PROBLEMS IN NONLINEAR DYNAMICS

by

Char-Ming Chin

Dissertation submitted to the Faculty of the

Virginia Polytechnic Institute and State University

in partial fulfillment of the requirements for the degree of

Doctor of Philosophy

in

Engineering Mechanics

APPROVED:

Professor Ali H. Nayfeh, Chairman

Professor Dean T. Mook

Professor Charles W. Smith

Professor Michael Renardy

Professor Scott L. Hendricks

December, 1993

Blacksburg, Virginia

PROBLEMS IN NONLINEAR DYNAMICS

by

Char-Ming Chin

Professor Ali H. Nayfeh, Chairman

Engineering Mechanics

(ABSTRACT)

Three types of problems in nonlinear dynamics are studied. First, we use a complex-variable invariant-manifold approach to determine the nonlinear normal modes of weakly nonlinear discrete systems with one-to-one and three-to-one internal resonances. Cubic geometric nonlinearities are considered. The system under investigation possesses similar nonlinear normal modes for the case of one-to-one internal resonance and nonsimilar nonlinear normal modes for the case of three-to-one internal resonance. In contrast with the case of no internal resonance, the number of nonlinear normal modes may be more than the number of linear normal modes. Bifurcations of the calculated nonlinear normal modes are investigated. For continuous systems without internal resonances, we consider a cantilever beam and compare two approaches for the determination of its nonlinear planar modes. In the first approach, the governing partial-differential system is discretized using the linear mode shapes and then the nonlinear mode shapes are determined from the discretized system. In the second approach, the boundary-value problem is treated directly by using the method of multiple scales. The results show that both approaches yield the same nonlinear modes because the discretization is performed using a complete set of basis functions, namely, the linear mode shapes.

Second, we study the nonlinear response of multi-degree-of-freedom systems with repeated natural frequencies to various parametric resonances. The linear part

of the system has a nonsemisimple one-to-one resonance. The character of the stability and various types of bifurcation are analyzed. The results are applied to the flutter of a simply supported panel in a supersonic airstream. In which case, the nonlinear ordinary differential equations governing the modulation of the amplitudes and phases of the excited modes are derived and used to calculate the equilibrium solutions and their stability and hence to identify the excitation parameters that suppress flutter and those that lead to complex motions. A combination of a shooting technique and Floquet theory is used to calculate limit cycles and their stability. The numerical results indicate the existence of a sequence of period-doubling bifurcations that culminates in chaos. The complex motions are characterized by using phase planes, power spectra, Lyapunov exponents, and dimensions. Moreover, bifurcation analyses in the case of fundamental parametric resonance reveal that the addition of quadratic nonlinearities change qualitatively as well as quantitatively the response of systems with cubic nonlinearities. The quadratic nonlinearities change the pitchfork bifurcation to a transcritical bifurcation. Cyclic-fold bifurcations, Hopf bifurcations of the nontrivial constant solutions, and period-doubling sequences leading to chaos are induced by these quadratic terms. The effects of quadratic nonlinearities for the case of principal parametric resonance are discussed.

Third, we investigate the transfer of energy from high- to low-frequency modes. The method of averaging is used to analyze the response of a two-degree-of-freedom system with widely spaced modal frequencies and cubic nonlinearities to a principal parametric resonance of the high-frequency mode. The conditions under which energy can be transferred from high- to low-frequency modes, as observed in the experiments, are determined. The interactions between the widely separated modes result in various bifurcations, the coexistence of multiple attractors, and chaotic

attractors. The results show that damping may be destabilizing. The analytical results are validated by numerically solving the original system.

Acknowledgements

This dissertation profited greatly from the excellent guidance, continuous encouragement, and infinite patience of my advisor, Professor Ali H. Nayfeh. I wish to express my sincere appreciation to him. I would also like to thank Professor Dean T. Mook for his continuous discussion and assistance during the course of this research. I am grateful to Professors Charles W. Smith, Michael Renardy, and Scott L. Hendricks for their precious comments and advices. Thanks are also due to the Air Force Office of Scientific Research for supporting this research under Grant No. F49620-92-J-0197.

To my family, I appreciate their warm care and strong support. Especially to my wife, Lei-Yi, without her endless encouragement, support, understanding, and sacrifice of all her time to take care of me and our children, Erica and Diana, it would have been impossible for me to finish this work.

I appreciate the friendship and assistance of Sally Shrader and other American friends. I move on with memories and appreciations. I dedicate this work to my father ('28-'85) and my mother.

Table of Contents

CHAPTER 1

INTRODUCTION

1.1 Problem Statement and Literature Review

1.1.1 Nonlinear Normal Modes

One of the most useful concepts in the study of linear systems is the normal mode. A basic property of these modes is invariance; that is, motion consisting of a single mode at any instant will consist only of that mode for all time. Linear systems and their modes possess many other properties that are very useful in a variety of applications. Recently, the concept of normal modes has been generalized to nonlinear systems. While most of the useful properties of linear modes cannot be duplicated in nonlinear systems, invariant motions on a two-dimensional manifold

can be found. Such motions have come to be known as nonlinear mode motions and have been the subject of much recent research.

Rosenberg (1962,1966) introduced the concept of nonlinear normal modes for undamped, multi-degree-of-freedom systems with n masses interconnected by strongly nonlinear symmetric springs. He classified nonlinear normal modes into similar and nonsimilar modes, depending on whether the positions of all masses at any instant are linearly or nonlinearly related to the position of any one of them. Rosenberg (1966) provided a theorem regarding the existence of similar normal modes in a symmetric, conservative system and discussed how the stability of nonlinear normal modes can be determined by using Floquet theory. Rosenberg and Kuo (1964) investigated nonsimilar normal modes of a discrete system. The number of nonlinear normal modes may be larger than the number of linear modes. Month and Rand (1980) illustrated how a Poincare map can be used to study the stability of similar nonlinear normal modes of a discrete system. Szemplinska-Stupnicka (1980) used the method of harmonic balance to construct nonlinear normal modes of discrete systems. Caughey and Vakakis (1991) and Vakakis and Caughey (1992) studied similar normal modes of discrete autonomous and nonautonomous systems. Pak, Rand, and Moon (1992) studied nonlinear normal modes of discrete systems. Rand, Pak, and Vakakis (1992) investigated bifurcations of nonlinear normal modes of a two-degree-of-freedom system. Vakakis and Rand (1992a,b) studied the local and global dynamics of a two-degree-of-freedom system by using Poincare maps.

Defining normal modes in terms of invariant manifolds, Shaw and Pierre (1991, 1993a,b) developed a method for constructing the nonlinear normal modes of conservative as well as nonconservative systems. In this approach, a nonlinear normal mode is an invariant manifold that is tangent to a linear modal hyperplane at the equilibrium point. Therefore, the number of nonlinear normal modes is the same

as the number of linear normal modes. Nayfeh and Nayfeh (1993a) showed that a perturbation method, such as the method of multiple scales (Nayfeh, 1973, 1981), can be used to obtain results equivalent to the invariant-manifold method of Shaw and Pierre. We note that the calculated modes are not valid in the case of internal resonance.

In this dissertation, we extend the approach of Nayfeh and Nayfeh and determine the nonlinear modes of a cantilever beam. Moreover, we employ the complex-variable approach of Nayfeh and Nayfeh to construct the nonlinear normal modes of systems with internal resonances. They are constructed by considering all the linear modes involved in the internal resonances.

1.1.2 Systems with Repeated Natural Frequencies

The mutual interactions among structural, inertial, and aerodynamic forces create many complicated physical phenomena. The principal phenomena of interest here are the dynamic aeroelastic instability of plates and shells (panel flutter) and the possible suppression of flutter by parametric excitations. It is well known that the aerodynamic loads on a panel increase as the wind speed increases. As the wind speed reaches some critical value (flutter speed), the panel motion itself creates significant pressure fluctuations which in turn modify the panel motion. Hence, a small disturbance can cause severe damage because of the resulting violent oscillations; this is called flutter. Because of structural nonlinearities, panel flutter does not usually lead to immediate structural failure. However, it will result in a sustained constant amplitude oscillation which may lead to long-time fatigue failure.

We study the possible suppression of flutter by parametric excitations and identify the parameters of the excitation that suppress flutter.

Physically, two natural frequencies of the structure coalesce as the flutter speed is reached; which means, mathematically, the linear operator of the corresponding discretized problem has a nonsemisimple structure. Therefore, we investigate the response of a weakly nonlinear system with a one-to-one internal resonance to various parametric resonances. Nonlinear modal interactions have been the subject of a great deal of recent research. For a weakly nonlinear system where there exists a special relationship between two or more natural frequencies of its linear modes and the excitation frequency, the nonlinearities can couple the modes, produce strong exchange of energy between modes, and lead to dangerously large responses in modes that are predicted by linear analysis to have insignificant response amplitudes. Moreover, the nonlinearities may put a cap on motions that are predicted by linear analysis to have infinitely large responses, as in systems with a nonsemisimple one-to-one internal resonance. In the presence of resonances, the long-time behavior of the system can contain large contributions due to several modes. The nature of these frequency relationships depends on the degree of the nonlinearity present in the system, the number of modes involved, and the character of the excitation. The resonances responsible for these modal interactions can be classified as autoparametric, or external combination, or parametric combination resonances.

Problems of parametric excitation of nonlinear dynamical systems are of importance in several branches of engineering, such as the vibrations of beam structures under dynamic loads, flow-induced vibrations, and control systems. The following brief review serves as an introduction to this subject. For a comprehensive review of the parametric response of nonlinear single- and

multiple-degree-of-freedom system, the reader is referred to Evan-Iwanowski (1976), Nayfeh and Mook (1979), Ibrahim (1985), Schmidt and Tondl (1986), and Nayfeh and Balachandran (1989, 1994).

Parametrically excited two-degree-of-freedom systems with quadratic nonlinearities and two-to-one autoparametric resonances were studied by Miles (1985), Nayfeh (1983b, 1983c, 1987a), Nayfeh and Zavodney (1986), Streit, Bajaj, and Krousgrill (1988), and Asrar (1991). Parametrically excited distributed-parameter systems with quadratic nonlinearities and two-to-one autoparametric resonances were studied by Miles (1984), Ibrahim and Barr (1975), Holmes (1986), Nayfeh (1987b), Gu and Sethna (1987), and Nayfeh and Nayfeh (1990).

Tso and Asmis (1974) analyzed the response of a two-degree-of-freedom system with cubic nonlinearities to a principal parametric resonance of the first mode. Tezak, Mook, and Nayfeh (1978) treated the nonlinear response of a hinged-clamped beam to principal and combination parametric resonances.

Parametrically excited systems with one-to-one autoparametric resonances whose linear parts are diagonal were studied by Asmis and Tso (1972), Ciliberto and Gollub (1985), Meron and Procaccia (1986), Simonelli and Gollub (1989), Feng and Sethna (1989), and Nayfeh and Pai (1989).

Parametrically excited systems having nonsemisimple linear structures were studied by Fu and Nemat-Nasser (1972a,b), Nayfeh and Mook (1979), Tezak, Nayfeh, and Mook (1982), Nayfeh (1983a), Namachchivaya and Malhotra (1992), and Nayfeh (1993). Fu and Nemat-Nasser used Floquet theory to analyze the parametric response of linear multi-degree-of-freedom systems with two repeated frequencies. Nayfeh and Mook (1979) used the method of multiple scales to analyze the response of linear multi-degree-of-freedom systems with two repeated frequencies to principal, fundamental, and combination parametric resonances. Nayfeh (1983a) used the

method of multiple scales to analyze the parametric response of linear systems with three repeated frequencies. Tezak, Nayfeh, and Mook (1982) used the method of multiple scales to determine the nonlinear response of multi-degree-of-freedom systems with two repeated frequencies to principal parametric resonances. They used the results to analyze the flutter of an isotropic panel in a supersonic stream. Namachchivaya and Malhotra (1992) used the method of normal forms to analyze the response of general two-degree-of-freedom nonlinear systems with two repeated frequencies to a principal parametric resonance. They found some interesting phenomena, such as homoclinic bifurcations, near the Bogdanov-Takens bifurcation point. Nayfeh (1993) presented normal forms for parametrically excited linear and nonlinear systems whose linear parts have nonsemisimple structures.

1.1.3 Systems with Widely Spaced Modal Frequencies

Recent experimental studies indicate that modal interactions can channel energy from a low-amplitude, high-frequency excitation into low-frequency, large-amplitude vibrations without a classical internal resonance or an external or parametric combination resonance involving the low-frequency mode. The presence of the low-frequency mode is accompanied by slow modulation of the amplitude and phase of the high-frequency mode where the frequency of the modulation is equal to the frequency of oscillation of the low-frequency mode.

In externally or parametrically excited multi-degree-of-freedom systems, modal interactions can occur when the excitation frequency is near the sum or difference of two or more linear natural frequencies. Dugundji and Mukhopadhyay (1973) experimentally and theoretically investigated the response of a thin cantilever beam

with an external base excitation at a frequency close to the sum of the natural frequencies of the first bending and first torsional modes. The excitation frequency was approximately 18 times the lowest-frequency component in the response. They found that the high-frequency excitation can produce a large-amplitude response in the low-frequency (first bending) mode through a combination resonance.

Haddow and Hasan (1988) conducted an experiment by parametrically exciting a flexible cantilever beam near twice the natural frequency of its fourth mode. Decreasing the excitation frequency, they found that a planar periodic response consisting essentially of the fourth mode lost stability, giving way to a nonplanar chaotic motion. They observed that as a result the energy seemed to cascade down through the modes, resulting eventually in a very low-frequency component in the response. Burton and Kolowith (1988) conducted an experiment similar to that of Haddow and Hasan. In certain regions of the parameter space, they observed chaotic motions where the lowest seven in-plane bending modes as well as the first torsional mode were present in the response. Cusumano and Moon (1989) presented experimental results for an externally excited cantilever beam. They observed a cascading of energy to low-frequency components in the response associated with nonplanar chaotic motions.

Recently, Anderson, Balachandran, and Nayfeh (1992) conducted experiments on a parametrically excited cantilever beam and found that modal interactions can transfer energy from a low-amplitude, high-frequency excitation into low-frequency, large-amplitude responses without a classical internal resonance or an external or parametric combination resonance involving the low-frequency mode. The only requirements they found are the existence of nonlinear coupling between the modes, which have widely separated natural frequencies. Nayfeh and Nayfeh (1993a) observed the same phenomenon in the response of an externally excited circular rod.

These experimental results indicate that the mechanism for the excitation of the low-frequency modes is due to slow modulations of the high-frequency modes. Nayfeh and Nayfeh (1993b) used an analytical model to explain the interactions between widely spaced modes of structures and determine conditions under which energy can be transferred from high-frequency to low-frequency modes, as observed in the experiments. Anderson, Nayfeh, and Balachandran (1993) used the method of averaging to analyze the response of the cantilever beam tested by Anderson, Balachandran, and Nayfeh. The analytical results are in qualitative agreement with the experimental results.

1.2 Objectives and Scope of the Dissertation

In this dissertation, we study three types of problems in nonlinear dynamics by employing various analytical approaches and numerical analyses.

In Chapter 2, we study the nonlinear normal modes of discrete systems with internal resonances and distributed-parameter systems, such as a cantilever beam, without internal resonances. In Section 2.1, we present methods for the study of nonlinear normal modes of weakly nonlinear discrete systems with one-to-one and three-to-one internal resonances. Cubic geometric nonlinearities are considered. The oscillator under investigation contains similar nonlinear normal modes for a one-to-one internal resonance and nonsimilar nonlinear normal modes for a three-to-one internal resonance. A mode bifurcation is possible when the structural parameters exceed certain values. The number of nonlinear normal modes of a

system is shown to be more than the number of normal modes of its associated linear system.

In Section 2.2, via the particular example of a cantilever beam, we discuss two approaches to the construction of the nonlinear normal modes of continuous systems. First, we summarize treatment of the discretized system. Here, a Galerkin procedure in terms of a complete set of basis functions is used to convert the partial-differential system into a system of ordinary-differential equations. Then, any of a number of techniques, including perturbation methods and invariant manifold techniques, can be applied to the discretized equations to obtain an approximation to the nonlinear modes. In the second approach, as shown in Section 2.2.2, we determine the nonlinear mode shapes and natural frequencies by applying the method of multiple scales directly to the governing partial-differential equation and boundary conditions. We show that treatment of the discretized system of a cantilever beam yields the same nonlinear modes obtained by treatment of the partial-differential system because the discretization is performed by using a complete set of basis functions that satisfy the boundary conditions, namely, the linear mode shapes.

In Chapter 3, we study the nonlinear response of parametrically excited systems with repeated natural frequencies. In Section 3.1, we use the method of normal forms to study the nonlinear response of two-degree-of-freedom systems with repeated natural frequencies and cubic nonlinearity to a principal parametric excitation. The linear part of the system has a nonsemisimple one-to-one resonance. The character of the stability and various types of bifurcation are analyzed. We reexamine the panel-flutter problem investigated by Tezak, Nayfeh, and Mook (1982). We show that, in the case of a simply supported panel in a supersonic airstream, only heteroclinic orbits can be observed near the Bogdanov-Takens bifurcation point, whereas a

homoclinic bifurcation can occur, resulting in the jump phenomenon. These results are interpreted by using the Shilnikov (1970) theorem. Some of the analytical results are verified by a numerical integration of the governing equations.

In Section 3.2, we summarize the analytical results for the case of fundamental parametric resonance. In Section 3.3, we use the method of multiple scales to study the nonlinear response of three-degree-of-freedom systems with a nonsemisimple structure to a combination parametric resonance, thereby extend the work of Tezak et al. to the case of combination parametric resonance. The numerical results indicate the existence of Hopf, cyclic-fold, and period-doubling bifurcations; chaotic responses; and different types of static bifurcations. In Section 3.4, we use the method of multiple scales to evaluate the effect of quadratic nonlinearities on the response of such systems to either a fundamental or a principal parametric resonance.

In Chapter 4, we consider the response of two nonlinearly coupled oscillators with widely spaced frequencies when the high-frequency mode is excited by a principal parametric resonance. Nayfeh and Nayfeh (1993b) studied the same system when the high-frequency mode is excited by a primary resonance. In this chapter, we use the method of averaging to investigate the solutions of the system and determine the conditions under which energy can be transferred from the high-frequency mode to the low-frequency mode. After an oscillation in the low-frequency mode occurs, we use numerical simulations to investigate some of the complexities in the system response.

In Chapter 5, we draw some conclusions and give few recommendations for further study.

CHAPTER 2

NONLINEAR NORMAL MODES

Methods for the study of nonlinear normal modes of weakly nonlinear discrete systems with one-to-one and three-to-one internal resonances are presented in Section 2.1. Cubic geometric nonlinearities are considered. The oscillator under investigation possesses similar nonlinear normal modes for a one-to-one internal resonance and nonsimilar nonlinear normal modes for a three-to-one internal resonance. A mode bifurcation is possible when the structural parameters exceed certain values. Hence, in contrast with the case of no internal resonance, the number of nonlinear normal modes may be more than the number of linear normal modes. In Section 2.2, two approaches for the determination of the nonlinear planar normal modes of a cantilever beam are compared. In the first approach, the governing partial-differential system is discretized by using the linear mode shapes and then the nonlinear mode shapes are determined from the discretized system. In the second approach, the boundary-value problem is treated directly by using the method of multiple scales. The results show that both approaches yield the same nonlinear

modes because the discretization is performed using a complete set of basis functions, namely, the linear mode shapes.

2.1 Discrete Systems with Internal Resonance

We construct the nonlinear modes of finite-degree-of-freedom systems governed by

$$\ddot{u}_j + \omega_j^2 u_j + f_j(u_1, u_2, ..., u_N) = 0 \text{ for } j = 1, 2, ..., N \tag{2.1}$$

in the presence of internal resonances. For simplicity, only cubic geometric nonlinearities are considered. Nayfeh and Nayfeh (1993a,b) showed that one can construct the nonlinear normal modes of equations, such as Eqs. (2.1), by using a perturbation method, such as the method of multiple scales, or the invariant-manifold approach with real or complex variables. Moreover, they showed that the algebra involved in implementing the invariant-manifold approach by using complex rather than real variables is less demanding. Hence, we will implement the invariant-manifold approach using complex variables. As a first step, we cast Eqs. (2.1) as a system of N first-order nonlinear complex-valued equations by using the transformation

$$u_j = \zeta_j + \bar{\zeta}_j, \quad \dot{u}_j = i\omega_j(\zeta_j - \bar{\zeta}_j) \tag{2.2}$$

The result is

$$\dot{\zeta}_j = i\omega_j\zeta_j + \frac{i}{2\omega_j} f_j[\zeta_1 + \bar{\zeta}_1, \zeta_2 + \bar{\zeta}_2, ..., \zeta_N + \bar{\zeta}_N] \tag{2.3}$$

2.1.1 The Case of No Internal Resonance

To construct the manifold that is tangent to the kth mode as the nonlinearity vanishes, we follow Nayfeh and Nayfeh (1993) and choose ζ_k and $\bar{\zeta}_k$ to parameterize the manifold. Thus, we let

$$\zeta_j(t) = h_j(\zeta_k, \bar{\zeta}_k) + ... \tag{2.4}$$

where

$$h_j(0,0) = 0 \text{ and } \frac{\partial h_j}{\partial \zeta_k}(0) = \frac{\partial h_j}{\partial \bar{\zeta}_k}(0) = 0$$

Then, the dynamics on the manifold is governed by

$$\dot{\zeta}_k = i\omega_k\zeta_k + \frac{i}{2\omega_k} f_k(\zeta_k + \bar{\zeta}_k) \tag{2.5}$$

For the case of cubic geometric nonlinearities,

$$f_j(u_1, u_2, ..., u_N) = f_{jk}u_k^3 + ... \tag{2.6}$$

Hence, Eq. (2.5) becomes

$$\dot{\zeta}_k = i\omega_k\zeta_k + \frac{if_{kk}}{2\omega_k}(\zeta_k + \bar{\zeta}_k)^3 + ... \tag{2.7}$$

Substituting Eq. (2.4) into Eq. (2.3) and using Eqs. (2.6) and (2.7), we obtain

$$\omega_k\left[\frac{\partial h_j}{\partial \zeta_k}\zeta_k - \frac{\partial h_j}{\partial \bar{\zeta}_k}\bar{\zeta}_k\right] - \omega_j h_j = \frac{f_{jk}}{2\omega_j}(\zeta_k + \bar{\zeta}_k)^3 + \ldots \tag{2.8}$$

The right-hand side of Eq. (2.8) suggests seeking h_j in the form

$$h_j = \Lambda_{1jk}\zeta_k^3 + \Lambda_{2jk}\zeta_k^2\bar{\zeta}_k + \Lambda_{3jk}\zeta_k\bar{\zeta}_k^2 + \Lambda_{4jk}\bar{\zeta}_k^3 \tag{2.9}$$

Substituting Eq. (2.9) into Eq. (2.8) and equating the coefficients of ζ_k^3, $\zeta_k^2\bar{\zeta}_k$, $\zeta_k\bar{\zeta}_k^2$, and $\bar{\zeta}_k^3$ on both sides, we have

$$\begin{aligned}
\Lambda_{1jk} &= \frac{f_{jk}}{2\omega_j(3\omega_k - \omega_j)}, \quad \Lambda_{2jk} = \frac{3f_{jk}}{2\omega_j(\omega_k - \omega_j)}, \\
\Lambda_{3jk} &= -\frac{3f_{jk}}{2\omega_j(\omega_k + \omega_j)}, \quad \Lambda_{4jk} = -\frac{f_{jk}}{2\omega_j(3\omega_k + \omega_j)}
\end{aligned} \tag{2.10}$$

Substituting Eqs. (2.9) and (2.10) into Eq. (2.2) yields

$$u_j = \frac{f_{jk}}{9\omega_k^2 - \omega_j^2}\left(\zeta_k^3 + \bar{\zeta}_k^3\right) + \frac{3f_{jk}}{\omega_k^2 - \omega_j^2}\left(\zeta_k^2\bar{\zeta}_k + \zeta_k\bar{\zeta}_k^2\right) + \ldots \tag{2.11}$$

It is clear from Eq. (2.11) that the constructed manifold is not valid when $\omega_j \approx 3\omega_k$ (three-to-one internal resonance) or $\omega_j \approx \omega_k$ (one-to-one internal resonance).

To express Eq. (2.11) in terms of u_k and $\dot{u}_k$, we note that

$$\begin{aligned}
\zeta_k^3 + \bar{\zeta}_k^3 &= \frac{\omega_k^2 u_k^3 - 3u_k\dot{u}_k^2}{4\omega_k^2} \\
\zeta_k^2\bar{\zeta}_k + \zeta_k\bar{\zeta}_k^2 &= \frac{\omega_k^2 u_k^3 + u_k\dot{u}_k^2}{4\omega_k^2}
\end{aligned} \tag{2.12}$$

Using Eqs. (2.12), we rewrite Eq. (2.11) as

$$u_j = \Gamma_{1jk} u_k^3 + \Gamma_{2jk} u_k \dot{u}_k^2 + \ldots \tag{2.13}$$

where

$$\Gamma_{1jk} = \frac{(7\omega_k^2 - \omega_j^2) f_{jk}}{(9\omega_k^2 - \omega_j^2)(\omega_k^2 - \omega_j^2)}, \quad \Gamma_{2jk} = \frac{6 f_{jk}}{(9\omega_k^2 - \omega_j^2)(\omega_k^2 - \omega_j^2)} \tag{2.14}$$

Differentiating Eq. (2.13) with respect to t and using Eqs. (2.1) when $j = k$, we have

$$\dot{u}_j = \left(3\Gamma_{1jk} - 2\omega_k^2 \Gamma_{2jk}\right) u_k^2 \dot{u}_k + \Gamma_{2jk} \dot{u}_k^3 + \ldots \tag{2.15}$$

To simplify the dynamics on the manifold, we use the method of normal forms (Nayfeh, 1993) and introduce the near-identity transformation

$$\zeta_k = \xi_k + h_k(\xi_k, \bar{\xi}_k) \tag{2.16}$$

and choose the h_k so that Eq. (2.7) takes the simplest possible form

$$\dot{\xi}_k = i\omega_k \xi_k + g_k(\xi_k, \bar{\xi}_k) \tag{2.17}$$

Substituting Eqs. (2.16) and (2.17) into Eq. (2.7) yields

$$g_k + i\omega_k \left[\frac{\partial h_k}{\partial \xi_k} \xi_k - \frac{\partial h_k}{\partial \bar{\xi}_k} \bar{\xi}_k - h_k \right] = \frac{i f_{kk}}{2\omega_k} (\xi_k + \bar{\xi}_k)^3 \tag{2.18}$$

We note that h_k can be chosen to eliminate the terms on the right-hand side of Eq. (2.18) except the resonance term, which is proportional to $\xi_k^2 \bar{\xi}_k$. Therefore, we choose g_k to eliminate this term; that is,

$$g_k = \frac{3if_{kk}}{2\omega_k}\xi_k^2\bar{\xi}_k \tag{2.19}$$

Then, we seek h_k in the form

$$h_k = \Lambda_{1k}\xi_k^3 + \Lambda_{2k}\xi_k^2\bar{\xi}_k + \Lambda_{3k}\xi_k\bar{\xi}_k^2 + \Lambda_{4k}\bar{\xi}_k^3 \tag{2.20}$$

Substituting Eq. (2.20) into Eq. (2.18), using Eq. (2.19), and equating the coefficients of ξ_k^3, $\xi_k\bar{\xi}_k^2$, and $\bar{\xi}_k^3$ on both sides, we obtain

$$\Lambda_{1k} = \frac{f_{kk}}{4\omega_k^2}, \quad \Lambda_{3k} = -\frac{3f_{kk}}{4\omega_k^2}, \quad \Lambda_{4k} = -\frac{f_{kk}}{8\omega_k^2} \tag{2.21}$$

We note that Λ_{2k} is arbitrary. Substituting Eq. (2.19) into Eq. (2.17), we obtain the normal form

$$\dot{\xi}_k = i\omega_k\xi_k + \frac{3if_{kk}}{2\omega_k}\xi_k^2\bar{\xi}_k + \ldots \tag{2.22}$$

Substituting Eqs. (2.20) and (2.16) into Eq. (2.2) and using Eqs. (2.21), we obtain

$$\begin{aligned} u_k = {} & \xi_k + \bar{\xi}_k + \frac{f_{kk}}{8\omega_k^2}(\xi_k^3 + \bar{\xi}_k^3) \\ & + \left[\Lambda_{2k} - \frac{3f_{kk}}{4\omega_k^2}\right](\xi_k^2\bar{\xi}_k + \xi_k\bar{\xi}_k^2) + \ldots \end{aligned} \tag{2.23}$$

To uniquely define the frequency of the fundamental component of oscillation, we choose Λ_{2k} to eliminate the term $\xi_k^2\bar{\xi}_k$. Therefore, Eq. (2.23) becomes

$$u_k = \xi_k + \bar{\xi}_k + \frac{f_{kk}}{8\omega_k^2}(\xi_k^3 + \bar{\xi}_k^3) + \ldots \tag{2.24}$$

2.1.2 The Case of Internal Resonance

To construct the manifold for two modes involved in an internal resonance, such as the rth and sth modes, we need a four-dimensional rather than a two-dimensional manifold. Thus, we seek a normal-mode motion of the form

$$\zeta_j(t) = h_j(\zeta_r, \bar{\zeta}_r, \zeta_s, \bar{\zeta}_s) + \ldots \quad \text{for } j \neq r \text{ and } s \tag{2.25}$$

For the case of cubic geometric nonlinearities, f_j can be expressed as

$$f_j(u_1, u_2, \ldots, u_N) = f_{jr}u_r^3 + f_{jrs}u_r^2 u_s + f_{jsr}u_r u_s^2 + f_{js}u_s^3 + \ldots \tag{2.26}$$

Hence, the dynamics on the manifold is governed by

$$\begin{aligned}\dot{\zeta}_r = i\omega_r\zeta_r + \frac{i}{2\omega_r}\Big[&f_{rr}(\zeta_r + \bar{\zeta}_r)^3 + f_{rrs}(\zeta_r + \bar{\zeta}_r)^2(\zeta_s + \bar{\zeta}_s) \\ &+ f_{rsr}(\zeta_r + \bar{\zeta}_r)(\zeta_s + \bar{\zeta}_s)^2 + f_{rs}(\zeta_s + \bar{\zeta}_s)^3\Big]\end{aligned} \tag{2.27}$$

$$\begin{aligned}\dot{\zeta}_s = i\omega_s\zeta_s + \frac{i}{2\omega_s}\Big[&f_{sr}(\zeta_r + \bar{\zeta}_r)^3 + f_{srs}(\zeta_r + \bar{\zeta}_r)^2(\zeta_s + \bar{\zeta}_s) \\ &+ f_{ssr}(\zeta_r + \bar{\zeta}_r)(\zeta_s + \bar{\zeta}_s)^2 + f_{ss}(\zeta_s + \bar{\zeta}_s)^3\Big]\end{aligned} \tag{2.28}$$

To determine the h_j, we substitute Eq. (2.25) into Eq. (2.3), use Eqs. (2.26)-(2.28), and obtain

$$\begin{aligned}&\omega_r\left(\frac{\partial h_j}{\partial \zeta_r}\zeta_r - \frac{\partial h_j}{\partial \bar{\zeta}_r}\bar{\zeta}_r\right) + \omega_s\left(\frac{\partial h_j}{\partial \zeta_s}\zeta_s - \frac{\partial h_j}{\partial \bar{\zeta}_s}\bar{\zeta}_s\right) - \omega_j h_j \\ &= \frac{1}{2\omega_j}\Big[f_{jr}(\zeta_r + \bar{\zeta}_r)^3 + f_{jrs}(\zeta_r + \bar{\zeta}_r)^2(\zeta_s + \bar{\zeta}_s) \\ &+ f_{jsr}(\zeta_r + \bar{\zeta}_r)(\zeta_s + \bar{\zeta}_s)^2 + f_{js}(\zeta_s + \bar{\zeta}_s)^3\Big] + \ldots\end{aligned} \tag{2.29}$$

The right-hand side of Eq. (2.29) suggests seeking h_j in the form

$$\begin{aligned} h_j = {} & \Lambda_1\zeta_r^3 + \Lambda_2\zeta_r^2\bar{\zeta}_r + \Lambda_3\zeta_r\bar{\zeta}_r^2 + \Lambda_4\bar{\zeta}_r^3 + \Lambda_5\zeta_s^3 + \Lambda_6\zeta_s^2\bar{\zeta}_s + \Lambda_7\zeta_s\bar{\zeta}_s^2 \\ & + \Lambda_8\bar{\zeta}_s^3 + \Lambda_9\zeta_r^2\zeta_s + \Lambda_{10}\zeta_r\bar{\zeta}_r\zeta_s + \Lambda_{11}\bar{\zeta}_r^2\zeta_s + \Lambda_{12}\zeta_r^2\bar{\zeta}_s \\ & + \Lambda_{13}\zeta_r\bar{\zeta}_r\bar{\zeta}_s + \Lambda_{14}\bar{\zeta}_r^2\bar{\zeta}_s + \Lambda_{15}\zeta_s^2\zeta_r + \Lambda_{16}\zeta_s\bar{\zeta}_s\zeta_r \\ & + \Lambda_{17}\bar{\zeta}_s^2\zeta_r + \Lambda_{18}\zeta_s^2\bar{\zeta}_r + \Lambda_{19}\zeta_s\bar{\zeta}_s\bar{\zeta}_r + \Lambda_{20}\bar{\zeta}_s^2\bar{\zeta}_r \end{aligned} \tag{2.30}$$

Substituting Eq. (2.30) into Eqs. (2.29) and equating each of the independent variables on both sides, we obtain

$$\Lambda_1 = \frac{f_{jr}}{2\omega_j(3\omega_r - \omega_j)}, \quad \Lambda_2 = \frac{3f_{jr}}{2\omega_j(\omega_r - \omega_j)}, \quad \Lambda_3 = -\frac{3f_{jr}}{2\omega_j(\omega_r + \omega_j)},$$

$$\Lambda_4 = -\frac{f_{jr}}{2\omega_j(3\omega_r + \omega_j)}, \quad \Lambda_5 = \frac{f_{js}}{2\omega_j(3\omega_s - \omega_j)},$$

$$\Lambda_6 = \frac{3f_{js}}{2\omega_j(\omega_s - \omega_j)}, \quad \Lambda_7 = -\frac{3f_{js}}{2\omega_j(\omega_s + \omega_j)},$$

$$\Lambda_8 = -\frac{f_{js}}{2\omega_j(3\omega_s + \omega_j)}, \quad \Lambda_9 = \frac{f_{jrs}}{2\omega_j(2\omega_r + \omega_s - \omega_j)},$$

$$\Lambda_{10} = \frac{f_{jrs}}{\omega_j(\omega_s - \omega_j)}, \quad \Lambda_{11} = -\frac{f_{jrs}}{2\omega_j(2\omega_r - \omega_s + \omega_j)},$$

$$\Lambda_{12} = \frac{f_{jrs}}{2\omega_j(2\omega_r - \omega_s - \omega_j)}, \quad \Lambda_{13} = -\frac{f_{jrs}}{\omega_j(\omega_s + \omega_j)},$$

$$\Lambda_{14} = -\frac{f_{jrs}}{2\omega_j(2\omega_r + \omega_s + \omega_j)}, \quad \Lambda_{15} = \frac{f_{jsr}}{2\omega_j(\omega_r + 2\omega_s - \omega_j)},$$

$$\Lambda_{16} = \frac{f_{jsr}}{\omega_j(\omega_r - \omega_j)}, \quad \Lambda_{17} = \frac{f_{jsr}}{2\omega_j(\omega_r - 2\omega_s - \omega_j)},$$

$$\Lambda_{18} = \frac{f_{jsr}}{2\omega_j(2\omega_s - \omega_r - \omega_j)}, \quad \Lambda_{19} = -\frac{f_{jsr}}{\omega_j(\omega_r + \omega_j)},$$

$$\Lambda_{20} = -\frac{f_{jsr}}{2\omega_j(\omega_r + 2\omega_s + \omega_j)}$$

Substituting the Λ_j into Eq. (2.30) and then substituting the result into Eqs. (2.25) and (2.2), we have

$$
\begin{aligned}
u_j = {} & \frac{f_{jr}}{9\omega_r^2 - \omega_j^2}(\zeta_r^3 + \bar{\zeta}_r^3) + \frac{3f_{jr}}{\omega_r^2 - \omega_j^2}(\zeta_r^2\bar{\zeta}_r + \zeta_r\bar{\zeta}_r^2) \\
& + \frac{f_{js}}{9\omega_s^2 - \omega_j^2}(\zeta_s^3 + \bar{\zeta}_s^3) + \frac{3f_{js}}{\omega_s^2 - \omega_j^2}(\zeta_s^2\bar{\zeta}_s + \zeta_s\bar{\zeta}_s^2) \\
& + \frac{f_{jrs}}{(2\omega_r + \omega_s)^2 - \omega_j^2}(\zeta_r^2\zeta_s + \bar{\zeta}_r^2\bar{\zeta}_s) + \frac{2f_{jrs}}{\omega_s^2 - \omega_j^2}(\zeta_s + \bar{\zeta}_s)\zeta_r\bar{\zeta}_r \\
& + \frac{f_{jrs}}{(2\omega_r - \omega_s)^2 - \omega_j^2}(\zeta_r^2\bar{\zeta}_s + \bar{\zeta}_r^2\zeta_s) + \frac{f_{jsr}}{(\omega_r + 2\omega_s)^2 - \omega_j^2}(\zeta_s^2\zeta_r + \bar{\zeta}_s^2\bar{\zeta}_r) \\
& + \frac{2f_{jsr}}{\omega_r^2 - \omega_j^2}(\zeta_r + \bar{\zeta}_r)\zeta_s\bar{\zeta}_s + \frac{f_{jsr}}{(2\omega_s - \omega_r)^2 - \omega_j^2}(\zeta_s^2\bar{\zeta}_r + \bar{\zeta}_s^2\zeta_r)
\end{aligned}
\tag{2.31}
$$

To express u_j in terms of u_r, $\dot{u}_r$, u_s, and $\dot{u}_s$, we use Eqs. (2.12), and the relations

$$
\begin{aligned}
u_r^2 u_s + \frac{\dot{u}_r^2 u_s}{\omega_r^2} &= 4(\zeta_s + \bar{\zeta}_s)\zeta_r\bar{\zeta}_r \\
\frac{u_r^2 u_s}{4} - \frac{\dot{u}_r^2 u_s}{4\omega_r^2} - \frac{\dot{u}_r\dot{u}_s u_r}{2\omega_r\omega_s} &= \zeta_r^2\zeta_s + \bar{\zeta}_r^2\bar{\zeta}_s \\
\frac{u_r^2 u_s}{4} - \frac{\dot{u}_r^2 u_s}{4\omega_r^2} + \frac{\dot{u}_r\dot{u}_s u_r}{2\omega_r\omega_s} &= \zeta_r^2\bar{\zeta}_s + \bar{\zeta}_r^2\zeta_s
\end{aligned}
\tag{2.32}
$$

and the relations obtained from Eqs. (2.32) by interchanging r and s. The result is

$$
\begin{aligned}
u_j = {} & \Gamma_{1jr}u_r^3 + \Gamma_{2jr}u_r\dot{u}_r^2 + \Gamma_{1js}u_s^3 + \Gamma_{2js}u_s\dot{u}_s^2 + \Gamma_{3jrs}u_r^2 u_s \\
& + \Gamma_{4jrs}\dot{u}_r^2 u_s + \Gamma_{5jrs}\dot{u}_r\dot{u}_s u_r + \Gamma_{3jsr}u_s^2 u_r + \Gamma_{4jsr}\dot{u}_s^2 u_r + \Gamma_{5jsr}\dot{u}_r\dot{u}_s u_s
\end{aligned}
\tag{2.33}
$$

where Γ_{1jk} and Γ_{2jk} are defined in Eqs. (2.14),

$$
\Gamma_{3jrs} = \frac{1}{4}f_{jrs}\left[\frac{2}{\omega_s^2 - \omega_j^2} + \frac{1}{(2\omega_r + \omega_s)^2 - \omega_j^2} + \frac{1}{(2\omega_r - \omega_s)^2 - \omega_j^2}\right] \tag{2.34}
$$

$$\Gamma_{4jrs} = \frac{f_{jrs}}{4\omega_r^2}\left[\frac{2}{\omega_s^2-\omega_j^2} - \frac{1}{(2\omega_r+\omega_s)^2-\omega_j^2} - \frac{1}{(2\omega_r-\omega_s)^2-\omega_j^2}\right] \tag{2.35}$$

$$\Gamma_{5jrs} = \frac{f_{jrs}}{2\omega_r\omega_s}\left[\frac{1}{(2\omega_r-\omega_s)^2-\omega_j^2} - \frac{1}{(2\omega_r+\omega_s)^2-\omega_j^2}\right] \tag{2.36}$$

and Γ_{3jsr}, Γ_{4jsr}, and Γ_{5jsr} can be obtained from Eqs. (2.34)-(2.36) by interchanging the subscripts r and s. It follows from Eqs. (2.34)-(2.36) that the constructed manifold will breakdown when $\omega_j \approx 2\omega_r \mp \omega_s$ or $\omega_j \approx \omega_s \pm 2\omega_r$, which are the cases of combination internal resonance. These cases are not discussed in this dissertation.

The dynamics on the manifold is governed by Eqs. (2.27) and (2.28). To simplify these equations, we introduce the near-identity transformation

$$\begin{aligned}\zeta_r &= \xi_r + h_r(\xi_r, \bar{\xi}_r, \xi_s, \bar{\xi}_s)\\ \zeta_s &= \xi_s + h_s(\xi_r, \bar{\xi}_r, \xi_s, \bar{\xi}_s)\end{aligned} \tag{2.37}$$

and choose h_r and h_s so that Eqs. (2.27) and (2.28) take the simplest possible form

$$\begin{aligned}\dot{\xi}_r &= i\omega_r\xi_r + g_r(\xi_r, \bar{\xi}_r, \xi_s, \bar{\xi}_s)\\ \dot{\xi}_s &= i\omega_s\xi_s + g_s(\xi_r, \bar{\xi}_r, \xi_s, \bar{\xi}_s)\end{aligned} \tag{2.38}$$

Substituting Eqs. (2.37) and (2.38) into Eqs. (2.27) and (2.28) yields

$$g_r + i\omega_r\left(\frac{\partial h_r}{\partial \xi_r}\xi_r - \frac{\partial h_r}{\partial \bar{\xi}_r}\bar{\xi}_r - h_r\right) + i\omega_s\left(\frac{\partial h_r}{\partial \xi_s}\xi_s - \frac{\partial h_r}{\partial \bar{\xi}_s}\bar{\xi}_s\right)$$
$$= \frac{i}{2\omega_r}\left[f_{rr}(\xi_r + \bar{\xi}_r)^3 + f_{rrs}(\xi_r + \bar{\xi}_r)^2(\xi_s + \bar{\xi}_s)\right. \tag{2.39}$$
$$\left. + f_{rsr}(\xi_r + \bar{\xi}_r)(\xi_s + \bar{\xi}_s)^2 + f_{rs}(\xi_s + \bar{\xi}_s)^3\right] + \ldots$$

$$g_s + i\omega_s\left(\frac{\partial h_s}{\partial \xi_s}\xi_s - \frac{\partial h_s}{\partial \bar{\xi}_s}\bar{\xi}_s - h_s\right) + i\omega_r\left(\frac{\partial h_s}{\partial \xi_r}\xi_r - \frac{\partial h_s}{\partial \bar{\xi}_r}\bar{\xi}_r\right)$$
$$= \frac{i}{2\omega_s}\left[f_{sr}(\xi_r + \bar{\xi}_r)^3 + f_{srs}(\xi_r + \bar{\xi}_r)^2(\xi_s + \bar{\xi}_s)\right. \tag{2.40}$$
$$\left. + f_{ssr}(\xi_r + \bar{\xi}_r)(\xi_s + \bar{\xi}_s)^2 + f_{ss}(\xi_s + \bar{\xi}_s)^3\right] + \ldots$$

The near-resonance terms depend on the internal resonance being considered.

(a) One-to-One Internal Resonance

When $\omega_s \approx \omega_r$, we choose g_r and g_s to eliminate the resonance and near-resonance terms on the right-hand sides of Eqs. (2.39) and (2.40), respectively; that is,

$$g_r = \frac{i}{2\omega_r}\left[3f_{rr}\xi_r^2\bar{\xi}_r + f_{rrs}(\xi_r^2\bar{\xi}_s + 2\xi_r\bar{\xi}_r\xi_s)\right.$$
$$\left. + f_{rsr}(\xi_s^2\bar{\xi}_r + 2\xi_s\bar{\xi}_s\xi_r) + 3f_{rs}\xi_s^2\bar{\xi}_s\right] + \ldots$$
$$g_s = \frac{i}{2\omega_s}\left[3f_{sr}\xi_r^2\bar{\xi}_r + f_{srs}(\xi_r^2\bar{\xi}_s + 2\xi_r\bar{\xi}_r\xi_s)\right. \tag{2.41}$$
$$\left. + f_{ssr}(\xi_s^2\bar{\xi}_r + 2\xi_s\bar{\xi}_s\xi_r) + 3f_{ss}\xi_s^2\bar{\xi}_s\right] + \ldots$$

Then, we seek and obtain h_r and h_s in the same form as h_j in Eq. (2.30) with the Λ_m being replaced by Λ_{mj} for m = 1,2,...,20 and j = r or s, except that Λ_{2j}, Λ_{6j}, Λ_{10j}, Λ_{12j}, Λ_{16j}, and Λ_{18j} are arbitrary. Following a procedure similar to that used in the case of no internal resonance, we choose the arbitrary coefficients so that the frequencies of the rth and sth components of oscillation are uniquely defined. The result is

$$u_r = \xi_r + \bar{\xi}_r + \frac{f_{rr}}{8\omega_r^2}(\xi_r^3 + \bar{\xi}_r^3) + \frac{f_{rrs}}{(\omega_r + \omega_s)(3\omega_r + \omega_s)}(\xi_r^2\xi_s + \bar{\xi}_r^2\bar{\xi}_s)$$
$$+ \frac{f_{rsr}}{4\omega_s(\omega_r + \omega_s)}(\xi_s^2\xi_r + \bar{\xi}_s^2\bar{\xi}_r) + \frac{f_{rs}}{9\omega_s^2 - \omega_r^2}(\xi_s^3 + \bar{\xi}_s^3) + \ldots \tag{2.42}$$

and u_s can be obtained from Eq. (2.42) by interchanging r and s.

(b) Three-to-One Internal Resonance

When $\omega_s \approx 3\omega_r$, g_r and g_s can be obtained from Eqs. (2.39) and (2.40) by eliminating the resonance and near-resonance terms; that is,

$$g_r = \frac{i}{2\omega_r}\left[3f_{rr}\xi_r^2\bar{\xi}_r + 2f_{rsr}\xi_s\bar{\xi}_s\xi_r + f_{rrs}\xi_s\bar{\xi}_r^2\right] + \ldots$$
$$g_s = \frac{i}{2\omega_s}\left[3f_{ss}\xi_s^2\bar{\xi}_s + 2f_{srs}\xi_r\bar{\xi}_r\xi_s + f_{sr}\xi_r^3\right] + \ldots \tag{2.43}$$

Following an approach similar to that used in the case of no internal resonance, we obtain

$$u_r = \xi_r + \bar{\xi}_r + \frac{f_{rr}}{8\omega_r^2}(\xi_r^3 + \bar{\xi}_r^3)$$
$$+ \frac{f_{rrs}}{\omega_r + \omega_s}\left[\frac{1}{3\omega_r + \omega_s}(\xi_r^2\xi_s + \bar{\xi}_r^2\bar{\xi}_s) + \frac{2}{\omega_s - \omega_r}(\xi_s + \bar{\xi}_s)\xi_r\bar{\xi}_r\right]$$
$$+ \frac{f_{rsr}}{4\omega_s}\left[\frac{1}{\omega_r + \omega_s}(\xi_s^2\xi_r + \bar{\xi}_s^2\bar{\xi}_r) + \frac{1}{\omega_s - \omega_r}(\xi_s^2\bar{\xi}_r + \bar{\xi}_s^2\xi_r)\right] \tag{2.44}$$
$$+ f_{rs}\left[\frac{3}{\omega_s^2 - \omega_r^2}(\xi_s + \bar{\xi}_s)\xi_s\bar{\xi}_s + \frac{1}{9\omega_s^2 - \omega_r^2}(\xi_s^3 + \bar{\xi}_s^3)\right] + \ldots$$

$$
\begin{aligned}
u_s = {} & \xi_s + \bar{\xi}_s + \frac{f_{ss}}{8\omega_s^2}(\xi_s^3 + \bar{\xi}_s^3) \\
& + \frac{f_{ssr}}{\omega_r + \omega_s}\left[\frac{1}{3\omega_s + \omega_r}(\xi_s^2\xi_r + \bar{\xi}_s^2\bar{\xi}_r) + \frac{2}{\omega_r - \omega_s}(\xi_r + \bar{\xi}_r)\xi_s\bar{\xi}_s\right] \\
& + \frac{f_{srs}}{4\omega_r}\left[\frac{1}{\omega_r + \omega_s}(\xi_r^2\xi_s + \bar{\xi}_r^2\bar{\xi}_s) + \frac{1}{\omega_r - \omega_s}(\xi_r^2\bar{\xi}_s + \bar{\xi}_r^2\xi_s)\right] \\
& + \frac{3f_{sr}}{\omega_r^2 - \omega_s^2}(\xi_r + \bar{\xi}_r)\xi_r\bar{\xi}_r + \frac{f_{ssr}}{(3\omega_s - \omega_r)(\omega_s - \omega_r)}(\xi_s^2\bar{\xi}_r + \bar{\xi}_s^2\xi_r) + \cdots
\end{aligned}
\tag{2.45}
$$

2.1.3 Nonlinear Normal Modes and Their Stability

In this section, we use Eqs. (2.38), (2.41), and (2.43) to calculate the nonlinear normal modes for the cases of one-to-one and three-to-one internal resonances and investigate their bifurcations.

(a) One-to-One Internal Resonance ($\omega_s \approx \omega_r$). To quantitatively describe the nearness of ω_r to ω_s, we introduce the detuning parameter σ defined as

$$\omega_s = \omega_r + \varepsilon\sigma, \tag{2.46a}$$

where ε is a small dimensionless parameter. Moreover, we scale ξ_r and ξ_s as $O(\varepsilon^{1/2})$ and express them in the polar form

$$\xi_m = \frac{1}{2}\varepsilon^{1/2}a_m(t)e^{i(\omega_m t + \beta_m(t))} \tag{2.46b}$$

Substituting Eqs. (2.46) into Eqs. (2.38) and (2.41) and separating the result into real and imaginary parts, we obtain the modulation equations

$$\dot{a}_r = -\frac{\varepsilon a_s}{8\omega_r}\left[(f_{rrs}a_r^2 + 3f_{rs}a_s^2)\sin\gamma + f_{rsr}a_r a_s \sin 2\gamma\right] \tag{2.47}$$

$$\dot{a}_s = \frac{\varepsilon a_r}{8\omega_s}\left[(f_{ssr}a_s^2 + 3f_{sr}a_r^2)\sin\gamma + f_{srs}a_r a_s \sin 2\gamma\right] \tag{2.48}$$

$$a_r\dot{\beta}_r = \frac{\varepsilon}{8\omega_r}\left[3f_{rr}a_r^3 + 2f_{rsr}a_s^2 a_r + (3f_{rrs}a_r^2 a_s + 3f_{rs}a_s^3)\cos\gamma + f_{rsr}a_s^2 a_r \cos 2\gamma\right] \tag{2.49}$$

$$a_s\dot{\beta}_s = \frac{\varepsilon}{8\omega_s}\left[3f_{ss}a_s^3 + 2f_{srs}a_r^2 a_s + (3f_{ssr}a_s^2 a_r + 3f_{sr}a_r^3)\cos\gamma + f_{srs}a_r^2 a_s \cos 2\gamma\right] \tag{2.50}$$

where

$$\gamma = \beta_s - \beta_r + \varepsilon\sigma t \tag{2.51}$$

Therefore, to the second approximation,

$$u_r = \varepsilon^{1/2}a_r\cos\phi + \varepsilon^{3/2}\left\{\frac{f_{rr}a_r^3}{32\omega_r^2}\cos 3\phi + \frac{f_{rs}a_s^3}{4(9\omega_s^2-\omega_r^2)}\cos(3\phi+3\gamma)\right.$$
$$\left. + \frac{f_{rrs}a_r^2 a_s}{4(\omega_r+\omega_s)(3\omega_r+\omega_s)}\cos(3\phi+\gamma) + \frac{f_{rsr}a_r a_s^2}{16\omega_s(\omega_r+\omega_s)}\cos(3\phi+2\gamma)\right\} + \ldots \tag{2.52}$$

$$u_s = \varepsilon^{1/2}a_s\cos(\phi+\gamma) + \varepsilon^{3/2}\left\{\frac{f_{sr}a_r^3}{4(9\omega_r^2-\omega_s^2)}\cos 3\phi + \frac{f_{ss}a_s^3}{32\omega_s^2}\cos(3\phi+3\gamma)\right.$$
$$\left. + \frac{f_{srs}a_r^2 a_s}{16\omega_r(\omega_r+\omega_s)}\cos(3\phi+\gamma) + \frac{f_{ssr}a_r a_s^2}{4(\omega_r+\omega_s)(3\omega_s+\omega_r)}\cos(3\phi+2\gamma)\right\} + \ldots \tag{2.53}$$

where the a_m and β_m are given by Eqs. (2.47)-(2.51) and

$$\phi = \omega_r t + \beta_r \tag{2.54}$$

It follows from Eqs. (2.52) and (2.53) that periodic solutions of the original system correspond to the fixed points of Eqs. (2.47)-(2.51); that is $\dot{a}_r = \dot{a}_s = 0$ and $\dot{\gamma} = 0$. It follows from Eqs. (2.47)-(2.51) that there are two possible types of fixed points: $(a_r, a_s) = (0,0)$ and $(a_r \neq 0, a_s \neq 0)$. The latter satisfies the following equations:

$$(f_{rrs}a_r^2 + 3f_{rs}a_s^2 + 2f_{rsr}a_r a_s \cos\gamma)\sin\gamma = 0 \tag{2.55}$$

$$(f_{ssr}a_s^2 + 3f_{sr}a_r^2 + 2f_{srs}a_r a_s \cos\gamma)\sin\gamma = 0 \tag{2.56}$$

$$\begin{aligned}\sigma &+ \frac{1}{8\omega_s}\left[3f_{ss}a_s^2 + 2f_{srs}a_r^2 + (3f_{ssr}a_s a_r + 3f_{sr}\frac{a_r^3}{a_s})\cos\gamma + f_{srs}a_r^2\cos 2\gamma\right] \\ &- \frac{1}{8\omega_r}\left[3f_{rr}a_r^2 + 2f_{rsr}a_s^2 + (3f_{rrs}a_r a_s + 3f_{rs}\frac{a_s^3}{a_r})\cos\gamma + f_{rsr}a_s^2\cos 2\gamma\right] = 0\end{aligned} \tag{2.57}$$

It follows from Eqs. (2.55) and (2.56) that there are two possibilities: $\sin\gamma = 0$ and $\sin\gamma \neq 0$. Next, we discuss these cases starting with the first.

(i) $\sin\gamma = 0$ or $\gamma = n\pi$ for $n = 0,1,2,...$

Letting $c = a_r/a_s$, we rewrite Eq. (2.57) as

$$\begin{aligned}(\omega_r f_{sr}\cos\gamma)c^4 + (\omega_r f_{srs} - \omega_s f_{rr})c^3 + [(\omega_r f_{ssr} - \omega_s f_{rrs})\cos\gamma]c^2 \\ + \left(\omega_r f_{ss} - \omega_s f_{rsr} + \frac{8\omega_r\omega_s}{3a_s^2}\sigma\right)c - \omega_s f_{rs}\cos\gamma = 0\end{aligned} \tag{2.58}$$

It follows from Eqs. (2.52), (2.53), (2.54), and (2.58) that, for a given ω_m, f_{mij}, a_s, and σ, $\cos\gamma = 1$ and $\cos\gamma = -1$ provide the same solutions. Hence, we focus on the case $\cos\gamma = 1$. Moreover, we consider after Month and Rand (1977,1980) and Vakakis and Rand (1992a,b) the case

$$\begin{aligned}f_{rr} &= K + 1, \quad f_{rrs} = -3, \quad f_{rsr} = 3, \quad f_{rs} = -1 \\ f_{sr} &= -1, \quad f_{srs} = 3, \quad f_{ssr} = -3, \quad f_{ss} = K + 1\end{aligned} \tag{2.59}$$

and $\omega_r = 1$.

When $\sigma = 0$ (i.e., $\omega_s = 1$), Eq. (2.58) can be rewritten as

$$\left(c^2 - 1\right)\left[c^2 + (K-2)c + 1\right] = 0 \tag{2.60}$$

whose solutions are

$$c = 1, \quad -1, \quad 1 - \frac{1}{2}K \pm \frac{1}{2}\sqrt{K(K-4)} \tag{2.61}$$

It follows from Eq. (2.61) that there are two real values for c, namely -1 and 1, when $K < 4$ and there are two additional real values when $K > 4$. Hence, there are only two normal modes when $K < 4$ and there are four normal modes when $K > 4$.

Here we perform a so-called local stability analysis. To each fixed-point solution we add a small disturbance, then substitute the sum into the equations governing the modulations of the amplitude and phase and retain only the linear terms in the result. Following such a procedure, one finds that the disturbance, $\delta\mathbf{x}$, is governed by an equation of the form:

$$\delta\dot{\mathbf{x}} = [D_x f]\delta\mathbf{x} \tag{2.62}$$

where $[D_x f]$ is the so-called Jacobian matrix, the matrix obtained by differentiating the right-hand side of the modulation equations with respect to the independent variables. $[D_x f]$ is evaluated at the fixed point. Equation (2.62) is a linear equation with constant coefficients; thus, its solution has the form

$$\delta\mathbf{x} = \mathbf{c}e^{\lambda t} \tag{2.63}$$

where λ is an eigenvalue of $[D_x f]$. There is one such solution for each λ. The disturbance is unstable if one or more of the eigenvalues has a real part greater than

zero. The boundary between stable and unstable solutions corresponds to one or more eigenvalues having a real part equal to zero and the rest having real parts less than zero.

Hence, the stability of the four solutions in Eq. (2.61) can be obtained from Eqs. (2.47)-(2.51) and (2.59). To accomplish this, we eliminate $\dot{\beta}_r$ and $\dot{\beta}_s$ from Eqs. (2.49)-(2.51), use Eq. (2.59), and obtain

$$\dot{\gamma} = \frac{3}{8}\varepsilon(K-2)\left(a_s^2 - a_r^2\right) + \frac{3}{8}\varepsilon\left(\frac{a_s^3}{a_r} - \frac{a_r^3}{a_s}\right) \tag{2.64}$$

when $a_r \neq 0$ and $a_s \neq 0$. Then the Jacobian matrix of Eqs. (2.47), (2.48), and (2.64) evaluated at the corresponding fixed point (a_r, a_s, γ) is

$$J = \varepsilon\begin{bmatrix} 0 & 0 & \chi_1 \\ 0 & 0 & -c\chi_1 \\ \chi_2 & \chi_3 & 0 \end{bmatrix} \tag{2.65}$$

where

$$\chi_1 = \frac{3}{8}(c-1)^2 a_s^3$$

$$\chi_2 = -\frac{3}{8}\left[3c^2 + \frac{1}{c^2} + 2(K-2)c\right]a_s \tag{2.66}$$

$$\chi_3 = \frac{3}{8}\left[c^3 + \frac{3}{c} + 2(K-2)\right]a_s$$

One of the eigenvalues of the matrix J is zero, and the other two eigenvalues are given by

$$\lambda^2 = \varepsilon^2(\chi_1\chi_2 - c\chi_1\chi_3)$$
$$= -\frac{9}{64}\varepsilon^2 a_s^4(c-1)^2\left[c^4 + 3c^2 + 3 + \frac{1}{c^2} + 4c(K-2)\right] \tag{2.67}$$

When $c = 1$, all three eigenvalues are zero and the normal mode $u_s = u_r$ is neutrally stable. When $c = -1$, the normal mode $u_s = -u_r$ is neutrally stable if $K \leq 4$ and unstable if $K > 4$.

For the periodic solutions bifurcating from $u_s = -u_r$ at K = 4, the values of c are given by

$$c^2 + (K-2)c + 1 = 0$$

Then, Eq. (2.67) becomes

$$\lambda^2 = -\frac{9}{64}\varepsilon^2 a_s^4(c-1)^2\left\{[(k-2)c+2]^2 + \left(c - \frac{1}{c}\right)^2\right\},$$

which is negative. Therefore, the bifurcating solutions are neutrally stable. As shown in the c-K plane in Fig. 2.1 for $\sigma = 0$, the normal mode $u_s = -u_r$ gives way to the other two similar normal modes via a supercritical pitchfork bifurcation at K = 4.

When $\sigma \neq 0$, Eq. (2.58) can be rewritten as

$$(1-c^2)\left[Kc + (1-c)^2\right]a_s^2 + \frac{8}{3}\sigma c = 0 \tag{2.68}$$

For a given σ, K, and a_s, Eq. (2.68) provides two or four real nontrivial roots for c, which in turn provide two or four approximate nonlinear normal modes. Variations of c with K for four values of σ are shown in Fig. 2.2. Comparing Figs. 2.1 and 2.2 shows that the parameter σ destroys the pitchfork bifurcation, which exists at $\sigma = 0$. The two approximate normal modes remain neutrally stable as K increases from

zero. When K exceeds a critical value, two global branches of solutions emerge: one branch being unstable and another branch being neutrally stable. For a dissipative system, the saddle-node bifurcation point, where the stable and unstable nontrivial constant solutions coalesce, corresponds to a vertical tangent. However, for the conservative system under consideration, the saddle-center point, where the unstable and neutrally stable constant solutions meet, is on the upper branch and near the left end or a vertical tangent of the curve. The saddle-center point moves away from the left end point of vertical tangencies as $|\sigma|$ increases. Moreover, the larger $|\sigma|$ is, the larger is the value of K at which the two additional modes appear.

In Fig. 2.3, we show variation of c with σ/a_s^2 for two values of K. When K = 3, there are only two normal modes, which are neutrally stable. When K = 5, there are two solutions when $\sigma > 0.564$ and $\sigma < -0.175$ and four solutions when $-0.175 < \sigma < 0.564$.

(ii) $\sin\gamma \neq 0$ and $\cos\gamma = 0$

It follows from Eqs. (2.55)-(2.57) that

$$a_s^2 = -\frac{f_{rrs}}{3f_{rs}}\,a_r^2 \tag{2.69}$$

$$a_r^2 = \frac{8\omega_r\omega_s f_{ssr}\sigma}{f_{ssr}(3\omega_s f_{rr} - \omega_r f_{srs}) + 3f_{sr}(3\omega_r f_{ss} - \omega_s f_{rsr})} \tag{2.70}$$

where the f_{mij} must satisfy the following constraints:

$$\begin{aligned} &f_{rrs}f_{rs} < 0, \quad f_{sr}f_{ssr} < 0, \quad 9f_{sr}f_{rs} = f_{ssr}f_{rrs} \\ &\sigma f_{ssr}[f_{ssr}(3\omega_s f_{rr} - \omega_r f_{srs}) + 3f_{sr}(3\omega_r f_{ss} - \omega_s f_{rsr})] > 0 \end{aligned} \tag{2.71}$$

The stability of the nontrivial constant solutions can be determined by investigating the eigenvalues of the corresponding Jacobian matrix. For example, for the case $\sin\gamma = 1$, $\omega_s \approx \omega_r = 1$, the eigenvalues of the Jacobian matrix are given by

$$\lambda^3 + \Gamma_1\lambda + \Gamma_2 = 0 \tag{2.72}$$

where

$$\Gamma_1 = -\frac{1}{16}\left[(f_{rrs} - f_{ssr})^2 + 2f_{rsr}f_{srs} - 3f_{rsr}f_{rr} - 3f_{srs}f_{ss}\right]a_r^2 a_s^2 \tag{2.73}$$

$$\Gamma_2 = \frac{1}{8}(3f_{rsr}f_{sr} - f_{srs}f_{rrs})a_s a_r^3 \sigma \tag{2.74}$$

Then, according to the Routh-Hurwitz criterion, the solution is unstable if either $\Gamma_2 \neq 0$ or $\Gamma_2 = 0$ and $\Gamma_1 < 0$ and neutrally stable if $\Gamma_2 = 0$ and $\Gamma_1 \geq 0$.

One case for $\Gamma_2 = 0$ is shown in Fig. 2.4. Unlike the previous cases, once the given f_{mij} satisfy the constraints (2.71) and one of the quantities a_r^2, a_s^2, and σ is specified, the other two quantities are uniquely determined.

(iii) $\sin\gamma \neq 0$ and $\cos\gamma \neq 0$

It follows from Eqs. (2.55)-(2.57) that

$$a_s^2 = \alpha_1 a_r^2 \tag{2.75}$$

$$a_r^2 = \frac{8\sigma}{\alpha_2 - \alpha_1\alpha_3} \tag{2.76}$$

$$\cos\gamma = \pm\frac{f_{rrs} + 3f_{rs}\alpha_1}{2f_{rsr}\sqrt{\alpha_1}} \tag{2.77}$$

provided that

$$-1 < \cos\gamma < 1, \quad \cos\gamma \neq 0,$$
$$\alpha_1 > 0 \quad \text{and} \quad \sigma(\alpha_2 - \alpha_1\alpha_3) > 0 \tag{2.78}$$

where

$$\alpha_1 = \frac{f_{srs}f_{rrs} - 3f_{rsr}f_{sr}}{f_{rsr}f_{ssr} - 3f_{srs}f_{rs}} \tag{2.79}$$

$$\alpha_2 = \frac{3f_{rr}}{\omega_r} + \frac{3f_{sr}f_{ssr}}{\omega_s f_{srs}} - \frac{f_{srs}}{\omega_s} - \frac{f_{rrs}^2}{\omega_r f_{rsr}} \tag{2.80}$$

$$\alpha_3 = \frac{3f_{ss}}{\omega_s} + \frac{3f_{rs}f_{rrs}}{\omega_r f_{rsr}} - \frac{f_{rsr}}{\omega_r} - \frac{f_{ssr}^2}{\omega_s f_{srs}} \tag{2.81}$$

Their stability can be determined as in the previous case.

(b) Three-to-One Internal Resonance ($\omega_s \approx 3\omega_r$). Substituting Eq. (2.46b) into Eqs. (2.38) and (2.43), letting $\omega_s = 3\omega_r + \varepsilon\sigma$, and separating the result into real and imaginary parts, we obtain the modulation equations

$$\dot{a}_r = -\frac{\varepsilon f_{rrs}}{8\omega_r} a_s a_r^2 \sin\gamma \tag{2.82}$$

$$\dot{a}_s = \frac{\varepsilon f_{sr}}{8\omega_s} a_r^3 \sin\gamma \tag{2.83}$$

$$a_r\dot{\beta}_r = \frac{\varepsilon}{8\omega_r}\left(3f_{rr}a_r^3 + 2f_{rsr}a_s^2 a_r + f_{rrs}a_s a_r^2 \cos\gamma\right) \tag{2.84}$$

$$a_s\dot{\beta}_s = \frac{\varepsilon}{8\omega_s}\left(3f_{ss}a_s^3 + 2f_{srs}a_r^2 a_s + f_{sr}a_r^3 \cos\gamma\right) \tag{2.85}$$

where

$$\gamma = \beta_s - 3\beta_r + \varepsilon\sigma t \tag{2.86}$$

Differentiating Eq. (2.86) with respect to t and using Eqs. (2.84) and (2.85), we obtain

$$\begin{aligned} a_r a_s \dot{\gamma} = a_r a_s \varepsilon\sigma &+ \frac{\varepsilon a_r}{8\omega_s}\left(3f_{ss}a_s^3 + 2f_{srs}a_r^2 a_s + f_{sr}a_r^3 \cos\gamma\right) \\ &- \frac{3\varepsilon a_s}{8\omega_r}\left(3f_{rr}a_r^3 + 2f_{rsr}a_s^2 a_r + f_{rrs}a_s a_r^2 \cos\gamma\right) \end{aligned} \tag{2.87}$$

Moreover, to the first approximation,

$$\begin{aligned} u_r &= \varepsilon^{1/2} a_r \cos(\omega_r t + \beta_r) + \ldots \\ u_s &= \varepsilon^{1/2} a_s \cos(3\omega_r t + 3\beta_r + \gamma) + \ldots \end{aligned} \tag{2.88}$$

It follows from Eqs. (2.88) that periodic solutions correspond to $\dot{a}_r = \dot{a}_s = 0$ and $\dot{\gamma} = 0$. Then, it follows from Eqs. (2.82) and (2.83) that the nontrivial constant solutions correspond to

$$\sin\gamma = 0 \quad \text{or} \quad \gamma = n\pi, \quad n = 0,1,2,\ldots \tag{2.89}$$

Next, we consider the special expressions for f_{mij} defined in Eqs. (2.59) with $\omega_r = 1$ and $\omega_s \approx 3\omega_r$. For a constant γ, Eq. (2.87) becomes

$$(\cos n\pi)a_r^3 + (27K + 21)a_s a_r^2 - (27\cos n\pi)a_s^2 a_r - \left[3(K - 17)a_s^3 + 24\sigma a_s\right] = 0 \tag{2.90}$$

For a given σ, n, and a_s, Eq. (2.90) yields one or three real roots. Substituting these roots into Eqs. (2.88) and recalling that $\gamma = n\pi$, we obtain

$$u_r = \varepsilon^{1/2} a_r \cos(t + \beta_r) + \ldots \tag{2.91}$$

$$u_s = \pm\varepsilon^{1/2} a_s\left[4\cos^3(t + \beta_r) - 3\cos(t + \beta_r)\right] + \ldots \tag{2.92}$$

or

$$u_s \approx \pm \frac{a_s}{a_r}\left(\frac{4}{\varepsilon a_r^2}u_r^3 - 3u_r\right) + \ldots \tag{2.93}$$

Therefore, the system possesses one or three approximate nonsimilar normal modes given by Eq. (2.93) when $\omega_s \approx 3\omega_r$. The stability of these modes can be determined by studying the stability of the corresponding fixed points of Eqs. (2.82), (2.83), and (2.87). In Figs. 2.5(a) and 2.5(b), we show the variation of a_r with K and σ, respectively.

2.1.4 Summary

The complex-valued invariant-manifold approach is used to construct the nonlinear normal modes of an N-degree-of-freedom system for the cases of one-to-one and three-to-one internal resonances. The dynamics of the modes are governed by four-dimensional autonomous systems of equations. The method of normal forms is used to simplify the dynamics on the invariant manifolds. The simplified equations are used to calculate the normal modes and investigate their bifurcations. In both cases, the number of nonlinear normal modes may exceed the number of linear normal modes, in contrast with the case of no internal resonance, where they are equal.

2.2 Nonlinear Normal Modes of a Cantilever Beam

In nondimensional form, the equation and boundary conditions governing planar motion of a metallic cantilever beam are given by (Crespo da Silva and Glynn, 1978)

$$\ddot{w} + w^{IV} + N[w(x,t)] = 0 \tag{2.94}$$

$$w = w' = 0 \quad \text{at } x = 0 \quad \text{and} \quad w'' = w''' = 0 \quad \text{at } x = 1 \tag{2.95}$$

where

$$N[w(x,t)] = \left[w' \left(w' w'' \right)' \right]' + \left[w' \int_1^x \int_0^x \left(\dot{w}'^2 + w' \ddot{w}' \right) dx\, dx \right]' \tag{2.96}$$

The overdot and prime indicate differentiation with respect to time t and the distance along the beam x, respectively; x and the transverse displacement w are nondimensionalized by the beam length L^* and the time is nondimensionalized by the characteristic time $L^{*2}\sqrt{\rho^* A^* / E^* I^*}$, where $E^* I^*$ is the rigidity of the beam, ρ^* is the beam density per unit length, and A^* is the beam cross-section area.

Hsieh, Shaw, and Pierre (1993) used the methodology of Shaw and Pierre (1993b) to treat the continuous system defined by Eqs. (2.94)-(2.96) as such. To this end, they defined the normal mode of this system as a two-dimensional invariant manifold that passes through a stable equilibrium point $(w, \dot{w}) = (0,0)$ of the system and is tangent to an eigenspace of the system linearized about this equilibrium. They chose the

displacement w_0 and velocity $\dot{w}_0$ at a particular point $x = x_0$ of the beam to describe the manifold and hence define the invariant manifold as

$$w(x,t) = W(w_o(t), \dot{w}_0(t), x, x_0)$$

$$\dot{w}(x,t) = \dot{W}(w_0(t), \dot{w}_0(t), x, x_0)$$

These geometric constraints are used to eliminate the explicit time dependence in Eq. (2.94) and the resulting spatial equations are solved asymptotically. Hsieh, Shaw, and Pierre (1993) pointed out that the selection of the reference point x_0 makes the procedure somewhat cumbersome. To overcome this shortcoming, Shaw and Pierre (1993b) modified the continuous approach by first discretizing the system by using the Galerkin procedure.

2.2.1 Treatment of the Discretized System

The linear mode shapes of Eqs. (2.94) and (2.95) with $N \equiv 0$ are given by

$$\phi_m(x) = \cosh z_m x - \cos z_m x + \beta(\sin z_m x - \sinh z_m x) \tag{2.97}$$

where

$$\beta = \frac{\cos z_m + \cosh z_m}{\sin z_m + \sinh z_m}, \tag{2.98}$$

the z_m are the roots of

$$1 + \cos z \cosh z = 0, \tag{2.99}$$

and the linear natural frequencies ω_m are given by z_m^2.

Since the boundary-value problem is self-adjoint, the eigenfunctions $\phi_m(x)$ corresponding to different eigenvalues ω_m are orthogonal. We define the inner product between $\phi_m(x)$ and $\phi_n(x)$ by

$$< \phi_m(x), \phi_n(x) > = \int_0^1 \phi_m(\tau)\phi_n(\tau)\, d\tau, \tag{2.100}$$

which becomes the Kronecker delta δ_{mn}; moreover,

$$< \phi_m^{iv}(x), \phi_n(x) > = \omega_m^2 \delta_{mn} \tag{2.101}$$

In discretizing the continuous problem, we approximate w(x,t) by an infinite series of linear eigenfunctions of the form

$$w(x,t) = \sum_{m=1}^{\infty} \phi_m(x) q_m(t) \tag{2.102}$$

Substituting Eq. (2.102) into Eq. (2.94) and taking the inner product of the resulting equation with $\phi_j(x)$, we have

$$\ddot{q}_j + \omega_j^2 q_j + G_j(q, \dot{q}, \ddot{q}) = 0 \quad \text{for } j = 1,2, \ldots \tag{2.103}$$

where

$$G_j(q, \dot{q}, \ddot{q}) = < \phi_j(x), N\left[\sum_{m=1}^{\infty} \phi_m(x) q_m(t), \sum_{m=1}^{\infty} \phi_m(x) \dot{q}_m(t), \sum_{m=1}^{\infty} \phi_m(x) \ddot{q}_m(t) \right] > \tag{2.104}$$

At this point, any of a variety of methods, including the normal-mode-manifold method in terms of real or complex variables and perturbation methods, can be used to construct the nonlinear modes. Nayfeh and Nayfeh (1993a) compare these methods and apply them to a system of the form of Eq. (2.103). They found that the methods yield equivalent results. For the procedural details, the reader is referred to Nayfeh and Nayfeh (1993a).

For the case of combined cubic geometric and inertial nonlinearities as indicated in Eq. (2.96), Eqs. (2.103) and (2.104) can be used to express the nonlinearity as

$$G_j(q_k, \dot{q}_k) = (g_{1jk} - \omega_k^2 g_{2jk}) q_k^3 + g_{2jk} q_k \dot{q}_k^2 + \cdots \tag{2.105}$$

where

$$g_{1jk} = < \phi_j(x),\ N_1(\phi_k(x)) > \tag{2.106}$$

$$g_{2jk} = < \phi_j(x),\ N_2(\phi_k(x)) > \tag{2.107}$$

$$N_1(\phi_k(x)) = \left[\phi_k' \left(\phi_k' \phi_k'' \right)' \right]' \tag{2.108}$$

$$N_2(\phi_k(x)) = \left(\phi_k' \int_1^x \int_0^x \phi_k'^2 \, dx \, dx \right)' \tag{2.109}$$

As shown in Nayfeh and Nayfeh (1993a), the kth nonlinear mode obtained by treatment of the discretized system can be written as

$$w_k(x,t) = \phi_k(x) q_k(t) + \sum_{j \neq k} \phi_j(x) \left[\Gamma_{1jk} q_k^3(t) + \Gamma_{2jk} q_k(t) \dot{q}_k^2(t) \right] + \cdots \tag{2.110}$$

where

$$\Gamma_{1jk} = \frac{1}{\Delta}\left[(7\omega_k^2 - \omega_j^2)g_{1jk} - (5\omega_k^2 - \omega_j^2)\omega_k^2 g_{2jk}\right] \tag{2.111}$$

$$\Gamma_{2jk} = \frac{1}{\Delta}\left[6g_{1jk} - (3\omega_k^2 + \omega_j^2)g_{2jk}\right] \tag{2.112}$$

$$\Delta = (\omega_k^2 - \omega_j^2)(9\omega_k^2 - \omega_j^2) \tag{2.113}$$

When $\omega_j \approx \omega_k$ (one-to-one internal resonance) or $\omega_j \approx 3\omega_k$ (three-to-one internal resonance), $\Delta = 0$ and this construction of the nonlinear mode breaks down. Hence, we assume ω_j is away from ω_k or $3\omega_k$. In addition to the kth linear mode, the summation in Eq. (2.110) captures the contributions of all other linear modes to the kth nonlinear mode. The modal motion is written in terms of $q_k(t)$, which is given by

$$q_k(t) = a_k \cos(\omega_{Nk}t + \beta_{k0}) + \frac{g_{1kk} - 2\omega_k^2 g_{2kk}}{32\omega_k^2} a_k^3 \cos(3\omega_{Nk}t + 3\beta_{k0}) + \cdots \tag{2.114}$$

where

$$\omega_{Nk} = \omega_k + \frac{1}{8\omega_k}(3g_{1kk} - 2\omega_k^2 g_{2kk})a_k^2 + \cdots, \tag{2.115}$$

which is the nonlinear natural frequency of the kth mode. Depending on the initial conditions, a_k and β_{k0} are constants which represent, respectively, first approximations to the amplitude and phase of the motion.

2.2.2 Direct Approach

In this section, we determine the nonlinear mode shapes and natural frequencies by applying the method of multiple scales directly to the governing partial-differential system, given by Eqs. (2.94)-(2.96). First, we introduce a small dimensionless parameter ε as a bookkeeping device and rewrite Eq. (2.94) as

$$\ddot{w} + w^{iv} + \varepsilon N[w(x,t)] = 0 \tag{2.116}$$

We seek a first-order uniform expansion in the form

$$w(x,t;\varepsilon) = w_0(x, T_0, T_1) + \varepsilon w_1(x, T_0, T_1) + \cdots \tag{2.117}$$

where $T_0 = t$ is a fast scale, characterizing motions occurring at one of the natural frequencies ω_k of the system, and $T_1 = \varepsilon t$ is a slow scale, characterizing the shift in the natural frequencies due to the nonlinearity. In terms of the T_n, the time derivative becomes

$$\frac{d}{dt} = D_0 + \varepsilon D_1 + \cdots \tag{2.118}$$

where $D_n = \partial/\partial T_n$. Substituting Eqs. (2.117) and (2.118) into Eqs. (2.116) and (2.95) and equating coefficients of like powers of ε, we obtain

Order ε^0

$$D_0^2 w_0 + w_0^{iv} = 0 \tag{2.119a}$$

$$w_0 = w_0' = 0 \quad \text{at } x = 0 \quad \text{and} \quad w_0'' = w_0''' = 0 \quad \text{at } x = 1 \tag{2.119b}$$

Order ε

$$D_0^2 w_1 + w_1^{iv} = -2D_0 D_1 w_0 - N(w_0, D_0 w_0, D_0^2 w_0) \tag{2.120a}$$

$$w_1 = w_1' = 0 \quad \text{at } x = 0 \quad \text{and} \quad w_1'' = w_1''' = 0 \quad \text{at } x = 1 \tag{2.120b}$$

To construct the nonlinear mode that reduces to the kth mode as the nonlinearity vanishes, we write the solution of Eqs. (2.119) as

$$w_0 = \phi_k(x)\left[A_k(T_1)e^{i\omega_k T_0} + \bar{A}_k(T_1)e^{-i\omega_k T_0}\right] \tag{2.121}$$

where the function A_k is to be determined by imposing the solvability condition at the next level of approximation.

Substituting Eq. (2.121) into Eq. (2.120a) and using Eqs. (2.96), (2.108), and (2.109), we obtain

$$\begin{aligned} D_0^2 w_1 + w_1^{iv} = & -2i\omega_k \phi_k(x)\left(A_k' e^{i\omega_k T_0} - \bar{A}_k' e^{-i\omega_k T_0}\right) \\ & - \left[N_1(\phi_k(x)) - \omega_k^2 N_2(\phi_k(x))\right]\left(A_k e^{i\omega_k T_0} + \bar{A}_k e^{-i\omega_k T_0}\right)^3 \\ & + \omega_k^2 N_2(\phi_k(x))\left(A_k e^{i\omega_k T_0} - \bar{A}_k e^{-i\omega_k T_0}\right)^2\left(A_k e^{i\omega_k T_0} + \bar{A}_k e^{-i\omega_k T_0}\right) \end{aligned} \tag{2.122}$$

Because the homogeneous part of Eqs. (2.122) and (2.120b) has a nontrivial solution, namely that given by Eq. (2.121), the inhomogeneous Eqs. (2.122) and (2.120b) have a solution only if a solvability condition is satisfied. This solvability condition demands that the right-hand sides of Eqs. (2.122) and (2.120b) be orthogonal to every solution of the homogeneous problem. For the case of no internal resonance, the solvability condition demands that

$$2i\omega_k A_k' + \left(3g_{1kk} - 2\omega_k^2 g_{2kk}\right)A_k^2 \bar{A}_k = 0 \tag{2.123}$$

where g_{1kk} and g_{2kk} are defined in Eqs. (2.106) and (2.107) for $j = k$, respectively. The amplitude and phase of the kth modal motion are governed by the modulation equation (2.123), which is in agreement with that obtained by attacking the discretized problem.

Using Eq. (2.123), we rewrite Eq. (2.122) as

$$D_0^2 w_1 + w_1^{iv} = (2\omega_k^2 g_{2kk} - g_{1kk})\phi_k(x)A_k^3 e^{3i\omega_k T_0} - f_1(x)A_k^3 e^{3i\omega_k T_0} - f_2(x)A_k^2\bar{A}_k e^{i\omega_k T_0} + cc \tag{2.124}$$

where

$$f_1(x) = N_1(\phi_k(x)) - 2\omega_k^2 N_2(\phi_k(x)) - (g_{1kk} - 2\omega_k^2 g_{2kk})\phi_k(x) \tag{2.125}$$

$$f_2(x) = 3N_1(\phi_k(x)) - 2\omega_k^2 N_2(\phi_k(x)) - (3g_{1kk} - 2\omega_k^2 g_{2kk})\phi_k(x) \tag{2.126}$$

Using separation of variables, we can express the solution of Eqs. (2.124) and (2.120b) as

$$w_1 = \frac{g_{1kk} - 2\omega_k^2 g_{2kk}}{8\omega_k^2}\phi_k(x)A_k^3 e^{3i\omega_k T_0} + h_1(x)A_k^3 e^{3i\omega_k T_0} + h_2(x)A_k^2\bar{A}_k e^{i\omega_k T_0} + cc \tag{2.127}$$

where $h_1(x)$ and $h_2(x)$ are solutions of the two two-point boundary-value problems

$$h_1^{iv} - 9\omega_k^2 h_1 = -f_1(x) \tag{2.128a}$$

$$h_1 = h_1' = 0 \quad \text{at } x = 0 \quad \text{and} \quad h_1'' = h_1''' = 0 \quad \text{at } x = 1 \tag{2.128b}$$

$$h_2^{iv} - \omega_k^2 h_2 = -f_2(x) \tag{2.129a}$$

$$h_2 = h_2' = 0 \quad \text{at } x = 0 \quad \text{and} \quad h_2'' = h_2''' = 0 \quad \text{at } x = 1 \tag{2.129b}$$

Equations (2.128) and (2.129) can be solved either numerically or analytically.

To compare the results presented in this section with those obtained in the preceding section, we replace A_k by the polar form

$$A_k = \frac{1}{2} a_k e^{i\beta_k} \tag{2.130}$$

in Eq. (2.123), separate real and imaginary parts, and obtain

$$a_k' = 0 \tag{2.131}$$

$$a_k \beta_k' = \frac{1}{8\omega_k} (3g_{1kk} - 2\omega_k^2 g_{2kk}) a_k^3 \tag{2.132}$$

Therefore, a_k is a constant and

$$\beta_k = \frac{3g_{1kk} - 2\omega_k^2 g_{2kk}}{8\omega_k} a_k^2 \varepsilon t + \beta_{k0} \tag{2.133}$$

where β_{k0} is a constant. Substituting Eqs. (2.121) and (2.127) into Eq. (2.117) and using Eqs. (2.130), (2.133), and (2.114), we obtain

$$w_k(x,t) = \phi_k(x) q_k(t) + \frac{1}{4} \varepsilon a_k^3 [h_1(x) \cos(3\omega_{Nk} t + 3\beta_{k0}) + h_2(x) \cos(\omega_{Nk} t + \beta_{k0})] + \cdots \tag{2.134}$$

We note that, to the first approximation,

$$a_k^3 \cos(\omega_{Nk} t + \beta_{k0}) = q_k^3 + \frac{\dot{q}_k^2 q_k}{\omega_k^2} \tag{2.135}$$

$$a_k^3 \cos(3\omega_{Nk}t + 3\beta_{k0}) = q_k^3 - \frac{3\dot{q}_k^2 q_k}{\omega_k^2} \tag{2.136}$$

Because ε is a bookkeeping device, we set it equal to unity and use Eqs. (2.135) and (2.136) to rewrite Eq. (2.134) as

$$w_k(x,t) = \phi_k(x)q_k(t) + \frac{1}{4}\left[(h_1(x) + h_2(x))q_k^3 + \frac{1}{\omega_k^2}(h_2(x) - 3h_1(x))\dot{q}_k^2 q_k\right] + \cdots \tag{2.137}$$

The spatial dependence of the correction to the linear mode shape is given by $h_1(x)$ and $h_2(x)$, which are the solutions of Eqs. (2.128) and (2.129). Solving Eqs. (2.128) and (2.129) by expanding $f_i(x)$ in terms of the $\phi_m(x)$ and substituting these solutions into Eq. (2.137), we obtain Eq. (2.110). Thus, discretization of Eqs. (2.128) and (2.129) is equivalent to discretization of the original problem.

Using Eqs. (2.108) and (2.109), we analytically solve for N_1 and N_2 and obtain

$$N_1(x) = z_k^4 \phi_k \phi_k'^2 + \phi_k''^3 + 4\phi_k' \phi_k'' \phi_k''' \tag{2.138}$$

$$N_2(x) = \phi_k'' \Lambda + \phi_k' \Lambda' \tag{2.139}$$

where

$$\begin{aligned}\Lambda(x) &= \int_1^x \int_0^x \phi_k'^2 \, dx \, dx \\ &= \frac{1}{4}\{\cosh^2 z_k x + \cos^2 z_k x - 4\cos z_k x \cosh z_k x - 6 \\ &\quad - \beta[\sinh 2z_k x + \sin 2z_k x - 4\sin z_k x \cosh z_k x - 4\cos z_k x \sinh z_k x + 4z_k(x-1)] \\ &\quad + \beta^2[\cosh^2 z_k x - \cos^2 z_k x - 4\sin z_k x \sinh z_k x + 2z_k^2(x^2-1)]\}\end{aligned} \tag{2.140}$$

and $\phi_k(x)$, β, and z_k are defined in Eqs. (2.97)-(2.99). We note that the boundary conditions require that $h_1 = h_2 = 0$ at $x = 0$.

Substituting Eqs. (2.138)-(2.140) into Eqs. (2.106) and (2.107) and carrying out the integration numerically, we calculate g_{1kk} and g_{2kk}. Using these values and those of N_1 and N_2, we calculate $f_1(x)$ and $f_2(x)$ from Eqs. (2.125) and (2.126). As an example for the first nonlinear mode, the $f_i(x)$ are plotted in Fig. 2.6. Having calculated $f_1(x)$ and $f_2(x)$, we solve Eqs. (2.128) and (2.129) for $h_1(x)$ and $h_2(x)$ numerically by using a Runge-Kutta scheme. Substituting for $h_1(x)$ and $h_2(x)$ in Eq. (2.137), we determine the deflection of the beam at any instant of time.

The results are plotted in Fig. 2.7. At any instant t^* when $\dot{q}_k(t^*) = 0$, we obtain the mode shape

$$W_k(x) = \phi_k(x)q_k^* + \frac{1}{4}(h_1(x) + h_2(x))q_k^{*3} + \cdots \tag{2.141}$$

where $q_k(t^*) = q_k^*$ is the maximum and $\dot{w}(x, t^*) = 0$. For a given q_k^*, which depends on the initial conditions, we compare the nonlinear mode shapes with the linear ones in Figs. 2.8 for the lowest three modes. As q_k^* exceeds a certain value q_{kc}^*, the correction terms in Eq. (2.141) due to the weakly nonlinearity qualitatively change the linear mode shape. Hence, the construction of the nonlinear normal mode breaks down. Moreover, the higher frequency the normal mode has, the lower value the q_{kc}^* has.

2.2.3 Summary

To construct the nonlinear normal modes of a cantilever beam, we present and compare two different approaches. First, we discretize the problem using a complete

set of basis functions that satisfy the boundary conditions, namely, the linear mode shapes. Then, the nonlinear modes are constructed by the method of multiple scales or an invariant-manifold approach. Then, the method of multiple scales is applied directly to the nonlinear partial-differential equation and boundary conditions. The nonlinear modes obtained with the direct approach are the same as those obtained by discretization.

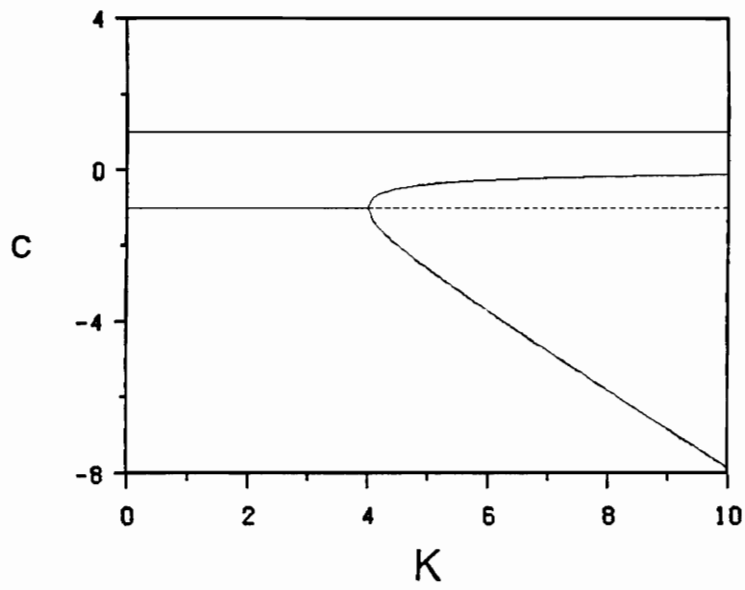

Figure 2.1. Variation of c with K for $\sigma = 0$, $\gamma = 2n\pi$, n = 0,1,2,... (one-to-one internal resonance); ___, neutrally stable solution; ---, unstable solution.

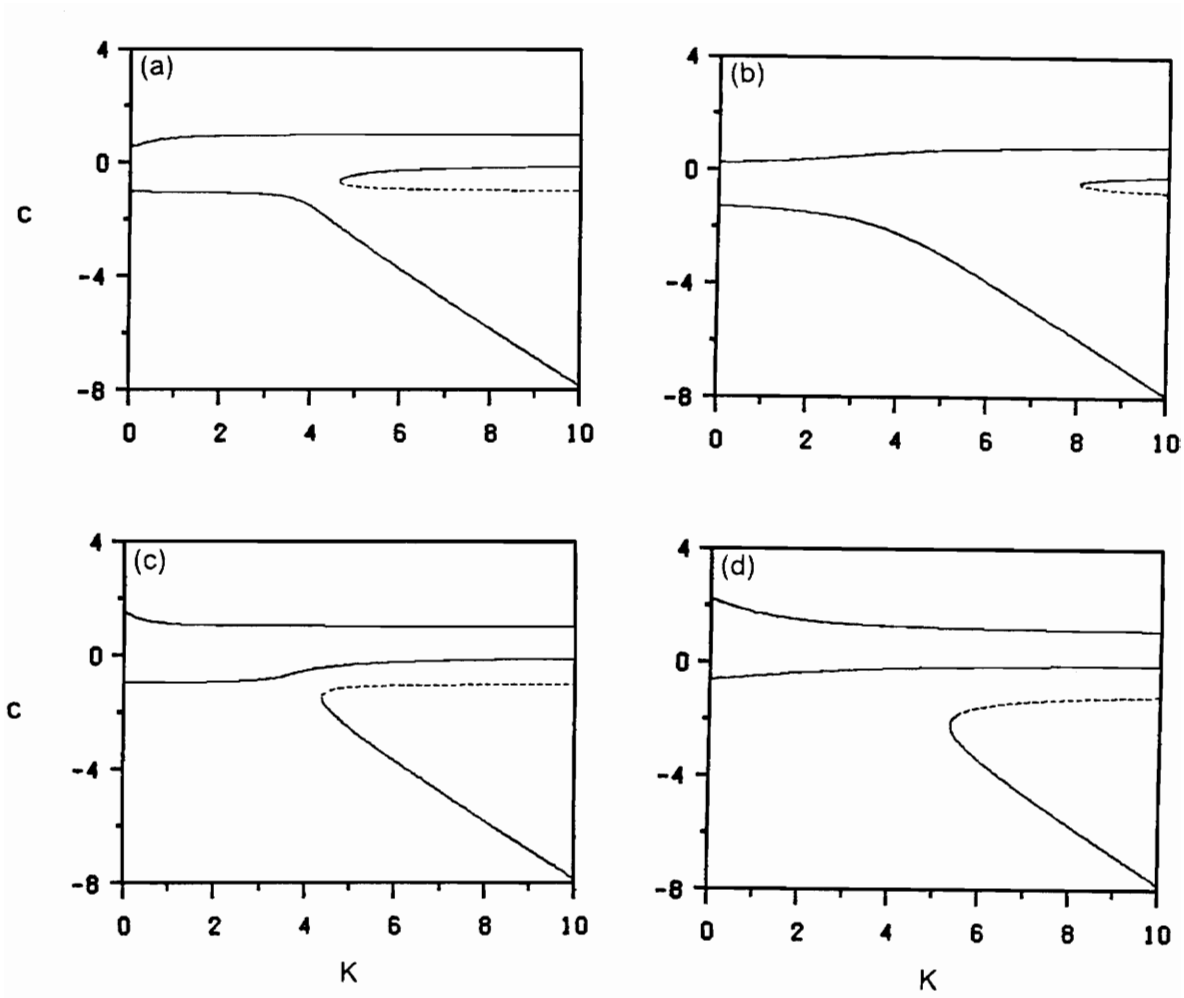

Figure 2.2. Variation of c with K for $\sigma \neq 0$, $a_s = 1$, $\gamma = 2n\pi$, $n = 0,1,2,...$ (one-to-one internal resonance), (a) $\sigma = -0.1$; (b) $\sigma = -1$; (c) $\sigma = 0.1$; (d) $\sigma = 1$; ___, neutrally stable solution; ---, unstable solution.

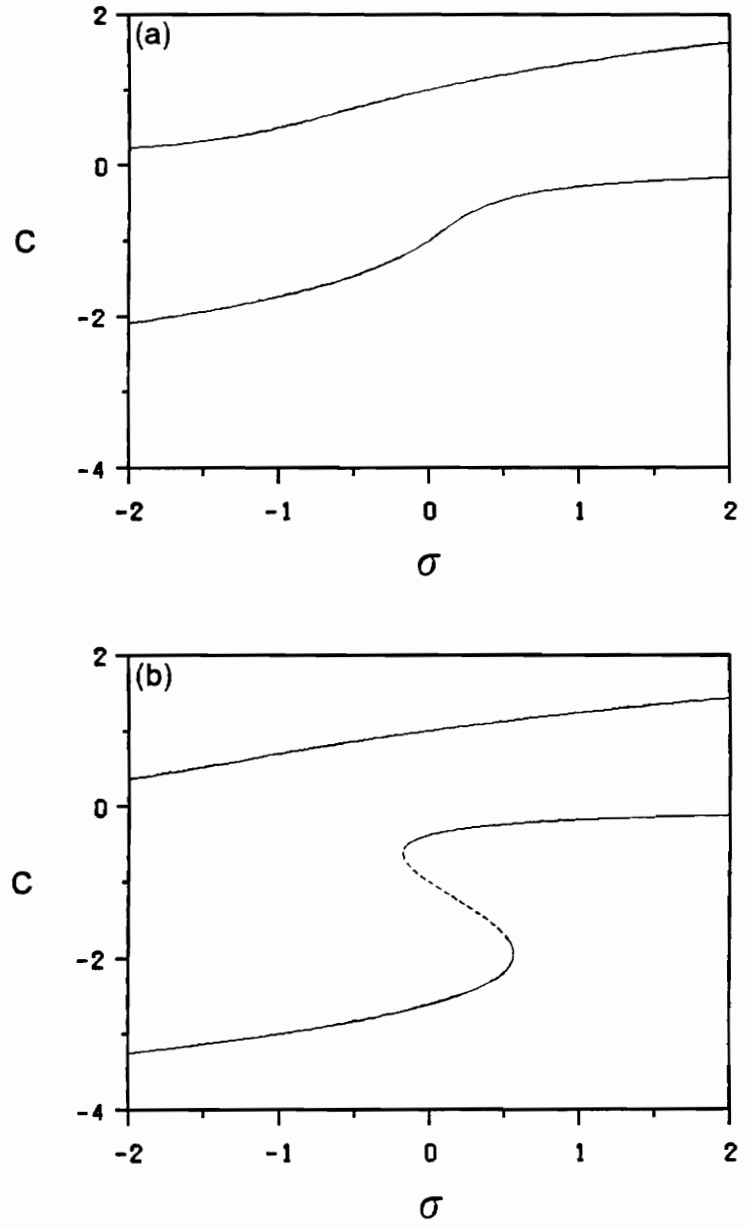

Figure 2.3. Variation of c with σ/a_s^2 for $a_s = 1$, $\gamma = 2n\pi$, $n = 0,1,2,...$ (one-to-one internal resonance), (a) $K = 3$; (b) $K = 5$; ___, neutrally stable solution; ---, unstable solution.

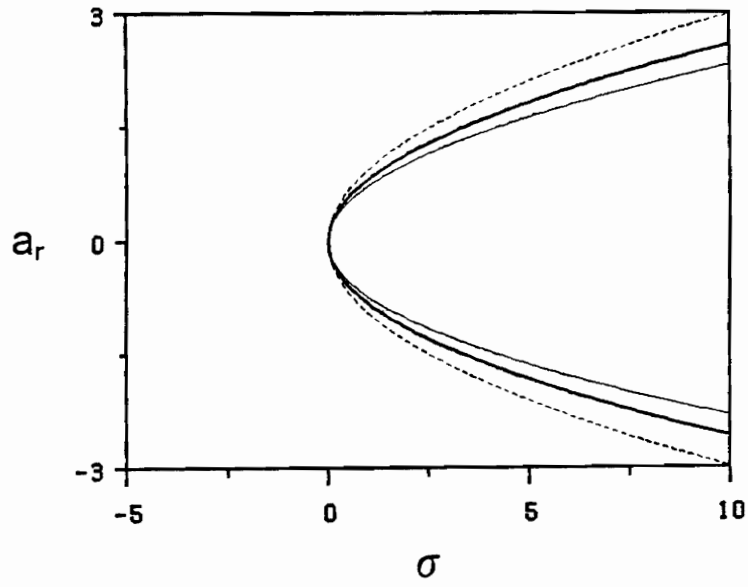

Figure 2.4. Variation of a_r with σ for the case of one-to-one internal resonance: $\gamma = (2n + 1/2)\pi$, $n = 0,1,2,...$, $f_{rrs} = 3$, $f_{rsr} = 3$, $f_{rs} = -1$, $f_{sr} = 1$, $f_{srs} = 3$, $f_{ssr} = -3$, $f_{ss} = 1$. In this case, $a_s = a_r$: ---, unstable solution ($f_{rr} = 4$, $\Gamma_1 < 0$); ___, neutrally stable solution ($f_{rr} = 5$, $\Gamma_1 = 0$); ___, neutrally stable solution ($f_{rr} = 6$, $\Gamma_1 > 0$).

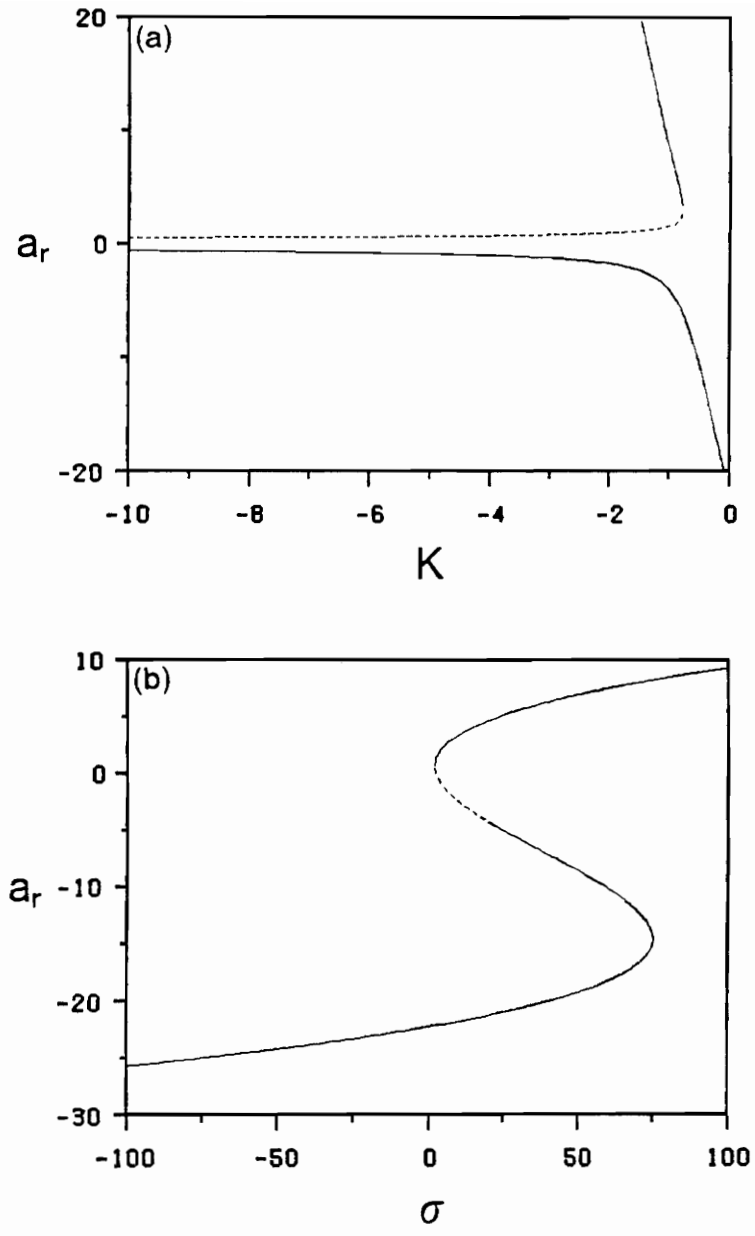

Figure 2.5. The nonlinear normal modes for the case of three-to-one internal resonance: (a) variation of a_r with K for $\sigma = 0$ and $a_s = 1$; (b) variation of a_r with σ for $K = 0$ and $a_s = 1$; $\gamma = 2n\pi$, $n = 0,1,2,...$, ___, neutrally stable solution; ---, unstable solution.

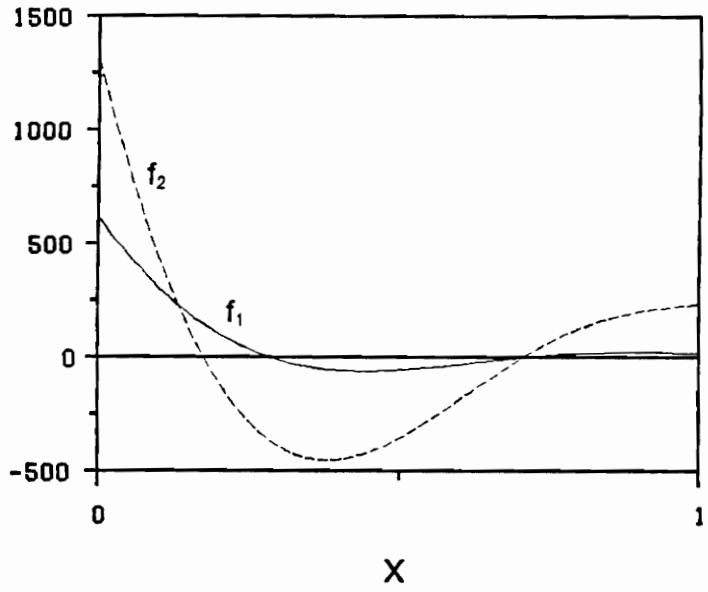

Figure 2.6. f_1 and f_2 as functions of x for the first nonlinear mode; the linear natural frequency $\omega_1 = 3.5160$, $g_{1kk} = 40.4407$, and $g_{2kk} = 4.5968$.

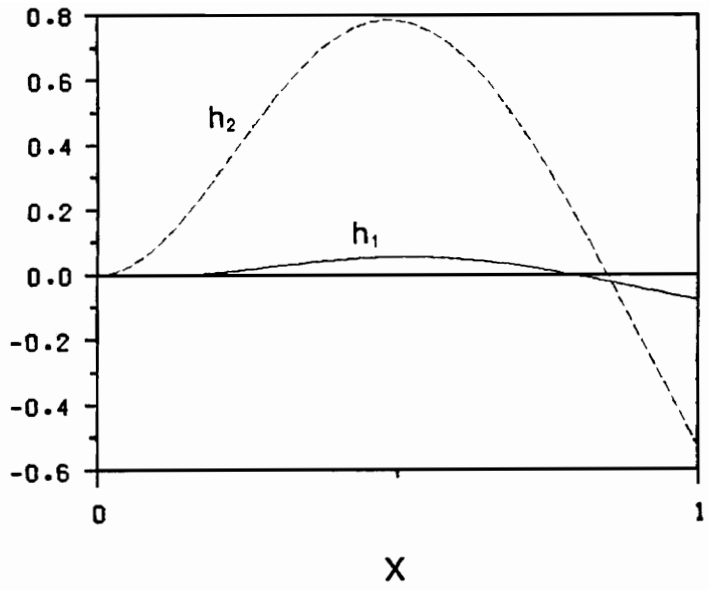

Figure 2.7. h_1 and h_2 as functions of x for the first nonlinear mode; these results include homogeneous solutions as well as particular solutions.

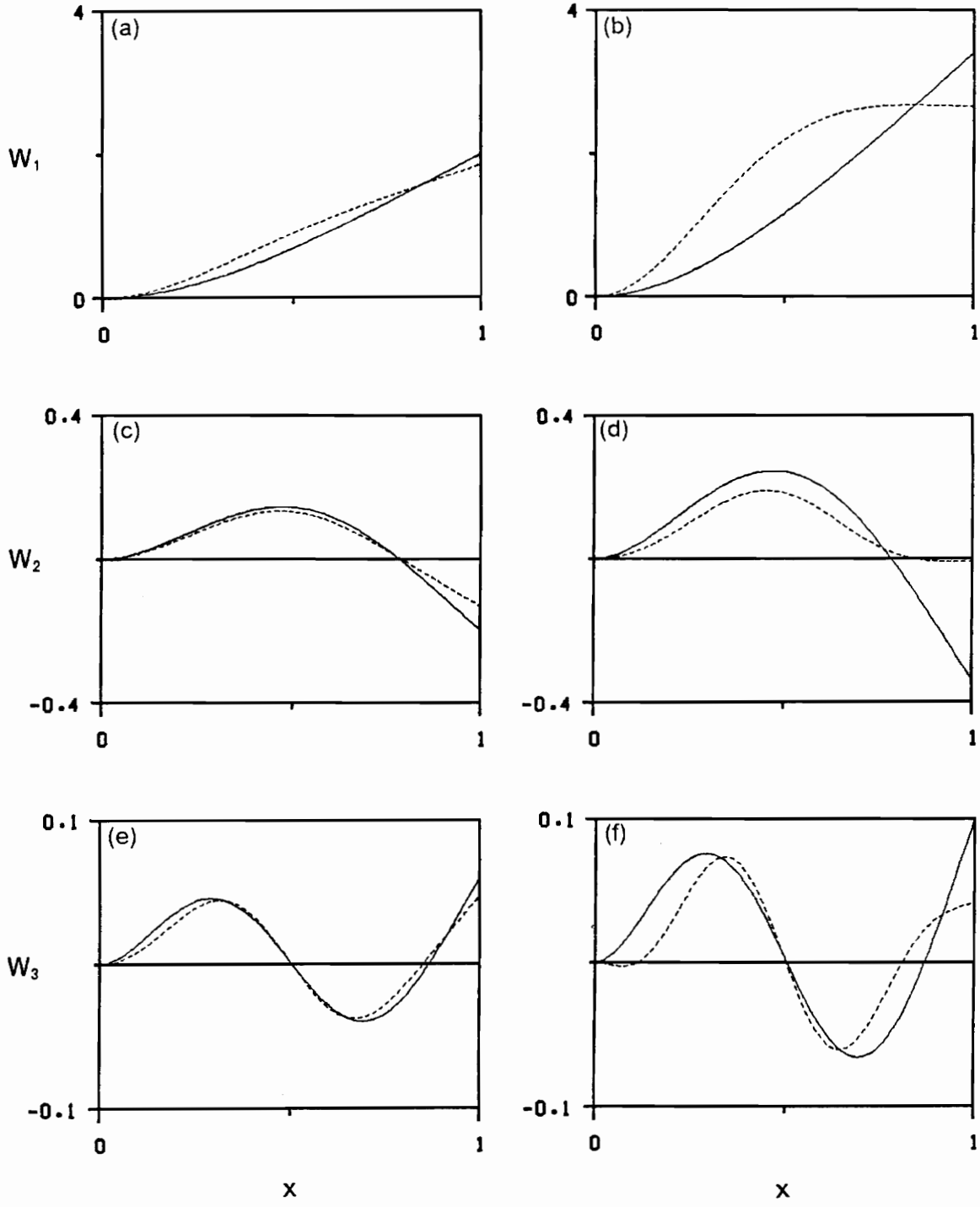

Figure 2.8. The comparison of linear (—) and nonlinear (---) mode shapes for the first mode (a) $q_1^* = 1.0$ and (b) $q_1^* = 1.7$; the second mode (c) $q_2^* = 0.10$ and (d) $q_2^* = 0.17$; the third mode (e) $q_3^* = 0.03$ and (f) $q_3^* = 0.05$.

CHAPTER 3

SYSTEMS WITH REPEATED NATURAL FREQUENCIES

The nonlinear response of multi-degree-of-freedom systems with repeated natural frequencies and cubic nonlinearity to various parametric resonances are studied in Sections 3.1-3.3. The linear part of the system has a nonsemisimple one-to-one internal resonance. These analyses are applied to the flutter of an isotropic simply supported panel in a supersonic airstream. The character of the stability and various types of bifurcation are analyzed. For the case of combination parametric resonance, the numerical results indicate the existence of Hopf, cyclic-fold, and period-doubling bifurcations; chaotic responses; and different types of static bifurcations. In Section 3.4, the influence of quadratic nonlinearities is investigated. The method of multiple scales is used to derive four first-order differential equations governing the modulation of the amplitudes and phases of the two modes for the cases of fundamental and principal parametric resonances.

Bifurcation analysis of the case of fundamental parametric resonance reveals that more complicated dynamics, such as period-doubling sequences leading to chaos, can be induced by these quadratic terms. The effects of quadratic nonlinearities for the case of principal parametric resonance are discussed.

3.1 Principal Parametric Resonance

3.1.1 Equation of Motion

The equations of motion for the aeroelasticity of plates and shells are well established (Dowell, 1975; Dowell and Ilgamov, 1988). The motion of a panel under a harmonic in-plane load in a supersonic airstream is governed by the following equation (Dowell, 1975):

$$D\frac{\partial^4 w}{\partial x^4} - (N_x^E + N_x)\frac{\partial^2 w}{\partial x^2} + \rho_m h\frac{\partial^2 w}{\partial t^2} + \mu_m\frac{\partial w}{\partial t} = -\frac{\rho_\infty U_\infty^2}{M_\infty}\left(\frac{\partial w}{\partial x} + \frac{1}{U_\infty}\frac{\partial w}{\partial t}\right) \quad (3.1)$$

where

$$N_x = \frac{Eh}{2l}\int_0^l \left(\frac{\partial w}{\partial \xi}\right)^2 d\xi \quad (3.2)$$

is the tension due to the bending-induced stretching of the panel, D is the flexural rigidity, w is the transverse deflection, x is the streamwise spatial coordinate, N_x^E is

the in-plane harmonic loading, E is the modulus of elasticity, h is the panel thickness, l is the panel length, and ρ_m and μ_m are the material density and damping, respectively. On the right-hand side of Eq. (3.1), piston theory is used to approximate the supersonic aerodynamic loads on the panel, where ρ_∞, U_∞, and M_∞ are the density, speed, and Mach number in the freestream.

Equation (3.1) can be rewritten in the following dimensionless form (* denotes dimensionless quantities):

$$\frac{\partial^4 w^*}{\partial x^{*4}} + \frac{\partial^2 w^*}{\partial t^{*2}} + \lambda^* \frac{\partial w^*}{\partial x^*} = \left[R_x^* + \alpha^* \int_0^2 \left(\frac{\partial w^*}{\partial \xi^*} \right)^2 d\xi^* \right] \frac{\partial^2 w^*}{\partial x^{*2}} - 2\mu^* \frac{\partial w^*}{\partial t^*}, \quad (3.3)$$

where

$$w^* = (l/h^2)w, \quad x^* = (2/l)x, \quad t^* = [4D^{1/2}/l^2(\rho_m h)^{1/2}]t,$$
$$\lambda^* = \rho_\infty U_\infty^2 l^3/8M_\infty D, \quad R_x^* = N_x^E l^2/4D = F\cos\Omega^* t^*,$$
$$\alpha^* = Eh^5/4l^2 D, \quad 2\mu^* = (l^2/4(\rho_m h D)^{1/2})(\mu_m + \rho_\infty U_\infty/M_\infty)$$

Following the Galerkin procedure, Tezak et al. (1982) expressed the deflection as an expansion in terms of the linear free-vibration modes and obtained a system of ordinary differential equations for the time-dependent coefficients (also called modal amplitudes) in this expansion. For flutter, two natural frequencies coalesce and the corresponding modal amplitudes are governed by equations having the following form:

$$\ddot{u}_1 + u_1 + 2\tilde{\mu}_1\dot{u}_1 + \tilde{\Lambda}_{11}u_1 + \tilde{\Lambda}_{12}u_2 + (2\cos\Omega\tau)(\tilde{f}_{11}u_1 + \tilde{f}_{12}u_2) + \tilde{\alpha}_{11}u_1^3 + \tilde{\alpha}_{12}u_1^2u_2 + \tilde{\alpha}_{13}u_1u_2^2 + \tilde{\alpha}_{14}u_2^3 = 0, \tag{3.4}$$

$$\ddot{u}_2 + u_1 + u_2 + 2\tilde{\mu}_2\dot{u}_2 + \tilde{\Lambda}_{21}u_1 + \tilde{\Lambda}_{22}u_2 + (2\cos\Omega\tau)(\tilde{f}_{21}u_1 + \tilde{f}_{22}u_2) + \tilde{\alpha}_{21}u_1^3 + \tilde{\alpha}_{22}u_1^2u_2 + \tilde{\alpha}_{23}u_1u_2^2 + \tilde{\alpha}_{24}u_2^3 = 0, \tag{3.5}$$

where $\tau = \omega^* t^*$ is the new independent variable; ω^* is the dimensionless natural frequency; the ratio Ω of the excitation frequency to the natural frequency is close to 2; the $\tilde{\Lambda}_{ij} = (\lambda^* - \lambda_c^*)C_{ij}$ are the aerodynamic detuning parameters; the C_{ij} are constants; λ_c^* is the critical value that causes two natural frequencies to merge and flutter to ensue; and the $\tilde{\mu}_i$, $\tilde{f}_{ij}$, and $\tilde{\alpha}_{ik}$ are constants related to the damping, in-plane loading, and nonlinear terms in Eq. (3.1), respectively. The case of a one-to-one internal resonance and a principal parametric excitation are studied.

It was shown that the remaining modal amplitudes decay.

Tezak, et al. (1982) used the method of multiple scales to obtain an approximate solution to Eqs. (3.4) and (3.5). One can obtain the same results by the method of normal forms, as we demonstrate in this section.

3.1.2 Scaling

Due to the nonsemisimple structure of the linear undamped operator, u_2 is much larger than u_1. Hence, introducing ε as a bookkeeping device, one assumes that

$$u_1 = \varepsilon v_1, \quad u_2 = \varepsilon^{1-\delta_1} v_2, \quad \tilde{\mu}_i = \varepsilon^{\delta_2}\mu_i, \quad \tilde{\Lambda}_{ij} = \varepsilon^{\delta_3}\Lambda_{ij}, \quad \tilde{f}_{ij} = \varepsilon^{\delta_4} f_{ij}, \quad \tilde{\alpha}_{ik} = \varepsilon^{\delta_5}\alpha_{ik}, \tag{3.6}$$

for $i = 1,2$, $j = 1,2$, $k = 1,2,3,4$, where the δ_m are unspecified (for the present) positive constants. Substituting Eq. (3.6) into Eqs. (3.4) and (3.5) yields

$$\begin{aligned}\ddot{v}_1 + v_1 + \varepsilon^{\delta_2}2\mu_1\dot{v}_1 + \varepsilon^{\delta_3}(\Lambda_{11}v_1 + \varepsilon^{-\delta_1}\Lambda_{12}v_2) + (2\cos\Omega\tau)\varepsilon^{\delta_4}(f_{11}v_1 + \varepsilon^{-\delta_1}f_{12}v_2) \\ + \varepsilon^{\delta_5+2}\left(\alpha_{11}v_1^3 + \varepsilon^{-\delta_1}\alpha_{12}v_1^2v_2 + \varepsilon^{-2\delta_1}\alpha_{13}v_1v_2^2 + \varepsilon^{-3\delta_1}\alpha_{14}v_2^3\right) = 0,\end{aligned} \tag{3.7}$$

$$\begin{aligned}\ddot{v}_2 + \varepsilon^{\delta_1}v_1 + v_2 + \varepsilon^{\delta_2}2\mu_2\dot{v}_2 + \varepsilon^{\delta_3}(\varepsilon^{\delta_1}\Lambda_{21}v_1 + \Lambda_{22}v_2) + (2\cos\Omega\tau)\varepsilon^{\delta_4}(\varepsilon^{\delta_1}f_{21}v_1 + f_{22}v_2) \\ + \varepsilon^{\delta_5+2}\left(\varepsilon^{\delta_1}\alpha_{21}v_1^3 + \alpha_{22}v_1^2v_2 + \varepsilon^{-\delta_1}\alpha_{23}v_1v_2^2 + \varepsilon^{-2\delta_1}\alpha_{24}v_2^3\right) = 0.\end{aligned} \tag{3.8}$$

Keeping the dominant terms only, we have

$$\ddot{v}_1 + v_1 + \varepsilon^{\delta_2}2\mu_1\dot{v}_1 + \varepsilon^{\delta_3-\delta_1}\Lambda_{12}v_2 + \varepsilon^{\delta_4-\delta_1}(2\cos\Omega\tau)f_{12}v_2 + \varepsilon^{\delta_5+2-3\delta_1}\alpha_{14}v_2^3 + \ldots = 0, \tag{3.9}$$

$$\ddot{v}_2 + \varepsilon^{\delta_1}v_1 + v_2 + \varepsilon^{\delta_2}2\mu_2\dot{v}_2 + \ldots = 0. \tag{3.10}$$

To bring the effects of the damping, aerodynamic loading, parametric resonance, and nonlinearity into the first approximation, we let

$$\delta_2 = \delta_3 - \delta_1 = \delta_4 - \delta_1 = \delta_5 + 2 - 3\delta_1 = \delta_1. \tag{3.11}$$

Hence, for an arbitrary δ_1, say 1,

$$\delta_2 = 1, \quad \delta_3 = 2, \quad \delta_4 = 2, \quad \text{and} \quad \delta_5 = 2, \tag{3.12}$$

and the scaled equations (3.9) and (3.10) become

$$\ddot{v}_1 + v_1 + 2\varepsilon\mu_1\dot{v}_1 + \varepsilon\Lambda_{12}v_2 + \varepsilon(2\cos\Omega\tau)f_{12}v_2 + \varepsilon\alpha_{14}v_2^3 + \ldots = 0, \tag{3.13}$$

$$\ddot{v}_2 + \varepsilon v_1 + v_2 + 2\varepsilon\mu_2\dot{v}_2 + \ldots = 0. \tag{3.14}$$

3.1.3 Method of Normal Forms

To simplify Eqs. (3.13) and (3.14) we use the method of normal forms (Nayfeh, 1993) and recast them in complex-valued form using the following transformation:

$$v_j = \eta_j + \bar{\eta}_j, \quad \dot{v}_j = i(\eta_j - \bar{\eta}_j), \quad j = 1,2 \tag{3.15}$$

where $\bar{\eta}_j$ is the complex conjugate of η_j. Hence, solving for η_j and $\bar{\eta}_j$, one obtains

$$\eta_j = \frac{1}{2}(v_j - i\dot{v}_j) \quad \text{and} \quad \bar{\eta}_j = \frac{1}{2}(\bar{v}_j + i\dot{\bar{v}}_j). \tag{3.16}$$

Differentiating the first of Eqs. (3.16) with respect to τ and using Eqs. (3.13)-(3.15) yields

$$\begin{aligned}\dot{\eta}_1 = i\eta_1 + \varepsilon\frac{i}{2}\big[&i2\mu_1(\eta_1 - \bar{\eta}_1) + \Lambda_{12}(\eta_2 + \bar{\eta}_2) \\ &+ f_{12}(z + \bar{z})(\eta_2 + \bar{\eta}_2) + \alpha_{14}(\eta_2 + \bar{\eta}_2)^3\big] + \ldots\end{aligned} \tag{3.17}$$

$$\dot{\eta}_2 = i\eta_2 + \varepsilon\frac{i}{2}\big[\eta_1 + \bar{\eta}_1 + i2\mu_2(\eta_2 - \bar{\eta}_2)\big] + \ldots \tag{3.18}$$

where $z = e^{i\Omega\tau}$.

To determine an approximation to the solution of Eqs. (3.17) and (3.18) by using the method of normal forms, we introduce the near-identity transformation

$$\eta_j = \xi_j + \varepsilon h_j(\xi_m, \bar{\xi}_m, z, \bar{z}) + \ldots, \qquad m = 1,2 \text{ for each } j = 1,2 \tag{3.19}$$

into Eqs. (3.17) and (3.18) and choose the h_j so that the resulting equations take the simplest possible form, the so-called normal form,

$$\dot{\xi}_j = i\xi_j + \varepsilon g_j(\xi_m, \bar{\xi}_m, z, \bar{z}) + \ldots, \qquad m = 1,2 \text{ for each } j = 1,2 \tag{3.20}$$

where the g_j consist of the resonance and near-resonance terms. Substituting Eqs. (3.19) and (3.20) into Eq. (3.17) and equating the coefficients of ε on both sides, we obtain

$$\begin{aligned} &g_1 + i\left(\frac{\partial h_1}{\partial \xi_1}\xi_1 - \frac{\partial h_1}{\partial \bar{\xi}_1}\bar{\xi}_1 + \frac{\partial h_1}{\partial \xi_2}\xi_2 - \frac{\partial h_1}{\partial \bar{\xi}_2}\bar{\xi}_2\right) + i\Omega\left(\frac{\partial h_1}{\partial z}z - \frac{\partial h_1}{\partial \bar{z}}\bar{z}\right) \\ &= ih_1 - \mu_1(\xi_1 - \bar{\xi}_1) + \frac{i}{2}\left[\Lambda_{12}(\xi_2 + \bar{\xi}_2) + f_{12}(z + \bar{z})(\xi_2 + \bar{\xi}_2) + \alpha_{14}(\xi_2 + \bar{\xi}_2)^3\right]. \end{aligned} \tag{3.21}$$

Choosing h_1 to eliminate the nonresonance terms in Eq. (3.21) leaves g_1 with the resonance and near-resonance terms; that is,

$$g_1 = -\mu_1\xi_1 + \frac{i}{2}(\Lambda_{12}\xi_2 + 3\alpha_{14}\xi_2{}^2\bar{\xi}_2 + f_{12}z\bar{\xi}_2) \tag{3.22}$$

The term proportional to $z\bar{\xi}_2$ is a near-resonance term because $\Omega \approx 2$ and the rest of the terms on the right-hand side of Eq. (3.22) are resonance terms. Substituting Eqs. (3.19) and (3.20) into Eq. (3.18), equating the coefficients of ε on both sides, and choosing h_2 to eliminate the nonresonance terms, we find that

$$g_2 = -\mu_2\xi_2 + \frac{i}{2}\xi_1. \tag{3.23}$$

Substituting Eqs. (3.22) and (3.23) into Eq. (3.20) and introducing a slow time scale $T_1 = \varepsilon\tau$ yields the normal form

$$\xi_1' = \frac{1}{\varepsilon}i\xi_1 - \mu_1\xi_1 + \frac{i}{2}(\Lambda_{12}\xi_2 + 3\alpha_{14}\xi_2^2\bar{\xi}_2 + f_{12}z\bar{\xi}_2) \tag{3.24}$$

$$\xi_2' = \frac{1}{\varepsilon} i\xi_2 - \mu_2\xi_2 + \frac{i}{2}\xi_1 \tag{3.25}$$

where $(\,)' = \dfrac{\partial(\,)}{\partial T_1}$.

Next, we introduce a detuning parameter σ defined by

$$\Omega = 2 + \varepsilon\sigma \tag{3.26}$$

where $\varepsilon\sigma$ is small compared with 1. Moreover, we express the ξ_j in the polar form

$$\xi_j = \frac{1}{2} a_j e^{i(\tau + \beta_j)} \tag{3.27}$$

recall that $z = \exp(i\Omega\tau)$, separate Eqs. (3.24) and (3.25) into real and imaginary parts, and obtain

$$a_1' = -\mu_1 a_1 - (\frac{1}{2}\Lambda_{12}a_2 + \frac{3}{8}\alpha_{14}a_2^3)\sin\gamma_1 - \frac{1}{2}f_{12}a_2\sin\gamma_2 \tag{3.28}$$

$$a_1\beta_1' = (\frac{1}{2}\Lambda_{12}a_2 + \frac{3}{8}\alpha_{14}a_2^3)\cos\gamma_1 + \frac{1}{2}f_{12}a_2\cos\gamma_2 \tag{3.29}$$

$$a_2' = -\mu_2 a_2 + \frac{1}{2}a_1\sin\gamma_1 \tag{3.30}$$

$$a_2\beta_2' = \frac{1}{2}a_1\cos\gamma_1 \tag{3.31}$$

where

$$\gamma_1 = \beta_2 - \beta_1 \text{ and } \gamma_2 = \sigma\tau - \beta_2 - \beta_1 \tag{3.32}$$

The equilibrium solutions of Eqs. (3.28)-(3.32) correspond to $a_j' = 0$ and $\gamma_j' = 0$. There are two possibilities:

(i) trivial solution: $a_1 = a_2 = 0$, (3.33)

(ii) nontrivial solution: $a_1 = a_2(\sigma^2 + 4\mu_2^2)^{1/2}$, (3.34)

$$a_2^2 = \frac{4}{3\alpha_{14}} \left\{ -\Lambda_{12} + \sigma^2 - 4\mu_1\mu_2 \pm [f_{12}^2 - 4\sigma^2(\mu_1 + \mu_2)^2]^{1/2} \right\}. \tag{3.35}$$

For nontrivial solutions, it follows from Eq. (3.35) that

$$f_{12} \geq 2|\sigma(\mu_1 + \mu_2)| \tag{3.36}$$

$$\alpha_{14}\left\{\Lambda_{12} + 4\mu_1\mu_2 - \sigma^2 - [f_{12}^2 - 4\sigma^2(\mu_1 + \mu_2)^2]^{1/2}\right\} \leq 0 \tag{3.37}$$

3.1.4 Stability of the Trivial Solution

Based on linear theory, the plate motion is unstable and the response grows exponentially with time if at least one of the eigenvalues has a positive real part. However, it is well known that, physically, the plate amplitude is limited by the nonlinear membrane forces induced by the plate motion (Lock and Fung, 1961; Dowell and Voss, 1965).

To determine the flutter boundaries for the linear problem, we use the Cartesian form

$$\xi_j = \frac{1}{2}(p_j - iq_j)e^{i(1 + \frac{1}{2}\varepsilon\sigma)\tau}, \quad j = 1,2 \tag{3.38}$$

to transform the nonautonomous system (3.24) and (3.25) into the four-dimensional autonomous system

$$\underline{x}' = L\underline{x} + \underline{N}(\underline{x}) \tag{3.39}$$

where

$$\underline{x} = \begin{bmatrix} p_1 \\ q_1 \\ p_2 \\ q_2 \end{bmatrix}, \quad \underline{N} = \frac{3}{8}\alpha_{14}(p_2^2 + q_2^2)\begin{bmatrix} q_2 \\ -p_2 \\ 0 \\ 0 \end{bmatrix}, \tag{3.40}$$

and

$$L = \frac{1}{2}\begin{bmatrix} -2\mu_1 & -\sigma & 0 & \Lambda_{12} - f_{12} \\ \sigma & -2\mu_1 & -\Lambda_{12} - f_{12} & 0 \\ 0 & 1 & -2\mu_2 & -\sigma \\ -1 & 0 & \sigma & -2\mu_2 \end{bmatrix}. \tag{3.41}$$

The eigenvalues λ of the matrix L satisfy the characteristic equation

$$\lambda^4 + r_1\lambda^3 + r_2\lambda^2 + r_3\lambda + r_4 = 0 \tag{3.42}$$

where

$$r_1 = 2(\mu_1 + \mu_2) \tag{3.43a}$$

$$r_2 = \mu_1^2 + \mu_2^2 + 4\mu_1\mu_2 + \frac{1}{2}(\Lambda_{12} + \sigma^2) \tag{3.43b}$$

$$r_3 = (\mu_1 + \mu_2)\left(2\mu_1\mu_2 + \frac{1}{2}\Lambda_{12} + \frac{1}{2}\sigma^2\right) \tag{3.43c}$$

$$r_4 = \frac{1}{4}\sigma^2(\mu_1 + \mu_2)^2 + \left(\mu_1\mu_2 + \frac{1}{4}\Lambda_{12} - \frac{1}{4}\sigma^2\right)^2 - \frac{1}{16}f_{12}^2 \tag{3.43d}$$

According to the Routh-Hurwitz criterion, at least one root of Eq. (3.42) has a positive real part if the following conditions are not satisfied:

$$r_1 > 0, \qquad r_1 r_2 - r_3 > 0, \tag{3.44a,b}$$

$$r_3(r_1 r_2 - r_3) - r_1^2 r_4 > 0, \qquad r_4 > 0. \tag{3.44c,d}$$

The flutter boundaries separating stable and unstable regions for the case of a simply supported panel can then be constructed to form the bifurcation diagram, as shown in Fig. 3.1. Stable trivial solutions exist in regions I and II only. As a control parameter is varied, the trivial equilibrium solution can undergo various types of bifurcations. The qualitative dynamical behavior near these bifurcation curves can be analyzed by using a combination of center manifold theory and the method of normal forms. The case of Bogdanov-Takens bifurcation is described in Section 3.1.7.

(a) Static Bifurcations of the Trivial Solution. The P curve in Fig. 3.1 corresponds to the condition $r_4 = 0$, where r_4 is defined in Eq. (3.43d). Thus, along this bifurcation curve, the linear operator L has a zero eigenvalue. As F crosses the P curve directly from region I into region III at a fixed Λ, a supercritical pitchfork bifurcation occurs. It can be identified by the normal form

$$y' = \varepsilon_1(F - F_{cr})y + \alpha_1 y^3, \quad \varepsilon_1 > 0 \text{ and } \alpha_1 < 0 \tag{3.45}$$

where F_{cr} is the bifurcation value. If F crosses from region II into region III, a subcritical pitchfork bifurcation occurs. It can be identified by the normal form

$$y' = \varepsilon_2(F - F_{cr})y + \alpha_2 y^3, \quad \varepsilon_2 > 0 \text{ and } \alpha_2 > 0 \tag{3.46}$$

In the case of supercritical bifurcation, the stable trivial solution loses stability and gives way to a stable nontrivial constant solution (or periodic solution of the original system) that smoothly grows with F, as shown in Fig. 3.2(a), where $(\varepsilon_1, \alpha_1) = (0.0033, -0.001)$ when $(\Lambda, F_{cr}) = (-300, 332.92)$. In the case of subcritical bifurcation, the solution jumps from a trivial to a nontrivial value as F increases past the bifurcation value, as shown in Fig. 3.2(b), where $(\varepsilon_2, \alpha_2) = (0.0058, 0.0028)$ when $(\Lambda, F_{cr}) = (100, 346.79)$.

(b) Hopf Bifurcation of the Trivial Solution. The H curve in Fig. 3.1 corresponds to the condition $r_3(r_1r_2 - r_3) - r_1^2 r_4 = 0$, where the r_j are defined in Eqs. (3.43). The linear operator L has a pair of purely imaginary eigenvalues along this bifurcation curve. As Λ crosses the H curve from region I into region IV or from region II into region V at a fixed F, a supercritical Hopf bifurcation occurs. It can be identified by the normal form

$$r' = \varepsilon_3(\Lambda - \Lambda_{cr})r + \alpha_3 r^3, \quad \varepsilon_3 > 0 \ \textit{and} \ \alpha_3 < 0 \tag{3.47a}$$

$$\theta' = \omega + \alpha_4 r^2, \quad \omega^2 = r_3/r_1 \ \textit{and} \ \alpha_4 < 0 \tag{3.47b}$$

where Λ_{cr} is the bifurcation value. In Figs. 3.3(a,b), the variation of the amplitude of the second mode with the aerodynamic detuning for two values of the excitation amplitude is shown. When F = 200 and Λ is increased slowly, the stable trivial solution loses stability across the Hopf bifurcation curve at $\Lambda_{cr} \simeq 326.41$, where $(\varepsilon_3, \alpha_3) = (0.0026, -0.0475)$ and $(\omega, \alpha_4) = (1.423, -0.0053)$. The amplitude of the periodic solution of the modulation equations (or quasiperiodic solution of the original system) gradually grows with increasing Λ, as show in Figs. 3.3(a) and 3.4(c,d). In Fig. 3.3(b), when Λ is increased from a low value, the trivial solution loses stability at $\Lambda \approx -416$ and a stable nontrivial constant solution starts to grow as Λ continues to

increase. When $\Lambda \approx 118$, a second, unstable nontrivial constant solution is possible and the unstable trivial solution regains its stability. It remains stable until $\Lambda \approx 453$, where $(\varepsilon_3, \alpha_3) = (0.0032, -0.04)$ and $(\omega, \alpha_4) = (1.140, -0.0158)$, a supercritical Hopf bifurcation occurs, and a periodic solution emerges. In the region of multivalued stable solutions, the response depends on the initial conditions. Starting from a stable nontrivial constant solution at a large value of Λ and then gradually decreasing Λ, one finds that the amplitude of the nontrivial solution would decrease until a stable trivial solution is reached. Starting from a periodic solution at a large value of Λ and gradually decreasing Λ, one finds that the solution would go through a reverse Hopf bifurcation to a stable trivial solution. As Λ continues to decrease, a jump occurs at the reverse pitchfork bifurcation point. Hence the stable branch of nontrivial constant solutions becomes the only realizable solution until it hits the trivial solution as Λ decreases.

3.1.5 Stability of Nontrivial Solutions

The Jacobian matrix of the autonomous system defined by Eqs. (3.28)-(3.32) evaluated at the nontrivial fixed points can be expressed as

$$J = \begin{bmatrix} -\mu_1 & J_{12} & J_{13} & -\frac{1}{2} f_{12} a_2 \cos \gamma_2 \\ \frac{1}{2} \sin \gamma_1 & -\mu_2 & \frac{1}{2} a_1 \cos \gamma_1 & 0 \\ \frac{1}{a_2} \cos \gamma_1 & J_{32} & J_{33} & \frac{f_{12}}{2a_1} a_2 \sin \gamma_2 \\ \frac{\sigma}{a_1} - \frac{1}{a_2} \cos \gamma_1 & \frac{\sigma}{a_2} + J_{32} & \frac{a_1}{a_2} \sin \gamma_1 + J_{33} & \frac{f_{12}}{2a_1} a_2 \sin \gamma_2 \end{bmatrix}, \quad (3.48a)$$

where

$$J_{12} = -\frac{1}{2} (\Lambda_{12} + \frac{9}{4} \alpha_{14} a_2^2) \sin \gamma_1 - \frac{1}{2} f_{12} \sin \gamma_2 \quad (3.48b)$$

$$J_{13} = -\frac{1}{2} (\Lambda_{12} + \frac{3}{4} \alpha_{14} a_2^2) a_2 \cos \gamma_1 \quad (3.48c)$$

$$J_{32} = -\frac{1}{a_1} [(\Lambda_{12} + \frac{3}{2} \alpha_{14} a_2^2) \cos \gamma_1 + f_{12} \cos \gamma_2] \quad (3.48d)$$

$$J_{33} = \left(-\frac{a_1}{2a_2} + \frac{\Lambda_{12}}{2a_1} a_2 + \frac{3\alpha_{14}}{8a_1} a_2^3 \right) \sin \gamma_1 \quad (3.48e)$$

Hence, the stability of a nontrivial equilibrium solution depends on the real parts of the eigenvalues of the matrix J. If the real part of each eigenvalue is negative, the corresponding equilibrium solution is asymptotically stable. If the real part of at least one of the eigenvalues is positive, the corresponding equilibrium solution is unstable. In regions II and V of Fig. 3.1, there are two nontrivial constant solutions; one is stable and one is unstable. And in region III, there is one nontrivial constant solution, which is stable. If the equilibrium solution becomes nonhyperbolic, a similar bifurcation

analysis can be conducted near the nontrivial fixed point by using the center manifold theory and the method of normal forms. As F is decreased across the line S, where $F = F_{cr}$, between regions I (or IV) and II (or V) for a fixed Λ, one real eigenvalue becomes positive and a saddle-node bifurcation occurs; it can be identified by the normal form

$$y' = \varepsilon_4(F - F_{cr}) - y^2, \quad \varepsilon_4 > 0 \tag{3.49}$$

In Figs. 3.2(b)-(f), as F decreases past the bifurcation point, the stable nontrivial constant solution loses stability and jumps down either to a stable trivial solution or to a periodic solution. The unstable branch of nontrivial constant solutions is unrealizable in either numerical or physical experiments.

3.1.6 Stability of Periodic Solutions

Using Floquet theory to check the stability of the periodic solutions in regions IV and V, one finds that only stable periodic solutions exist in region IV, whereas stable periodic solutions and stable nontrivial constant solutions coexist in part of region V, as shown in Figs. 3.2(e,f) and 3.3. In the latter case, the response depends on the initial conditions. In Figs. 3.2(c,d) and 3.5, the mean value of the amplitude of the periodic solution decreases while its period increases as F increases, and eventually a reverse Hopf bifurcation produces a stable trivial solution. In Figs. 3.2(e,f), when Λ is either near the value where the Bogdanov-Takens bifurcation occurs or away from the Hopf-bifurcation curve, the mean value of the amplitude of the periodic solution first decreases with F, then starts to increase somewhere beneath the unstable branch of nontrivial constant solutions (saddles). At this point, the periodic

solution is stable in a sense that the corresponding Floquet multipliers lie within the unit circle. However, as shown in Fig. 3.5 for fixed values of Λ, the period of the limit cycle tends to infinity as F increases, suggesting the occurrence of a homoclinic orbit.

If a system has an orbit homoclinic to a saddle focus, which has one positive real eigenvalue λ_1, $\lambda_2 = \bar{\lambda}_3 = -\alpha + i\omega$, and Real$(-\lambda_i) > \alpha$ for i = 4,5,...,n, where α and ω are positive, Shilnikov (1970) showed that the system has a stable periodic orbit on one side of the homoclinic orbit and no recurrent behavior on the other if the eigenvalues of this saddle satisfy the inequality

$$\delta \equiv \alpha/\lambda_1 > 1, \tag{3.50}$$

which is the case in the current study.

The projections of the unstable manifolds of the saddle are shown in Fig. 3.6 for $\Lambda = 1000$. Before the homoclinicity condition is reached, the unstable manifold leads to a limit cycle in one direction and to a sink in the other, as shown in part (a) for $F = 330$. As F increases, the limit cycle grows and its period increases, as shown in Fig. 3.6(b) for $F = 335$. At $F = F_h \approx 340.853$, the periodic orbit passes through the saddle focus, forming the homoclinic orbit. The eigenvalues of the saddle focus are $\lambda_1 = 0.4656$, $\lambda_{2,3} = -1.2334 \pm 4.2036i$, and $\lambda_4 = -2.9324$. Hence, $\delta = 2.649 > 1$. Therefore, according to the Shilnikov theorem, when $F < F_h$, the system has a stable limit cycle, and when $F > F_h$ it has no recurrent behavior, explaining the results in Fig. 3.6.

In Fig. 3.7, when Λ increases from approximately 510.5 for $F = 400$, where a supercritical Hopf bifurcation occurs and a limit cycle is born, the period of the limit cycle increases and tends to infinity as $\Lambda \to \Lambda_h \approx 734.16$. In Fig. 3.8(a) for $\Lambda = 530$, the unstable manifold of the saddle leads to a limit cycle in one direction and to a sink in the other. As Λ increases further, the limit cycle grows and approaches the

homoclinic orbit, as shown in part (b) for $\Lambda = 630$ and part (c) for $\Lambda = 734.1614$, respectively. The eigenvalues of the saddle focus at $\Lambda = \Lambda_h$, where a homoclinic orbit occurs, are $\lambda_1 = 0.7262$, $\lambda_{2,3} = -1.2334 \pm 3.0807i$, and $\lambda_4 = -3.193$. Clearly, $\delta = 1.698 > 1$. Therefore, according to the Shilnikov theorem, the system has a stable limit cycle for $\Lambda < \Lambda_h$ and no recurrent behavior for $\Lambda > \Lambda_h$, again explaining the results in Fig. 3.8.

3.1.7 Bogdanov-Takens Bifurcation of the Trivial Solution

Analyzing a similar type of system, Namachchivaya and Malhotra (1992) observed an interesting phenomenon: a homoclinic bifurcation near the Bogdanov-Takens bifurcation point, which is the intersection of two codimension-one bifurcation varieties, the static bifurcation and the Hopf bifurcation. The corresponding linear operator has a double-zero eigenvalue.

For the case of a simply supported panel in a supersonic stream, the critical values $\Lambda_{cr} = 679.2$ and $F_{cr} = 519.6$ at point c_1 in Fig. 3.1 are obtained by satisfying the two conditions $r_3 = 0$ and $r_4 = 0$, where r_3 and r_4 are defined in (3.43c,d). The corresponding linear operator L_{cr} has the Jordan form

$$\hat{J} = P^{-1} L_{cr} P = \begin{bmatrix} 0 & 1 & 0 & 0 \\ 0 & 0 & 0 & 0 \\ 0 & 0 & -(\mu_1 + \mu_2) & 1 \\ 0 & 0 & 0 & -(\mu_1 + \mu_2) \end{bmatrix}. \tag{3.51}$$

Center manifold theory (Carr, 1981) can then be applied near this nonhyperbolic fixed point to reduce the fourth-order system to a second-order equation defined on a

two-dimensional center manifold. Substituting $\underline{x} = P\underline{y}$ into Eq. (3.39) and premultiplying by P^{-1} yields

$$\underline{y'} = \hat{J}\underline{y} + P^{-1}(L - L_{cr})P\underline{y} + P^{-1}\underline{N}(P\underline{y}). \tag{3.52}$$

The center manifold of the decoupled system has the form

$$y_3 = h_1(y_1, y_2, \Lambda, F) \tag{3.53a}$$

$$y_4 = h_2(y_1, y_2, \Lambda, F). \tag{3.53b}$$

Since the nonlinearities are cubic, this center manifold can be approximated by cubic functions. Therefore, the dynamics of the center manifold is governed by equations of the following form:

$$\begin{bmatrix} y_1' \\ y_2' \end{bmatrix} = J \begin{bmatrix} y_1 \\ y_2 \end{bmatrix} + E(\Lambda, F) \begin{bmatrix} y_1 \\ y_2 \end{bmatrix} + \tilde{\underline{N}}(y_1, y_2), \tag{3.54}$$

where

$$J = \begin{bmatrix} 0 & 1 \\ 0 & 0 \end{bmatrix}, \quad \tilde{\underline{N}} = \varepsilon \begin{bmatrix} \alpha_1 y_1^{\,3} + \alpha_2 y_1^{\,2} y_2 + \alpha_3 y_1 y_2^{\,2} + \alpha_4 y_2^{\,3} \\ \alpha_5 y_1^{\,3} + \alpha_6 y_1^{\,2} y_2 + \alpha_7 y_1 y_2^{\,2} + \alpha_8 y_2^{\,3} \end{bmatrix}, \tag{3.55}$$

and E is a 2x2 submatrix of $P^{-1}(L - L_{cr})P$. Letting

$$B = J + E = \begin{bmatrix} b_{11} & b_{12} \\ b_{21} & b_{22} \end{bmatrix}, \tag{3.56}$$

$$det\, B = b_{11}b_{22} - b_{21}b_{12}, \quad \text{and} \quad tr\, B = b_{11} + b_{22},$$

one can introduce the transformation

$$\begin{bmatrix} \eta_1 \\ \eta_2 \end{bmatrix} = \begin{bmatrix} 1 & 0 \\ b_{11} & b_{12} \end{bmatrix} \begin{bmatrix} y_1 \\ y_2 \end{bmatrix} \tag{3.57}$$

to transform Eq. (3.54) into the following form:

$$\begin{bmatrix} \eta_1' \\ \eta_2' \end{bmatrix} = \begin{bmatrix} 0 & 1 \\ -det\, B & tr\, B \end{bmatrix} \begin{bmatrix} \eta_1 \\ \eta_2 \end{bmatrix} + \underline{\tilde{N}}(\eta_1, \eta_2). \tag{3.58}$$

Again, one can use the method of normal forms to simplify Eq. (3.58).

For the time being, one can drop det (B) and tr (B) because they are sufficiently small. Then, we consider

$$\underline{\eta'} = J\,\underline{\eta} + \underline{\tilde{N}}(\underline{\eta}), \tag{3.59}$$

and introduce a near-identity transformation as well as the normal form

$$\underline{\eta} = \underline{\xi} + \varepsilon \underline{h}(\underline{\xi}) + \ldots\ , \tag{3.60a}$$

$$\underline{\xi'} = J\underline{\xi} + \varepsilon \underline{g}(\underline{\xi}) + \ldots\ . \tag{3.60b}$$

Substituting Eqs. (3.60) into (3.59) yields

$$\begin{bmatrix} g_1 \\ g_2 \end{bmatrix} + \begin{bmatrix} \dfrac{\partial h_1}{\partial \xi_1} & \dfrac{\partial h_1}{\partial \xi_2} \\ \dfrac{\partial h_2}{\partial \xi_1} & \dfrac{\partial h_2}{\partial \xi_2} \end{bmatrix} \begin{bmatrix} 0 & 1 \\ 0 & 0 \end{bmatrix} \begin{bmatrix} \xi_1 \\ \xi_2 \end{bmatrix} - \begin{bmatrix} 0 & 1 \\ 0 & 0 \end{bmatrix} \begin{bmatrix} h_1 \\ h_2 \end{bmatrix} = \begin{bmatrix} \alpha_1 \xi_1^{\,3} + \alpha_2 \xi_1^{\,2} \xi_2 + \alpha_3 \xi_1 \xi_2^{\,2} + \alpha_4 \xi_2^{\,3} \\ \alpha_5 \xi_1^{\,3} + \alpha_6 \xi_1^{\,2} \xi_2 + \alpha_7 \xi_1 \xi_2^{\,2} + \alpha_8 \xi_2^{\,3} \end{bmatrix}. \tag{3.61}$$

The form of the nonlinearity suggests seeking the g_i and h_i in the following forms:

$$h_1 = \Gamma_1 \xi_1^3 + \Gamma_2 \xi_1^2 \xi_2 + \Gamma_3 \xi_1 \xi_2^2 + \Gamma_4 \xi_2^3 \tag{3.62a}$$

$$h_2 = \Gamma_5 \xi_1^3 + \Gamma_6 \xi_1^2 \xi_2 + \Gamma_7 \xi_1 \xi_2^2 + \Gamma_8 \xi_2^3 \tag{3.62b}$$

$$g_1 = \Lambda_1 \xi_1^3 + \Lambda_2 \xi_1^2 \xi_2 + \Lambda_3 \xi_1 \xi_2^2 + \Lambda_4 \xi_2^3 \tag{3.62c}$$

$$g_2 = \Lambda_5 \xi_1^3 + \Lambda_6 \xi_1^2 \xi_2 + \Lambda_7 \xi_1 \xi_2^2 + \Lambda_8 \xi_2^3 \tag{3.62d}$$

Substituting Eq. (3.62) into Eq. (3.61) yields

$$\begin{aligned} &\Lambda_1 \xi_1^3 + \Lambda_2 \xi_1^2 \xi_2 + \Lambda_3 \xi_1 \xi_2^2 + \Lambda_4 \xi_2^3 + \xi_2 (3\Gamma_1 \xi_1^2 + 2\Gamma_2 \xi_1 \xi_2 + \Gamma_3 \xi_2^2) \\ &\quad - (\Gamma_5 \xi_1^3 + \Gamma_6 \xi_1^2 \xi_2 + \Gamma_7 \xi_1 \xi_2^2 + \Gamma_8 \xi_2^3) \\ &\quad = \alpha_1 \xi_1^3 + \alpha_2 \xi_1^2 \xi_2 + \alpha_3 \xi_1 \xi_2^2 + \alpha_4 \xi_2^3 \end{aligned} \tag{3.63}$$

$$\begin{aligned} &\Lambda_5 \xi_1^3 + \Lambda_6 \xi_1^2 \xi_2 + \Lambda_7 \xi_1 \xi_2^2 + \Lambda_8 \xi_2^3 + \xi_2 (3\Gamma_5 \xi_1^2 + 2\Gamma_6 \xi_1 \xi_2 + \Gamma_7 \xi_2^2) \\ &\quad = \alpha_5 \xi_1^3 + \alpha_6 \xi_1^2 \xi_2 + \alpha_7 \xi_1 \xi_2^2 + \alpha_8 \xi_2^3 \end{aligned} \tag{3.64}$$

Equating the coefficients of ξ_1^3, $\xi_1^2 \xi_2$, $\xi_1 \xi_2^2$, and ξ_2^3 on both sides of Eqs. (3.63) and (3.64), one has

$$C\underline{\Gamma} = \underline{\alpha} - \underline{\Lambda} \tag{3.65}$$

where

$$C = \begin{bmatrix} 0 & 0 & 0 & 0 & -1 & 0 & 0 & 0 \\ 3 & 0 & 0 & 0 & 0 & -1 & 0 & 0 \\ 0 & 2 & 0 & 0 & 0 & 0 & -1 & 0 \\ 0 & 0 & 1 & 0 & 0 & 0 & 0 & -1 \\ 0 & 0 & 0 & 0 & 0 & 0 & 0 & 0 \\ 0 & 0 & 0 & 0 & 3 & 0 & 0 & 0 \\ 0 & 0 & 0 & 0 & 0 & 2 & 0 & 0 \\ 0 & 0 & 0 & 0 & 0 & 0 & 1 & 0 \end{bmatrix}, \tag{3.66}$$

Here $\underline{\Gamma}$, $\underline{\alpha}$, and $\underline{\Lambda}$ are column vectors having the components Γ_m, α_m, and Λ_m, respectively.

Because C is a singular matrix, the system (3.65) has a solution if and only if $\underline{\alpha} - \underline{\Lambda}$ is orthogonal to every nontrivial solution $\underline{u}$ of the adjoint homogeneous problem; that is, $C^T\underline{u} = \underline{0}$. One then has

$$\underline{u} = (0,0,0,0,1,0,0,0)^T \quad \text{and} \quad (3,0,0,0,0,1,0,0)^T$$

and accordingly obtains

$$\Lambda_5 = \alpha_5 \tag{3.67a}$$

$$3\Lambda_1 + \Lambda_6 = 3\alpha_1 + \alpha_6 \tag{3.67b}$$

One can solve Eq. (3.65) for $\underline{\Gamma}$ for all values of the α_m, and hence Λ_k, $k = 2,3,4,7,$and 8 can be set equal to zero. If one has $\Lambda_1 = 0$ and accounts for the two unfolding parameters, $\beta_1 = -det\,(B)$ and $\beta_2 = tr\,(B)$, the corresponding truncated normal form of Eq. (3.58) can be expressed as

$$\xi_1' = \xi_2 \tag{3.68a}$$

$$\xi_2' = \beta_1\xi_1 + \beta_2\xi_2 + \gamma_1\xi_1^3 + \gamma_2\xi_1^2\xi_2. \tag{3.68b}$$

where

$$\beta_1 = -0.009(\Lambda - \Lambda_{cr}) + 0.023(F - F_{cr}) \tag{3.69a}$$

$$\beta_2 = 0.012(\Lambda - \Lambda_{cr}) - 0.019(F - F_{cr}) \tag{3.69b}$$

$$\gamma_1 = \varepsilon\alpha_5 = 0.028 \tag{3.69c}$$

$$\gamma_2 = \varepsilon(3\alpha_1 + \alpha_6) = -0.097. \tag{3.69d}$$

The global bifurcation behavior arising from this local codimension-two bifurcation is well known (Guckenheimer and Holmes,1983)

3.1.8 Summary

The nonlinear response of two-degree-of-freedom systems with one-to-one internal and principal parametric resonances is obtained by the method of normal forms. The same technique along with center manifold theory are used to analyze the bifurcation behavior near the nonhyperbolic fixed points. Since the stability of hyperbolic fixed points or periodic solutions can be studied by the corresponding eigenvalues or Floquet multipliers, respectively, one would then obtain a clearer picture of the dynamic behavior from the bifurcation diagram. In the case of a simply supported panel in a supersonic stream, qualitative changes can be predicted when

either the forcing amplitude or the aerodynamic pressure is varied across a bifurcation curve. It is shown that the trivial solutions can lose stability through three types of bifurcations: supercritical and subcritical pitchfork bifurcations, supercritical Hopf bifurcations, and Bogdanov-Takens bifurcations. The stability of the equilibrium and periodic solutions are investigated. The Shilnikov theorem is used to explain the numerical results obtained near the formation of an orbit homoclinic to a saddle-focus fixed point. A comparison between the numerical time integration of the modulation equations and the original governing equations is shown in Figs. 3.9-3.11. In Fig. 3.9, we show the effect of ε, which appears in the scaling process. Better agreement is reached when $\varepsilon = 0.01$, which is also used for the results obtained in Figs. 3.10 and 3.11. By introducing this ε, one can observe that u_2 is much larger than u_1, which is consistent with the inherent nonsemisimple structure of the system under investigation.

3.2 *Fundamental Parametric Resonance*

Considering the case $\Omega \approx 1$ and following an analysis similar to that described in the preceding section, one obtains, for the two modes whose natural frequencies coalesce, the following modulation equations:

$$A_1' = -\mu_1 A_1 + i\left[\left(\frac{1}{2}\Lambda_{12} + \phi_1\right)A_2 + \phi_2 \bar{A}_2 e^{i\sigma T_1} + \frac{3}{2}\alpha_{14} A_2^2 \bar{A}_2\right] \tag{3.70}$$

$$A_2' = -\mu_2 A_2 + \frac{1}{2} i A_1 \tag{3.71}$$

where

$$\phi_1 = \frac{5}{9} f_{12}^2 - \frac{1}{3} f_{12}(f_{11} + f_{22}), \tag{3.72}$$

$$\phi_2 = \frac{1}{2} f_{12}^2 - \frac{1}{2} f_{12}(f_{11} + f_{22}), \tag{3.73}$$

$( )' = \dfrac{\partial( )}{\partial T_1}$, $T_1 = \varepsilon\tau$, and $\Omega = 1 + \varepsilon\sigma$.

Comparing Eqs. (3.70)-(3.73) with Eqs. (3.24) and (3.25) by letting $\xi_j = A_j \exp(i\tau)$, one notes that there are only quantitative changes between these two cases, namely $\Omega \approx 1$ and $\Omega \approx 2$, for the system in the current study, which has cubic nonlinearities only. Once the quadratic nonlinearities are involved geometrically or inertially, dramatically qualitative changes would occur in the response of the system to the fundamental parametric excitation, as shown in Section 3.4.

3.3 Combination Parametric Resonance

We consider the nonlinear response of a three-degree-of-freedom system with a nonsemisimple one-to-one internal resonance to a combination parametric resonance. Specifically, we determine a second-order approximate solution of the following dimensionless equations:

$$\ddot{u}_1 + u_1 + 2\tilde{\mu}_1 \dot{u}_1 + \sum_{n=1}^{3} \tilde{\Lambda}_{1n} u_n + (2\cos\Omega t) \sum_{n=1}^{3} \tilde{f}_{1n} u_n + \sum_{n=1}^{3}\sum_{p=1}^{3}\sum_{q=1}^{3} \tilde{\Gamma}_{1npq} u_n u_p u_q = 0, \tag{3.74}$$

$$\ddot{u}_2 + u_1 + u_2 + 2\tilde{\mu}_2\dot{u}_2 + \sum_{n=1}^{3}\tilde{\Lambda}_{2n}u_n + (2\cos\Omega t)\sum_{n=1}^{3}\tilde{f}_{2n}u_n + \sum_{n=1}^{3}\sum_{p=1}^{3}\sum_{q=1}^{3}\tilde{\Gamma}_{2npq}u_n u_p u_q = 0, \quad (3.75)$$

$$\ddot{u}_3 + \omega_3^2 u_3 + 2\tilde{\mu}_3\dot{u}_3 + \sum_{n=1}^{3}\tilde{\Lambda}_{3n}u_n + (2\cos\Omega t)\sum_{n=1}^{3}\tilde{f}_{3n}u_n + \sum_{n=1}^{3}\sum_{p=1}^{3}\sum_{q=1}^{3}\tilde{\Gamma}_{3npq}u_n u_p u_q = 0, \quad (3.76)$$

when $\Omega \approx \omega_3 \pm 1$. In Eqs. (3.74)-(3.76) time was made dimensionless by using the natural frequency ω_1 of the first two modes. The $\tilde{\mu}_i$, $\tilde{\Lambda}_{in}$, $\tilde{f}_{in}$, and $\tilde{\Gamma}_{inpq}$ are constants related to the damping, aerodynamic detuning, in-plane loading, and nonlinearity due to the bending-induced stretching of the panel.

3.3.1 Analytical Solution

We use the method of multiple scales to determine a second-order approximate solution of Eqs. (3.74)-(3.76) for the case of combination parametric resonance for small- but finite-amplitude motions. To this end, we introduce a small dimensionless parameter ε as a bookkeeping device. Because u_2 is much larger than u_1 due to the nonsemisimple structure of the linear undamped operator, we scale the variables as

$$u_1 = \varepsilon v_1, \quad u_2 = \varepsilon^{1-\delta_1} v_2, \quad u_3 = \varepsilon^{1-\delta_2} v_3 \quad (3.77a)$$

and the parameters as

$$\tilde{\mu}_i = \varepsilon^{\delta_3}\mu_i, \quad \tilde{\Lambda}_{in} = \varepsilon^{\delta_4}\Lambda_{in}, \quad \tilde{f}_{in} = \varepsilon^{\delta_5} f_{in}, \quad \tilde{\Gamma}_{inpq} = \varepsilon^{\delta_6}\Gamma_{inpq} \quad (3.77b)$$

for $i,n,p,q = 1,2,3$, where the δ_m are positive constants to be determined in the course of the analysis. Substituting Eqs. (3.77) into Eqs. (3.74)-(3.76) leads to

$$\ddot{v}_1 + v_1 + \varepsilon^{\delta_3} 2\mu_1 \dot{v}_1 + \varepsilon^{\delta_4}(\Lambda_{11} v_1 + \varepsilon^{-\delta_1}\Lambda_{12} v_2 + \varepsilon^{-\delta_2}\Lambda_{13} v_3) + (2\cos\Omega t)\varepsilon^{\delta_5}(f_{11} v_1 + \varepsilon^{-\delta_1} f_{12} v_2 + \varepsilon^{-\delta_2} f_{13} v_3) + \varepsilon^{2+\delta_6-3\delta_1}\Gamma_{1222} v_2^3 = 0 \tag{3.78}$$

$$\ddot{v}_2 + \varepsilon^{\delta_1} v_1 + v_2 + \varepsilon^{\delta_3} 2\mu_2 \dot{v}_2 + \varepsilon^{\delta_4}(\varepsilon^{\delta_1}\Lambda_{21} v_1 + \Lambda_{22} v_2 + \varepsilon^{\delta_1-\delta_2}\Lambda_{23} v_3) + (2\cos\Omega t)\varepsilon^{\delta_5}(\varepsilon^{\delta_1} f_{21} v_1 + f_{22} v_2 + \varepsilon^{\delta_1-\delta_2} f_{23} v_3) + \varepsilon^{2+\delta_6-2\delta_1}\Gamma_{2222} v_2^3 = 0 \tag{3.79}$$

$$\ddot{v}_3 + \omega_3^2 v_3 + \varepsilon^{\delta_3} 2\mu_3 \dot{v}_3 + \varepsilon^{\delta_4}(\varepsilon^{\delta_2}\Lambda_{31} v_1 + \varepsilon^{\delta_2-\delta_1}\Lambda_{32} v_2 + \Lambda_{33} v_3) + (2\cos\Omega t)\varepsilon^{\delta_5}(\varepsilon^{\delta_2} f_{31} v_1 + \varepsilon^{\delta_2-\delta_1} f_{32} v_2 + f_{33} v_3) + \varepsilon^{2+\delta_6-3\delta_1+\delta_2}\Gamma_{3222} v_2^3 = 0 \tag{3.80}$$

To determine a uniformly valid approximate solution that exhibits the effects of the repeated frequency, nonlinearity, and combination parametric resonance, we introduce the time scales

$$T_0 = t, \quad T_1 = \varepsilon t, \quad \text{and} \quad T_2 = \varepsilon^2 t \tag{3.81}$$

In terms of these scales, the time derivatives become

$$\frac{d}{dt} = D_0 + \varepsilon D_1 + \varepsilon^2 D_2, \tag{3.82}$$

$$\frac{d^2}{dt^2} = D_0^2 + 2\varepsilon D_0 D_1 + \varepsilon^2(D_1^2 + 2D_0 D_2) + \ldots \tag{3.83}$$

where $D_n \equiv \partial/\partial T_n$. We seek a second-order uniform approximation to the solution of Eqs. (3.78)-(3.80) in the form

$$v_m(t;\varepsilon) \simeq v_{m0}(T_0, T_1, T_2) + \varepsilon v_{m1}(T_0, T_1, T_2) + \varepsilon^2 v_{m2}(T_0, T_1, T_2) \tag{3.84}$$

Substituting Eqs. (3.81)-(3.84) into Eqs. (3.78)-(3.80) yields

$$
\begin{aligned}
&D_0^2 v_{10} + v_{10} + \varepsilon(D_0^2 v_{11} + v_{11} + 2D_0 D_1 v_{10}) + \varepsilon^2(D_0^2 v_{12} + v_{12} + 2D_0 D_2 v_{10} + D_1^2 v_{10} \\
&\quad + 2D_0 D_1 v_{11}) + \varepsilon^{\delta_3} 2\mu_1 D_0 v_{10} + \varepsilon^{\delta_4}(\Lambda_{11} v_{10} + \varepsilon^{-\delta_1}\Lambda_{12} v_{20} + \varepsilon^{1-\delta_1}\Lambda_{12} v_{21} \\
&\quad + \varepsilon^{-\delta_2}\Lambda_{13} v_{30} + \varepsilon^{1-\delta_2}\Lambda_{13} v_{31}) + (2\cos\Omega t)\varepsilon^{\delta_5}(f_{11} v_{10} + \varepsilon^{-\delta_1} f_{12} v_{20} \\
&\quad + \varepsilon^{1-\delta_1} f_{12} v_{21} + \varepsilon^{-\delta_2} f_{13} v_{30} + \varepsilon^{1-\delta_2} f_{13} v_{31}) \\
&\quad + \varepsilon^{2+\delta_6-3\delta_1}\Gamma_{1222} v_{20}^3 = 0
\end{aligned} \tag{3.85}
$$

$$
\begin{aligned}
&D_0^2 v_{20} + v_{20} + \varepsilon(D_0^2 v_{21} + v_{21} + 2D_0 D_1 v_{20}) + \varepsilon^2(D_0^2 v_{22} + v_{22} + 2D_0 D_2 v_{20} + D_1^2 v_{20} \\
&\quad + 2D_0 D_1 v_{21}) + \varepsilon^{\delta_1} v_{10} + \varepsilon^{\delta_3} 2\mu_2 D_0 v_{20} + \varepsilon^{\delta_4}(\varepsilon^{\delta_1}\Lambda_{21} v_{10} + \Lambda_{22} v_{20} + \varepsilon^{\delta_1-\delta_2}\Lambda_{23} v_{30}) \\
&\quad + (2\cos\Omega t)\varepsilon^{\delta_5}(\varepsilon^{\delta_1} f_{21} v_{10} + f_{22} v_{20} + \varepsilon f_{22} v_{21} \\
&\quad + \varepsilon^{\delta_1-\delta_2} f_{23} v_{30} + \varepsilon^{1+\delta_1-\delta_2} f_{23} v_{31}) + \varepsilon^{2+\delta_6-2\delta_1}\Gamma_{2222} v_{20}^3 = 0
\end{aligned} \tag{3.86}
$$

$$
\begin{aligned}
&D_0^2 v_{30} + \omega_3^2 v_{30} + \varepsilon(D_0^2 v_{31} + \omega_3^2 v_{31} + 2D_0 D_1 v_{30}) + \varepsilon^2(D_0^2 v_{32} + \omega_3^2 v_{32} + 2D_0 D_2 v_{30} + D_1^2 v_{30} \\
&\quad + 2D_0 D_1 v_{31}) + \varepsilon^{\delta_3} 2\mu_3 D_0 v_{30} + \varepsilon^{\delta_4}(\varepsilon^{\delta_2}\Lambda_{31} v_{10} + \varepsilon^{\delta_2-\delta_1}\Lambda_{32} v_{20} + \Lambda_{33} v_{30}) \\
&\quad + (2\cos\Omega t)\varepsilon^{\delta_5}(\varepsilon^{\delta_2} f_{31} v_{10} + \varepsilon^{\delta_2-\delta_1} f_{32} v_{20} + \varepsilon^{1+\delta_2-\delta_1} f_{32} v_{21} + f_{33} v_{30} \\
&\quad + \varepsilon f_{33} v_{31}) + \varepsilon^{\delta_6+2-3\delta_1+\delta_2}\Gamma_{3222} v_{20}^3 = 0
\end{aligned} \tag{3.87}
$$

(I) The case of $\Omega \simeq \omega_3 - 1$. To quantitatively describe the nearness of this resonance, we introduce a detuning parameter, σ, defined by

$$
\Omega = \omega_3 - 1 + \varepsilon^2\sigma \tag{3.88}
$$

To determine the effects of the repeated frequency, nonlinearity, and combination parametric resonance, we must at least include the terms containing $f_{13}v_{30}\cos\Omega t$, $\Lambda_{12}v_{20}$, and $\Gamma_{1222}v_{20}^3$ in Eq. (3.85), v_{10} in Eq. (3.86), $f_{32}v_{20}\cos\Omega t$ in Eq. (3.87), and all the damping terms. Initially it may appear that we have two options:

1. $\delta_5 - \delta_2 = 1$, $\delta_1 = 1$, $\delta_4 - \delta_1 = 1$, $\delta_6 + 2 - 3\delta_1 = 1$, and $\delta_5 + \delta_2 - \delta_1 = 1$ (3.89)

2. $\delta_5 - \delta_2 = 2$, $\delta_1 = 2$, $\delta_4 - \delta_1 = 2$, $\delta_6 + 2 - 3\delta_1 = 2$, and $\delta_5 + \delta_2 - \delta_1 = 2$ (3.90)

The first choice yields

$$\delta_1 = 1, \quad \delta_2 = \frac{1}{2}, \quad \delta_4 = 2, \quad \delta_5 = \frac{3}{2}, \quad \text{and} \quad \delta_6 = 2 \tag{3.91}$$

whereas the second choice yields

$$\delta_1 = 2, \quad \delta_2 = 1, \quad \delta_3 = 2, \quad \delta_4 = 4, \quad \delta_5 = 3, \quad \text{and} \quad \delta_6 = 6 \tag{3.92}$$

The first choice must be discarded, otherwise the coefficient of the term $f_{12}v_{20}\cos\Omega t$ would be order $\varepsilon^{1/2}$, which is bigger than ε, the coefficient of $D_\delta^2 v_{11}$. Consequently, the damping terms should be $O(\varepsilon^2)$; that is, $\delta_3 = 2$.

Using the second choice and equating coefficients of like powers of ε leads to the following:

$$\begin{aligned} \textit{Order } \varepsilon^0\text{:} \quad & D_0^2 v_{10} + v_{10} = 0 \\ & D_0^2 v_{20} + v_{20} = 0 \\ & D_0^2 v_{30} + \omega_3^2 v_{30} = 0 \end{aligned} \tag{3.93}$$

$$\begin{aligned} \textit{Order } \varepsilon^1\text{:} \quad & D_0^2 v_{11} + v_{11} = -2D_0 D_1 v_{10} - 2f_{12} v_{20} \cos\Omega T_0 \\ & D_0^2 v_{21} + v_{21} = -2D_0 D_1 v_{20} \\ & D_0^2 v_{31} + \omega_3^2 v_{31} = -2D_0 D_1 v_{30} \end{aligned} \tag{3.94}$$

$$\begin{aligned} \textit{Order } \varepsilon^2\text{:} \quad & D_0^2 v_{12} + v_{12} = -2D_0 D_2 v_{10} - D_1^2 v_{10} - 2D_0 D_1 v_{11} - 2\mu_1 D_0 v_{10} - \Lambda_{12} v_{20} \\ & -2\cos\Omega T_0 (f_{12} v_{21} + f_{13} v_{30}) - \Gamma_{1222} v_{20}^3 \\ & D_0^2 v_{22} + v_{22} = -2D_0 D_2 v_{20} - D_1^2 v_{20} - 2D_0 D_1 v_{21} - v_{10} - 2\mu_2 D_0 v_{20} \\ & D_0^2 v_{32} + \omega_3^2 v_{32} = -2D_0 D_2 v_{30} - D_1^2 v_{30} - 2D_0 D_1 v_{31} - 2\mu_3 D_0 v_{30} - 2f_{32} v_{20} \cos\Omega T_0 \end{aligned} \tag{3.95}$$

The solutions of Eqs. (3.93) can be expressed as

$$v_{j0} = A_j(T_1, T_2)\exp(iT_0) + cc, \quad j = 1,2$$
$$v_{30} = A_3(T_1, T_2)\exp(i\omega_3 T_0) + cc \tag{3.96}$$

where cc indicates the complex conjugate of the preceding terms and the A_n (n = 1,2, and 3) are arbitrary complex-valued functions at this point. Substituting Eqs. (3.96) into Eqs. (3.94) and eliminating the secular terms yields

$$D_1 A_1 = D_1 A_2 = D_1 A_3 = 0 \tag{3.97}$$

Then it follows that

$$v_{11} = f_{12}\left(\frac{A_2 e^{i(\Omega+1)T_0}}{(\Omega+1)^2 - 1} + \frac{\bar{A}_2 e^{i(\Omega-1)T_0}}{(\Omega-1)^2 - 1} \right) + cc \tag{3.98}$$

$$v_{21} = v_{31} = 0 \tag{3.99}$$

Substituting Eqs. (3.96)-(3.99) into Eqs. (3.95) and eliminating the secular terms, we obtain the following modulation equations:

$$A_1' = -\mu_1 A_1 + \frac{1}{2} i(\Lambda_{12} A_2 + f_{13} A_3 e^{-i\sigma T_2} + 3\Gamma_{1222} A_2^2 \bar{A}_2) \tag{3.100}$$

$$A_2' = -\mu_2 A_2 + \frac{1}{2} i A_1 \tag{3.101}$$

$$A_3' = -\mu_3 A_3 + \frac{i}{2\omega_3} f_{32} A_2 e^{i\sigma T_2} \tag{3.102}$$

Introducing the polar representation

$$A_m(T_2) = \frac{1}{2} a_m(T_2) e^{i\beta_m(T_2)} \tag{3.103}$$

into Eqs. (3.100)-(3.102) and separating real and imaginary parts, we obtain

$$a_1' = -\mu_1 a_1 - \frac{1}{2}\Lambda_{12} a_2 \sin\gamma_1 + \frac{1}{2} f_{13} a_3 \sin\gamma_2 - \frac{3}{8}\Gamma_{1222} a_2^3 \sin\gamma_1 \tag{3.104}$$

$$a_2' = -\mu_2 a_2 + \frac{1}{2} a_1 \sin\gamma_1 \tag{3.105}$$

$$a_3' = -\mu_3 a_3 - \frac{1}{2\omega_3} f_{32} a_2 \sin(\gamma_1 + \gamma_2) \tag{3.106}$$

$$a_1\beta_1' = \frac{1}{2}\Lambda_{12} a_2 \cos\gamma_1 + \frac{1}{2} f_{13} a_3 \cos\gamma_2 + \frac{3}{8}\Gamma_{1222} a_2^3 \cos\gamma_1 \tag{3.107}$$

$$a_2\beta_2' = \frac{1}{2} a_1 \cos\gamma_1 \tag{3.108}$$

$$a_3\beta_3' = \frac{1}{2\omega_3} f_{32} a_2 \cos(\gamma_1 + \gamma_2) \tag{3.109}$$

where

$$\gamma_1 = \beta_2 - \beta_1 \quad \text{and} \quad \gamma_2 = \sigma T_2 + \beta_1 - \beta_3 \tag{3.110}$$

Using Eqs. (3.107)-(3.109) and differentiating Eqs. (3.110), we obtain

$$a_1 a_2 \gamma_1' = (\frac{1}{2} a_1^2 - \frac{1}{2}\Lambda_{12} a_2^2 - \frac{3}{8}\Gamma_{1222} a_2^4) \cos\gamma_1 - \frac{1}{2} f_{13} a_2 a_3 \cos\gamma_2 \tag{3.111}$$

$$\begin{aligned} a_1 a_3 \gamma_2' = a_1 a_3 \sigma + (\frac{1}{2}\Lambda_{12} + \frac{3}{8}\Gamma_{1222} a_2^2) a_2 a_3 \cos\gamma_1 + \frac{1}{2} f_{13} a_3^2 \cos\gamma_2 \\ - \frac{f_{32}}{2\omega_3} a_1 a_2 \cos(\gamma_1 + \gamma_2) \end{aligned} \tag{3.112}$$

Hence, Eqs. (3.104)-(3.106), (3.111) and (3.112) form a fifth-order autonomous system (I), which governs the modulation of the amplitude and phase of the motion of the system.

It follows from Eqs. (3.77a), (3.88), and (3.96) that

$$u_1 \simeq \varepsilon a_1 \cos(t + \beta_2 - \gamma_1) \tag{3.113}$$

$$u_2 \simeq \varepsilon^{-1} a_2 \cos(t + \beta_2) \tag{3.114}$$

$$u_3 \simeq a_3 \cos[(\Omega + 1)t + \beta_2 - \gamma_1 - \gamma_2] \tag{3.115}$$

where a_1, a_2, a_3, β_2, γ_1, and γ_2 are solutions of Eqs. (3.104)-(3.112) above. Of particular interest are the solutions that correspond to constant values of a_1, a_2, and a_3, which are discussed in the next section. These are called fixed-point solutions.

The deflection of the panel at any given point is a weighted sum of the three functions given in Eqs. (3.113)-(3.115). Hence, the deflection is not, in general, a periodic function of time, even when the a_n are constants. However, when the amplitudes are constant, it follows from Eqs. (3.111) and (3.112) that the γ_n are also constant and then from Eqs. (3.107)-(3.109) that the derivatives of the β_n are also constant. Hence, the first two modes have the same constant frequency, $1 + \beta_2'$, but are not in phase; the third mode also has a constant frequency, $\Omega + 1 + \beta_2'$, which is exactly the sum of the frequencies of the excitation and the first two modes. Therefore, the deflections of the panel corresponding to the fixed-point solutions are also not periodic in time. Finally, we note that either all the a_n are zero or none is zero.

(II) The case of $\Omega \simeq \omega_3 + 1$. Following an analysis similar to that described in the previous case, we assume $\Omega = \omega_3 + 1 + \varepsilon^2\sigma$ and obtain the following fifth-order autonomous system (II):

$$a_1' = -\mu_1 a_1 - \frac{1}{2}\Lambda_{12} a_2 \sin\gamma_1 - \frac{1}{2} f_{13} a_3 \sin\hat{\gamma}_2 - \frac{3}{8}\Gamma_{1222} a_2^3 \sin\gamma_1 \tag{3.116}$$

$$a_2' = -\mu_2 a_2 + \frac{1}{2} a_1 \sin\gamma_1 \tag{3.117}$$

$$a_3' = -\mu_3 a_3 - \frac{1}{2\omega_3} f_{32} a_2 \sin(\hat{\gamma}_2 - \gamma_1) \tag{3.118}$$

$$a_1 a_2 \gamma_1' = (\frac{1}{2} a_1^2 - \frac{1}{2}\Lambda_{12} a_2^2 - \frac{3}{8}\Gamma_{1222} a_2^4)\cos\gamma_1 - \frac{1}{2} f_{13} a_2 a_3 \cos\hat{\gamma}_2 \tag{3.119}$$

$$\begin{aligned} a_1 a_3 \hat{\gamma}_2' = a_1 a_3 \sigma - (\frac{1}{2}\Lambda_{12} + \frac{3}{8}\Gamma_{1222} a_2^2) a_2 a_3 \cos\gamma_1 - \frac{1}{2} f_{13} a_3^2 \cos\hat{\gamma}_2 \\ - \frac{f_{32}}{2\omega_3} a_1 a_2 \cos(\hat{\gamma}_2 - \gamma_1) \end{aligned} \tag{3.120}$$

$$\hat{\gamma}_2 = \sigma T_2 - \beta_1 - \beta_3 \tag{3.121}$$

By inspecting both fifth-order autonomous systems (I) and (II), we note that their solutions can be related by some mapping, for example,

$$(a_1, a_2, a_3, \gamma_1, \gamma_2)_{(I)} \quad <====> \quad (a_1, -a_2, -a_3, -\gamma_1, \hat{\gamma}_2)_{(II)} \tag{3.122}$$

Therefore, we only focus on the analysis for system (I), which is the case of $\Omega \simeq \omega_3 - 1$.

3.3.2 Fixed-Point Solutions

The so-called fixed-point solutions correspond to the a_n and the γ_n being constants. Hence, we set the left-hand sides of Eqs. (3.104)-(3.106), (3.111) and (3.112) equal to zero and solve the resulting equations by a Newton-Raphson method. The trivial solution is possible for all values of the various parameters. Nontrivial solutions are possible for a restricted set of parameters. All the present results are based on the following set of parameters: $\omega_3 = 2.722$, $\mu_1 = \mu_2 = 1.233$, $\sigma^* = 8.1079\sigma$, $\Lambda_{12} = -0.0230\Lambda$, $f_{12} = 0.0468F$, $f_{13} = 0.0176F$, $f_{32} = -0.02F$, and $\Gamma_{1222} = 1.258$.

Some possible fixed-point solutions are shown in Fig. 3.12. In part (a), the amplitude of the second mode, a_2, is shown as a function of a measure of the amplitude of the parametric excitation, F. For this curve, the aerodynamic and forcing detuning factors (Λ and σ^*, respectively) are constant. In part (b), a_2 is shown as a function of the aerodynamic detuning, and the frequency and amplitude of the excitation are constant. In both parts, the stable solutions are represented by solid lines and the unstable solutions are represented by broken lines.

In part (a), the aerodynamic detuning, Λ, is such that flutter would occur if there were no parametric excitation. In this case, the nonlinearity limits the amplitude of the predicted flutter motion to a finite value. In the lower left-hand corner of the figure, one can see that the influence of the parametric excitation is stabilizing initially: the trivial solution is unstable, and the amplitude of the flutter motion, represented here by a_2, decreases as the amplitude of the excitation, F, increases. Just before F reaches 750 at point A, a_2 reaches zero; the unstable trivial solution and the stable nontrivial solution merge to form a stable trivial solution. The trivial solution remains stable to small perturbations until F reaches 868 approximately.

However, for $747 < F < 868$ at point C, a relatively large-amplitude stable solution also exists; consequently a large disturbance could evolve into a potentially catastrophic motion. When $F > 868$, the trivial solution is unstable to all disturbances and a large-amplitude solution is the only possibility. The instability that occurs at $F = 868$, approximately, is known as a subcritical or an inverse pitchfork bifurcation and, because of the large jump in the value of a_2, is particularly dangerous. The point labelled B in part (a) is called a saddle-node bifurcation.

In part (b), the results correspond to a relatively large-amplitude excitation. When there is no excitation, flutter occurs when Λ reaches 265 approximately. Consequently, the large-amplitude solution at negative values of Λ would not have occurred without the parametric excitation. As Λ increases from a large negative value, the stable trivial solution bifurcates into a stable nontrivial solution and an unstable trivial solution at $\Lambda = -1864$ approximately. This instability, which is called a pitchfork bifurcation, is not associated with a sudden large increase in the amplitude of the solution and, therefore, is not as potentially dangerous as the subcritical instability shown in part (a).

Before discussing fixed-point solutions further, we discuss the stability of the fixed-point solutions.

3.3.3 Stability of Fixed-Point Solutions

To study the stability of the trivial fixed-point solutions, we introduce the Cartesian [instead of the polar, Eq. (3.103)] transformation

$$A_j = \frac{1}{2}(p_j - iq_j)\exp(\frac{1}{2}i\sigma T_2), \quad j = 1,2 \tag{3.123}$$

$$A_3 = \frac{1}{2}(p_3 - iq_3)\exp(\frac{3}{2}i\sigma T_2) \tag{3.124}$$

into Eqs. (3.100)-(3.102) and obtain

$$p_1' = -\frac{1}{2}\sigma q_1 - \mu_1 p_1 + \frac{1}{2}\Lambda_{12} q_2 + \frac{1}{2} f_{13} q_3 + \frac{3}{8}\Gamma_{1222} q_2 (p_2^2 + q_2^2) \tag{3.125}$$

$$q_1' = \frac{1}{2}\sigma p_1 - \mu_1 q_1 - \frac{1}{2}\Lambda_{12} p_2 - \frac{1}{2} f_{13} p_3 - \frac{3}{8}\Gamma_{1222} p_2 (p_2^2 + q_2^2) \tag{3.126}$$

$$p_2' = -\frac{1}{2}\sigma q_2 - \mu_2 p_2 + \frac{1}{2} q_1 \tag{3.127}$$

$$q_2' = \frac{1}{2}\sigma p_2 - \mu_2 q_2 - \frac{1}{2} p_1 \tag{3.128}$$

$$p_3' = -\frac{3}{2}\sigma q_3 - \mu_3 p_3 + \frac{1}{2\omega_3} f_{32} q_2 \tag{3.129}$$

$$q_3' = \frac{3}{2}\sigma p_3 - \mu_3 q_3 - \frac{1}{2\omega_3} f_{32} p_2 \tag{3.130}$$

The fixed-point solutions correspond to $p_i' = q_i' = 0$ for i = 1, 2, and 3.

The fifth-order modulation equations in the polar representation are more convenient for the analysis of the stability of the nontrivial solutions.

In Fig. 3.13, the stability boundaries corresponding to the results in Fig. 3.12 are shown. (The figure is known as a bifurcation diagram.) In region I, the only constant solution possible is the trivial solution and it is stable. In region II, the trivial constant solution is unstable and a single, stable, nontrivial, solution exists. In region III one trivial and two nontrivial constant solutions exist. The large-amplitude and trivial solutions are stable.

To connect Fig. 3.13 with Fig. 3.12, we consider what happens when F increases from zero when Λ is 709, as in part (a) of Fig. 3.12. In Fig. 3.13, we see that $\Lambda = 709$ is clearly above the flutter boundary at $F = 0$, which is approximately $\Lambda = 265$; hence, the trivial solution is unstable, the panel is in flutter. As F increases along the vertical line at $\Lambda = 709$ in Fig 3.13, the amplitude of the flutter, represented by a_2 in part (a) of Fig. 3.12, decreases until at $F = 747$, approximately, a_2 reaches zero and F crosses the solid boundary from region II into region I in Fig. 3.13. As F increases further, it soon crosses into region III, where three constant solutions exist, as shown in part (a) of Fig. 3.12. When F reaches 868 approximately, it crosses from region III into the upper portion of region II; the trivial constant solution again is unstable and only a single, stable nontrivial constant solution exists. Now as F continues to increase, the amplitude of the response will increase as shown in part (a) of Fig. 3.12. The solid lines in Fig. 3.13 correspond to pitchfork bifurcations in Fig. 3.12, and the broken lines correspond to saddle-node bifurcations.

3.3.4 Additional Numerical Results

For the bifurcation diagram in Fig. 3.14, σ^* has been decreased from -25 to -50. In addition to the pitchfork and saddle-node bifurcations that occur at $\sigma^* = -25$, there is an island of Hopf bifurcations. Inside this island, the real part of a pair of complex conjugate eigenvalues is positive, the fixed points are unstable foci, and the modulation equations possess oscillatory solutions. To demonstrate the consequences of the Hopf bifurcation on the solutions of the modulation equations, we show in Fig. 3.15 force-response curves for $\sigma^* = -50$ and two values of Λ. In Fig. 3.15(a), $\Lambda = 2474$ and there are no Hopf bifurcations. Consequently, the only possible

solutions of the modulation equations are fixed points. There are two saddle-node bifurcations. Between these bifurcations, two nontrivial stable fixed points coexist, and hence the response depends on the initial conditions. Outside these bifurcation values, only one solution is stable; it is nontrivial. Hence, the response is unique and nontrivial. When $\Lambda = 3000$, in addition to the two saddle-node bifurcations, there are two Hopf bifurcations labelled H_1 and H_2 on the force-response curve. When F is set at a small positive value, the nontrivial constant solution is stable. As F is increased, the response amplitude decreases until F exceeds a critical value corresponding to the left Hopf bifurcation, point H_1. Then, the solution of the modulation equations becomes periodic (i.e., a limit cycle develops) and it is stable with four Floquet multipliers being inside the unit circle and one multiplier being unity. As F is increased further, the amplitude of the limit cycle first grows, then decreases, and vanishes at the right Hopf bifurcation, point H_2. For this value of Λ, in addition to the coexistence of two unstable fixed points, a stable fixed point coexists with a stable limit cycle.

As σ^* decreases below -50, the Hopf bifurcation island and the pitchfork bifurcation curve move closer to each other. At $\sigma^* = -100$, they almost touch, as shown in Fig. 3.16(a). In Fig. 3.16(b), we show the force-response curves for $\sigma^* = -100$ and $\Lambda = 9000$. The right Hopf bifurcation almost coincides with the pitchfork bifurcation. In contrast with the dynamics for $\sigma^* = -50$, now the dynamics between the two Hopf bifurcations is much more complicated.

The general picture for the dynamics between the Hopf bifurcation values in Fig. 3.16(b) is summarized in Fig. 3.17. By inspecting Eqs. (3.104)-(3.106), (3.111), and (3.112), we see that they are invariant if a_1, a_2, or a_3 change sign. Hence, eight different solutions may coexist. Starting from a value of F below $F_1 = 3282.3$ and choosing the initial conditions that lead to the nontrivial stable constant solution on

the lower branch and gradually increasing F, one finds that the response amplitude will decrease until the supercritical Hopf bifurcation value F_1 is reached. As F is increased beyond F_1, the constant solution loses stability and a small stable periodic orbit (limit cycle) is born. When the nontrivial constant solution is followed by the periodic solution as a supercritical Hopf bifurcation occurs, these eight possible periodic solutions of the same branch group into four different sets and each set consists of (a_1, a_2, a_3) and $(a_1, a_2, -a_3)$ as a pair of solutions. Two-dimensional projections of the periodic orbits of branch I onto the $a_3 - a_1$ plane are shown in Fig. 3.18 for $F_1 < F \leq F_3$. One of the Floquet multipliers approaches $+1$ at both end points. A supercritical Hopf bifurcation occurs at $F = F_1$, whereas a cyclic-fold bifurcation occurs at $F = F_3$. When F is increasing, nothing occurs at $F = F_2$.

As F increases from F_1 to F_3, the pair of stable periodic orbits of each set approach each other in such a way that $a_3 \to 0$. As F passes through F_3, these two orbits become unstable and jump to two other stable orbits on a new branch (branch II). A similar behavior is also detected along this new branch in Fig. 3.19 when F decreases from F_3 to F_2, where one of the Floquet multipliers approaches $+1$. The pair of orbits would lose stability by touching each other and jump to branch I (as shown in Fig. 3.18). Hence 16 possible stable periodic solutions coexist when $F_2 \leq F \leq F_3$.

As F increases from F_3 to F_4, one of the Floquet multipliers approaches -1, where a period-doubling bifurcation occurs. In Fig. 3.20, two-dimensional projections of the periodic orbits onto the $a_2 - a_1$ plane and the FFT's of a_2 show that a sequence of period-doubling bifurcations occurs as F increases from F_2 to F_8. These bifurcations give rise to solutions of period 2T, 4T, 8T, etc. As we know, this is one of the eight possible sequences for the same parameters.

Another period-doubling sequence is obtained from the other end, as shown in Fig. 3.21. As F decreases from $F = 5858.4$ to F_{13}, the stable period-one solution loses stability through a period-doubling bifurcation, resulting in a stable period-two solution. As F decreases further, a cascade of period-doubling bifurcations occurs, resulting in periodic solutions of period 4T, 8T, 16T, 32T,..., culminating in chaos. In Figs. 3.22(a)-(c), we show a two-dimensional projection of the chaotic attractor onto the $a_2 - a_1$ plane, the FFT of the a_2 signal, and the Lyapunov exponents at $F = 5000$, which is between F_8 and F_9. For the nonlinear deterministic system under investigation, the period-doubling sequence leads to increasing complexity of regular periodic motions (Fig. 3.22(a)), which is one of the known routes to chaos. The broad spectrum in Fig. 3.22(b) indicates a possible chaotic motion. The Lyapunov exponents measure the sensitivity of the system to changes in initial conditions (Moon, 1987). Since the system of equations is explicitly known, we calculated the complete spectrum of the Lyapunov exponents; the result is shown in Fig. 3.22(c). Clearly, one of the Lyapunov exponents is positive, implying a chaotic motion. The Lyapunov exponents can be used to calculate a lower bound for the fractal dimension, the Lyapunov dimension (Kaplan & Yorke, 1978; Farmer, 1983), as

$$d_L = k + \frac{\sum_{m=1}^{k} \lambda_m}{|\lambda_{k+1}|}, \tag{3.131}$$

where the λ_m are the Lyapunov exponents, ordered from the largest to the smallest and k is defined by $\sum_{m=1}^{k} \lambda_m > 0$ and $\sum_{m=1}^{k+1} \lambda_m < 0$. In the present case, we have $d_L \simeq 2.169$, a non-integer dimension, which represents a fractured structure of chaotic (strange) attractors. The structure between F_2 and F_{14} is an example of a bubble structure (Knobloch and Weiss, 1983).

3.3.5 Summary

A combination of analytical and numerical techniques is used to analyze the nonlinear response of three-degree-of-freedom systems with a nonsemisimple one-to-one internal resonance and cubic nonlinearity to a combination parametric excitation. The method of multiple scales is used to derive five first-order autonomous equations governing the modulation of the amplitudes and phases. The analysis is applied to an isotropic simply supported panel in a supersonic stream. The existence and stability of different types of attractors are obtained numerically. The static bifurcations, such as supercritical and subcritical pitchfork and saddle-node bifurcations, are located for some values of the detuning of the parametric excitation. Conditions for supercritical Hopf bifurcations are found. Between the Hopf bifurcations, cyclic-fold bifurcations and period-doubling sequences leading to chaos are obtained.

3.4 The Effects of Quadratic Nonlinearities

3.4.1 Modulation Equations

We consider the following two-degree-of-freedom system in dimensionless form:

$$\ddot{u}_1 + u_1 + 2\tilde{\mu}_1\dot{u}_1 + \sum_{n=1}^{2}\tilde{\Lambda}_{1n}u_n + (2\cos\Omega t)\sum_{n=1}^{2}\tilde{f}_{1n}u_n + \sum_{n=1}^{2}\sum_{p=1}^{2}\Gamma_{1np}u_nu_p + \sum_{n=1}^{2}\sum_{p=1}^{2}\sum_{q=1}^{2}\Gamma_{1npq}u_nu_pu_q = 0, \tag{3.132}$$

$$\ddot{u}_2 + u_1 + u_2 + 2\tilde{\mu}_2\dot{u}_2 + \sum_{n=1}^{2}\tilde{\Lambda}_{2n}u_n + (2\cos\Omega t)\sum_{n=1}^{2}\tilde{f}_{2n}u_n + \sum_{n=1}^{2}\sum_{p=1}^{2}\Gamma_{2np}u_nu_p + \sum_{n=1}^{2}\sum_{p=1}^{2}\sum_{q=1}^{2}\Gamma_{2npq}u_nu_pu_q = 0, \tag{3.133}$$

where time was made dimensionless by using the repeated linear natural frequency of the system. The nonsemisimple structure is adjusted by the detuning parameters $\tilde{\Lambda}_{mn}$ (associated with the aerodynamic loading in the panel-flutter case), whereas $\tilde{\mu}_m$, $\tilde{f}_{mn}$, Ω, Γ_{mnp}, and Γ_{mnpq} are constants related to the damping, forcing amplitude and frequency, and the coefficients of the quadratic and cubic nonlinearities, respectively.

Because of the nonsemisimple linear part of the system, u_2 is expected to be much larger than u_1. Introducing ε as a bookkeeping device, we scale the variables as

$$u_1 = \varepsilon v_1, \quad u_2 = \varepsilon^{1-\delta_1} v_2,$$
$$\tilde{\mu}_m = \varepsilon^{\delta_2}\mu_m, \quad \tilde{\Lambda}_{mn} = \varepsilon^{\delta_3}\Lambda_{mn}, \quad \tilde{f}_{mn} = \varepsilon^{\delta_4} f_{mn}, \tag{3.134}$$

for m,n = 1,2, where the δ_k are positive constants to be determined in the course of the analysis. Substituting Eq. (3.134) into Eqs. (3.132) and (3.133) yields

$$\ddot{v}_1 + v_1 + 2\varepsilon^{\delta_2}\mu_1\dot{v}_1 + \varepsilon^{\delta_3}(\Lambda_{11}v_1 + \varepsilon^{-\delta_1}\Lambda_{12}v_2) + \varepsilon^{\delta_4}(2\cos\Omega t)(f_{11}v_1 + \varepsilon^{-\delta_1}f_{12}v_2)$$
$$+ \varepsilon^{-1}\sum_{n=1}^{2}\sum_{p=1}^{2}\Gamma_{1np}u_n u_p + \varepsilon^{-1}\sum_{n=1}^{2}\sum_{p=1}^{2}\sum_{q=1}^{2}\Gamma_{1npq}u_n u_p u_q = 0, \tag{3.135}$$

$$\ddot{v}_2 + \varepsilon^{\delta_1}v_1 + v_2 + 2\varepsilon^{\delta_2}\mu_2\dot{v}_2 + \varepsilon^{\delta_3}(\varepsilon^{\delta_1}\Lambda_{21}v_1 + \Lambda_{22}v_2) + \varepsilon^{\delta_4}(2\cos\Omega t)(\varepsilon^{\delta_1}f_{21}v_1 + f_{22}v_2)$$
$$+ \varepsilon^{\delta_1-1}\sum_{n=1}^{2}\sum_{p=1}^{2}\Gamma_{2np}u_n u_p + \varepsilon^{\delta_1-1}\sum_{n=1}^{2}\sum_{p=1}^{2}\sum_{q=1}^{2}\Gamma_{2npq}u_n u_p u_q = 0. \tag{3.136}$$

To determine a uniformly valid second-order approximate solution of Eqs. (3.135) and (3.136), we introduce two time scales defined by

$$T_0 = t \text{ and } T_1 = \varepsilon^{\delta_5}t \tag{3.137}$$

where δ_5 is another positive constant to be determined. In terms of these scales, the time derivatives become

$$\frac{d}{dt} = D_0 + \varepsilon^{\delta_5}D_1 + \ldots \tag{3.138}$$

$$\frac{d^2}{dt^2} = D_0^2 + 2\varepsilon^{\delta_5}D_0D_1 + \ldots \tag{3.139}$$

where $D_n \equiv \partial/\partial T_n$. We seek a uniform approximation to the solution of Eqs. (3.135) and (3.136) in the form

$$v_m(t;\varepsilon) = v_{m0}(T_0, T_1) + \varepsilon^{\delta_5} v_{m1}(T_0, T_1) + \ldots \tag{3.140}$$

Substituting Eqs. (3.137)-(3.140) into Eqs. (3.135) and (3.136) leads to

$$\begin{aligned} &D_0^2 v_{10} + v_{10} + \varepsilon^{\delta_5}(D_0^2 v_{11} + v_{11} + 2D_0 D_1 v_{10}) \\ &\quad + 2\varepsilon^{\delta_2}\mu_1 D_0 v_{10} + \varepsilon^{\delta_3}(\Lambda_{11} v_{10} + \varepsilon^{-\delta_1}\Lambda_{12} v_{20}) \\ &\quad + \varepsilon^{\delta_4}(2\cos\Omega T_0)(f_{11} v_{10} + \varepsilon^{-\delta_1} f_{12} v_{20} + \varepsilon^{-\delta_1+\delta_5} f_{12} v_{21}) \\ &\quad + \varepsilon(\Gamma_{111} v_{10}^2 + \varepsilon^{-\delta_1}\Gamma_{112} v_{10} v_{20} + \varepsilon^{-2\delta_1}\Gamma_{122} v_{20}^2 + 2\varepsilon^{-2\delta_1+\delta_5}\Gamma_{122} v_{20} v_{21}) \\ &\quad + \varepsilon^{2-3\delta_1}\Gamma_{1222} v_{20}^3 + \ldots = 0, \end{aligned} \tag{3.141}$$

$$\begin{aligned} &D_0^2 v_{20} + v_{20} + \varepsilon^{\delta_5}(D_0^2 v_{21} + v_{21} + 2D_0 D_1 v_{20}) \\ &\quad + \varepsilon^{\delta_1} v_{10} + 2\varepsilon^{\delta_2}\mu_2 D_0 v_{20} + \varepsilon^{\delta_3}(\varepsilon^{\delta_1}\Lambda_{21} v_{10} + \Lambda_{22} v_{20}) \\ &\quad + \varepsilon^{\delta_4}(2\cos\Omega T_0)(\varepsilon^{\delta_1} f_{21} v_{10} + f_{22} v_{20} + \varepsilon^{\delta_5} f_{22} v_{21}) \\ &\quad + \varepsilon(\varepsilon^{\delta_1}\Gamma_{211} v_{10}^2 + \Gamma_{212} v_{10} v_{20} + \varepsilon^{-\delta_1}\Gamma_{222} v_{20}^2 + 2\varepsilon^{-\delta_1+\delta_5}\Gamma_{222} v_{20} v_{21}) \\ &\quad + \varepsilon^{2-2\delta_1}\Gamma_{2222} v_{20}^3 + \ldots = 0. \end{aligned} \tag{3.142}$$

(a) The Case of Fundamental Parametric Resonance. We assume that

$$\Omega = 1 + \frac{1}{2}\varepsilon^{\delta_5}\sigma, \tag{3.143}$$

where δ_5 is a positive constant and σ is a detuning parameter. To balance the effects of the internal and fundamental parametric resonances, damping, and nonlinearities, we must at least include the terms proportional to $\Lambda_{12}v_{20}$, $f_{12}v_{21}\cos\Omega T_0$, $\Gamma_{112}v_{10}v_{20}$, and $\Gamma_{1222}v_{20}^3$ in Eq. (3.141), v_{10} in Eq. (3.142), and all the damping terms. Thus, we let

$$\delta_5 = \delta_2 = \delta_3 - \delta_1 = \delta_4 - \delta_1 + \delta_5 = 1 - \delta_1 = 2 - 3\delta_1 = \delta_1. \tag{3.144}$$

Hence, $\delta_1 = \frac{1}{2}$, $\delta_2 = \frac{1}{2}$, $\delta_3 = 1$, $\delta_4 = \frac{1}{2}$, and $\delta_5 = \frac{1}{2}$. Substituting for the δ_k in Eqs. (3.141) and (3.142) and equating coefficients of like powers of ε, we obtain

Order ε^0:

$$D_0^2 v_{10} + v_{10} = -(2\cos\Omega T_0) f_{12} v_{20} - \Gamma_{122} v_{20}^2 \tag{3.145a}$$

$$D_0^2 v_{20} + v_{20} = 0 \tag{3.145b}$$

Order $\varepsilon^{1/2}$:

$$\begin{aligned} D_0^2 v_{11} + v_{11} = &-2D_0 D_1 v_{10} - 2\mu_1 D_0 v_{10} - \Lambda_{12} v_{20} - (2\cos\Omega T_0)(f_{11} v_{10} + f_{12} v_{21}) \\ &- \Gamma_{112} v_{10} v_{20} - 2\Gamma_{122} v_{20} v_{21} - \Gamma_{1222} v_{20}^3 \end{aligned} \tag{3.146a}$$

$$D_0^2 v_{21} + v_{21} = -2D_0 D_1 v_{20} - 2\mu_2 D_0 v_{20} - v_{10} - (2\cos\Omega T_0) f_{22} v_{20} - \Gamma_{222} v_{20}^2 \tag{3.146b}$$

The solution of Eq. (3.145b) can be expressed as

$$v_{20} = A_2(T_1)\exp(iT_0) + cc, \tag{3.147}$$

where cc indicates the complex conjugate of the preceding terms. Substituting Eq. (3.147) into Eq. (3.145a) and solving for v_{10}, we obtain

$$\begin{aligned} v_{10} = A_1(T_1)e^{iT_0} + \frac{f_{12}}{(\Omega+1)^2 - 1} A_2 e^{i(\Omega+1)T_0} + \frac{f_{12}}{(\Omega-1)^2 - 1} \bar{A}_2 e^{i(\Omega-1)T_0} \\ + \frac{1}{3}\Gamma_{122} A_2^2 e^{2iT_0} - \Gamma_{122} A_2 \bar{A}_2 + cc \end{aligned} \tag{3.148}$$

Substituting Eqs. (3.147) and (3.148) into (3.146b) and eliminating the secular terms, we have

$$A_2' = -\mu_2 A_2 + \frac{1}{2} i A_1 \tag{3.149}$$

where the prime indicates the derivative with respect to T_1. Therefore,

$$
\begin{aligned}
v_{21} = & \left(\frac{f_{22}}{(\Omega+1)^2-1} + \frac{f_{12}}{\left[(\Omega+1)^2-1\right]^2} \right) A_2 e^{i(\Omega+1)T_0} \\
& + \left(\frac{f_{22}}{(\Omega-1)^2-1} + \frac{f_{12}}{\left[(\Omega-1)^2-1\right]^2} \right) \bar{A}_2 e^{i(\Omega-1)T_0} \\
& + \left(\frac{1}{3}\Gamma_{222} + \frac{1}{9}\Gamma_{122} \right) A_2^2 e^{2iT_0} + (\Gamma_{122} - \Gamma_{222}) A_2 \bar{A}_2 + cc
\end{aligned}
\tag{3.150}
$$

Substituting Eqs. (3.147), (3.148), and (3.150) into Eq. (3.146a), using Eq. (3.143), and eliminating the secular terms, we obtain

$$
\begin{aligned}
A_1' = & -\mu_1 A_1 + i \left[\left(\frac{1}{2}\Lambda_{12} + \chi_1 \right) A_2 + \chi_2 \bar{A}_2 e^{i\sigma T_1} + 2\chi_3 A_2^2 e^{-\frac{1}{2}i\sigma T_1} \right. \\
& \left. + 2\chi_4 A_2 \bar{A}_2 e^{\frac{1}{2}i\sigma T_1} + 4\chi_5 A_2^2 \bar{A}_2 \right]
\end{aligned}
\tag{3.151}
$$

where

$$
\chi_1 = \frac{5}{9} f_{12}^2 - \frac{1}{3} f_{12}(f_{11} + f_{22}) \tag{3.152}
$$

$$
\chi_2 = \frac{1}{2} f_{12}^2 - \frac{1}{2} f_{12}(f_{11} + f_{22}) \tag{3.153}
$$

$$
\chi_3 = \frac{1}{12}\Gamma_{122} f_{11} + \frac{1}{36}(19\Gamma_{122} - 9\Gamma_{112} + 3\Gamma_{222}) f_{12} - \frac{1}{2}\Gamma_{122} f_{22} \tag{3.154}
$$

$$
\chi_4 = -\frac{1}{2}\Gamma_{122} f_{11} + \frac{1}{18}(19\Gamma_{122} - 3\Gamma_{112} - 9\Gamma_{222}) f_{12} - \frac{1}{3}\Gamma_{122} f_{22} \tag{3.155}
$$

$$
\chi_5 = \frac{1}{72}\Gamma_{122}(38\Gamma_{122} - 15\Gamma_{112} - 30\Gamma_{222}) + \frac{3}{8}\Gamma_{1222} \tag{3.156}
$$

(b) The Case of Principal Parametric Resonance. Following an analysis similar to that described in the preceding section with proper scaling, which accounts for the balance of the effects of the repeated frequency, damping, principal parametric resonance, and nonlinearities, we let

$$\Omega = 2 + \varepsilon^{\delta_5}\sigma, \tag{3.157}$$

and obtain the modulation equations

$$A_1' = -\mu_1 A_1 + i\left(\frac{1}{2}\Lambda_{12}A_2 + \frac{1}{2}f_{12}\bar{A}_2 e^{i\sigma T_1} + 4\chi_5 A_2^2\bar{A}_2\right) \tag{3.158}$$

$$A_2' = -\mu_2 A_2 + i\frac{1}{2}A_1 \tag{3.159}$$

It follows from Eq. (3.156) that, when Ω is near 2, the quadratic terms modify the effective nonlinearity coefficient. Hence, if the signs of Γ_{1222} and χ_5 are the same, the quadratic terms have only a quantitative effect on the system response. On the other hand, if Γ_{1222} and χ_5 have opposite signs, the quadratic terms affect the response qualitatively as well as quantitatively. We will not consider this case any further.

Introducing the polar representation

$$A_m(T_1) = \frac{1}{2}a_m(T_1)e^{i\beta_m(T_1)} \tag{3.160}$$

into Eqs. (3.149) and (3.151) and separating real and imaginary parts, we have

$$\begin{aligned} a_1' = {} & -\mu_1 a_1 - \left(\frac{1}{2}\Lambda_{12} + \chi_1 + \chi_5 a_2^2\right)a_2 \sin\gamma_1 - \chi_2 a_2 \sin\gamma_2 \\ & - \chi_3 a_2^2 \sin\left[\frac{1}{2}(3\gamma_1 - \gamma_2)\right] - \chi_4 a_2^2 \sin\left[\frac{1}{2}(\gamma_1 + \gamma_2)\right] \end{aligned} \tag{3.161}$$

$$a_2' = -\mu_2 a_2 + \frac{1}{2} a_1 \sin \gamma_1 \tag{3.162}$$

$$\begin{aligned} a_1 a_2 \gamma_1' = &\left[\frac{1}{2} a_1^2 - \left(\frac{1}{2} \Lambda_{12} + \chi_1 \right) a_2^2 - \chi_5 a_2^4 \right] \cos \gamma_1 - \chi_2 a_2^2 \cos \gamma_2 \\ &- \chi_3 a_2^3 \cos\left[\frac{1}{2} (3\gamma_1 - \gamma_2) \right] - \chi_4 a_2^3 \cos\left[\frac{1}{2} (\gamma_1 + \gamma_2) \right] \end{aligned} \tag{3.163}$$

$$\begin{aligned} a_1 a_2 \gamma_2' = a_1 a_2 \sigma &- \left[\frac{1}{2} a_1^2 + \left(\frac{1}{2} \Lambda_{12} + \chi_1 \right) a_2^2 + \chi_5 a_2^4 \right] \cos \gamma_1 - \chi_2 a_2^2 \cos \gamma_2 \\ &- \chi_3 a_2^3 \cos\left[\frac{1}{2} (3\gamma_1 - \gamma_2) \right] - \chi_4 a_2^3 \cos\left[\frac{1}{2} (\gamma_1 + \gamma_2) \right] \end{aligned} \tag{3.164}$$

where

$$\gamma_1 = \beta_2 - \beta_1 \tag{3.165}$$

$$\gamma_2 = \sigma T_1 - \beta_2 - \beta_1 \tag{3.166}$$

The fixed-point solutions correspond to $a_i' = 0$ and $\gamma_i' = 0$ for $i = 1,2$. The trivial solution is possible for all values of the various parameters. Nontrivial solutions are possible for a restricted set of parameters. In the absence of quadratic nonlinearities ($\chi_3 = \chi_4 = 0$), nontrivial solutions are obtained in closed form, whereas in the presence of quadratic nonlinearities, nontrivial solutions are obtained numerically.

3.4.2 Trivial Solution and Its Stability

To study the stability of the trivial solution, we find it convenient to express the A_m in the Cartesian form

$$A_m(T_1) = \frac{1}{2}(p_m(T_1) - iq_m(T_1))e^{\frac{1}{2}i\sigma T_1} \tag{3.167}$$

Substituting Eq. (3.167) into Eqs. (3.149) and (3.151) and separating real and imaginary parts, we obtain

$$p_1' = -\frac{1}{2}\sigma q_1 - \mu_1 p_1 + (\frac{1}{2}\Lambda_{12} + \chi_1 - \chi_2)q_2 + 2\chi_3 p_2 q_2 + \chi_5 q_2(p_2^2 + q_2^2) \tag{3.168}$$

$$\begin{aligned} q_1' = \quad & \frac{1}{2}\sigma p_1 - \mu_1 q_1 - (\frac{1}{2}\Lambda_{12} + \chi_1 + \chi_2)p_2 - (\chi_3 + \chi_4)p_2^2 + (\chi_3 - \chi_4)q_2^2 \\ & - \chi_5 p_2(p_2^2 + q_2^2) \end{aligned} \tag{3.169}$$

$$p_2' = -\frac{1}{2}\sigma q_2 - \mu_2 p_2 + \frac{1}{2}q_1 \tag{3.170}$$

$$q_2' = \frac{1}{2}\sigma p_2 - \mu_2 q_2 - \frac{1}{2}p_1 \tag{3.171}$$

The trivial solution corresponds to $p_i' = q_i' = 0$ for $i = 1,2$. The stability of this solution can be determined by the eigenvalues of the Jacobian matrix of Eqs. (3.168)-(3.171) evaluated at $p_i = q_i = 0$. They are given by

$$\lambda^4 + r_1\lambda^3 + r_2\lambda^2 + r_3\lambda + r_4 = 0, \tag{3.172}$$

where

$$r_1 = 4\mu, \quad r_2 = 4\mu^2 + \sigma^2 + 2S, \tag{3.173a,b}$$

$$r_3 = 2\mu(\sigma^2 + 2S), \quad r_4 = \mu^2\sigma^2 + S^2 - \frac{1}{4}\chi_2^2, \tag{3.173c,d}$$

$$2\mu = \mu_1 + \mu_2, \quad S = \mu_1\mu_2 + \frac{1}{4}(\Lambda_{12} + 2\chi_1 - \sigma^2). \tag{3.173e,f}$$

According to the Routh-Hurwitz criterion, at least one root of Eq. (3.172) has a positive real part if the following conditions are not satisfied:

$$r_1 > 0, \quad r_1 r_2 - r_3 > 0, \quad r_3(r_1 r_2 - r_3) - r_1^2 r_4 > 0, \quad r_4 > 0. \tag{3.174}$$

All the present results are based on the following set of parameters: $\mu_1 = \mu_2 = 1.233$, $\sigma^* = 8.1079\sigma$, $\Lambda_{12} = -0.0230\Lambda$, $\chi_1 = -9.35F^2 x 10^{-4}$, and $\chi_2 = -7.66F^2 x 10^{-5}$. We consider two systems: (I) a system without quadratic nonlinearities (i.e., $\chi_3 = \chi_4 = 0$ and $\chi_5 = 0.472$) and (II) a system with quadratic nonlinearities (i.e., $\chi_3 = -0.019F$, $\chi_4 = 0.0016F$, and $\chi_5 = 0.468$). We note that the stability boundaries of the trivial solution are the same for both systems. However, the quadratic nonlinearities have a profound effect on the resulting bifurcations.

(a) Static Bifurcations of the Trivial Solution. When one of the roots of Eq. (3.172) moves into the right-half plane along the real axis as a control parameter is varied, the trivial solution loses stability via a static bifurcation. This bifurcation corresponds to $r_4 = 0$, where r_4 is defined in Eq. (3.173d). The locus of this bifurcation is labeled curve 1 in Fig. 3.23. Using the method of multiple scales, we computed the normal form of the dynamics near this bifurcation; it reveals the difference between the two systems.

For system I, the static bifurcation is of the pitchfork type. At a fixed F, the normal form can be expressed as

$$y' = \varepsilon_1(\Lambda - \Lambda_{cr})y + \alpha y^3, \tag{3.175}$$

where Λ_{cr} is the bifurcation value. As Λ crosses the static bifurcation curve directly from region I into region III at a fixed F, $\varepsilon_1 > 0$ and $\alpha < 0$, which indicates a pitchfork bifurcation. In Fig. 3.24(a), $(\varepsilon_1, \alpha) = (0.00085, -0.00268)$ when $(F, \Lambda_{cr}) = (100, -689.63)$. The stable trivial solution loses stability and gives way to a

stable nontrivial constant solution (or periodic solution of the original system) that smoothly grows with Λ. If Λ crosses the curve from region II into region III, $\varepsilon_1 < 0$ and $\alpha > 0$, which indicates a subcritical (reverse) pitchfork bifurcation. In Fig. 3.24(a), $(\varepsilon_1, \alpha) = (-0.0031, 0.00853)$ when $(F, \Lambda_{cr}) = (100, 257.98)$. The solution jumps from a trivial to a nontrivial value as Λ decreases past the bifurcation value.

For system II, the static bifurcation is of the transcritical type. At a fixed value of F, the normal form can be expressed as

$$y' = \varepsilon_1(\Lambda - \Lambda_{cr})y + \delta y^2. \tag{3.176}$$

As Λ crosses the static bifurcation curve directly from region I into region III at a fixed value of F, $\varepsilon_1 > 0$ and $\delta > 0$, which indicates a transcritical bifurcation. In Fig. 3.24(b), $(\varepsilon_1, \delta) = (0.00085, 0.00483)$ when $(F, \Lambda_{cr}) = (100, -689.63)$. The trivial solution exchanges stability with a nontrivial constant solution, which smoothly grows with Λ. If Λ crosses the curve from region II into region III, $\varepsilon_1 < 0$ and $\delta < 0$, which also indicates a transcritical bifurcation. In Fig. 3.24(b), $(\varepsilon_1, \delta) = (-0.0031, -0.2356)$ when $(F, \Lambda_{cr}) = (100, 257.98)$. As Λ decreases past the bifurcation value, a transcritical bifurcation occurs and results in an exchange of stability between the trivial and a nontrivial constant solution. Instead of a jump, the constant solution grows smoothly in the other direction as Λ decreases. Hence, between the two static bifurcation values, two nontrivial constant solutions $\pm a_2$ coexist for system I, whereas two pairs of constant solutions $\pm a_2$ coexist for system II. Which one is realizable physically depends on the initial conditions.

(b) Hopf Bifurcation of the Trivial Solution. When a pair of complex-conjugate eigenvalues of the Jacobian matrix of Eqs. (3.168)-(3.171) evaluated at the trivial fixed point crosses transversely into the right-half plane as a control parameter is varied, the trivial solution loses stability via a Hopf bifurcation. The locus of the Hopf

bifurcation is $r_3(r_1r_2 - r_3) - r_1^2r_4 = 0$, where the r_j are defined in Eqs. (3.173). The Hopf bifurcation curve is labeled curve 2 in Fig. 3.23. As Λ crosses this curve from region I or II at a fixed F, a supercritical Hopf bifurcation occurs for both systems I and II. The normal form describing this bifurcation is

$$r' = \varepsilon_2(\Lambda - \Lambda_{cr})r + \alpha_R r^3, \quad \varepsilon_2 > 0 \text{ and } \alpha_R < 0 \tag{3.177a}$$

$$\theta' = \omega + \alpha_I r^2, \quad \omega^2 = r_3/r_1 \text{ and } \alpha_I < 0 \tag{3.177b}$$

where Λ_{cr} is the bifurcation value. When $(F, \Lambda_{cr}) = (100, 442.61)$, $(\varepsilon_2, \alpha_R) = (0.00363, -0.03767)$ and $(\omega, \alpha_I) = (0.9875, -0.0215)$ for system I, whereas $(\varepsilon_2, \alpha_R) = (0.00363, -0.0705)$ and $(\omega, \alpha_I) = (0.9875, -0.2707)$ for system II. The stable trivial solution loses stability and gives way to a stable periodic solution (or an amplitude- and phase-modulated solution of the original system) that gradually grows with increasing Λ.

3.4.3 Nontrivial Solutions and Their Stability

A Newton-Raphson procedure is used to compute the nontrivial constant solutions numerically. The eigenvalues of the Jacobian matrix of the nontrivial constant solutions are monitored to detect possible bifurcations. A two-point boundary-value algorithm is used to compute periodic solutions and the eigenvalues of the monodromy matrix are monitored to detect possible bifurcations.

The bifurcation diagrams for systems I and II for $\sigma^* = 25$ are shown in Fig. 3.23. Clearly, the quadratic nonlinearities dramatically modify the bifurcation diagram. In addition to transforming the pitchfork bifurcation curve into a transcritical bifurcation

curve, the quadratic nonlinearities extend the region of nontrivial constant solutions by decreasing the slope of the saddle-node bifurcation curve, produce a new branch of Hopf bifurcations, and create a period-doubling bifurcation curve.

For $\sigma^* = 25$ and $F = 100$, we show variation of a_2 with Λ in Fig. 3.24(a) in the absence of the quadratic terms and in Fig. 3.24(b) in the presence of the quadratic terms. As Λ increases from -1000, the trivial solution loses stability via a pitchfork bifurcation in part (a) and a transcritical bifurcation in part (b). Either one results in a value of a_2 that smoothly grows with Λ. If we start with the trivial solution at $\Lambda \approx$ 257.98 and then increase Λ, we find that the solution remains trivial until Λ exceeds $\Lambda \approx$ 442.61, where a_2 undergoes a supercritical Hopf bifurcation. As a result, the trivial solution gives way to a small stable limit cycle for a_1, a_2, γ_1 and γ_2, which corresponds to a quasiperiodic solution or a synchronized solution with a period much larger than that of the excitation. As Λ increases, in part (a), the mean amplitude of the limit cycle grows until it reaches a vertical tangent at $\Lambda \simeq 669.1907$, where its period approaches ∞, as shown in Fig. 3.25, suggesting the occurrence of a homoclinic orbit.

As stated in Section 3.1.6, if a system has a homoclinic orbit at a saddle focus and the eigenvalues of the saddle focus satisfy the Shilnikov inequality in Eq. (3.50), Shilnikov (1970) showed that the system has a stable periodic orbit on one side of the homoclinic orbit and no recurrent behavior on the other. Two-dimensional projections of the unstable manifolds of the saddle are shown in Fig. 3.26. Before the homoclinicity condition is reached, the unstable manifold of the saddle focus leads to a limit cycle in one direction and to a sink in the other, as shown in part (a) at $\Lambda = 610$. As Λ increases, the limit cycle grows and its period increases, as shown in part (b) at $\Lambda = 640$. At $\Lambda = \Lambda_h \simeq 669.1907$, the periodic orbit passes through the saddle focus, forming the homoclinic orbit. The eigenvalues of the saddle focus at Λ_h are

(0.7245, $-1.2334 \pm 3.0951i$, -3.1912). Hence, $\delta = 1.702 > 1$ and the conditions of the Shilnikov theorem are satisfied. Therefore, when $\Lambda < \Lambda_h$, the system has a stable limit cycle, and when $\Lambda > \Lambda_h$, it has no local recurrent behavior. Consequently, as Λ increases past Λ_h, a jump to the stable branch of nontrivial constant solutions is expected, as shown in part (d).

If we start with the trivial solution for system II at $\Lambda = 300$ and slowly increase Λ, we find that the solution remains trivial until Λ exceeds 442.61 approximately, where a_2 undergoes a supercritical Hopf bifurcation. The small limit cycle born by the Hopf bifurcation increases in size and its period increases with Λ, as shown in Fig. 3.27. As Λ approaches 458.3363, the period of the limit cycle approaches infinity, suggesting the formation of a homoclinic orbit. Indeed this is the case as evident from the two-dimensional projections of the orbit onto the $a_2 - a_1$ plane shown in Fig. 3.28. In part (a), the unstable manifold of the saddle focus tends to a sink in one direction and to a limit cycle in the other direction. As Λ increases, the limit cycle increases in size and at $\Lambda \approx 458.3363$ becomes homoclinic to the saddle. The eigenvalues of the saddle are (0.7501, -1.1639, $-2.2598 \pm 1.7952i$). According to the Shilnikov theorem, in a general system without symmetries, we only consider the positive eigenvalue (real or complex pair) with smallest real part and the negative eigenvalue (real or complex pair) with real part of smallest modulus in the Shilnikov inequality. Here, $\delta = 1.1639/0.7501$ is greater than unity, conditions of the Shilnikov theorem are satisfied. Hence, a limit cycle exists on one side of the homoclinic orbit and no local recurrent behavior exists on the other side, as shown in Fig. 3.28. Consequently the response jumps to the sink, corresponding to the branch of large nontrivial constant solutions.

Starting with the trivial solution at $\Lambda = 300$ and slowly decreasing Λ, we find that the response remains trivial until Λ decreases past 257.98, where the trivial solution

loses stability and jumps up to the stable nontrivial constant solution via a subcritical pitchfork bifurcation in Fig. 3.24(a), whereas it exchanges stability with a nontrivial constant solution via a transcritical bifurcation in Fig. 3.24(b). As Λ decreases further, the amplitude of the constant solution in (a) decreases to zero, whereas the magnitude of the amplitude in (b) smoothly increases first then decreases until $\Lambda \simeq -690.79$, where a saddle-node bifurcation occurs. As a result, the constant solution jumps to the trivial solution.

In Fig. 3.29, we set $F = 80 < 90.193$, which is the minimum value on curve 1 in Fig. 3.23. The trivial solution gives way to a limit cycle via a supercritical Hopf bifurcation as Λ increases from a small value. The limit cycle remains stable all the way in part (a), whereas in part (b), the limit cycle increases in size and its period increases with Λ until $\Lambda \simeq 425.54$, where an orbit homoclinic to the saddle focus forms. The eigenvalues of the saddle are $(0.7423, -1.3308, -2.1725 \pm 2.943i)$. Therefore, the conditions for the Shilnikov theorem are satisfied with $\delta = 1.3308/0.7423$ being greater than unity. Consequently, a limit cycle is expected to exist for $\Lambda < 425.54$ and no local recurrent behavior is expected for $\Lambda > 425.54$, resulting in a jump to a far away solution. In this case, the jump is to a large-amplitude nontrivial constant solution.

When Λ decreases from 500, the mean amplitude of the limit cycle slowly decreases to zero in part (a), whereas in part (b), the only stable solution is the nontrivial constant solution, which decreases to a value where a saddle-node bifurcation occurs. As a result, the response jumps down to the trivial solution.

In Fig. 3.30, we show variation of a_2 with F for $\sigma^* = 25$ and $\Lambda = 500$. For small values of F, the response consists of a stable limit cycle in (a). As F increases, the limit cycle decreases in size and disappears via a reversed supercritical Hopf bifurcation, giving way to the trivial solution. As F increases further, the trivial solution loses stability via a subcritical pitchfork bifurcation and jumps up to the

stable constant solution. As F decreases from a large value, the stable nontrivial constant solution decreases, undergoes a saddle-node bifurcation, and jumps down to a limit cycle. In (b), as F increases from a small value, the response remains to be a limit cycle until an orbit homoclinic to a saddle focus forms at $F \simeq 77.133$. The eigenvalues of the saddle focus are $(0.781, -1.31, -2.202 \pm 3.133i)$. The conditions for the Shilnikov theorem are satisfied with $\delta = 1.31/0.781$ being greater than unity. Therefore, there is no local recurrent behavior beyond the formation of the homoclinic orbit and the response jumps up to a constant solution.

When F lies between 106.14 and 110.1 in Fig. 3.30(b), the trivial solution is stable. If the initial conditions are chosen to lead to the trivial solution, it loses stability via a supercritical Hopf bifurcation as F decreases or via a transcritical bifurcation as F increases. As F decreases past the Hopf bifurcation value, the mean amplitude of the limit cycle grows and reaches a vertical tangent at $F \simeq 105.277$, where an orbit homoclinic to a saddle focus forms. As a result the response jumps to a constant solution. As F increases past the transcritical bifurcation value, $|a_2|$ increases until a Hopf bifurcation occurs at $F \simeq 117.47$.

When F increases from a small value at $\Lambda = 592.37$, corresponding to the intersection of curves 1 and 2 in Fig. 3.23, the response is given by a small limit cycle whose mean amplitude first grows slowly and then decreases, as shown in Fig. 3.31. As F increases, the limit cycles gets closer and closer to the unstable nontrivial fixed point (saddle focus), resulting in the formation of homoclinic orbits at $F \simeq 109.447$ in part (a) and $F \simeq 76.715$ in part (b). The eigenvalues of the corresponding saddle focus are $(0.680, -1.233 \pm 1.764i, -3.147)$ in (a) and $(0.894, -1.291, -2.268 \pm 3.233i)$ in (b). The Shilnikov conditions are satisfied with δ being greater than unity. Consequently, there is no recurrent behavior beyond the formation of the homoclinic orbit. Therefore, a jump to a constant solution occurs in both cases.

Next, we increase σ^* to 50. The bifurcation diagrams are shown in parts (a) and (b) of Fig. 3.32 for systems I and II, respectively. Clearly, the dynamics of system II is much more complex than that of system I. A cyclic-fold bifurcation curve (curve 5, which is close to curve 2) and a period-doubling bifurcation curve (curve 4) emerge. They are not connected. A small gap exists between $\Lambda \simeq 605$ and 609. Inside this gap, a possible homoclinic bifurcation is responsible for the instability of the periodic solution.

In Fig. 3.33, we show the force-response curves at $\Lambda = -1500$. As F increases from a small value, the response remains trivial until it loses stability via a supercritical pitchfork bifurcation in (a) and via a transcritical bifurcation in (b). As a result, the response becomes nontrivial and constant. In part (b), as F increases further, $|a_2|$ increases and then loses stability via a Hopf bifurcation. When F decreases from 200, the initial conditions determine the response in (b). If it is the constant solution, it will jump down to the trivial solution via a saddle-node bifurcation as F decreases. If it is the limit cycle, it will finally get to the trivial solution by going through a reverse Hopf bifurcation followed by a transcritical bifurcation.

In Fig. 3.34, we show the force-response curves at $\Lambda = 606$ and 750 for systems I and II. Clearly, the quadratic nonlinearities produce complexity in the dynamics. In Fig. 3.34(b), as F increases from a small value at $\Lambda = 606$, the limit cycle grows and gets close to its basin boundary at $F \simeq 149.717$. The eigenvalues of the saddle focus are $(2.0516, -1.2613, -2.8619 \pm 5.3i)$. As F increases further, the stable limit cycle collides with its basin and results in a jump. When F decreases past $F_{cr} \simeq 152.49$, a cyclic-fold bifurcation occurs. The response jumps to a far away attractor.

If the initial conditions are chosen to lead to the trivial solution when F lies between 155.27 and 177.81, it will undergo a transcritical bifurcation as F increases. The ensuing constant solution grows in magnitude and loses stability via a Hopf

bifurcation. If F increases further, the periodic solution loses stability via a sequence of period-doubling bifurcations, culminating in chaos.

In Fig. 3.34(d), the middle and right branches of limit cycles behave qualitatively as those in (b). On the other hand, the left branch of limit cycles loses stability via a sequence of period-doubling bifurcation starting at $F \simeq 122.4$ and culminating in chaos. However, the chaotic attractor is very close to its basin boundary. A boundary crisis (Grebogi et al., 1983) occurs at a value of F slightly below 139.1, resulting in the destruction of the attractor and its basin. In Fig. 3.35, we show the time trace of a trajectory initiated in the region that used to be occupied by the chaotic attractor for $F < 1.39.1$. The trajectory bounces around in the region formerly occupied by the chaotic attractor but finally leaves it to the constant attractor.

A sequence of period-doubling bifurcations leading to chaos is shown in Fig. 3.36 at $\Lambda = 900$. The broad spectrum shown in Fig. 3.36(p) at $F = 139.385$ and the corresponding Lyapunov exponents (0.013, 0.0, −3.405, −3.724) confirm the chaotic nature of this attractor.

3.4.4 Summary

We consider the effects of quadratic nonlinearities on the response of a parametrically excited two-degree-of-freedom system with cubic nonlinearities and a nonsemisimple one-to-one internal resonance. For the case of fundamental parametric resonance, the quadratic nonlinearities qualitatively modify the response of the excited system. They change the static bifurcation of the trivial solution from a pitchfork bifurcation to a transcritical bifurcation. They also produce cyclic-fold, period-doubling, and Hopf bifurcations in the nontrivial constant solutions. However,

the quadratic nonlinearities only quantitatively change the response of the system with cubic nonlinearities to the principal parametric resonance if the coefficient of the nonlinear term in the modulation equations does not change sign.

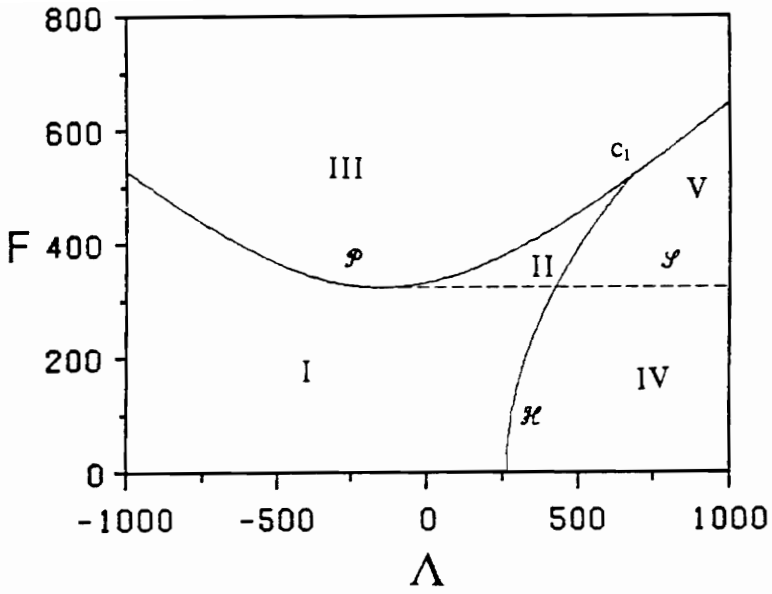

Figure 3.1. Various regions of interest obtained from the linear and nonlinear stability analyses for a simply supported panel, $\omega^* = 8.1076$, $\sigma = 25/\omega^*$, $\mu_1 = \mu_2 = 10/\omega^*$, $\Lambda_{12} = -99.2\Lambda/\omega^{*4}$, $f_{12} = 202.5F/\omega^{*4}$, and $\alpha_{14} = 5729/\omega^{*4}$. The P and H curves define the linear flutter boundaries. The P curve corresponds to pitchfork bifurcations, the H curve corresponds to Hopf bifurcations, and the S curve corresponds to saddle-node bifurcations.

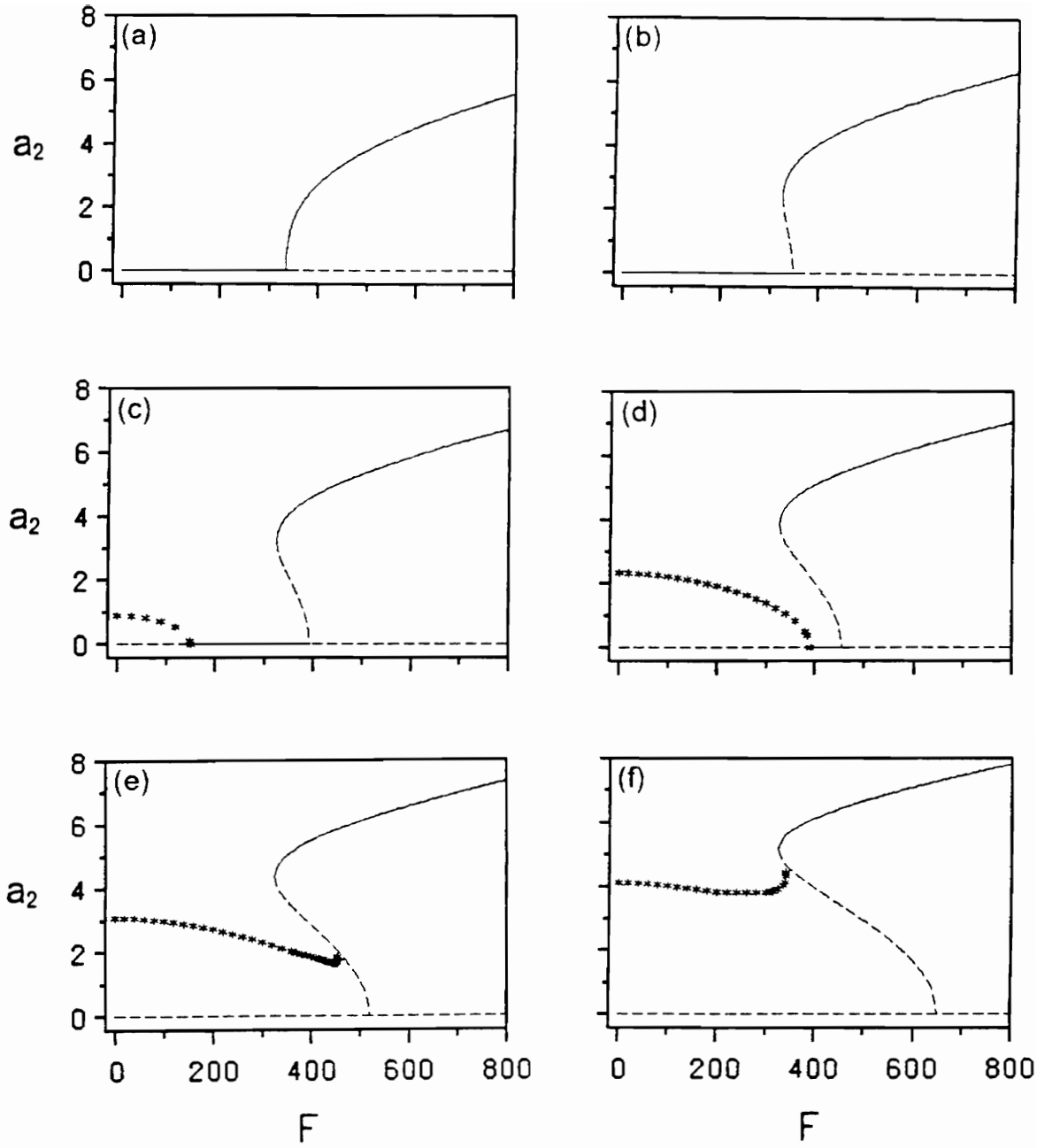

Figure 3.2. Variation of the amplitude of the second mode with the amplitude of the parametric excitation. (a) $\Lambda = -300$; (b) $\Lambda = 100$; (c) $\Lambda = 300$; (d) $\Lambda = 500$; (e) $\Lambda = 679.2$; and (f) $\Lambda = 1000$. ___, Stable constant solution; ---, unstable constant solution; and ***, mean amplitude of the periodic solution.

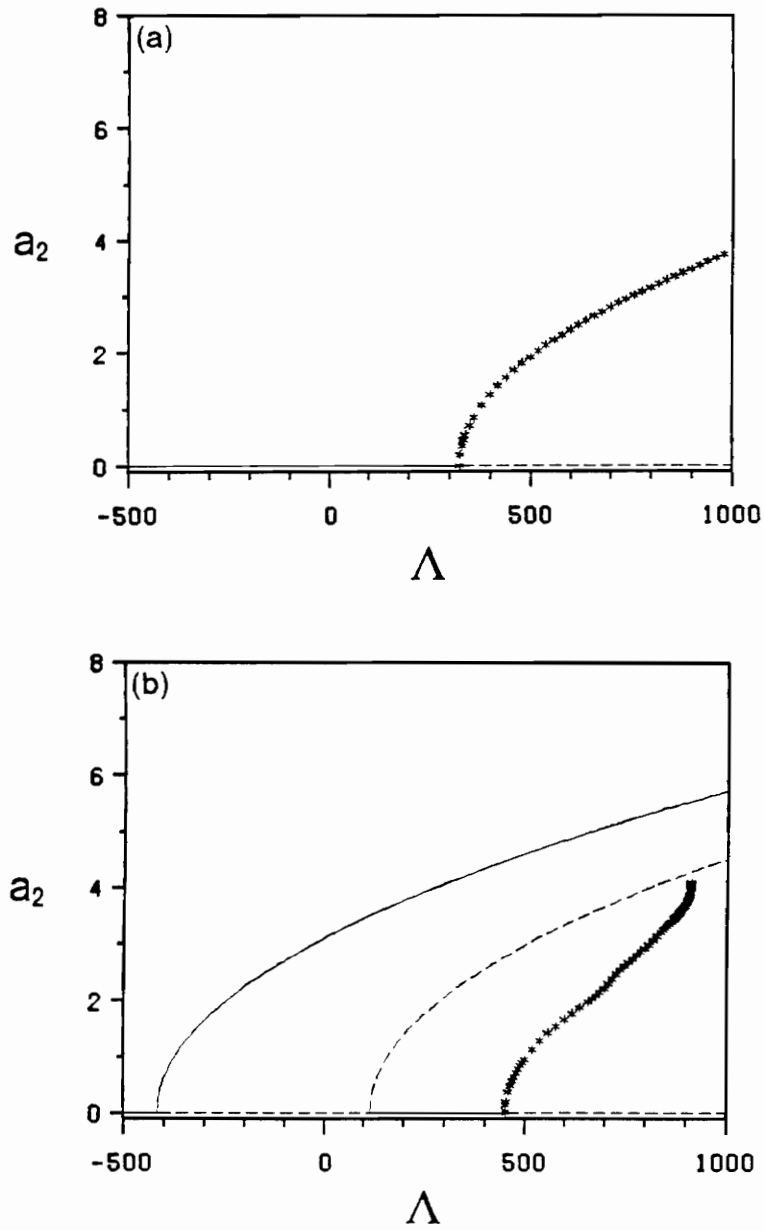

Figure 3.3. Variation of the amplitude of the second mode a_2 with the aerodynamic detuning: (a) F = 200; (b) F = 350. ___, Stable constant solution; ---, unstable constant solution; and ***, mean amplitude of the periodic solution.

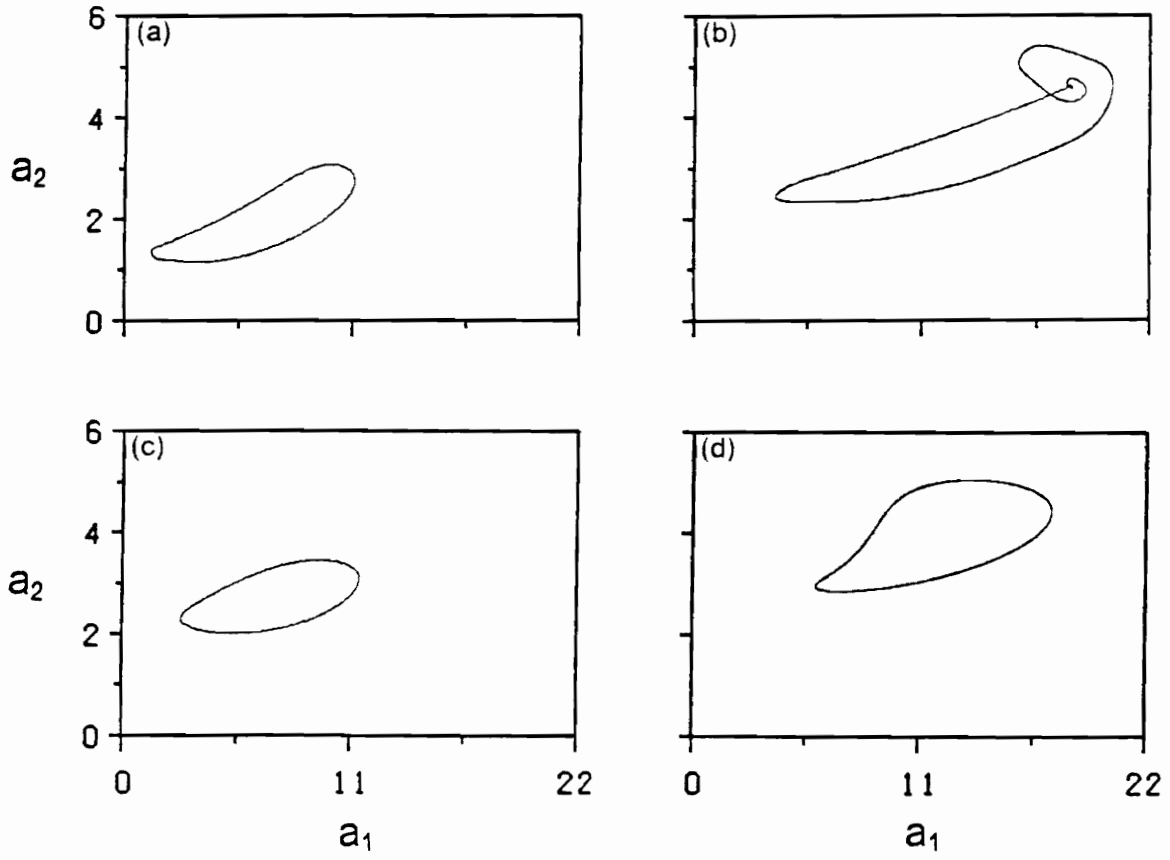

Figure 3.4. A two-dimensional projection of the phase portrait onto the $a_2 - a_1$ plane: $(\Lambda,F) =$ (a) (679.2,340); (b) (1000,340); (c) (679.2,200); and (d) (1000,200).

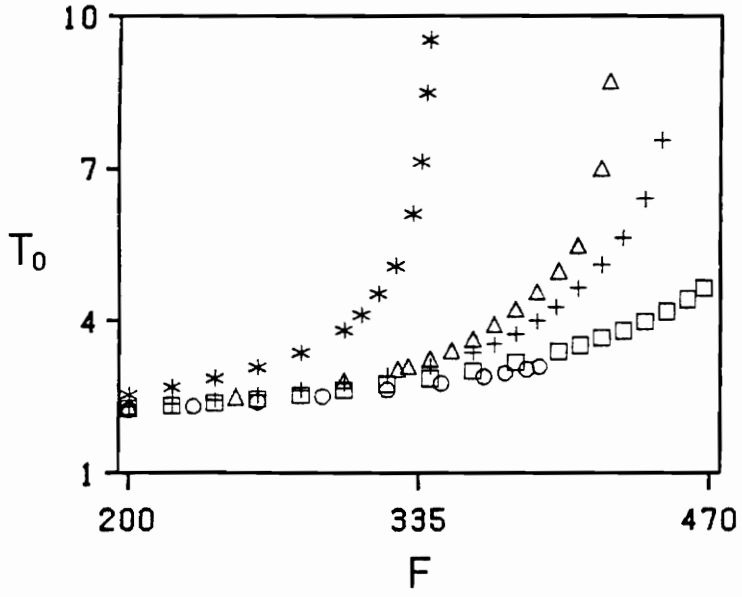

Figure 3.5. Variation of the period of the periodic motion with the amplitude of the parametric excitation. ○ $\Lambda = 500$; □ $\Lambda = 600$; + $\Lambda = 679$; Δ $\Lambda = 700$; * $\Lambda = 1000$.

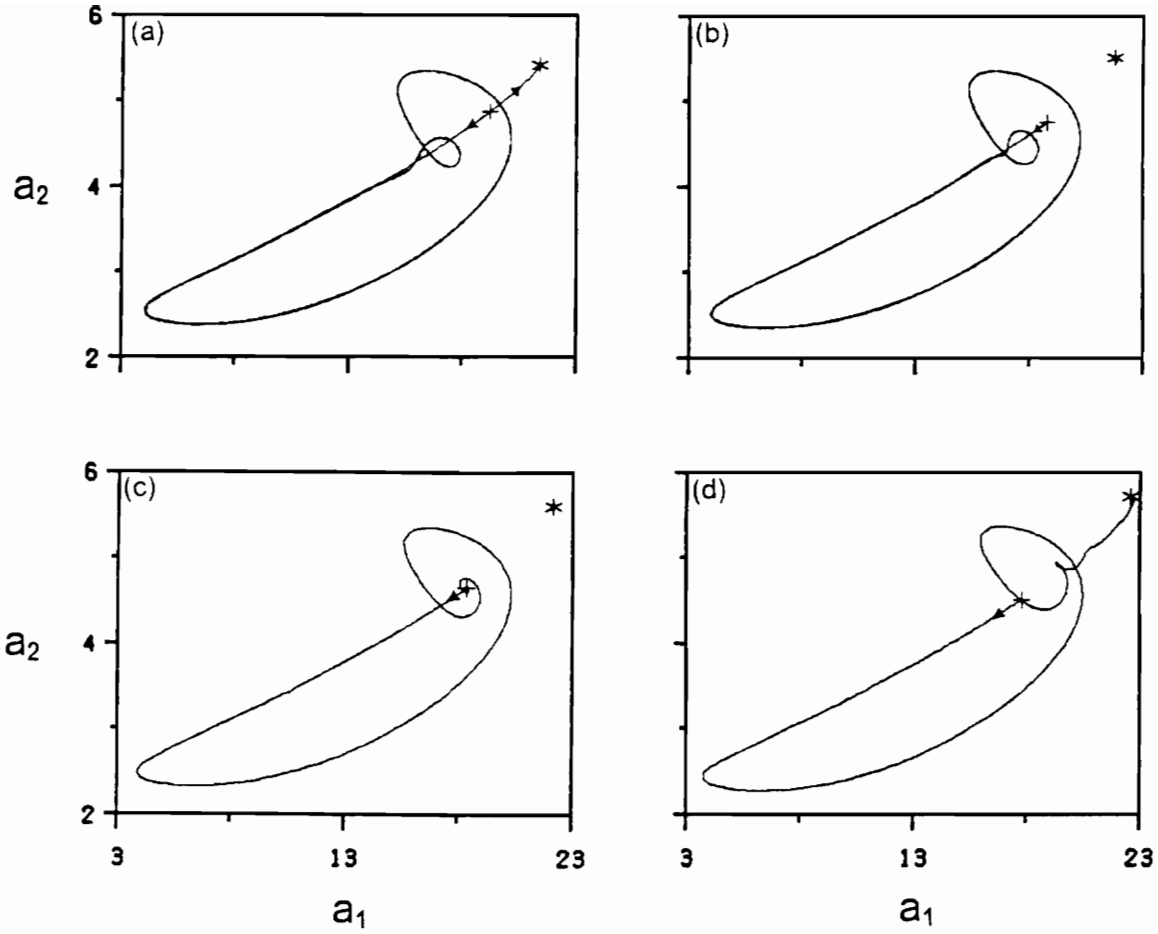

Figure 3.6. A two-dimensional projection of an unstable manifold onto the $a_2 - a_1$ plane for $\Lambda = 1000$ and F = (a) 330 (both directions are included); (b) 335; (c) 340.853; (d) 350. + denotes a saddle and * denotes a sink.

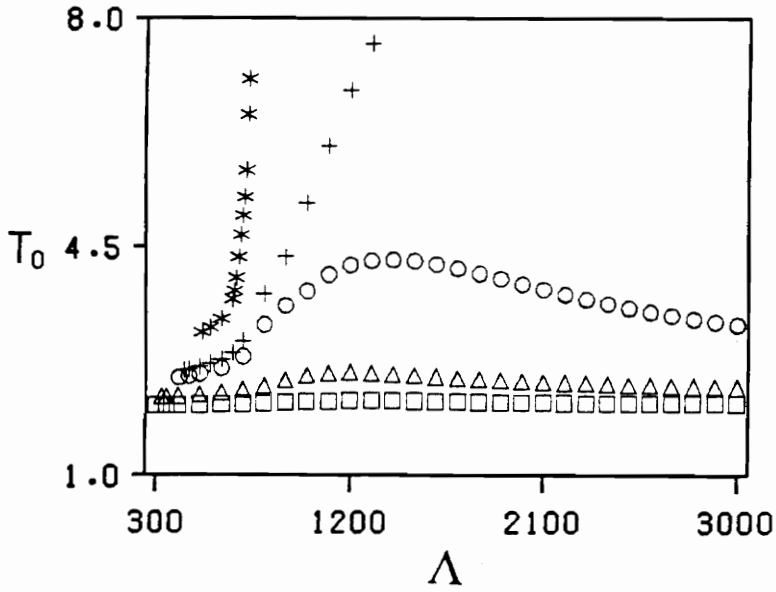

Figure 3.7. Variation of the period of the periodic motion with the aerodynamic detuning. □ F = 100; Δ F = 200; ○ F = 300; + F = 325; * F = 400.

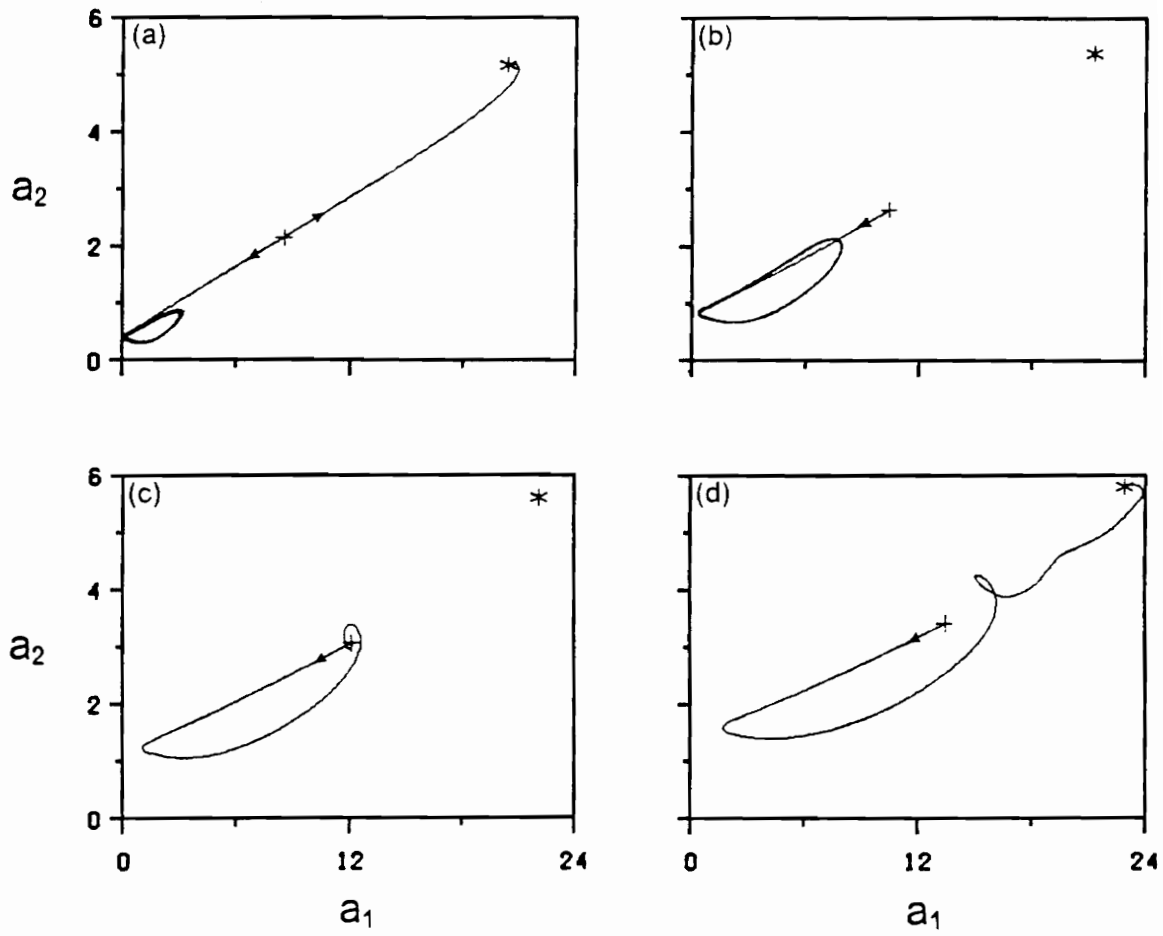

Figure 3.8. A two-dimensional projection of an unstable manifold onto the $a_2 - a_1$ plane for $F = 400$ and $\Lambda =$ (a) 530 (both directions are included); (b) 630; (c) 734.161; (d) 830. + denotes a saddle and * denotes a sink.

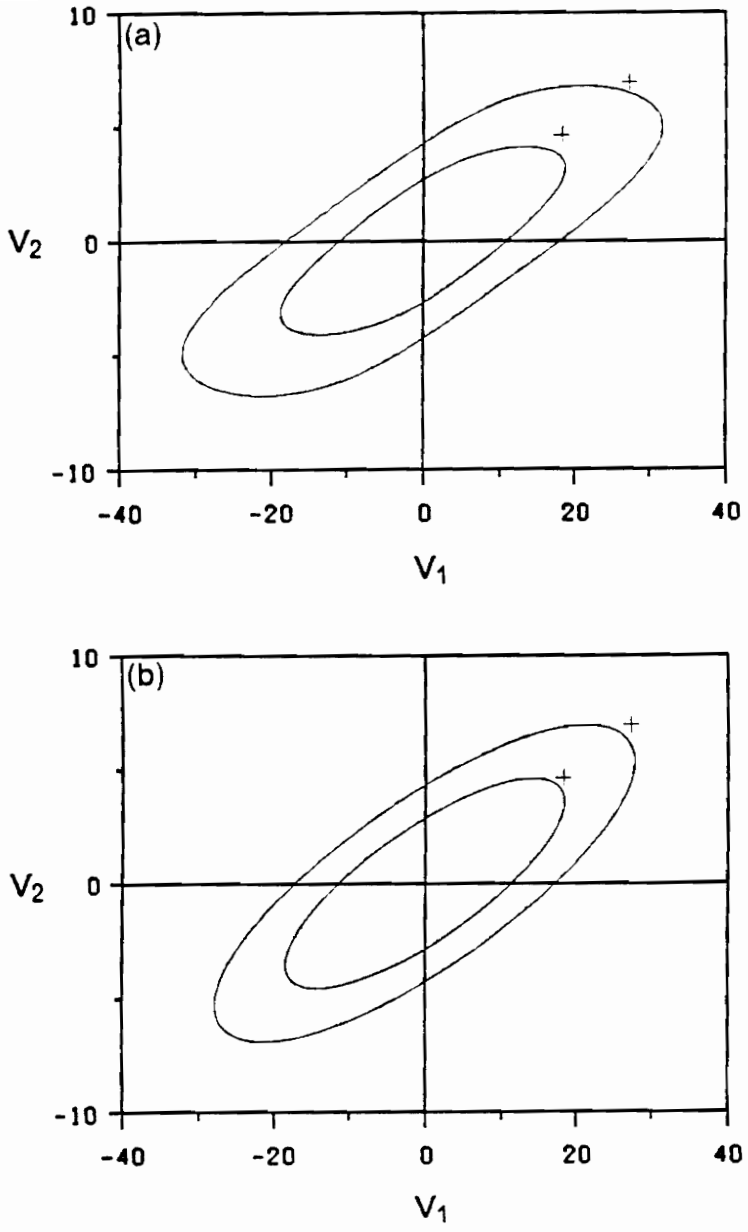

Figure 3.9. Comparison between the numerical time integration of the modulation equations (+) and the original governing equations for $(\Lambda,F) = (0,500)$ and $(0,1000)$ (outer loop), (a) $\varepsilon = 0.1$; (b) $\varepsilon = 0.01$.

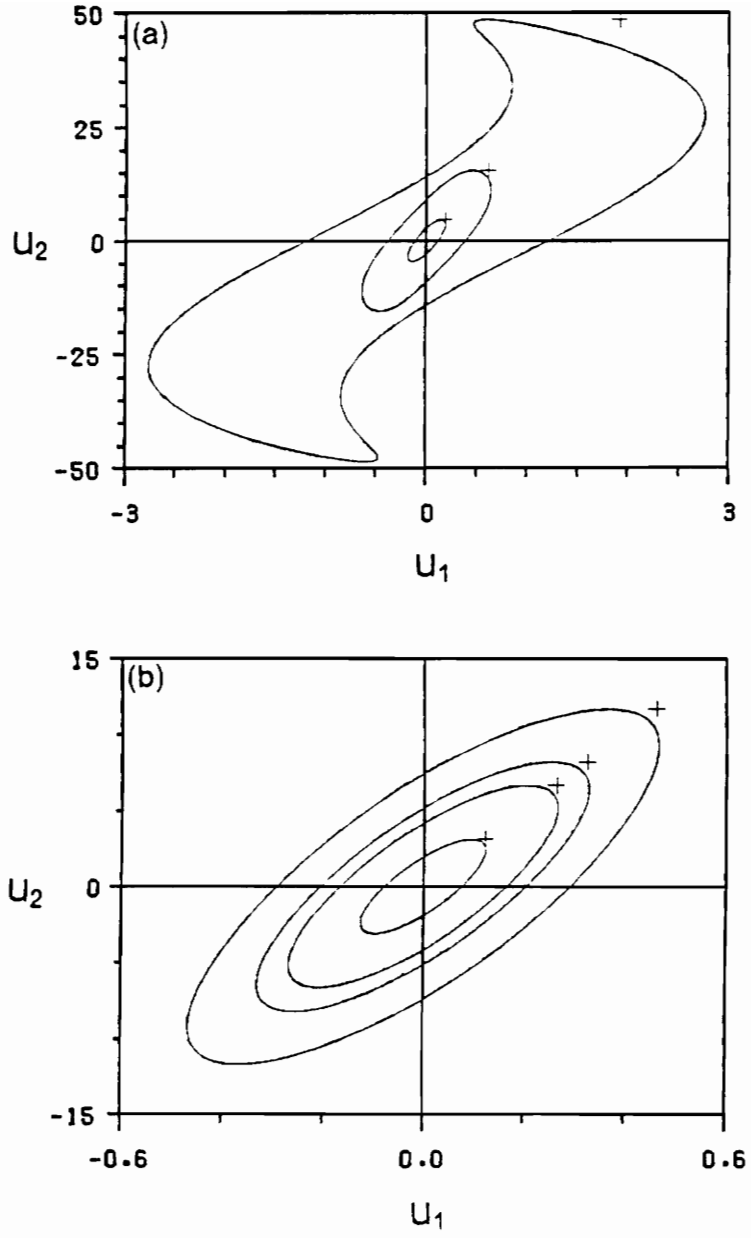

Figure 3.10. Comparison between the numerical time integration of the modulation equations (+) and the original governing equations for $\varepsilon = 0.01$, (a) $\Lambda = 0$, $F = 500$, 5000, and 50000 (outer loop); (b) $F = 500$, $\Lambda = -500$, 1000, 2000, and 5000 (outer loop).

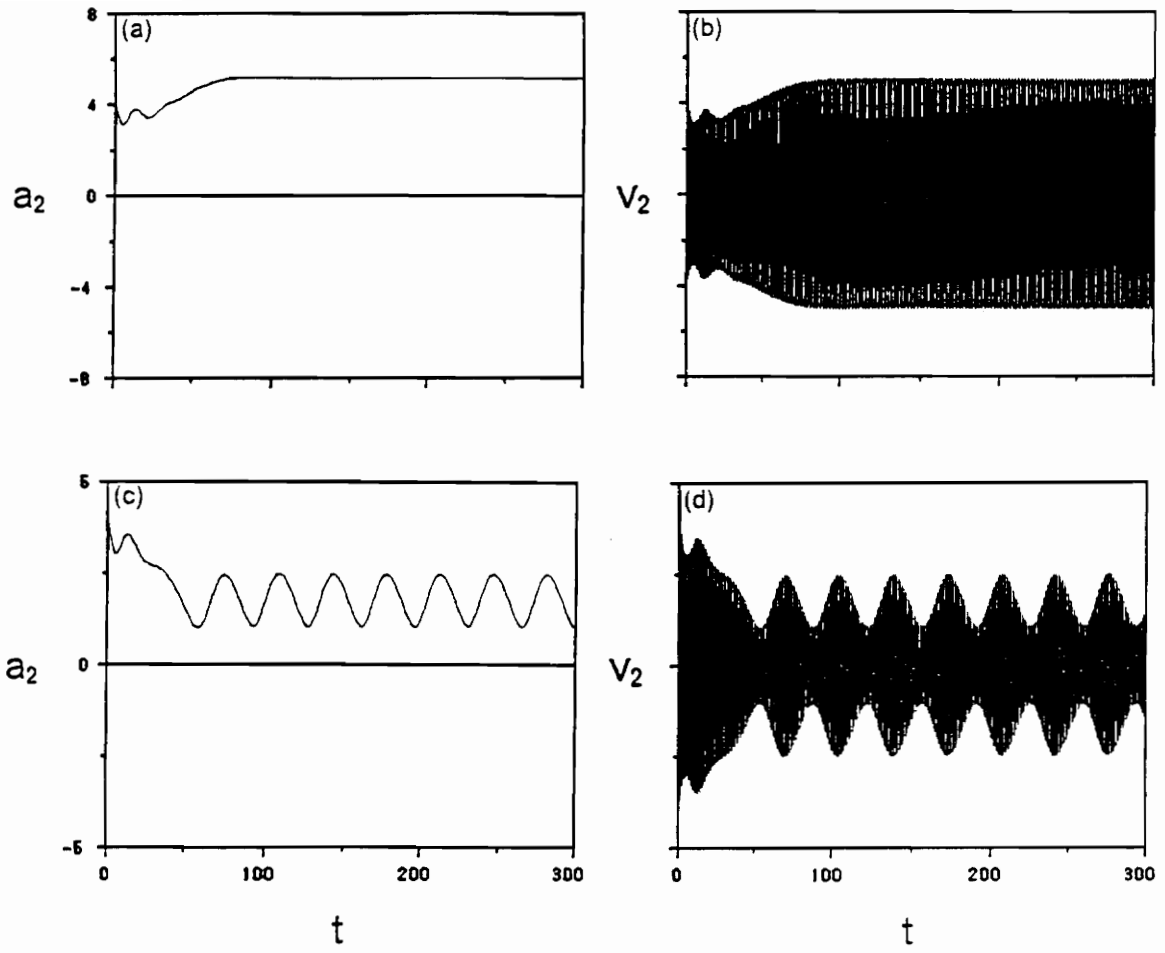

Figure 3.11. Comparison between the numerical time integration of the modulation equations (left) and the original governing equations (right). $(\Lambda,F) = (600,379)$ for (a) and (b); $(\Lambda,F) = (600,329)$ for (c) and (d).

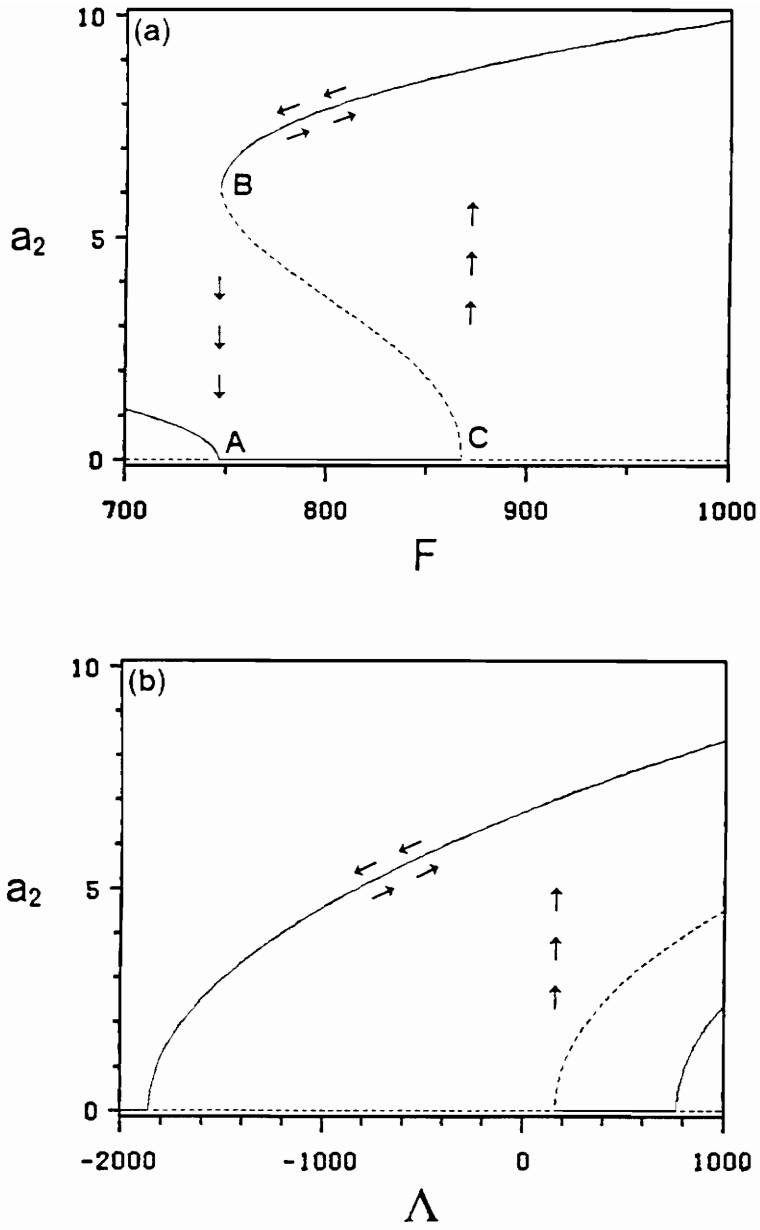

Figure 3.12. (a) The amplitude-response curve for $\Lambda = 709$ and $\sigma^* = -25$; (b) a_2 as a function of Λ for $F = 800$, $\sigma^* = -25$;
___, stable constant solution; ---, unstable constant solution.

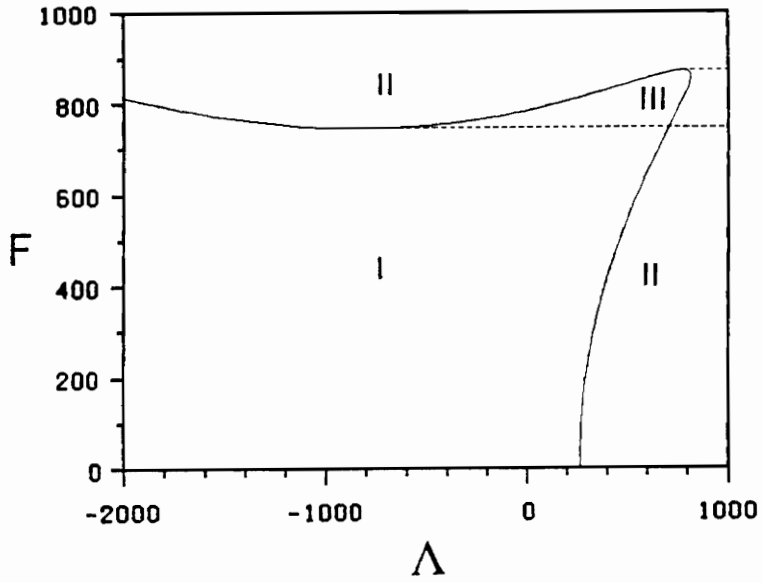

Figure 3.13. Bifurcation diagram for $\sigma^* = -25$; ___, pitchfork bifurcation curve; —, saddle-node bifurcation curve. Region I: stable trivial solutions; region II: unstable trivial solutions; region III: stable trivial solutions and nontrivial constant solutions.

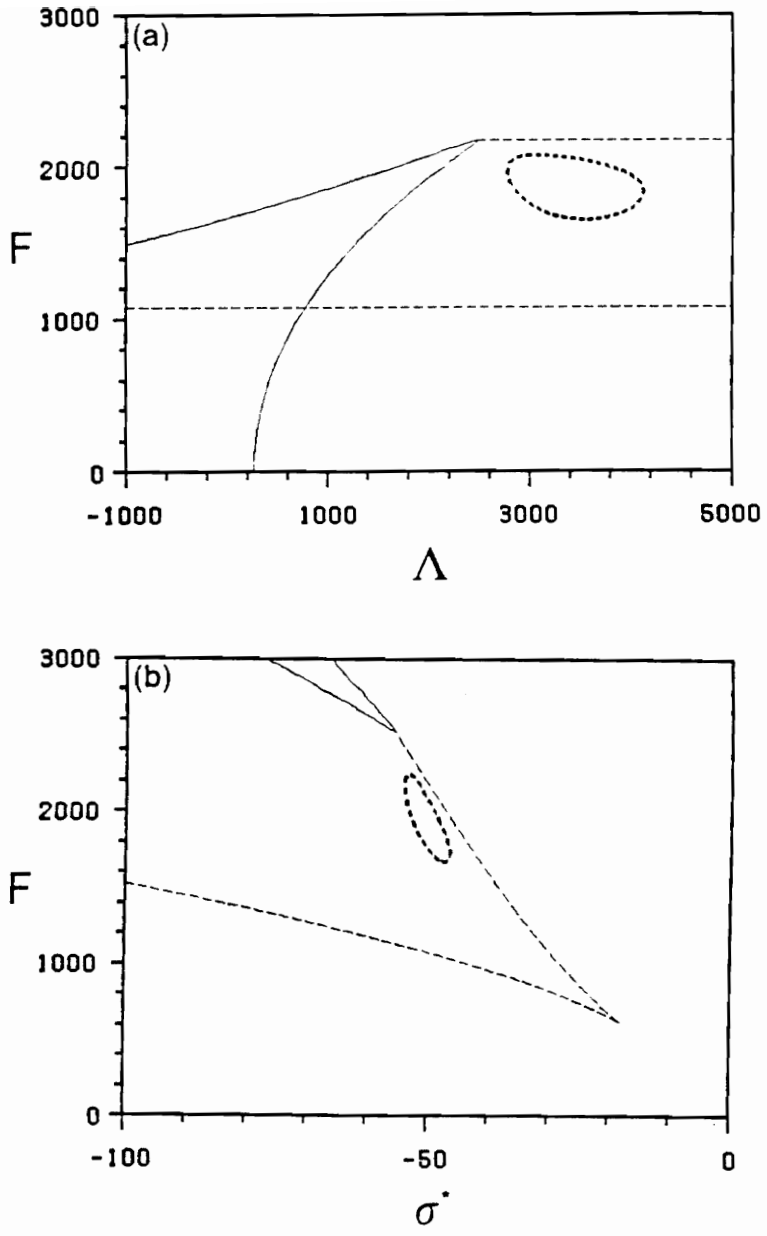

Figure 3.14. Bifurcation diagrams for (a) $\sigma^* = -50$ and (b) $\Lambda = 3000$: ___, pitchfork bifurcation curve; —, saddle-node bifurcation curve; and ---, Hopf bifurcation curve.

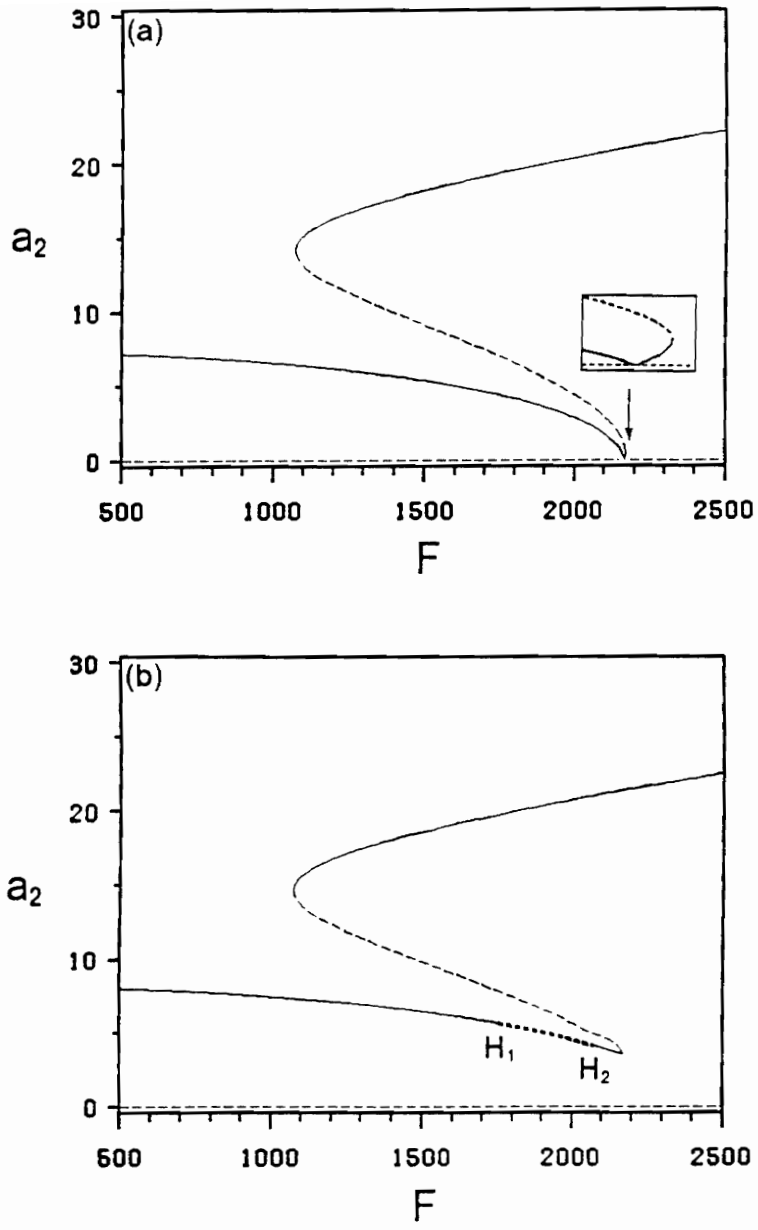

Figure 3.15. The amplitude-response curves for $\sigma^* = -50$ (a) $\Lambda = 2474$, (b) $\Lambda = 3000$: ___, stable constant solution; ---, unstable constant solution; and -·-, stable periodic solution.

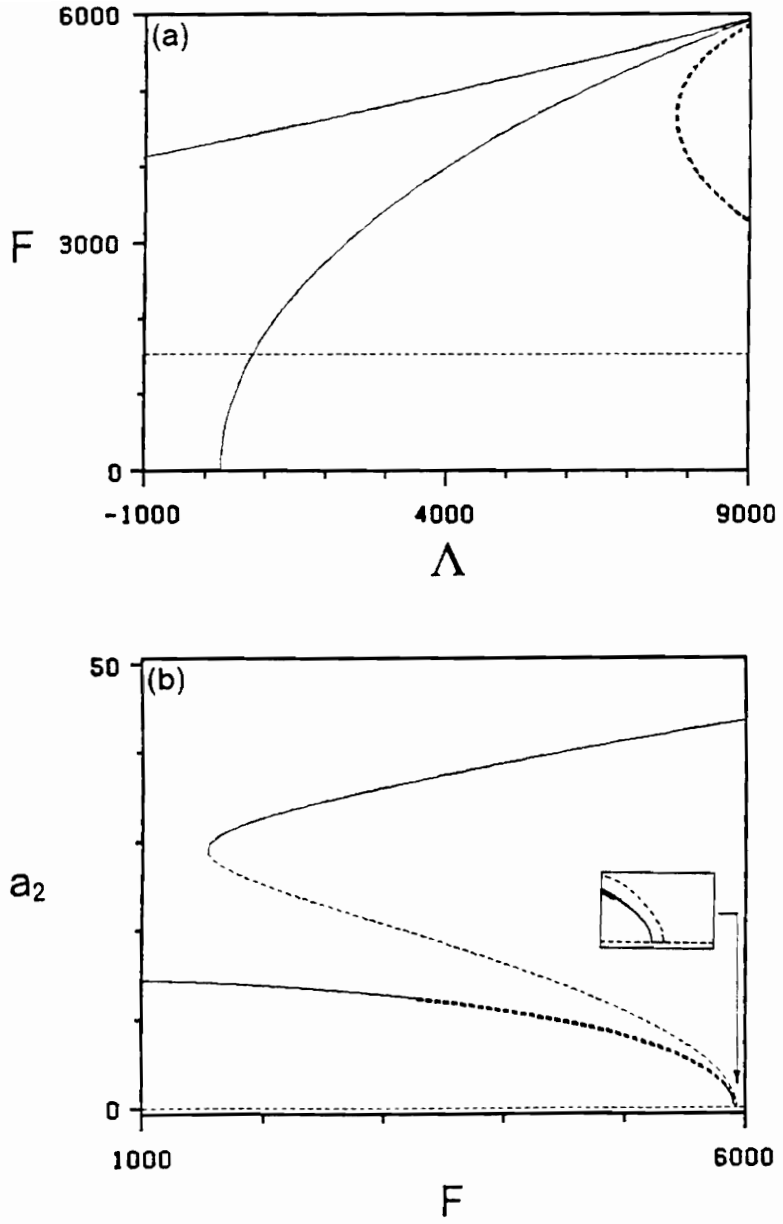

Figure 3.16. (a) Bifurcation diagram for $\sigma^* = -100$; ___, pitchfork bifurcation curve; —, saddle-node bifurcation curve; ---, Hopf bifurcation curve; (b) amplitude-response curve for $\Lambda = 9000$, $\sigma^* = -100$; ___, stable constant solution; ---, unstable constant solution; ▬, unsteady solution.

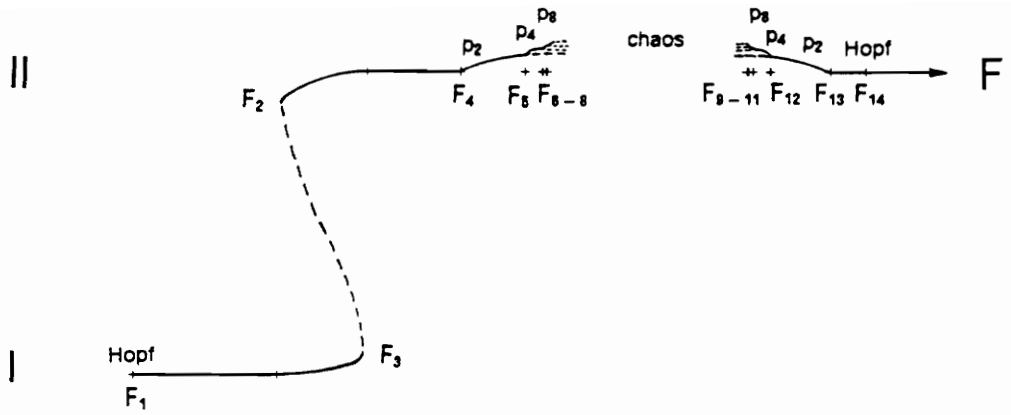

Figure 3.17. A bifurcation diagram illustrating the stages leading to chaos between the Hopf bifurcation values in Figure 3.16(b), where on branch I: F_1(supercritical Hopf) = 3282.3, and F_3(cyclic-fold bifurcation) = 4096.20; on branch II: F_2(cyclic-fold bifurcation) = 3785.96, F_4(p-2) = 4428.58, F_5(p-4) = 4655.78, F_6(p-8) = 4716.88, F_7(p-16) = 4730.93, F_8(p-32) = 4734.03, F_9(p-32) = 5443.06, F_{10}(p-16) = 5447.38, F_{11}(p-8) = 5463.98, F_{12}(p-4) = 5526.08, F_{13}(p-2) = 5737.58, and F_{14}(supercritical Hopf) = 5859.

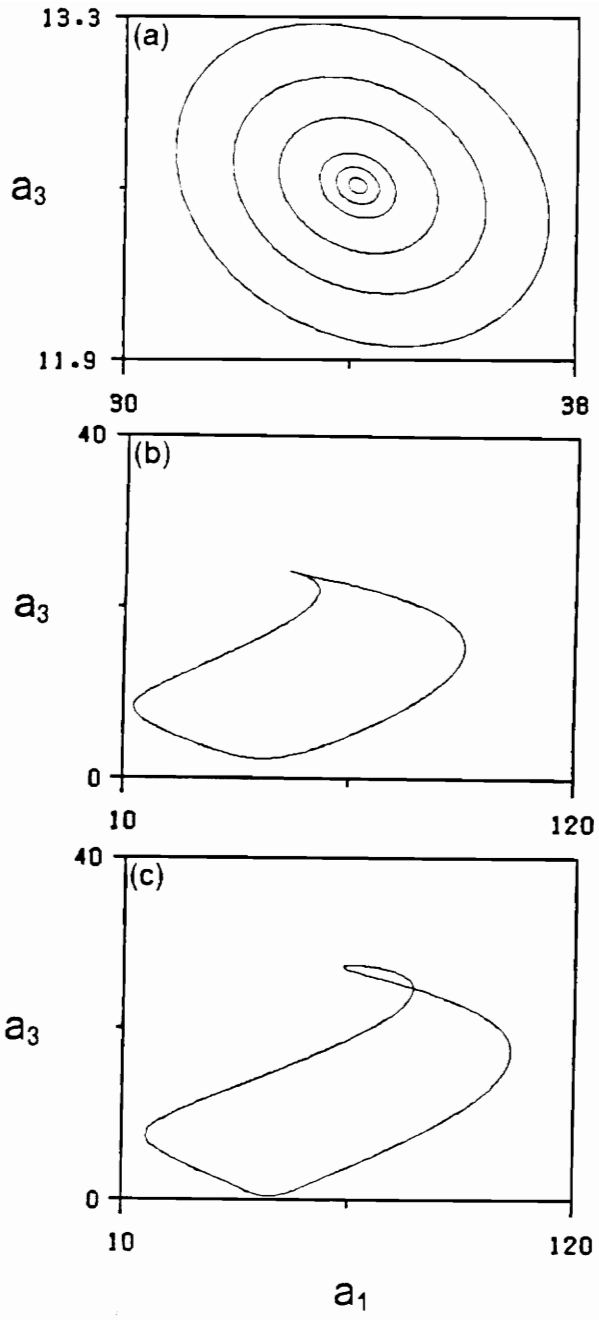

Figure 3.18. Two-dimensional projections of the periodic orbits of branch I onto the $a_3 - a_1$ plane; (a) $F > F_1$ ($F_1 = 3282.3$; from inner to outer loop: $F = 3282.345$, 3282.36, 3282.4, 3282.6, 3283, and 3283.8, respectively.); (b) $F = F_2$; (c) $F = F_3$.

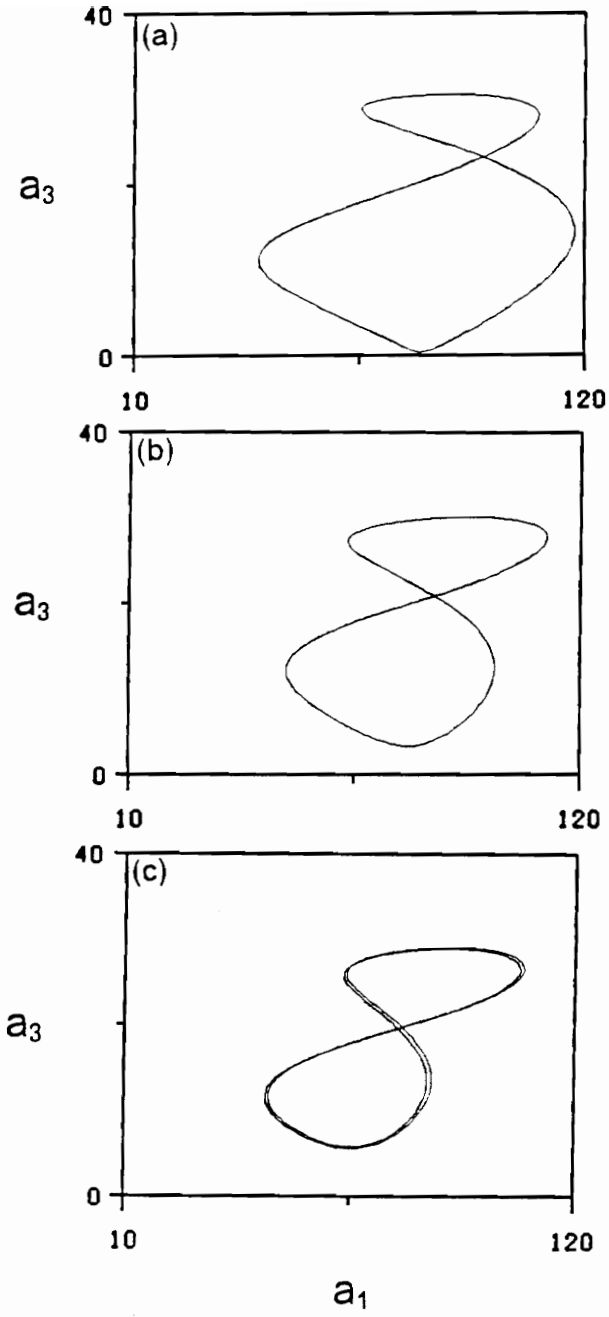

Figure 3.19. Two-dimensional projections of the periodic orbits of branch II onto the $a_3 - a_1$ plane; (a) $F = F_2$; (b) $F = F_3$; (c) $F = F_4$.

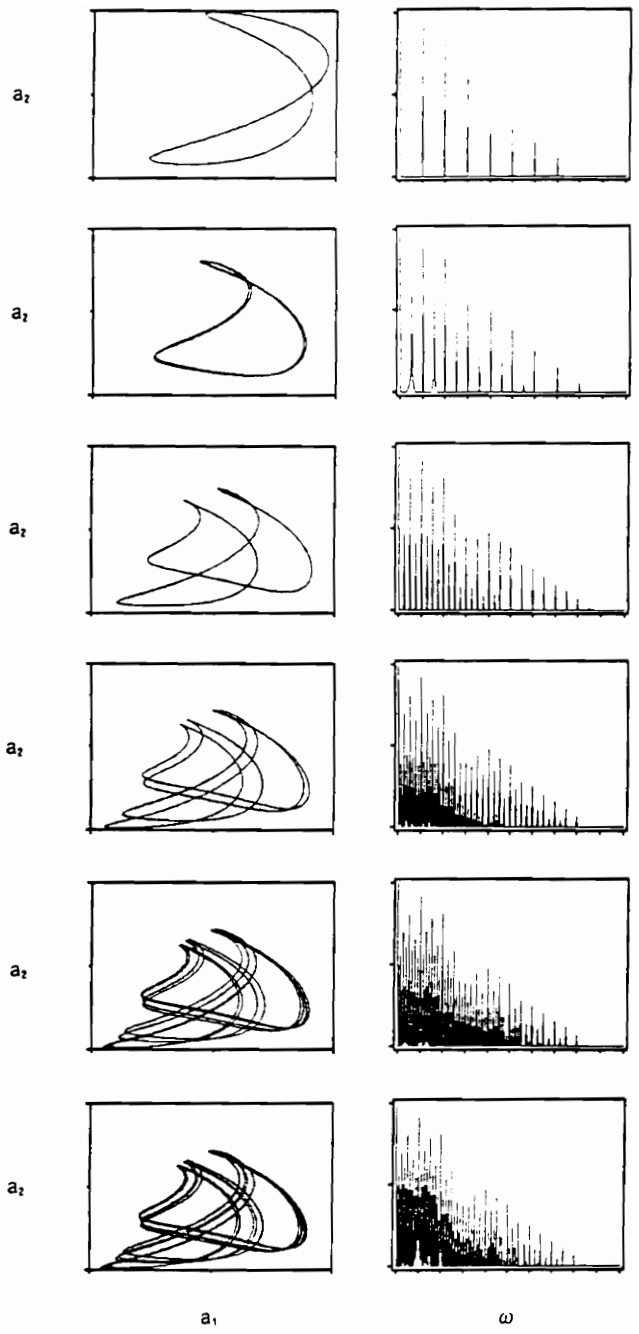

Figure 3.20. A period-doubling sequence from F_2 (top) to F_8 (bottom). (Left): Two-dimensional projections of the periodic orbits onto the $a_2 - a_1$ plane; (right): FFT spectrum of a_2.

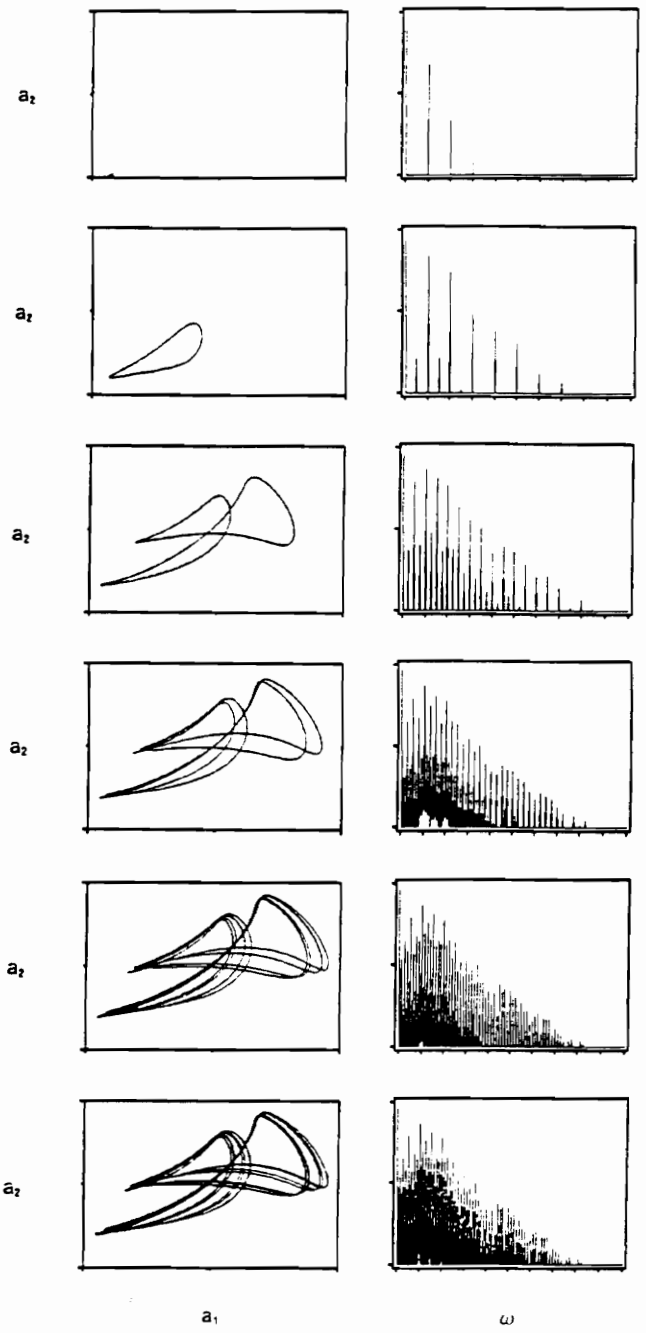

Figure 3.21. A sequence of period-doubling bifurcations from $F = 5858.4$ (top) to F_9 (bottom). (Left): Two-dimensional projections of the periodic orbits onto the $a_2 - a_1$ plane; (right): FFT spectrum of a_2.

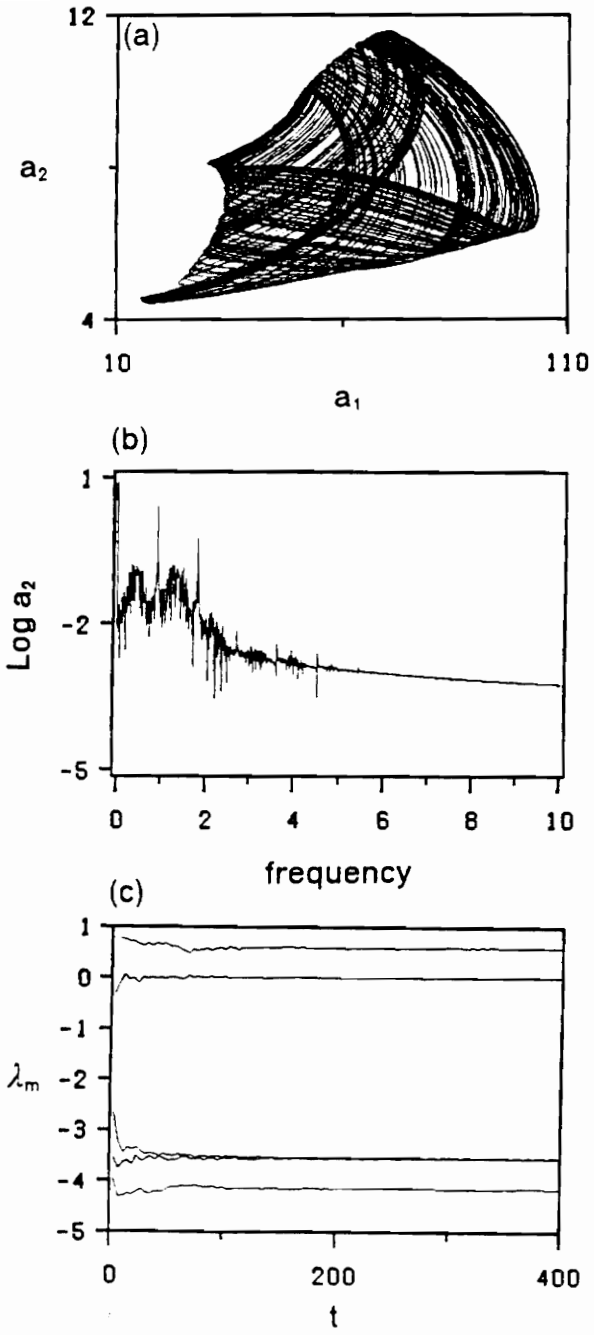

Figure 3.22. (a) A two-dimensional projection of the chaotic attractor onto the $a_2 - a_1$ plane for $F = 5000$; (b) the FFT of a_2; (c) the evolution of the five Lyapunov exponents λ_m with time.

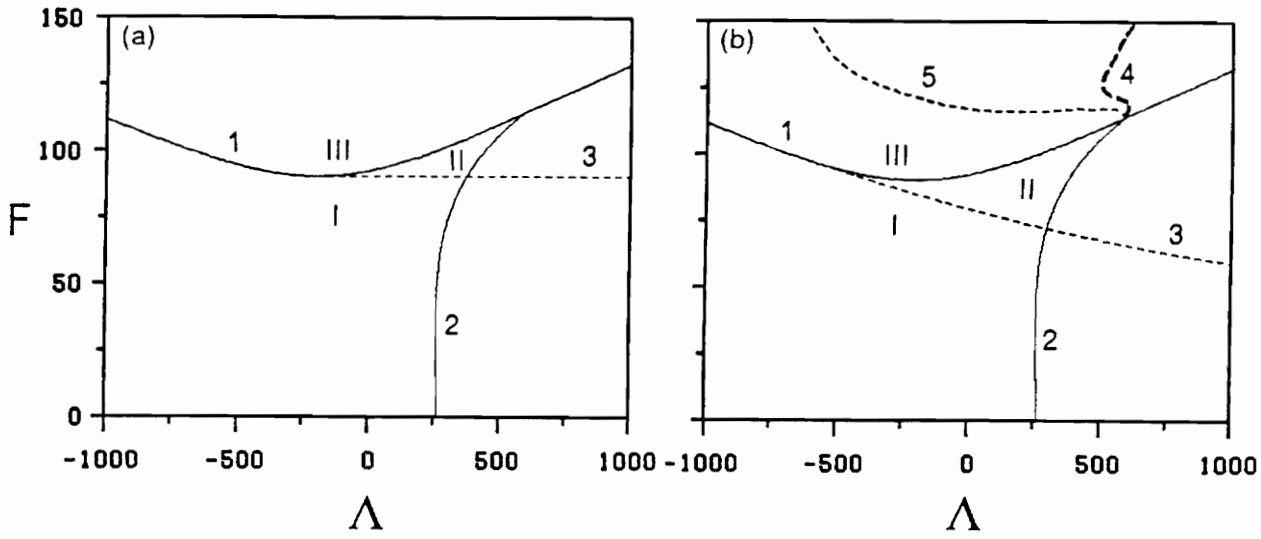

Figure 3.23. Bifurcation diagrams for $\sigma^* = 25$. (a) System I, curve #1: pitchfork bifurcation, #2: Hopf bifurcation, and #3: saddle-node bifurcation. (b) System II, curve #1: transcritical bifurcation, #2: Hopf bifurcation, #3: saddle-node bifurcation, #4: period-doubling bifurcation, and #5: Hopf bifurcation. Region I: stable trivial solutions; region II: coexistence of stable trivial solutions and nontrivial constant solutions; and region III: unstable trivial solutions.

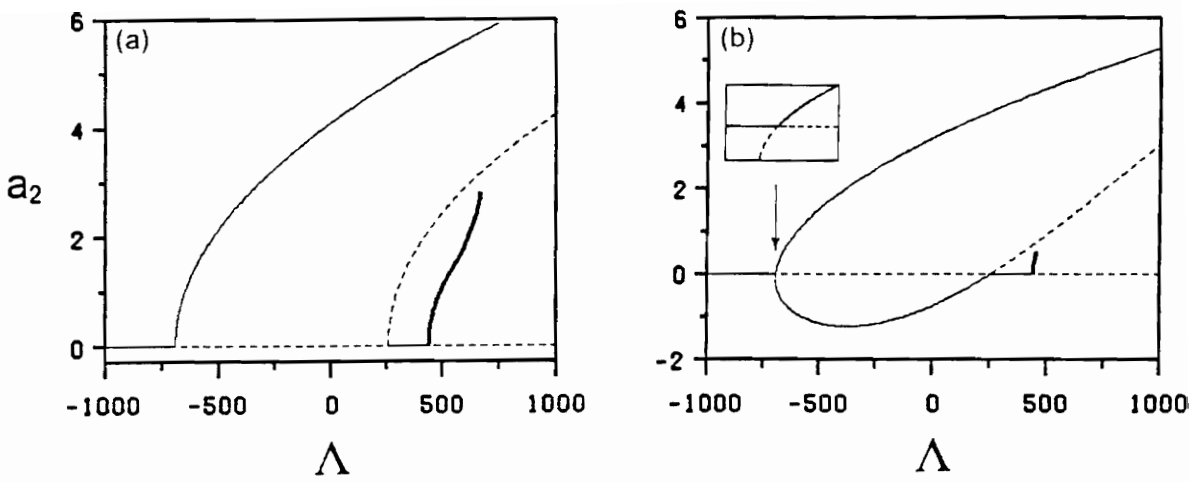

Figure 3.24. Variation of a_2 with Λ at $\sigma^* = 25$ and $F = 100$ for (a) system I and (b) system II:
___, stable constant solution; ---, unstable constant solution; and —, mean amplitude of the periodic solution.

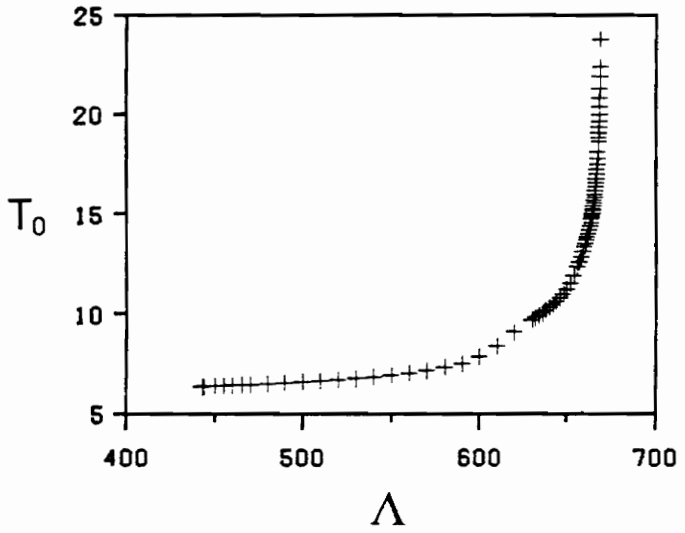

Figure 3.25. Variation of the period of the limit cycle (Figure 3.24a) with Λ.

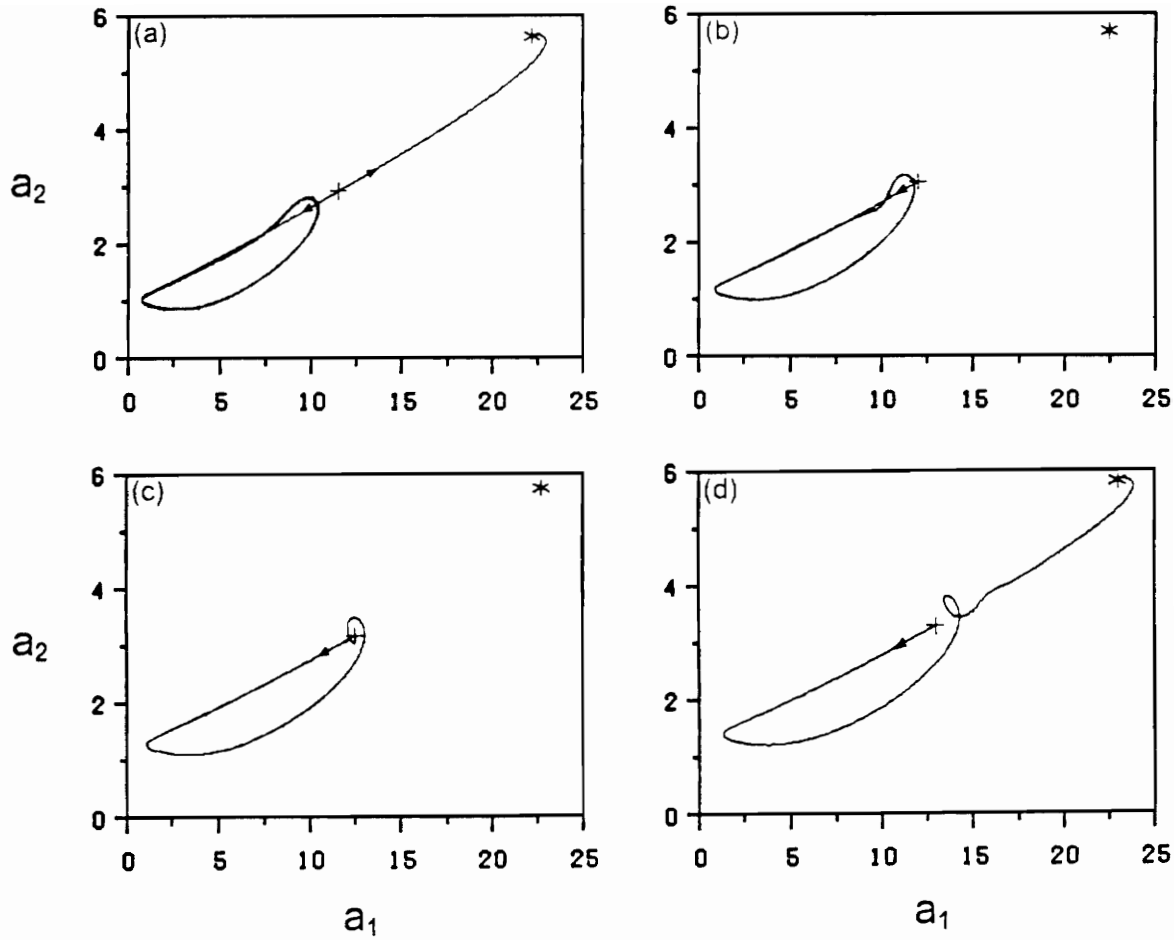

Figure 3.26. A two-dimensional projection of the unstable manifold of the saddle focus onto the $a_2 - a_1$ plane at $F = 100$ and $\Lambda =$ (a) 610 (both directions are included); (b) 640; (c) 669.1907; (d) 700 for system I. + denotes a saddle and * denotes a sink.

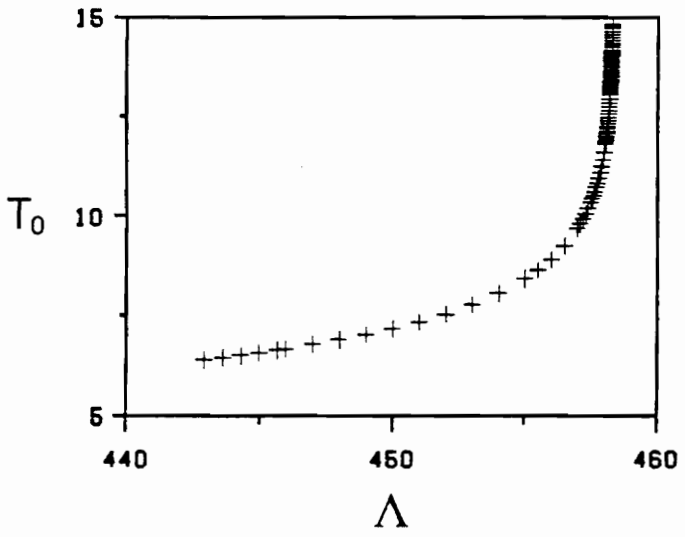

Figure 3.27. Variation of the period of the limit cycle (Figure 3.24b) with Λ.

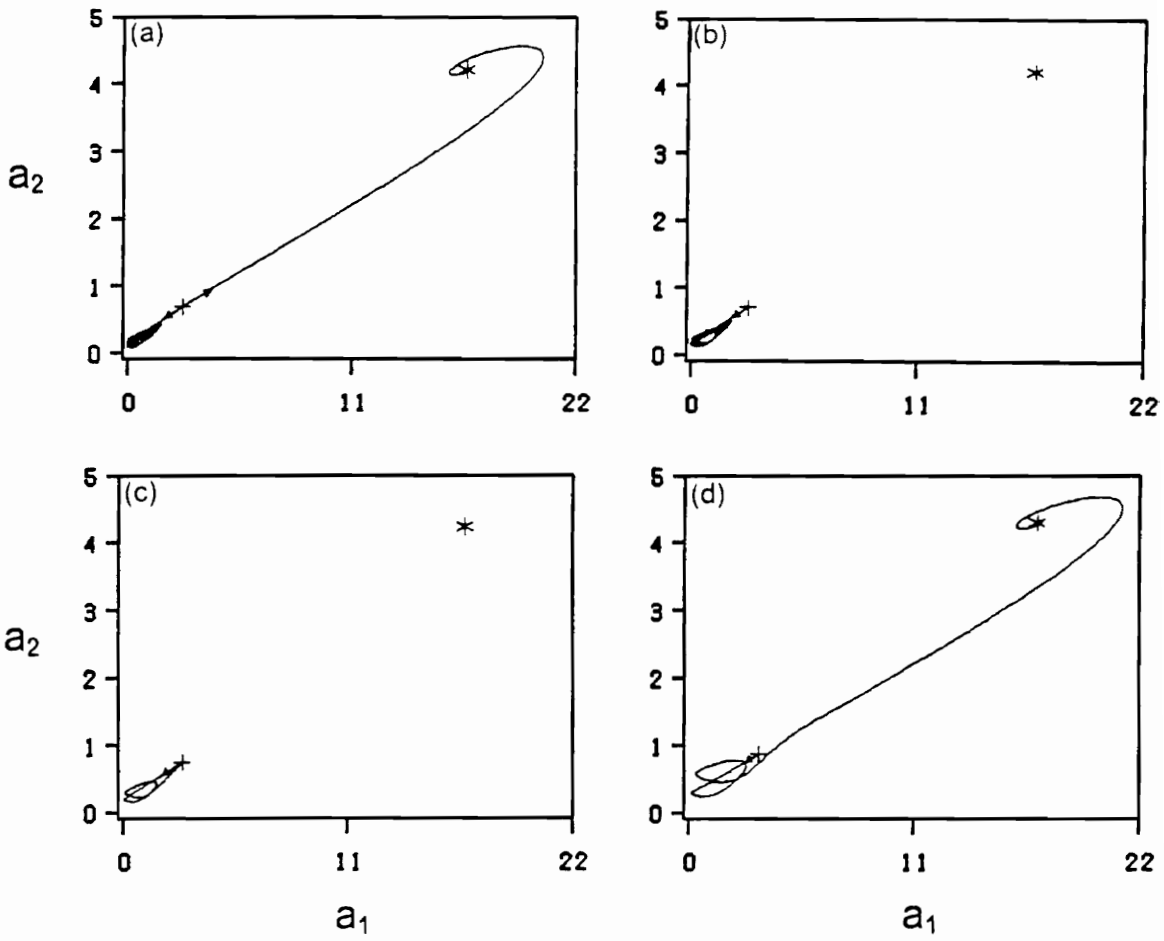

Figure 3.28. A two-dimensional projection of the unstable manifold of the saddle focus onto the $a_2 - a_1$ plane at $F = 100$ and $\Lambda =$ (a) 445 (both directions are included); (b) 450; (c) 458.3363; (d) 490 for system II. + denotes a saddle and * denotes a sink.

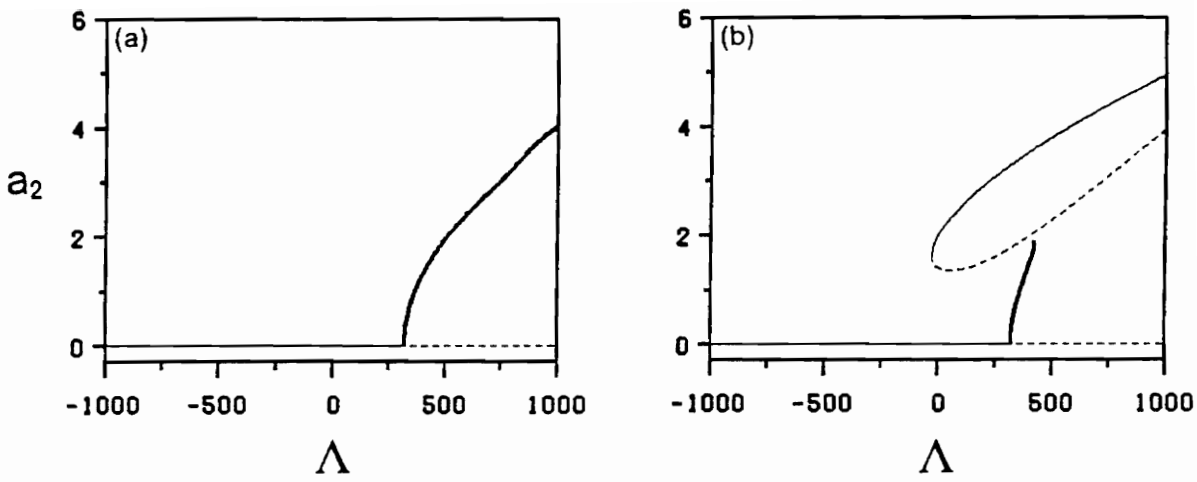

Figure 3.29. Variation of a_2 with Λ at $\sigma^* = 25$ and $F = 80$ for (a) system I and (b) system II:
___, stable constant solution; ---, unstable constant solution; and —, mean amplitude of the periodic solution.

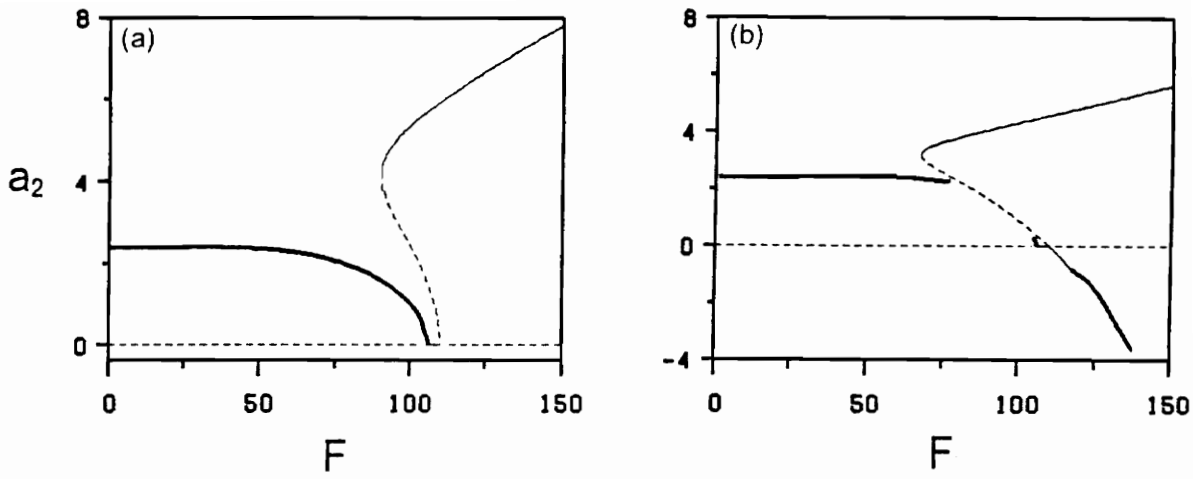

Figure 3.30. Variation of a_2 with F at $\sigma^* = 25$ and $\Lambda = 500$ for (a) system I and (b) system II:

___, stable constant solution; ---, unstable constant solution; and —, mean amplitude of the periodic solution.

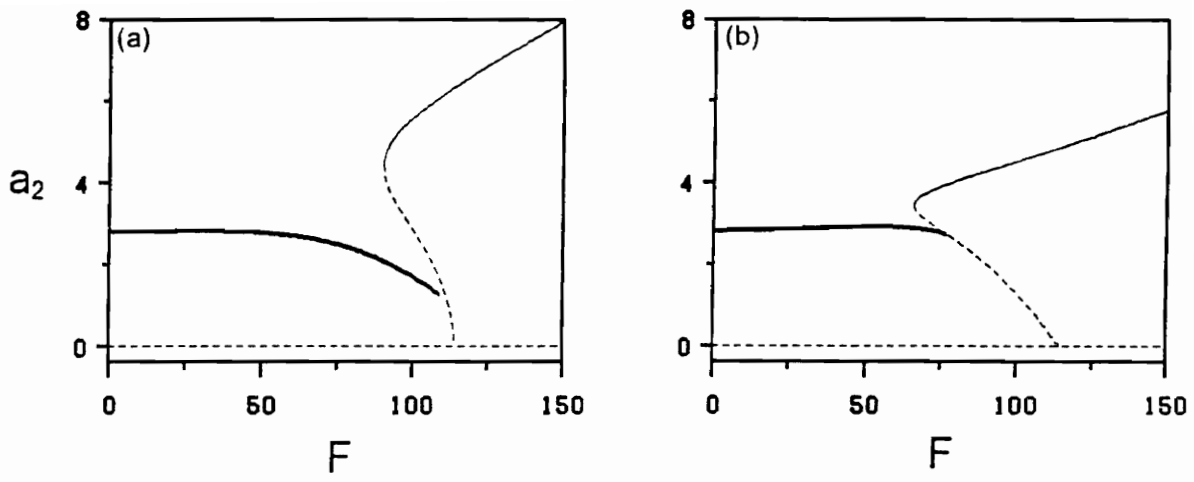

Figure 3.31. Variation of a_2 with F at $\sigma^* = 25$ and $\Lambda = 592.37$ for (a) system I and (b) system II:
___, stable constant solution; ---, unstable constant solution; and —, mean amplitude of the periodic solution.

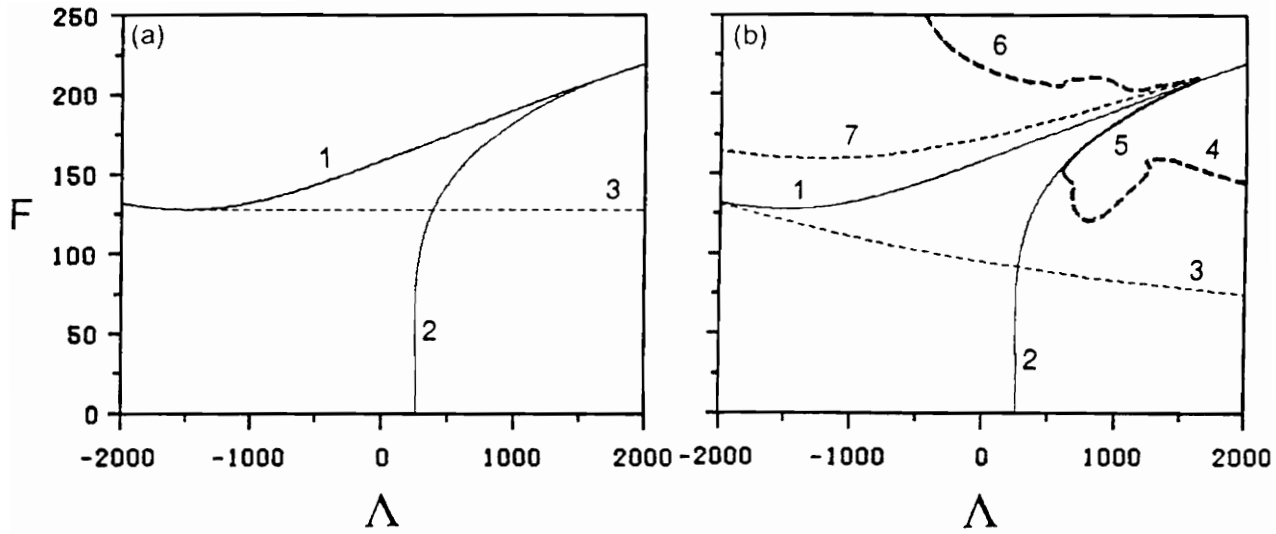

Figure 3.32. Bifurcation diagrams for $\sigma^* = 50$. (a) System I, curve #1: pitchfork bifurcation, #2: Hopf bifurcation, and #3: saddle-node bifurcation. (b) System II, curve #1: transcritical bifurcation, #2: Hopf bifurcation, #3: saddle-node bifurcation, #4: period-doubling bifurcation, #5: cyclic-fold bifurcation, #6: period-doubling bifurcation, and #7: Hopf bifurcation.

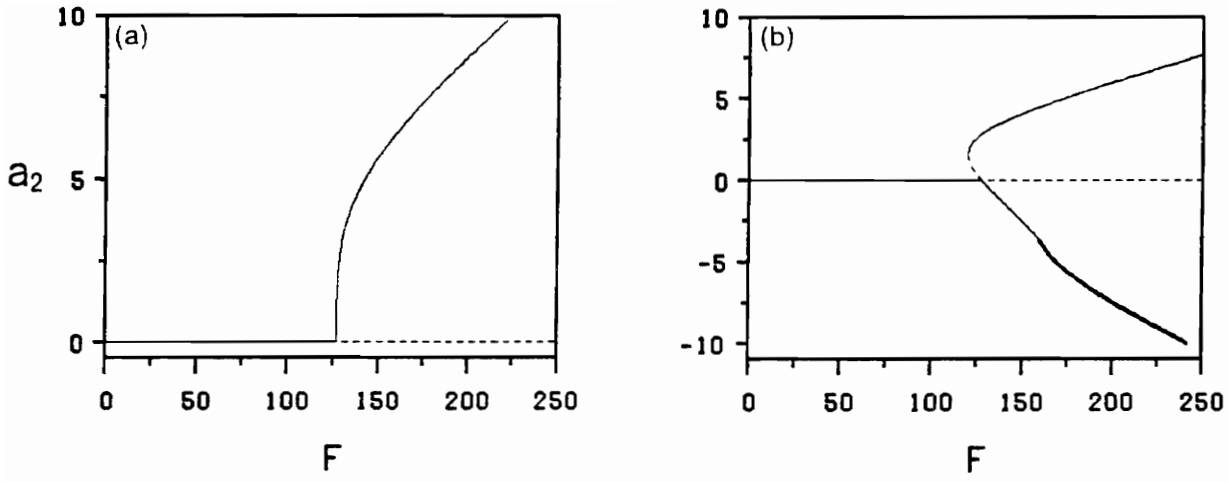

Figure 3.33. Variation of a_2 with F at $\sigma^* = 50$ and $\Lambda = -1500$ for (a) system I and (b) system II.
___, Stable constant solution; ---, unstable constant solution; and —, mean amplitude of the periodic solution.

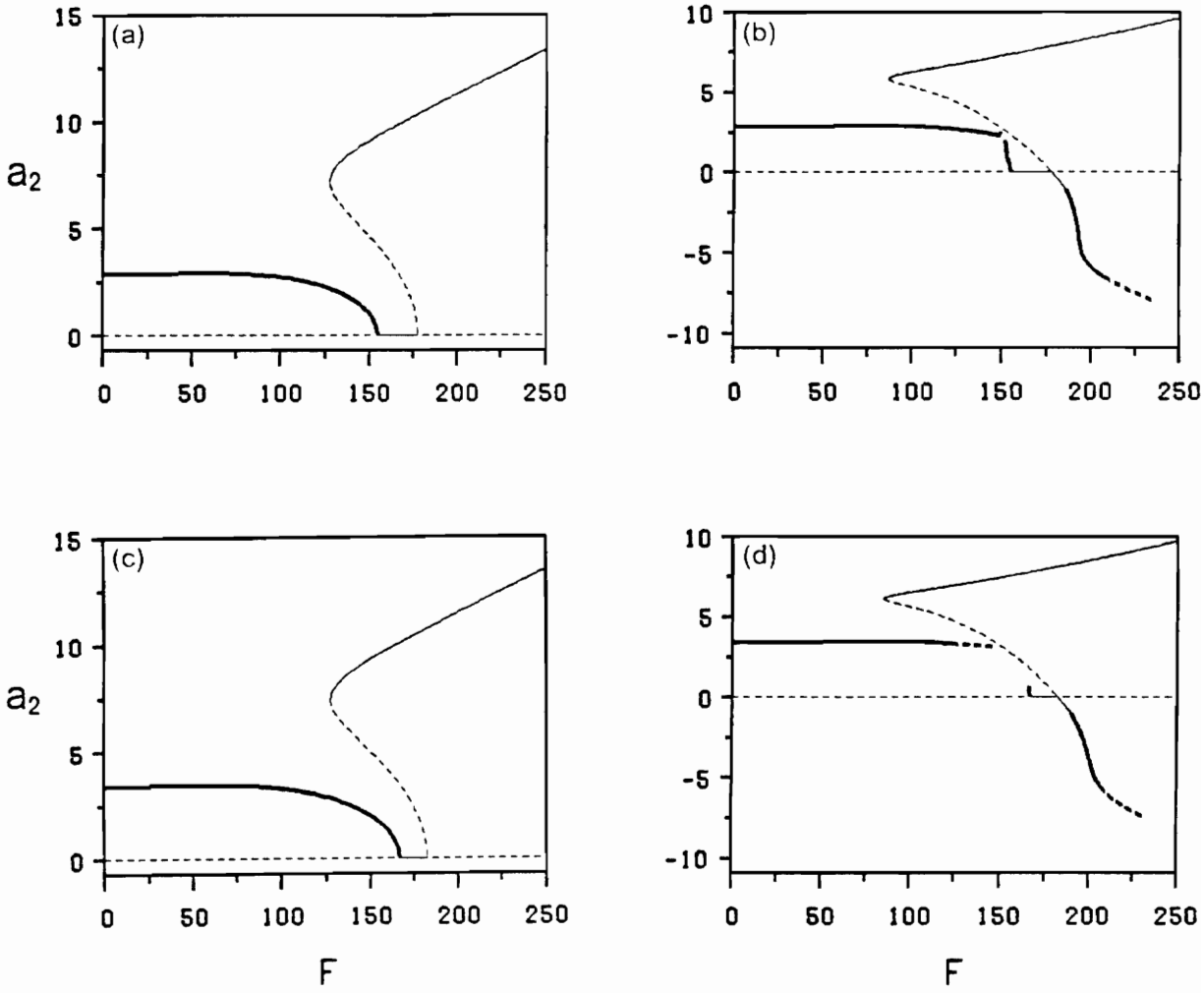

Figure 3.34. Variation of a_2 with F at $\sigma^* = 50$. $\Lambda = 606$ for (a) system I and (b) system II; $\Lambda = 750$ for (c) system I and (d) system II. ___, Stable constant solution; —, unstable constant solution; and — , mean amplitude of the periodic solution.

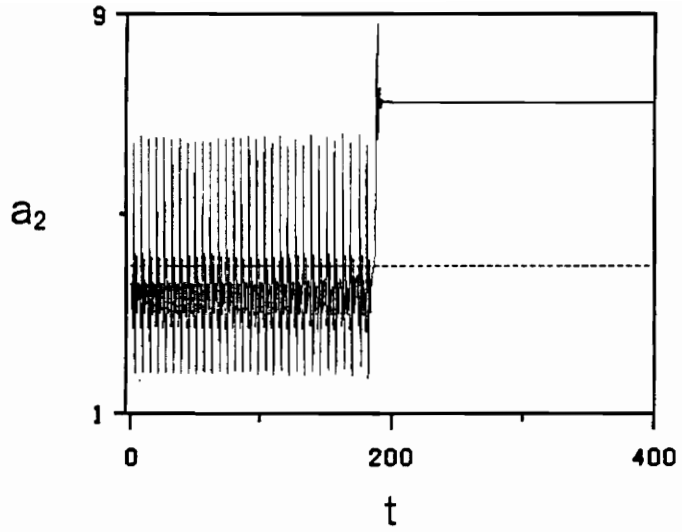

Figure 3.35. The time history of a_2 at $\sigma^* = 50$, $\Lambda = 750$, and $F = 139.1$, where a crisis occurs.

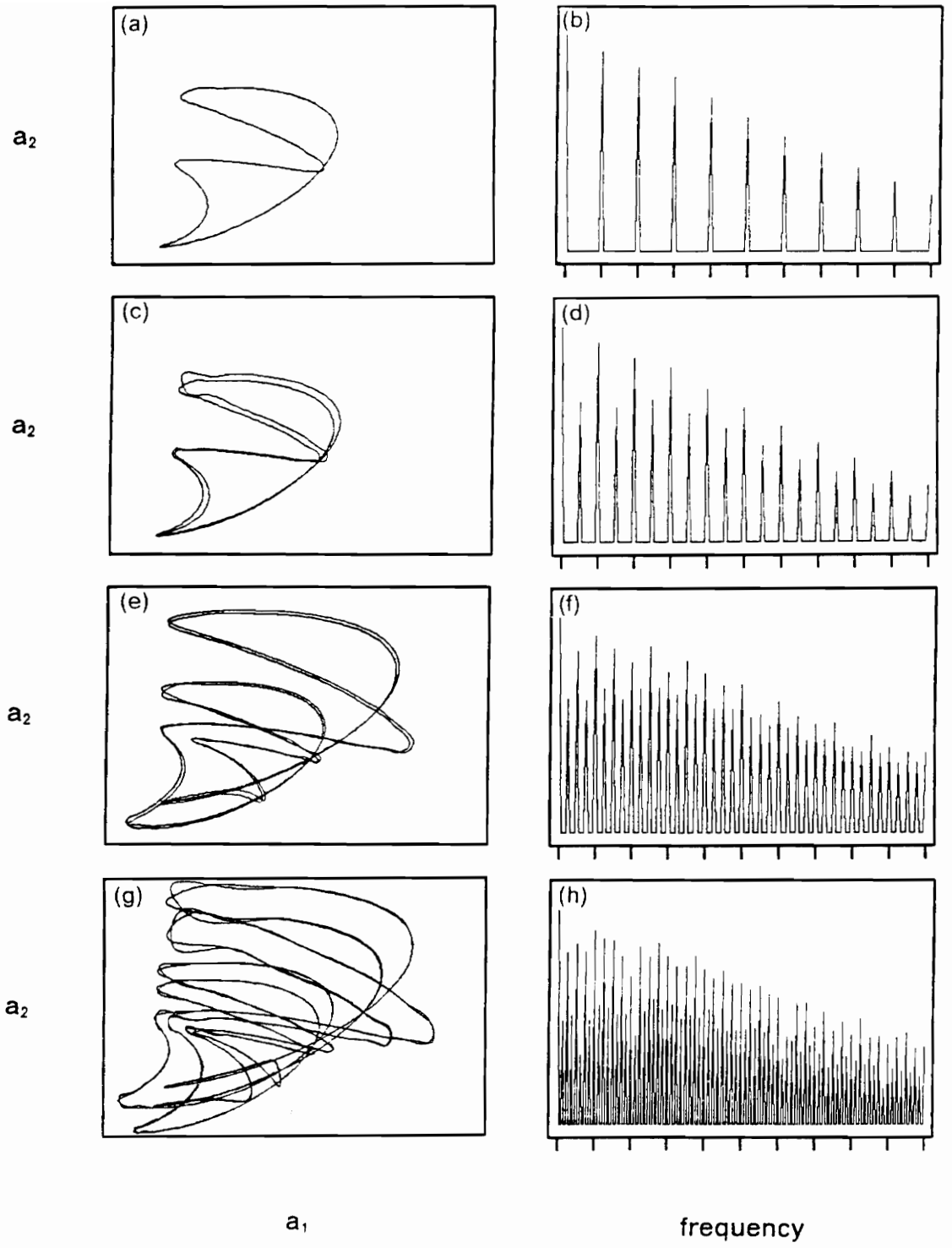

Figure 3.36. A period-doubling sequence leading to chaos at $\sigma^* = 50$ and $\Lambda = 900$. (Left): Two-dimensional projections of the periodic orbits onto the $a_2 - a_1$ plane; (right): FFT spectrum of a_2; (a,b) p-1, $F = 124.3$, (c,d) p-2, $F = 124.4$, (e,f) p-4, $F = 137.6$, and (g,h) p-8, $F = 139.15$.

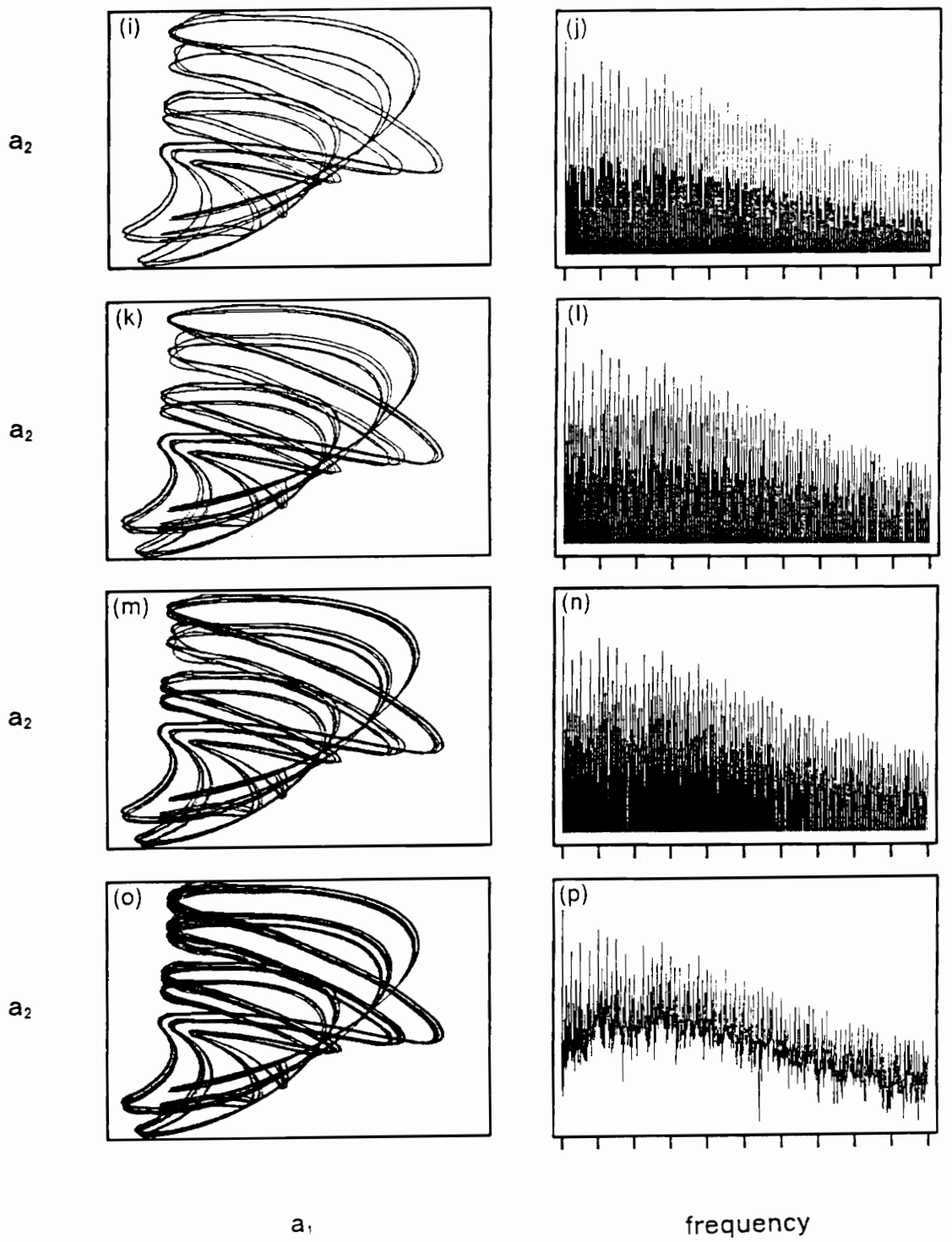

Figure 3.36. continued, (i,j) p-16, F = 139.332, (k,l) p-32, F = 139.3703, (m,n) p-64, F = 139.3787, and (o,p) chaos, F = 139.385.

CHAPTER 4

SYSTEMS WITH WIDELY SPACED MODAL FREQUENCIES

A modal discretization is commonly used in the analysis of weakly nonlinear continuous systems. We always rely on a general knowledge of modal interactions to select the modes necessary to represent the response. Hence, it is essential for us to understand the nature of all possible modal interactions. In this chapter, we consider the response of two nonlinearly coupled oscillators with widely spaced frequencies when the high-frequency mode is excited by a principal parametric resonance. Specifically, we consider the system

$$\ddot{u}_1 + 2\mu_1\omega_1\dot{u}_1 + \omega_1^2 u_1 = -\left(\alpha_1 u_1^3 + \alpha_2 u_1 u_2^2\right) \tag{4.1}$$

$$\ddot{u}_2 + 2\hat{\mu}_2\omega_2\dot{u}_2 + \omega_2^2 u_2 = \alpha_3 u_2^3 + \alpha_4 u_1^2 u_2 + u_2 f \cos\Omega t \tag{4.2}$$

where $\omega_1^*/\omega_2^* \ll 1$. The system has linear viscous damping given by the coefficients μ_1 and $\hat{\mu}_2$, cubic nonlinearities with the coefficients α_i^*, and a parametric excitation $f\cos\Omega^* t^*$, which is applied only to the high-frequency mode. Nayfeh and Nayfeh (1993b) studied the same system when the high-frequency mode is excited by a primary resonance. In this chapter, we use the method of averaging to investigate the solutions of Eqs. (4.1) and (4.2) when $\Omega^* \approx 2\omega_2^*$. The averaged equations are used to determine the conditions under which energy can be transferred from the high-frequency mode to the low-frequency mode. After an oscillation in the low-frequency mode occurs, we use numerical simulations to investigate some of the complexities in the system response.

4.1 Modulation Equations

To identify the relative sizes of the various terms in the equations, we first introduce dimensionless variables given by

$$t = \omega_2^* t^*, \quad u_1^* = c_1^* u_1, \quad u_2^* = c_2^* u_2, \quad \text{and} \quad \Omega^* = \omega_2^* \Omega \tag{4.3}$$

and a small dimensionless parameter

$$\varepsilon = \omega_1^*/\omega_2^* \tag{4.4}$$

Substituting these dimensionless variables into Eqs. (4.1) and (4.2) yields

$$\ddot{u}_1 + 2\varepsilon\mu_1\dot{u}_1 + \varepsilon^2 u_1 = -\varepsilon^2\left(4\alpha_1 u_1^3 + \alpha_2 u_1 u_2^2\right) \tag{4.5}$$

$$\ddot{u}_2 + 2\varepsilon\mu_2\dot{u}_2 + u_2 = \varepsilon\left(\alpha_3 u_2^3 + \alpha_4 u_1^2 u_2 + u_2 f\cos\Omega t\right) \tag{4.6}$$

where

$$\alpha_1 = \frac{c_1^{*2}\alpha_1^*}{4\omega_1^{*2}}, \quad \alpha_2 = \frac{c_2^{*2}\alpha_2^*}{\omega_1^{*2}}, \quad \alpha_3 = \frac{c_2^{*2}\alpha_3^*}{\omega_1^*\omega_2^*},$$
$$\alpha_4 = \frac{c_1^{*2}\alpha_4^*}{\omega_1^*\omega_2^*}, \quad \mu_2 = \frac{\hat{\mu}_2}{\varepsilon}, \quad \text{and} \quad f = \frac{f^*}{\omega_1^*\omega_2^*} \tag{4.7}$$

For the case of principal parametric resonance of the high-frequency mode, we introduce a detuning parameter σ defined by

$$\frac{1}{4}\Omega^2 = 1 + \varepsilon\sigma \tag{4.8}$$

We apply the variation of parameters transformation

$$u_2 = a(t)\cos\phi \tag{4.9}$$

$$\dot{u}_2 = -\frac{1}{2}a(t)\Omega\sin\phi \tag{4.10}$$

$$\phi = \frac{1}{2}\left[\Omega t + \beta(t)\right] \tag{4.11}$$

to Eqs. (4.5) and (4.6) and obtain

$$\ddot{u}_1 + 2\varepsilon\mu_1\dot{u}_1 + \varepsilon^2 u_1 = -\varepsilon^2\left(4\alpha_1 u_1^3 + \alpha_2 u_1 a^2\cos^2\phi\right) \tag{4.12}$$

$$\dot{a} = -\varepsilon\frac{2g}{\Omega}\sin\phi \tag{4.13}$$

$$a\dot{\beta} = -\varepsilon \frac{4g}{\Omega} \cos \phi \tag{4.14}$$

where

$$\begin{aligned} g = {} & \sigma a \cos \phi + \mu_2 a\Omega \sin \phi + \alpha_3 a^3 \cos^3 \phi \\ & + \alpha_4 u_1^2 a \cos \phi + af \cos \phi \cos \Omega t \end{aligned} \tag{4.15}$$

It follows from Eq. (4.12) that whereas u_1 is $O(1)$, $\dot{u}_1$ is $O(\varepsilon)$ and $\ddot{u}_1$ is $O(\varepsilon^2)$. Therefore, Eq. (4.12) can be rewritten as a pair of first-order equations as

$$\dot{u}_1 = \varepsilon v_1 \tag{4.16}$$

$$\dot{v}_1 = -\varepsilon\left(u_1 + 2\mu_1 v_1 + 4\alpha_1 u_1^3 + \alpha_2 u_1 a^2 \cos^2 \phi\right) \tag{4.17}$$

It follows from Eqs. (4.13), (4.14), (4.16), and (4.17) that u_1, v_1, a, and β are slowly varying. Consequently, averaging these equations from 0 to $2\pi/\Omega$, we obtain the modulation equations

$$\dot{a} = -\varepsilon a(\mu_2 + \frac{1}{4} f \sin \beta) \tag{4.18}$$

$$a\dot{\beta} = -\varepsilon a(\sigma + \frac{3}{4} \alpha_3 a^2 + \alpha_4 u_1^2 + \frac{1}{2} f \cos \beta) \tag{4.19}$$

$$\dot{u}_1 = \varepsilon v_1 \tag{4.20}$$

$$\dot{v}_1 = -\varepsilon(u_1 + 2\mu_1 v_1 + 4\alpha_1 u_1^3 + \frac{1}{2} \alpha_2 u_1 a^2) \tag{4.21}$$

where we have set $\Omega = 2$. Because ε appears as a common factor in the right-hand sides of Eqs. (4.18)-(4.21), the character of the motion does not depend on the value

of ε. While ε must be small for the averaging approximation to be valid, its value only determines the speed at which the motion evolves; the amplitude and stability of the response are independent of its value.

4.2 Fixed Points and Their Stability

The fixed points of the modulation equations (4.18)-(4.21) represent periodic motions of the high-frequency mode accompanied by static responses of the low-frequency mode. Setting the time derivatives in Eqs. (4.18)-(4.21) equal to zero, we obtain two types of fixed points: $a = 0$ or $a \neq 0$.

4.2.1 Fixed Points with $a = 0$

It is convenient to use the Cartesian form for $u_2(t)$ in studying the stability of the trivial fixed point of the high-frequency mode. To this end, we introduce the transformation

$$p = a\cos\frac{1}{2}\beta \quad \text{and} \quad q = -a\sin\frac{1}{2}\beta \tag{4.22}$$

into Eqs. (4.18)-(4.21) and obtain

$$\dot{p} = -\varepsilon\left[\mu_2 p + \left(\frac{1}{2}\sigma - \frac{1}{4}f\right)q + \frac{3}{8}\alpha_3 q\left(p^2+q^2\right) + \frac{1}{2}\alpha_4 u_1^2 q\right] \tag{4.23}$$

$$\dot{q} = -\varepsilon\left[\mu_2 q - \left(\frac{1}{2}\sigma + \frac{1}{4}f\right)p - \frac{3}{8}\alpha_3 p\left(p^2+q^2\right) - \frac{1}{2}\alpha_4 u_1^2 p\right] \tag{4.24}$$

$$\dot{u}_1 = \varepsilon v_1 \tag{4.25}$$

$$\dot{v}_1 = -\varepsilon\left[u_1 + 2\mu_1 v_1 + 4\alpha_1 u_1^3 + \frac{1}{2}\alpha_2 u_1 (p^2 + q^2)\right] \tag{4.26}$$

Solving for the fixed points from Eqs. (4.25) and (4.26) when $p = q = 0$ gives

$$v_1 = 0 \quad \text{and either} \quad u_1 = 0 \quad \text{or} \quad \pm\sqrt{-\frac{1}{4\alpha_1}} \tag{4.27}$$

To determine the stability of the fixed point (p, q, u_1, v_1) = (0, 0, 0, 0), we evaluate the Jacobian matrix of Eqs. (4.23)-(4.26) at this point, solve for the eigenvalues, and obtain

$$\lambda = -\varepsilon\left(\mu_2 \pm \sqrt{\frac{f^2}{16} - \frac{\sigma^2}{4}}\right), \quad -\varepsilon\left(\mu_1 \pm \sqrt{\mu_1^2 - 1}\right) \tag{4.28}$$

Hence, the trivial solution is asymptotically stable when $f^2 < 4(\sigma^2 + 4\mu_2^2)$ and unstable when $f^2 > 4(\sigma^2 + 4\mu_2^2)$, provided that the μ_i are positive. A pitchfork bifurcation occurs at $f^2 = 4(\sigma^2 + 4\mu_2^2)$. The eigenvalues of the Jacobian matrix evaluated at the fixed point (p, q, u_1, v_1) = $\left(0, 0, \pm\sqrt{-\frac{1}{4\alpha_1}}, 0\right)$ and $\alpha_1 < 0$ are

$$\lambda = -\varepsilon\left(\mu_2 \pm \sqrt{\frac{f^2}{16} - \left(\frac{\sigma}{2} - \frac{\alpha_4}{8\alpha_1}\right)^2}\right), \quad -\varepsilon\left(\mu_1 \pm \sqrt{\mu_1^2 + 2}\right) \tag{4.29}$$

Therefore, this fixed point is a saddle since one of the λ_j is always real and positive.

4.2.2 Fixed Points with $a \neq 0$

Setting the right-hand sides of Eqs. (4.18)-(4.21) equal to zero and solving for σ and u_1 in terms of a, we obtain

$$\sigma = -\frac{3}{4}\alpha_3 a^2 - \alpha_4 u_1^2 \pm \sqrt{\frac{f^2}{4} - 4\mu_2^2} \tag{4.30}$$

$$u_1 = 0 \quad \text{or} \quad \pm\sqrt{-\frac{2 + \alpha_2 a^2}{8\alpha_1}} \tag{4.31}$$

The Jacobian matrix of Eqs. (4.18)-(4.21) evaluated at one of these fixed points is

$$J = -\varepsilon \begin{bmatrix} 0 & \frac{1}{4} af\cos\beta & 0 & 0 \\ \frac{3}{2}\alpha_3 a & 2\mu_2 & 2\alpha_4 u_1 & 0 \\ 0 & 0 & 0 & -1 \\ \alpha_2 u_1 a & 0 & \Gamma & 2\mu_1 \end{bmatrix} \tag{4.32}$$

where

$$\Gamma = 1 + 12\alpha_1 u_1^2 + \frac{1}{2}\alpha_2 a^2 \tag{4.33}$$

When $u_1 = 0$, the eigenvalues of J are

$$\begin{aligned} \lambda = &-\varepsilon\left(\mu_2 \pm \sqrt{\mu_2^2 + \frac{3}{8}\alpha_3 a^2 f\cos\beta}\right), \\ &-\varepsilon\left(\mu_1 \pm \sqrt{\mu_1^2 - 1 - \frac{1}{2}\alpha_2 a^2}\right) \end{aligned} \tag{4.34}$$

It follows from Eqs. (4.34) that Hopf bifurcations are not possible because the damping coefficients μ_i are positive. Therefore, we do not expect oscillatory solutions involving u_1 to occur in the neighborhood of fixed points with $u_1 = 0$. However, pitchfork

bifurcations are possible. They give rise to saddle foci, which could play an important role in homoclinic bifurcations.

Fixed points with $u_1 \neq 0$ are possible when $\alpha_1(2 + \alpha_2 a^2) < 0$. In this case, we write the equation for the eigenvalues in the form

$$\lambda^4 + \varepsilon r_1 \lambda^3 + \varepsilon^2 r_2 \lambda^2 + \varepsilon^3 r_3 \lambda + \varepsilon^4 r_4 = 0 \tag{4.35}$$

where

$$r_1 = 2(\mu_1 + \mu_2) \tag{4.36}$$

$$r_2 = -2 - \alpha_2 a^2 - \frac{3}{8}\alpha_3 a^2 f \cos\beta + 4\mu_1\mu_2 \tag{4.37}$$

$$r_3 = -\frac{3}{4}\mu_1\alpha_3 a^2 f \cos\beta - 4\mu_2 - 2\mu_2\alpha_2 a^2 \tag{4.38}$$

$$r_4 = \frac{1}{16\alpha_1}(2 + \alpha_2 a^2)(6\alpha_1\alpha_3 - \alpha_2\alpha_4)a^2 f \cos\beta \tag{4.39}$$

The Routh-Hurwitz criterion guarantees that all of the eigenvalues have negative real parts if

$$r_1 > 0, \quad r_1 r_2 - r_3 > 0, \quad r_3(r_1 r_2 - r_3) - r_1^2 r_4 > 0, \quad r_4 > 0 \tag{4.40}$$

Of particular interest is the case where condition (4.40c) is violated because in this case a complex-conjugate pair of eigenvalues will have a zero or positive real part and a Hopf bifurcation may occur, leading to oscillatory motions of u_1.

4.3 Numerical Results

The frequency-response curves for $\mu_1 = 0.25$, $\mu_2 = 0.5$, $f = 2.5$, $\alpha_1 = \alpha_3 = 1$, $\alpha_2 = -2$, and $\alpha_4 = 3$ are depicted in Fig. 4.1. When σ decreases from a large value or Ω decreases and approaches twice the natural frequency of the high-frequency mode, both u_1 and u_2 are trivial and stable. The trivial a solution remains stable until a pitchfork bifurcation occurs, which leads to stable finite-amplitude values of a corresponding to periodic oscillations in u_2 with u_1 remaining trivial and stable. As σ decreases below zero, another pitchfork bifurcation occurs for both modes. The constant branch solution for a bifurcates into two branches: a stable branch that slowly grows with decreasing σ and a saddle-focus branch. For the low-frequency mode, the trivial u_1 solution loses stability and gives way to slowly growing stable constant solutions: u_1 and $-u_1$. Hence, the motion will consist of periodic oscillations in u_2 accompanied by a positive or negative nonzero static deflection in u_1. When σ decreases past approximately -0.2888, a supercritical Hopf bifurcation of the nontrivial constant a and u_1 solutions occurs. The ensuing motion will then consist of oscillatory u_1 motions accompanied by modulated u_2 responses, as observed in the experiments.

Next, we fix the excitation frequency and vary the excitation amplitude f. The results are shown in Fig. 4.2 for $\sigma = -0.289$. As f increases from zero, the system remains motionless until a subcritical pitchfork bifurcation occurs. The high-frequency mode suddenly starts to oscillate with a finite and constant amplitude, whereas the low-frequency mode remains unexcited until a supercritical pitchfork bifurcation takes place. When f exceeds about 2.5, a supercritical Hopf bifurcation

occurs, resulting in oscillatory solutions in u_1 accompanied by slow modulations of the amplitude and phase of the high-frequency mode, as observed in the experiment.

In Fig. 4.3, the boundaries between constant and oscillatory motions of u_1 for various damping values are shown. Below these curves, oscillations in u_1 decay to a constant value and above them oscillations in u_1 are sustained. As indicated in part (a), for fixed values of μ_1 and σ, the larger μ_2 is, the larger is the critical force amplitude required to generate oscillations in u_1. In part (b), for fixed values of μ_2 and σ, increasing the damping coefficient μ_1 of the low-frequency mode does not always increase the value of the critical force amplitude. That is, increasing μ_1 will destabilize the system for some excitation amplitudes and frequencies.

Next, we study the dynamics of the system in the neighborhood of the unstable foci shown in Fig. 4.1 and summarize the results in Fig. 4.4. Three branches of solutions are found. On branch I, as σ decreases from the supercritical Hopf bifurcation value σ_1 to σ_8, the limit cycle born at σ_1 increases in size, deforms, and then undergoes a sequence of period-doubling bifurcations, leading to chaos, as shown in Figs. 4.5(a)-(f). The responses come in pairs as solutions with u_1 and $-u_1$ coexist. As σ decreases further, a sequence of reverse period-doubling bifurcations occurs, leading to a singly winding limit cycle, as shown in Figs. 4.5(g)-(i). This is an example of a bubble structure (Knobloch and Weiss, 1983).

Inspection of Figs. 4.5(j)-(k) indicates the formation of an orbit homoclinic to the saddle focus as σ decreases slightly below $\sigma = -0.55799$. It is clear from Figs. 4.5(l) and 4.6(a) that the twin limit cycles are very near to the saddle focus. To confirm this, we plot in Fig. 4.7 variation of the period T_0 of the period-one solution with σ. Clearly, this period approaches ∞ as $\sigma \to \sigma_c \approx -0.55799$.

As σ decreases below σ_c, a chaotic attractor is expected to occur according to the Shilnikov theorem. Shilnikov (1970) first proved this theorem for any third-order system that can be written in the form

$$\dot{x}_i = f_i(x_1, x_2, x_3), \quad i = 1,2,3$$

if there is an orbit Γ homoclinic to a saddle focus in the state space of the system. We denote the eigenvalues or characteristic exponents of the saddle focus by $\lambda_1, \lambda_2, \lambda_3$ such that $\lambda_3 = \bar{\lambda}_2 = -\alpha + i\omega$ with ω being different from zero and α positive. The Shilnikov theorem says that if $\lambda_1 > 0$ and $\delta = \alpha/\lambda_1 < 1$, the trajectories in the neighborhood of Γ form a homoclinic structure that contains a countable set of saddle periodic orbits and hence a state trajectory wanders "randomly" between the unstable periodic trajectories. In other words, the system behavior is chaotic. The Shilnikov theorem has been extended to higher-dimensional systems of the form

$$\dot{x}_i = f_i(x_1, x_2, ..., x_n), \quad i = 1,2,..,n$$

if there is an orbit Γ homoclinic to a saddle focus with the characteristic exponents $\lambda_1 > 0$, $\lambda_2 = \bar{\lambda}_3 = -\alpha + i\omega$, Real $(-\lambda_i) > \alpha$ for $i = 4,5, ...n$, and $\delta = \alpha/\lambda_1 < 1$. This theorem can be applied to our system and hence proves the existence of homoclinic or Shilnikov chaos.

The critical value σ_c of σ at which the homoclinic orbit exists is equal to -0.55799 approximately. The eigenvalues of the saddle focus at σ_c are $(0.648, -0.5 \pm 0.855i, -1.148)$. Clearly, $\delta = 0.772 < 1$, and therefore the Shilnikov theorem implies the existence of chaos for $\sigma < \sigma_c$. In Figs. 4.6(a) and (b), we show the twin periodic orbits and their spectra at $\sigma = -0.55799$, just before the formation of the homoclinic orbit, and in Figs. 4.6(c) and (d), we show the chaotic attractor and its spectrum at $\sigma = -0.558$, just after the formation of the homoclinic orbit. The broad

spectrum of this attractor shown in Fig. 4.6(d) and its Lyapunov exponents (0.015, 0.0, -0.982, -1.195) confirm its chaotic nature.

When σ decreases further, this chaotic attractor persists for a while and is followed by a reverse homoclinic bifurcation, which results in two asymmetric limit cycles. In Figs. 4.8(a) and (b), we show a chaotic attractor and its spectrum at $\sigma = -0.564904$, and in Figs. 4.8(c) and (d), we show one of the twin periodic attractors and its spectrum at $\sigma = -0.564905$. The periodic attractor shown in Fig. 4.8(c) is very close to an orbit Γ that is homoclinic to the saddle focus indicated by the + sign. To confirm this, we plot in Fig. 4.9 variation of the period T_0 of the period-one motion for values of σ between -0.5650 and $\sigma_c \approx -0.564905$. Clearly, T_0 approaches ∞ as σ approaches σ_c from below. The eigenvalues of the saddle focus at σ_c are $(0.653, -0.5 \pm 0.858i, -1.153)$. Hence, $\delta = 0.766 < 1$. Consequently, the Shilnikov theorem predicts periodic orbits for $\sigma < \sigma_c$ and chaos for $\sigma > \sigma_c$. As a result, decreasing σ below σ_c results in the disappearance of the chaotic attractor and the appearance of two asymmetric periodic orbits, as shown in Fig. 4.8. A second bubble structure occurs in the interval $-0.578 \leq \sigma \leq -0.564905$, as shown in Fig. 4.10. In Figs. 4.10(a)-(c), we show a sequence of period-doubling bifurcations, leading to two chaotic attractors of the form shown in (c). The corresponding FFT's are shown in Fig. 4.11. These two attractors then merge as shown in Fig. 4.10(d). The resulting chaotic attractor deforms and bifurcates back to two other asymmetric chaotic attractors of the form shown in (g). These chaotic attractors undergo a sequence of reverse period-doubling bifurcations, as shown in Figs. 4.10(h)-(k). As σ decreases below -0.578, the twin asymmetric attractors undergo a reverse symmetry-breaking bifurcation, which is followed by a cyclic-fold bifurcation at $\sigma = \sigma_{15}$, resulting in the termination of this branch solution and a jump to branch III.

Branch II appears to be an isolated one, which only exists for a short frequency interval. If a periodic orbit exists on this branch, it bifurcates into a chaotic attractor as σ increases or decreases. It follows from Fig. 4.12 that, as σ increases from -0.54912, the period T_0 of the limit cycle increases and approaches ∞ as σ approaches $\sigma_c \approx -0.548686$, indicating the formation of an orbit homoclinic to the saddle focus. The eigenvalues of the saddle focus are $(0.641, -0.5 \pm 0.851i, -1.141)$ and hence $\delta = 0.78 < 1$. Consequently, according to the Shilnikov theorem, the symmetric singly winding limit cycle bifurcates into a chaotic attractor as σ increases past σ_c. In Figs. 4.13(a) and (b), we show the symmetric singly winding attractor and its spectrum that exist just before the formation of the homoclinic orbit, and in Figs. 4.13(c) and (d), we show the chaotic attractor and its spectrum that exist just after the formation of the homoclinic orbit. As σ increases further, the chaotic attractor persists until a boundary crisis (Grebogi et al., 1983) occurs at $\sigma = \sigma_{16}$. It involves a chaotic attractor colliding with its own basin boundary, resulting in the destruction of the attractor and leading to one of the twin limit cycles of branch I, as shown in Fig. 4.14.

When σ decreases from -0.54912, the limit cycle undergoes a symmetry-breaking bifurcation. As σ decreases further, an intermittently chaotic motion occurs. It can be seen from Figs. 4.15(d)-(f) and 4.16(a) that the extent of this intermittency seems to spread out as σ decreases. In Fig. 4.16(b) for $\sigma = \sigma_{17}$, a crisis or chaos quenching occurs, resulting in one of the twin limit cycles of branch I.

On branch III, a cyclic-fold bifurcation occurs at $\sigma = \sigma_{18}$, leading to one of the period-four orbits on branch I. As σ decreases, the symmetric limit cycle undergoes a symmetry-breaking bifurcation followed by a sequence of period-doubling bifurcation, culminating in chaos, as shown in Fig. 4.17. The two ensuing chaotic attractors merge at $\sigma = -0.76$, as shown in Fig. 4.18. They are closely related to the

unstable manifolds of the upper branch of the saddle foci of Fig. 4.1. As σ decreases further, the chaotic attractor deforms, increases in size, and approaches the lower branch of saddle foci, as shown in Fig. 4.19. While the chaotic attractor is growing and intricately winding, the lower saddle focus moves toward it and splits into two at $\sigma = -1.5$. As σ decreases to σ_c, the chaotic attractor collides with its basin boundary (boundary crisis), resulting in its destruction. At values of σ just below σ_c, a trajectory initiated in the state space occupied by the ghost of the chaotic attractor will bounce around chaotically for a finite time until it collides with one of the saddle foci and then suddenly moves off toward some other distant attractor (Fig. 4.20); in this case the only attractor is the trivial one.

4.4 Summary

We investigate the response of a parametrically excited two-degree-of-freedom system with cubic nonlinearities and widely spaced modal frequencies. The method of averaging is used to derive a system of four first-order ordinary differential equations describing the modulation of the displacement and velocity of the low-frequency mode and the amplitude and phase of the high-frequency mode. In Fig. 4.21, we compare the results of numerically integrating the modulation equations and the original equations (4.13)-(4.17) for $\varepsilon = 0.01$ and three values of σ. Clearly, the averaging approximation accurately predicts the occurrence of period-doubling bifurcations for a small ε.

We study the equilibrium solutions of the averaged equations in some detail and determine the conditions under which energy can be transferred from the

high-frequency to the low-frequency mode. Oscillations of the low-frequency mode are accompanied by slow amplitude and phase modulations of the high-frequency mode, as observed in the experiments.

Even for the simple model of current study, many interesting complexities due to nonlinear interactions are found after an oscillation in the low-frequency mode is created. These include bubble structures (the occurrence of cascades of period-doubling and reverse period-doubling bifurcations), homoclinic bifurcations, the coexistence of multiple attractors, cyclic-fold and symmetry-breaking bifurcations, the merger of two chaotic attractors, boundary crises, intermittent chaos, and chaos quenching.

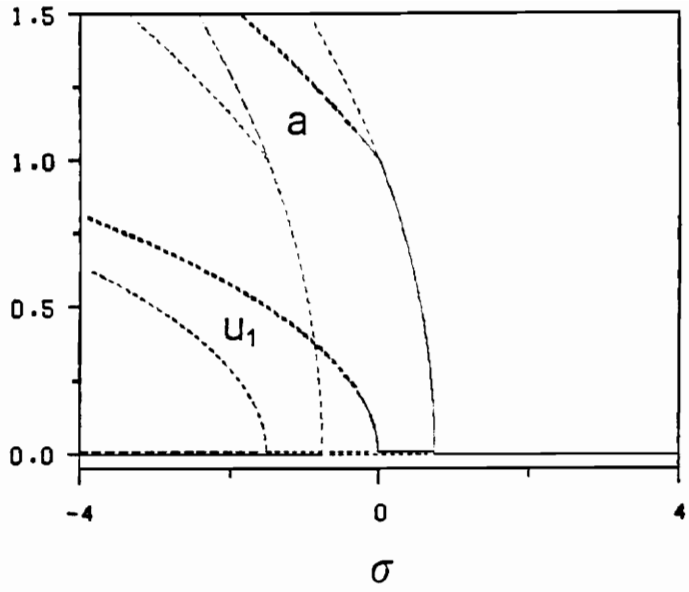

Figure 4.1. Frequency-response curves for $\alpha_1 = \alpha_3 = 1$, $\alpha_2 = -2$, $\alpha_4 = 3$, $\mu_1 = 0.25$, $\mu_2 = 0.5$, and $f = 2.5$; ____ stable nodes, ---- unstable foci, – – saddles (two positive and two negative real eigenvalues), and ---- saddle foci.

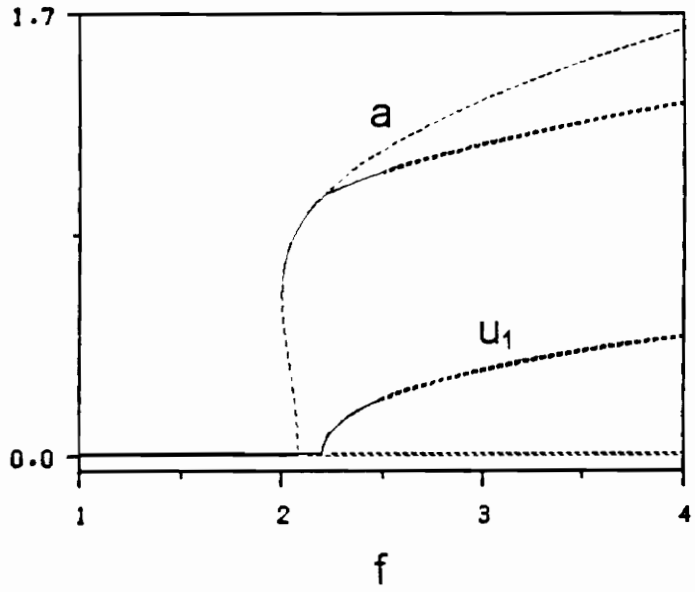

Figure 4.2. Force-response curves for $\alpha_1 = \alpha_3 = 1$, $\alpha_2 = -2$, $\alpha_4 = 3$, $\mu_1 = 0.25$, $\mu_2 = 0.5$, and $\sigma = -0.289$; ____ stable nodes, ---- unstable foci, and ---- saddle foci.

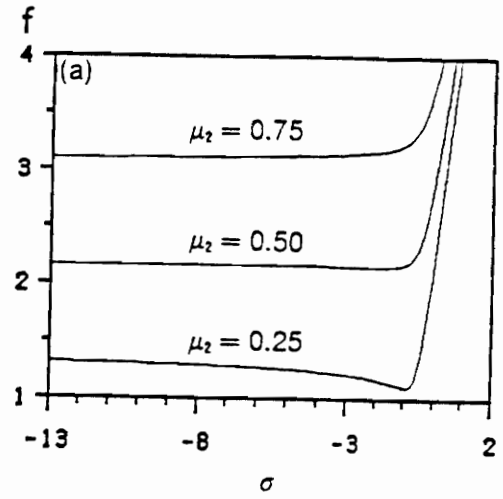

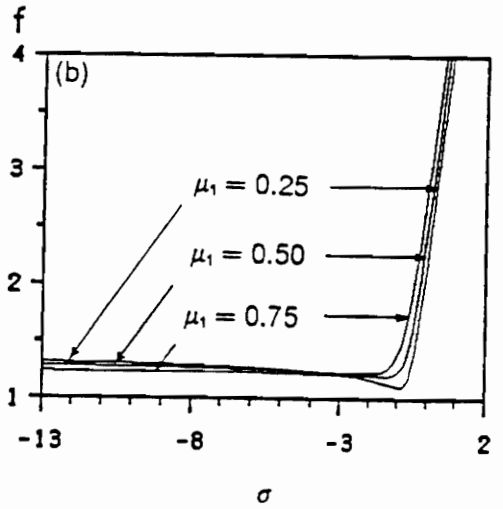

Figure 4.3. Boundaries between constant and oscillatory motions of u_1 for $\alpha_1 = \alpha_3 = 1$, $\alpha_2 = -2$, $\alpha_4 = 3$, and various damping values: (a) $\mu_2 = 0.25$, 0.50, and 0.75 for a fixed $\mu_1 = 0.25$ and (b) $\mu_1 = 0.25$, 0.50, and 0.75 for a fixed $\mu_2 = 0.25$.

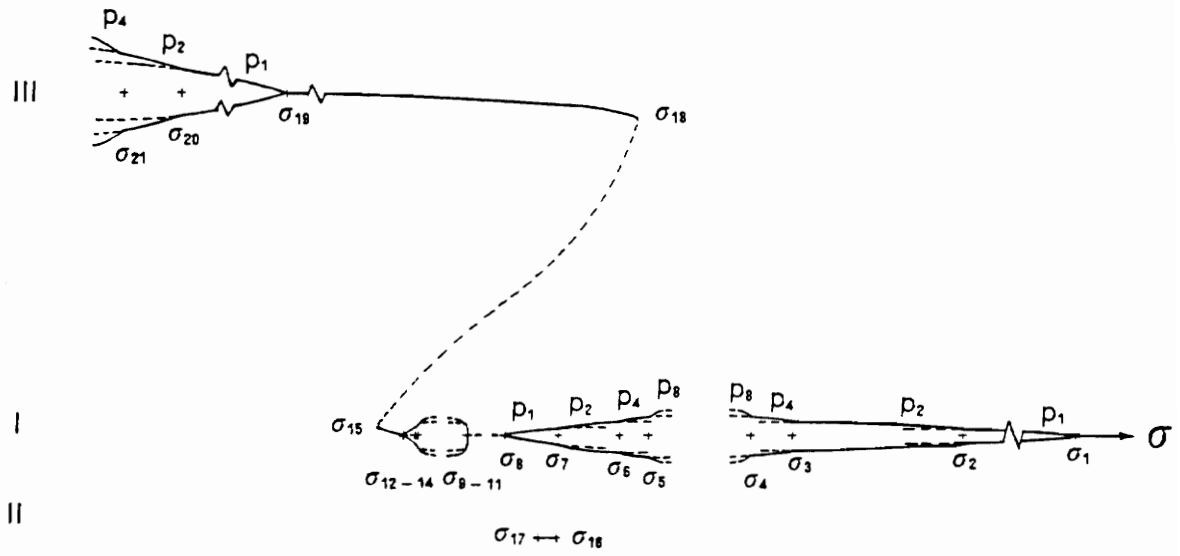

Figure 4.4. Bifurcation diagram illustrating the various stages leading to chaos in the neighborhood of the unstable foci, where on branch I: σ_1(supercritical Hopf) = −0.2888, σ_2(p-2) = −0.471, σ_3(p-4) = −0.503, σ_4(p-8) = −0.511, σ_5(reversed p-8) = −0.5305, σ_6(reversed p-4) = −0.536, σ_7(reversed p-2) = −0.5478, σ_8(homoclinic bifurcation) = −0.55799, σ_9(reversed homoclinic bifurcation) = −0.564904, σ_{10}(p-2) = −0.565, σ_{11}(p-4) = −0.565057, σ_{12}(reversed p-4) = −0.5744, σ_{13}(reversed p-2) = −0.575, σ_{14}(reversed symmetry-breaking) = −0.5772, and σ_{15}(cyclic-fold bifurcation) = −0.582366; on branch II: σ_{16}(crisis) = −0.5481, and σ_{17}(crisis) = −0.55165; on branch III: σ_{18}(cyclic-fold bifurcation) = −0.533, σ_{19}(symmetry-breaking) = −0.67; σ_{20}(p-2) = −0.73, and σ_{21}(p-4) = −0.741.

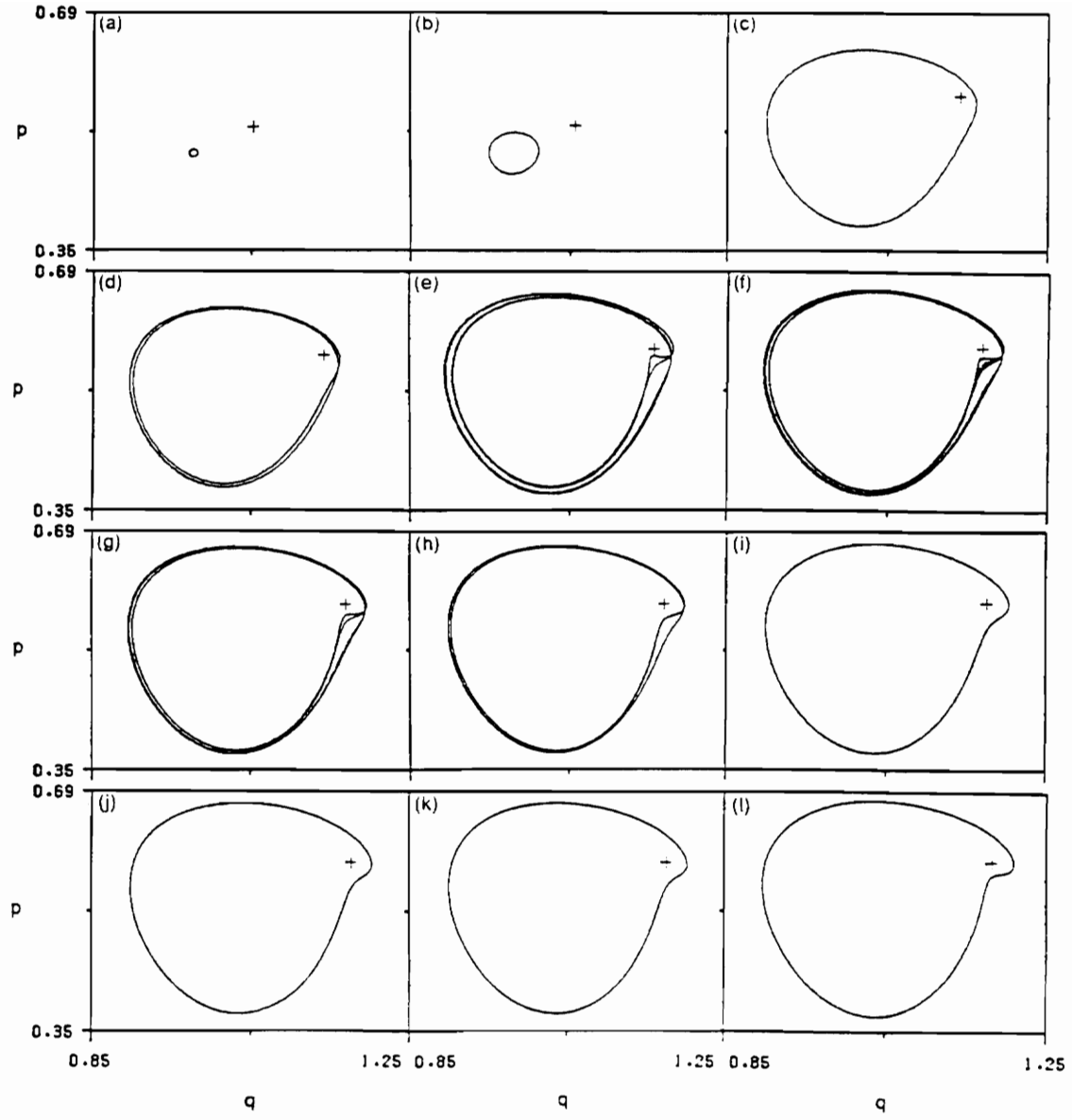

Figure 4.5. Two-dimensional projections of the phase portraits onto the p – q plane at σ = (a) −0.2889, (b) −0.297, (c) −0.47, (d) −0.472, (e) −0.51, (f) −0.527, (g) −0.533, (h) −0.54, (i) −0.548, (j) −0.549, (k) −0.55, and (l) −0.55799 on branch I. They show a sequence of period-doubling bifurcations leading to chaos followed by a reverse period-doubling sequence of bifurcations. In the figures, + denotes the saddle focus.

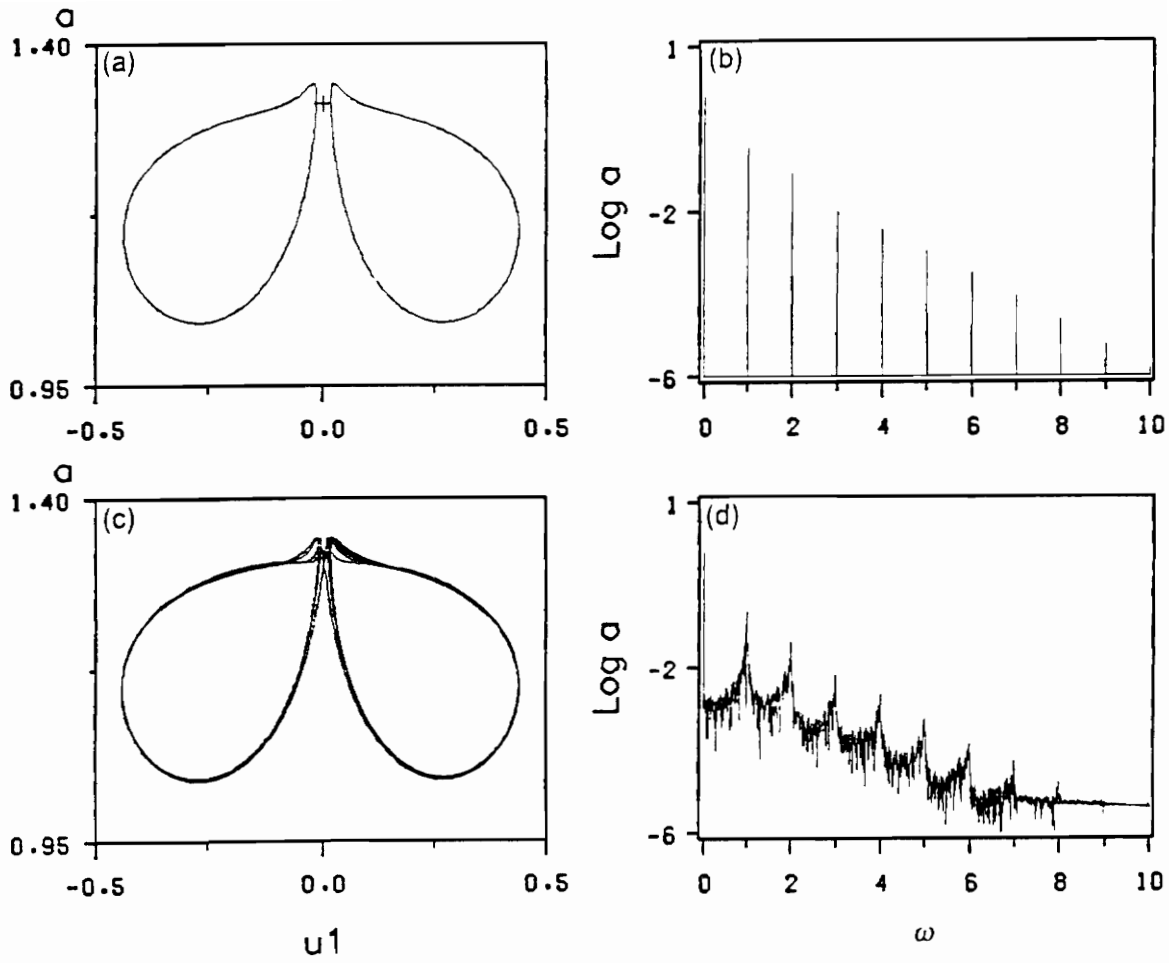

Figure 4.6. (a) A two-dimensional projection of the twin limit cycles onto the $a - u_1$ plane and (b) the FFT of a at $\sigma = -0.55799$; (c) A two-dimensional projection of the chaotic attractor onto the $a - u_1$ plane and (d) the FFT of a at $\sigma = -0.558$. In (a) and (c), + denotes the saddle focus.

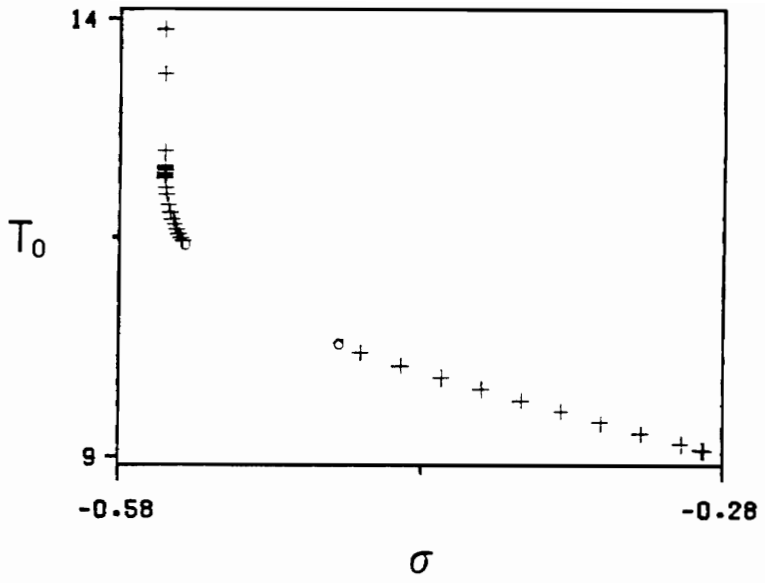

Figure 4.7. Variation of the period of the period-one motion with the detuning parameter σ. The symbol o marks the onset of period-doubling bifurcations.

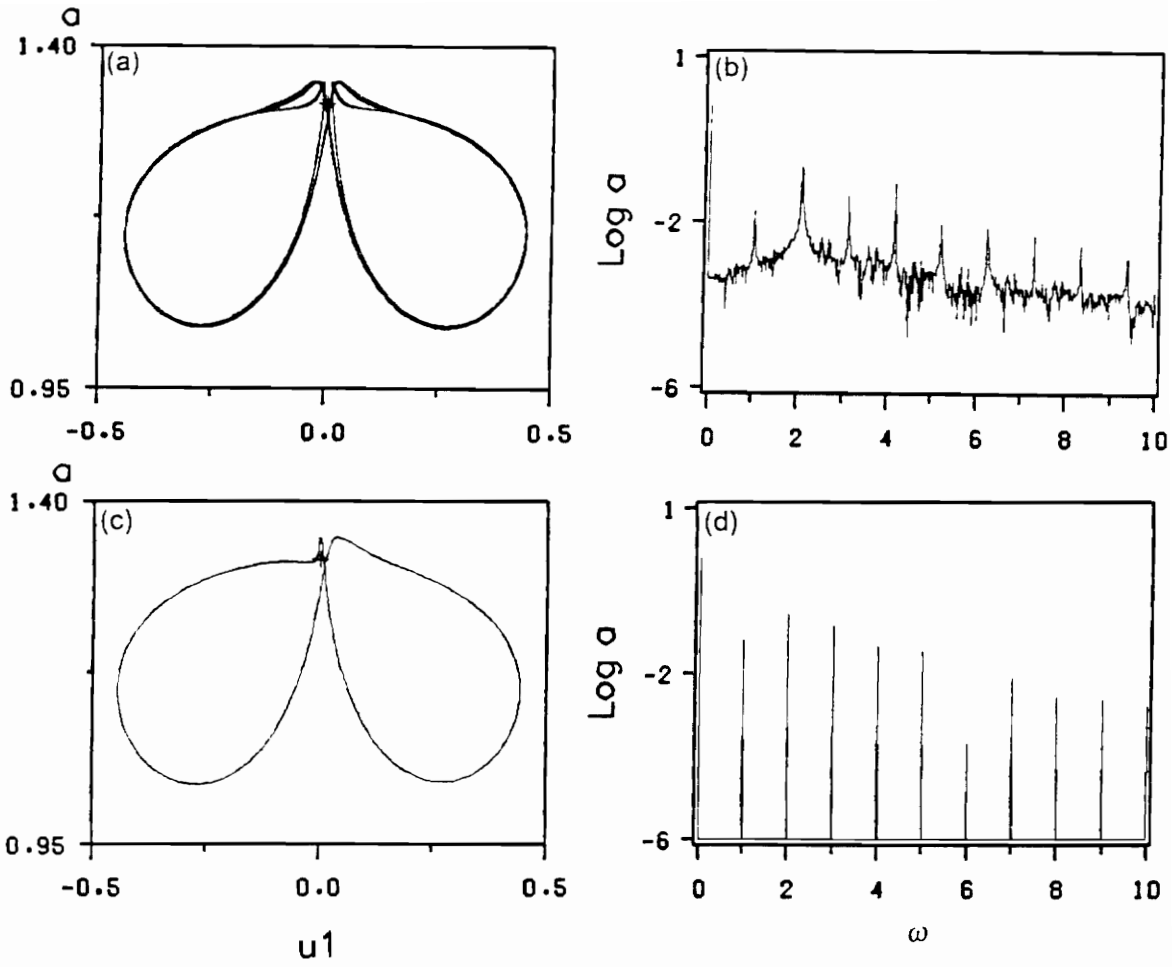

Figure 4.8. (a) A two-dimensional projection of the chaotic attractor onto the $a - u_1$ plane and (b) the FFT of a at $\sigma = -0.564904$; (c) A two-dimensional projection of one of the asymmetric limit cycles onto the $a - u_1$ plane and (d) the FFT of a at $\sigma = -0.564905$. In (a) and (c), + denotes the saddle focus.

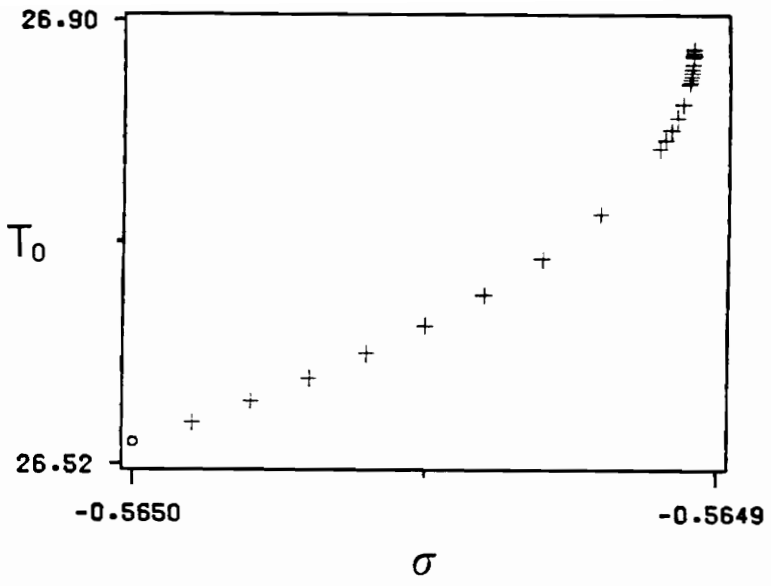

Figure 4.9. Variation of the period of the period-one motion with the detuning parameter σ. The symbol o marks the onset of period-doubling bifurcations.

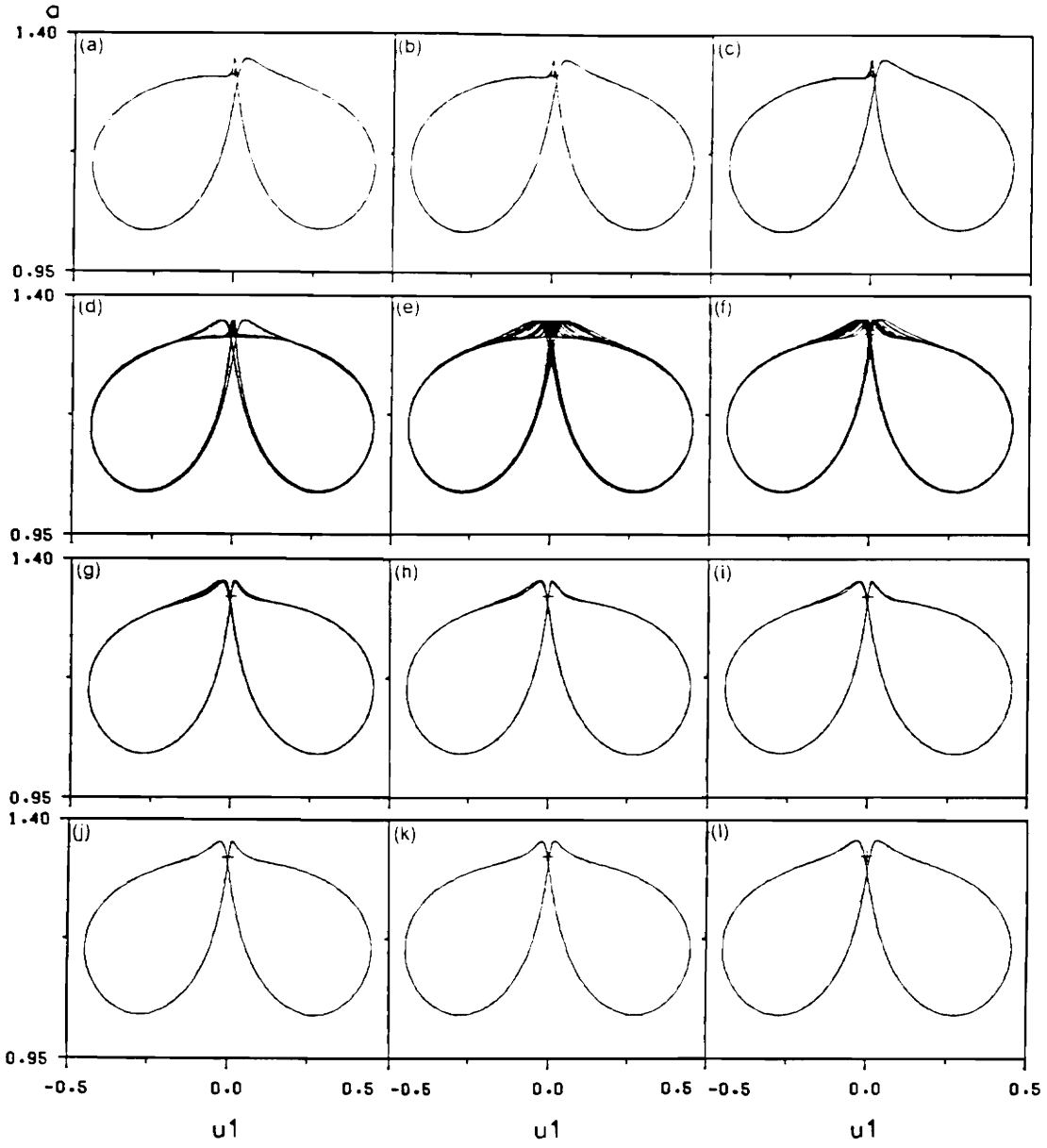

Figure 4.10. Two-dimensional projections of the phase portraits onto the $a - u_1$ plane at $\sigma =$ (a) -0.565, (b) -0.56505, (c) -0.5651, (d) -0.5652, (e) -0.57, (f) -0.573, (g) -0.574, (h) -0.5743, (i) -0.5745, (j) -0.5751, (k) -0.578, and (l) -0.582365. They show a sequence of period-doubling bifurcations leading to chaos followed by a reverse period-doubling sequence of bifurcations and symmetry-breaking bifurcation. In the figures, + denotes the saddle focus.

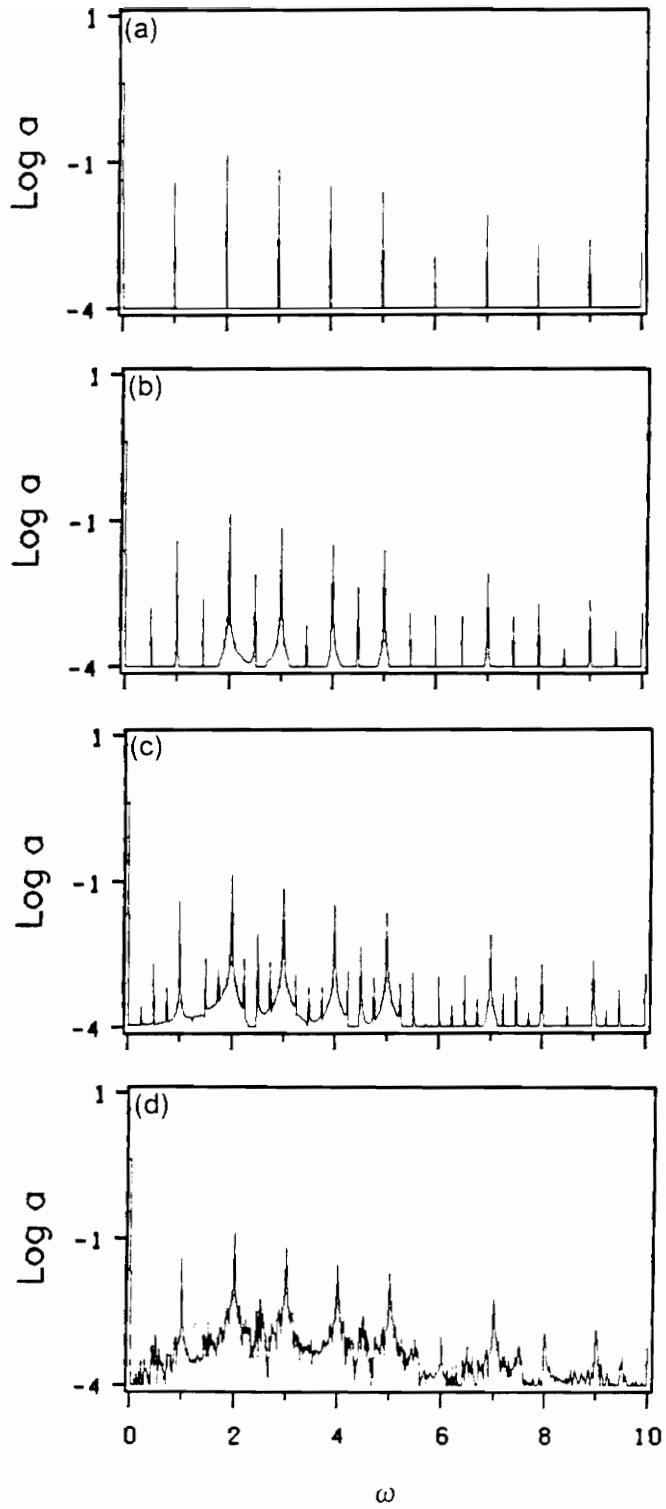

Figure 4.11. The FFT of a at $\sigma =$ (a) -0.565, (b) -0.56505, (c) -0.56507, and (d) -0.5651.

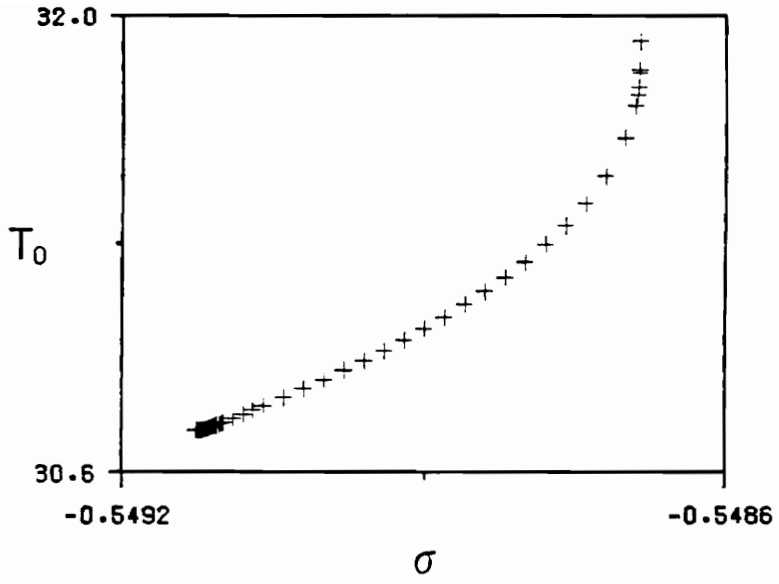

Figure 4.12. Variation of the period of the period-one motion of branch II. with the detuning parameter σ.

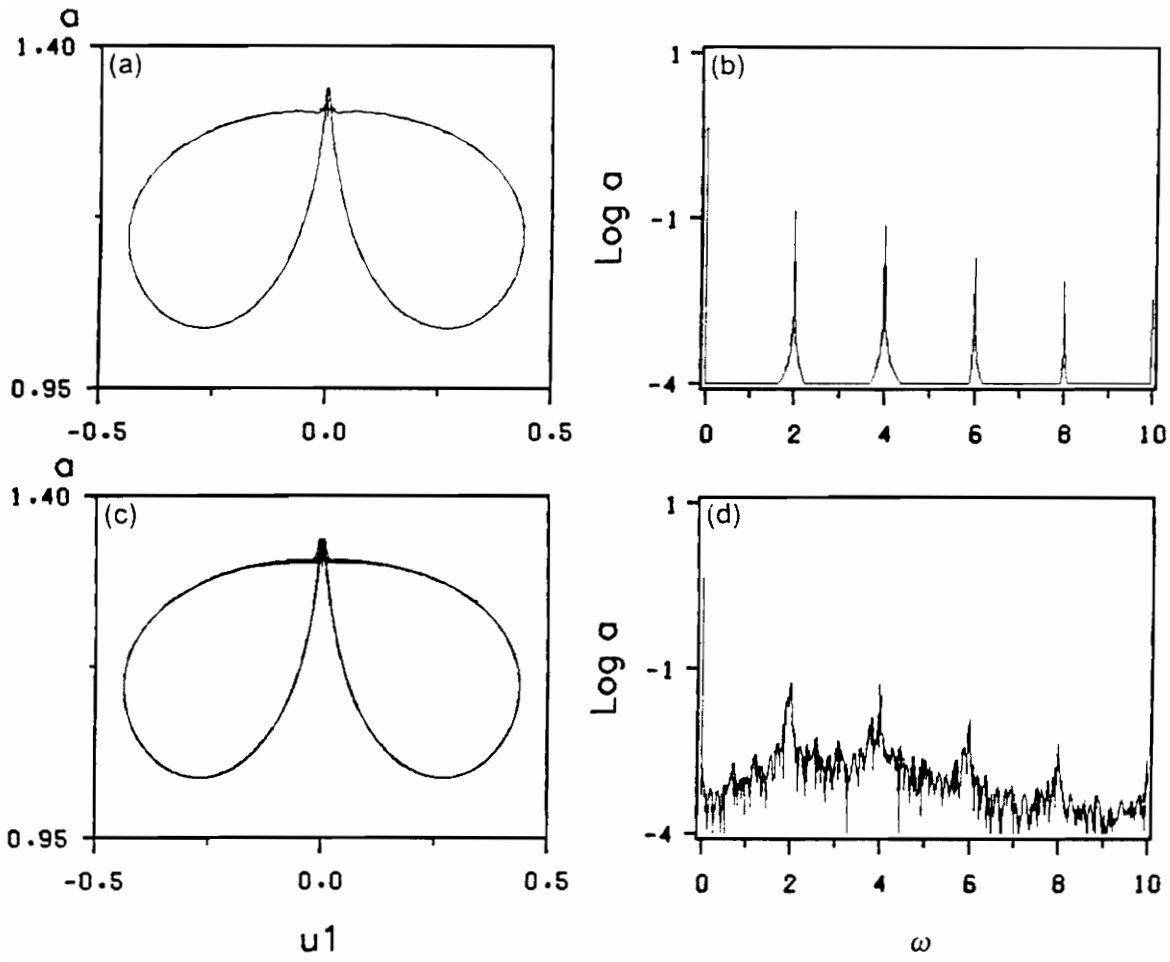

Figure 4.13. (a) A two-dimensional projection of the limit cycle onto the $a - u_1$ plane and (b) the FFT of a at $\sigma = -0.5486861$; (c) A two-dimensional projection of the chaotic attractor onto the $a - u_1$ plane and (d) the FFT of a at $\sigma = -0.548685$. In (a) and (c), + denotes the saddle focus.

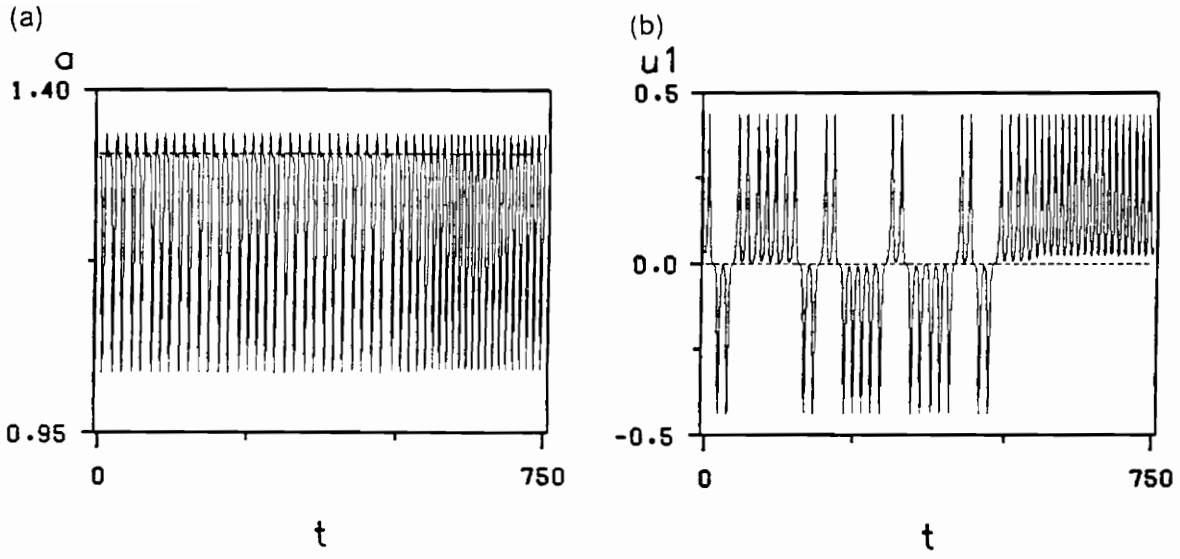

Figure 4.14. The time histories of a in (a) and u_1 in (b) at $\sigma = -0.5481$, where a crisis occurs.

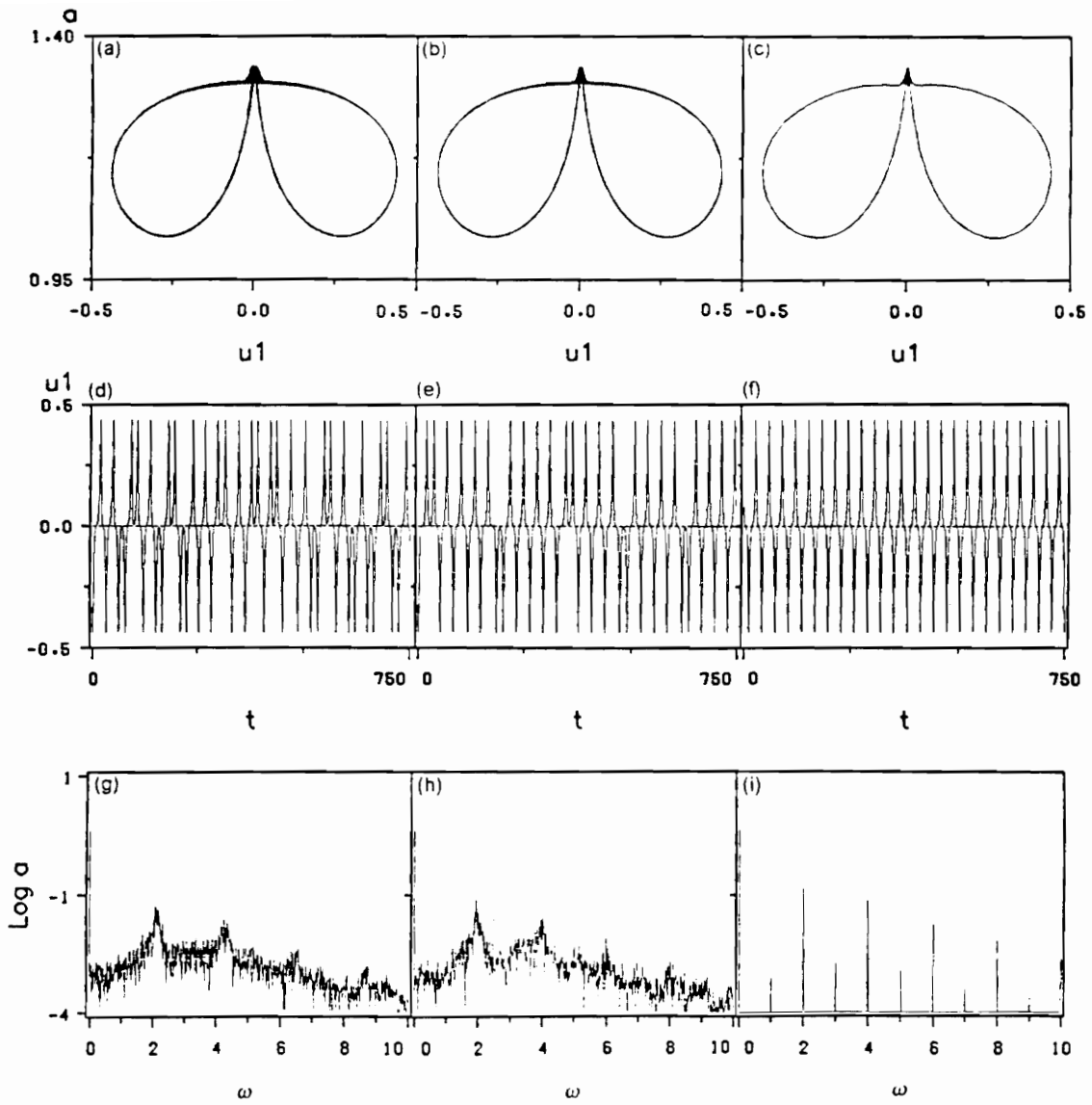

Figure 4.15. From right to left: $\sigma = -0.549126$, -0.5498, and -0.551, where (a)-(c) show the two-dimensional projections of the attractors onto the $a - u_1$ plane; (d)-(f) show the time histories of u_1; and (g)-(i) show the FFT of a.

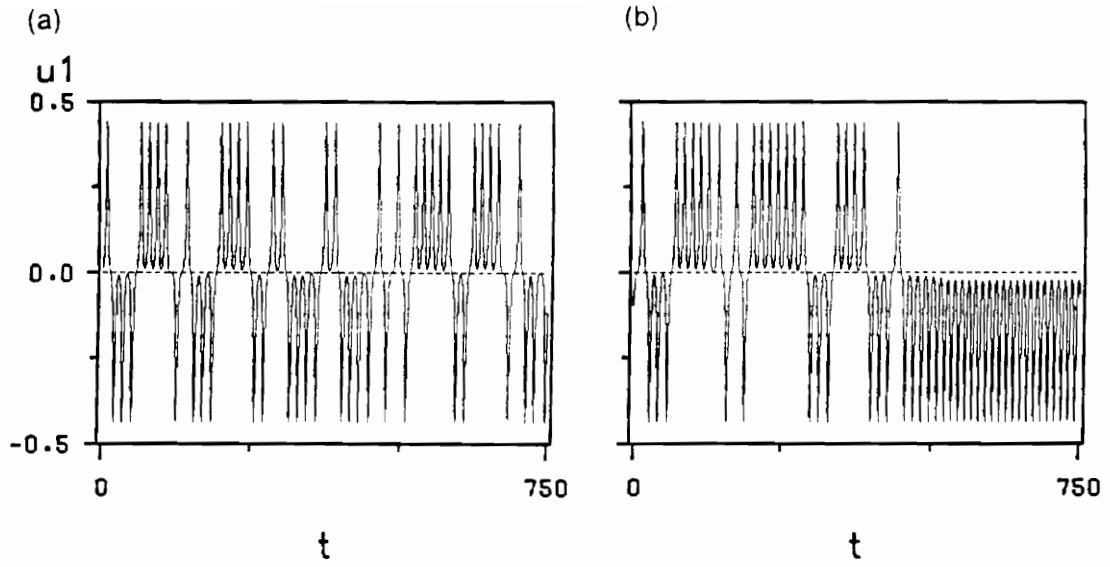

Figure 4.16. The time histories of u_1 at σ = (a) −0.5516 and (b) −0.55165 after a crisis had occurred.

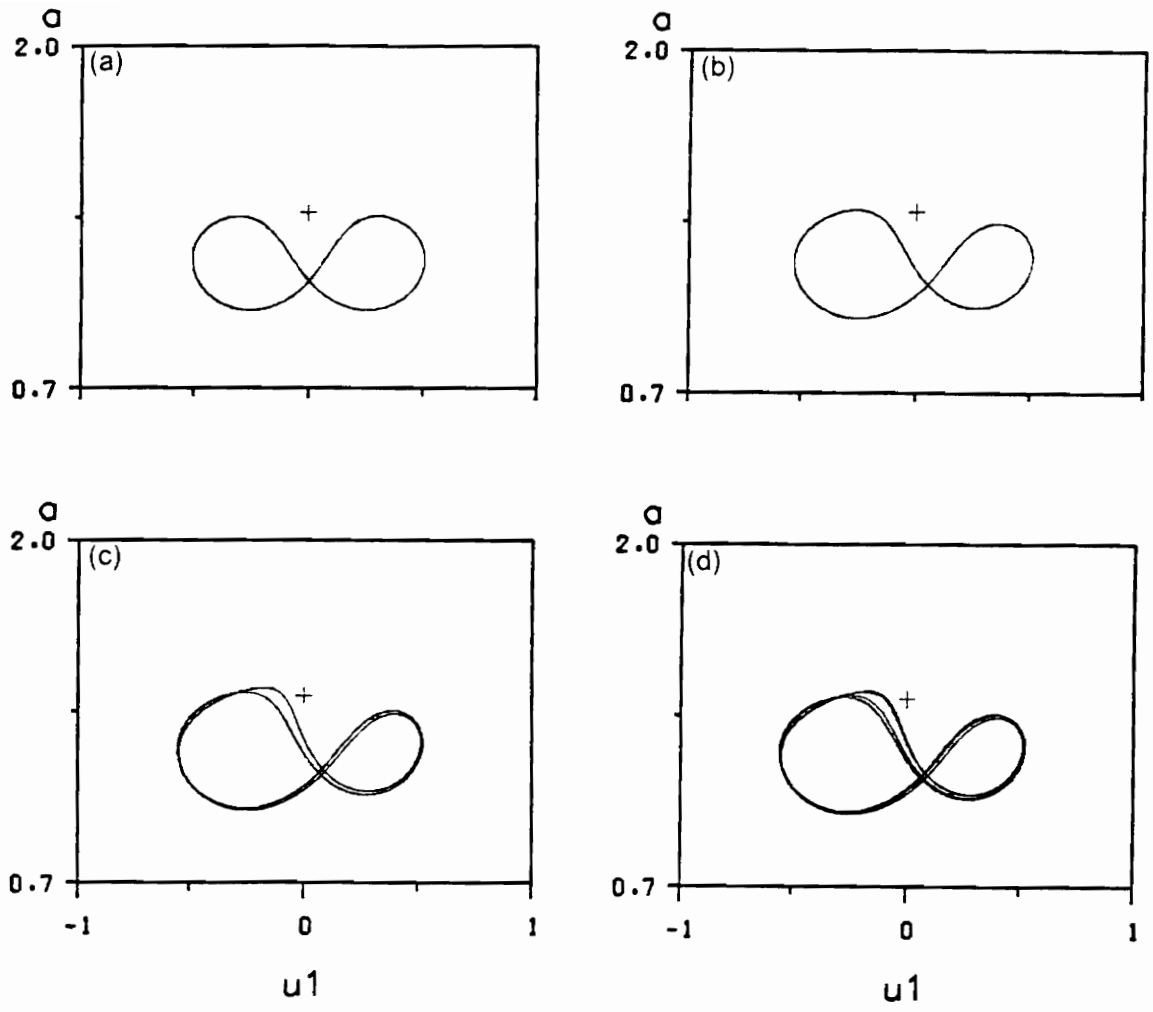

Figure 4.17. The projections of the periodic orbits onto the $a - u_1$ plane at $\sigma =$ (a) -0.65, (b) -0.69, (c) -0.74, and (d) -0.743 on branch III. They show a symmetry-breaking bifurcation followed by a sequence of period-doubling bifurcations. In the figures, + denotes a fixed point on the upper branch of saddle foci shown in Figure 4.1.

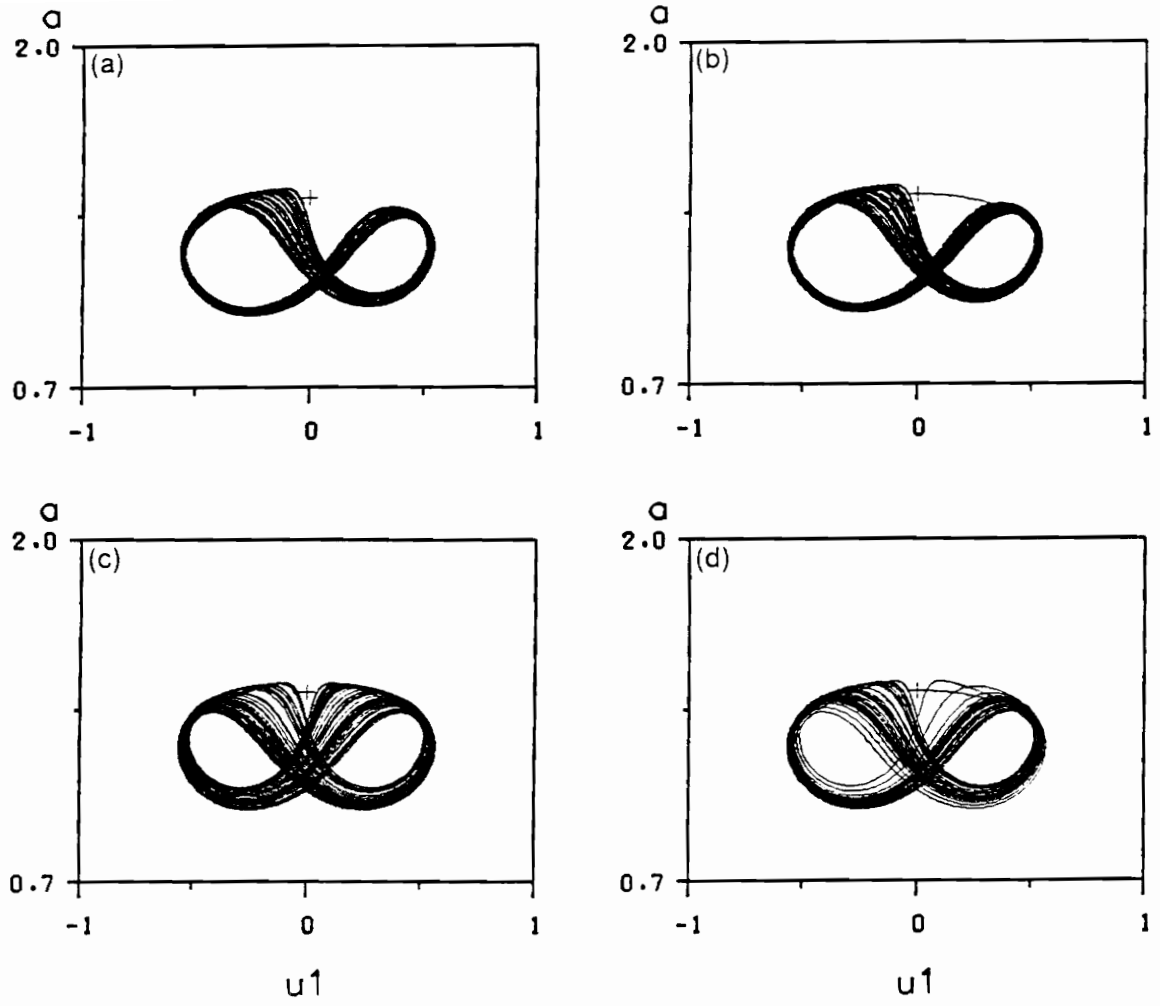

Figure 4.18. The projections of the chaotic attractors onto the $a - u_1$ plane at (a) $\sigma = -0.75999$ and (c) $\sigma = -0.76$. (b) and (d) show the unstable manifolds of the corresponding upper saddle foci (denoted by +) to (a) and (c), respectively.

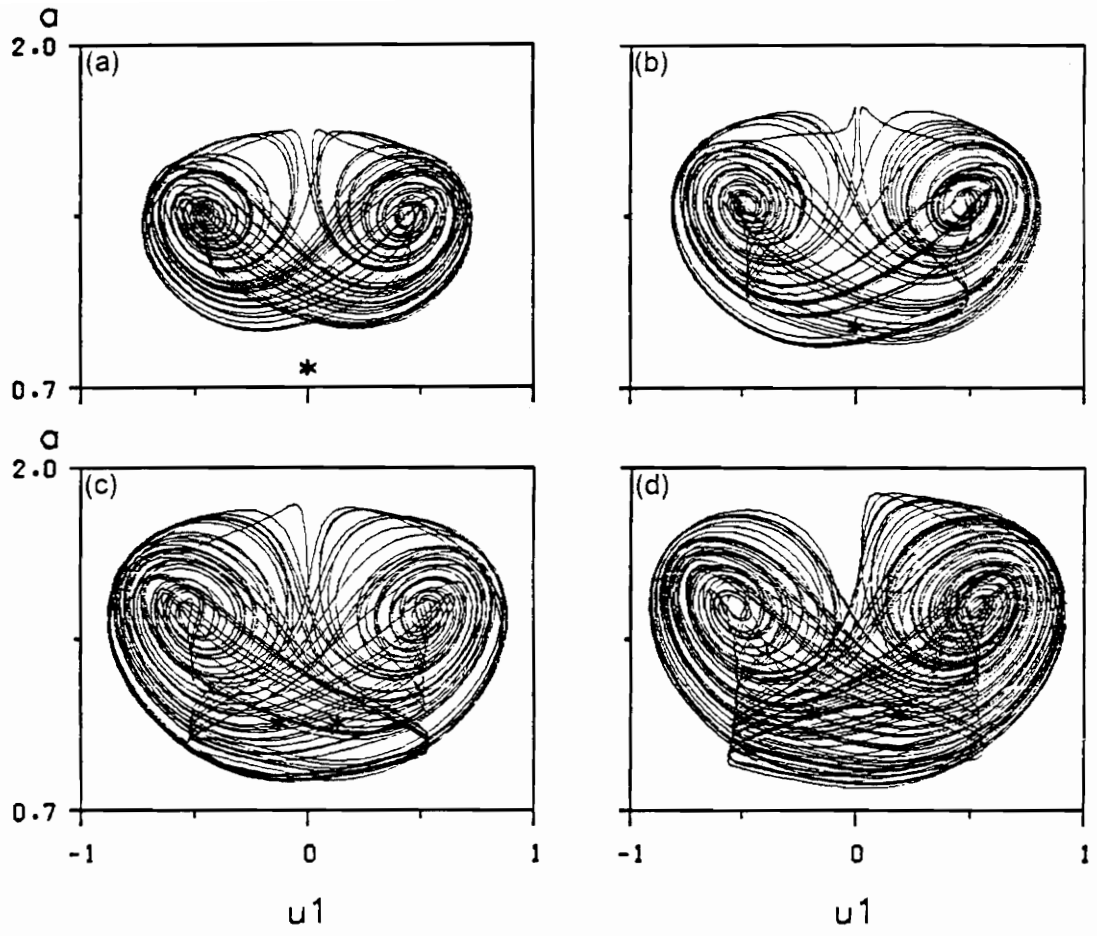

Figure 4.19. The projections of the phase portraits onto the $a - u_1$ plane at $\sigma =$ (a) -1.2, (b) -1.4, (c) -1.6, and (d) -1.72. The nontrivial fixed point denoted by * is the one on the lower branch of saddle foci in Figure 4.1. It starts to grow as σ decreases from -0.75.

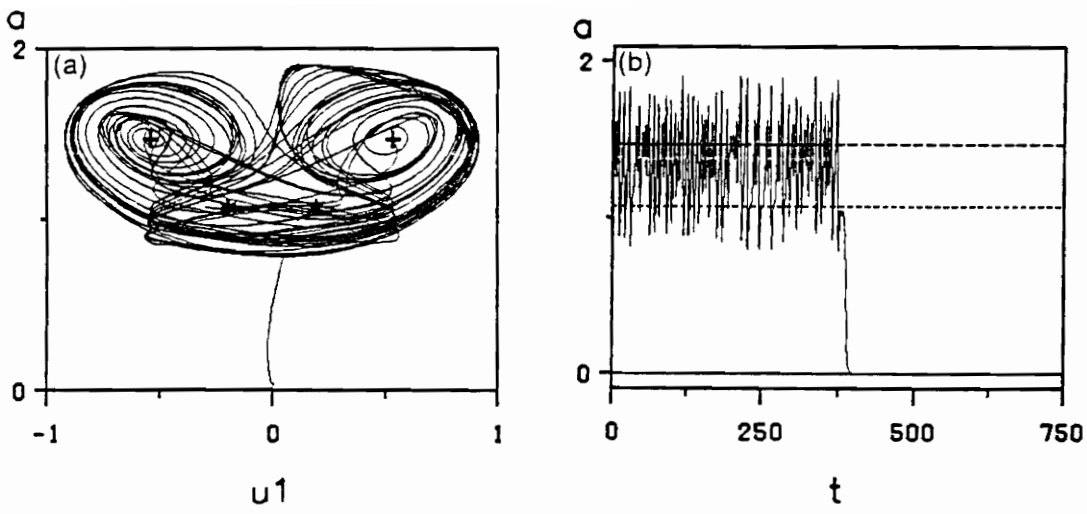

Figure 4.20. (a) The projection of the phase portrait onto the $a - u_1$ plane and (b) the time history of a at $\sigma = -1.725$. The saddle focus is denoted by * in (a) or lower dashed line in (b), whereas the unstable focus is denoted by + in (a) or upper dashed line in (b).

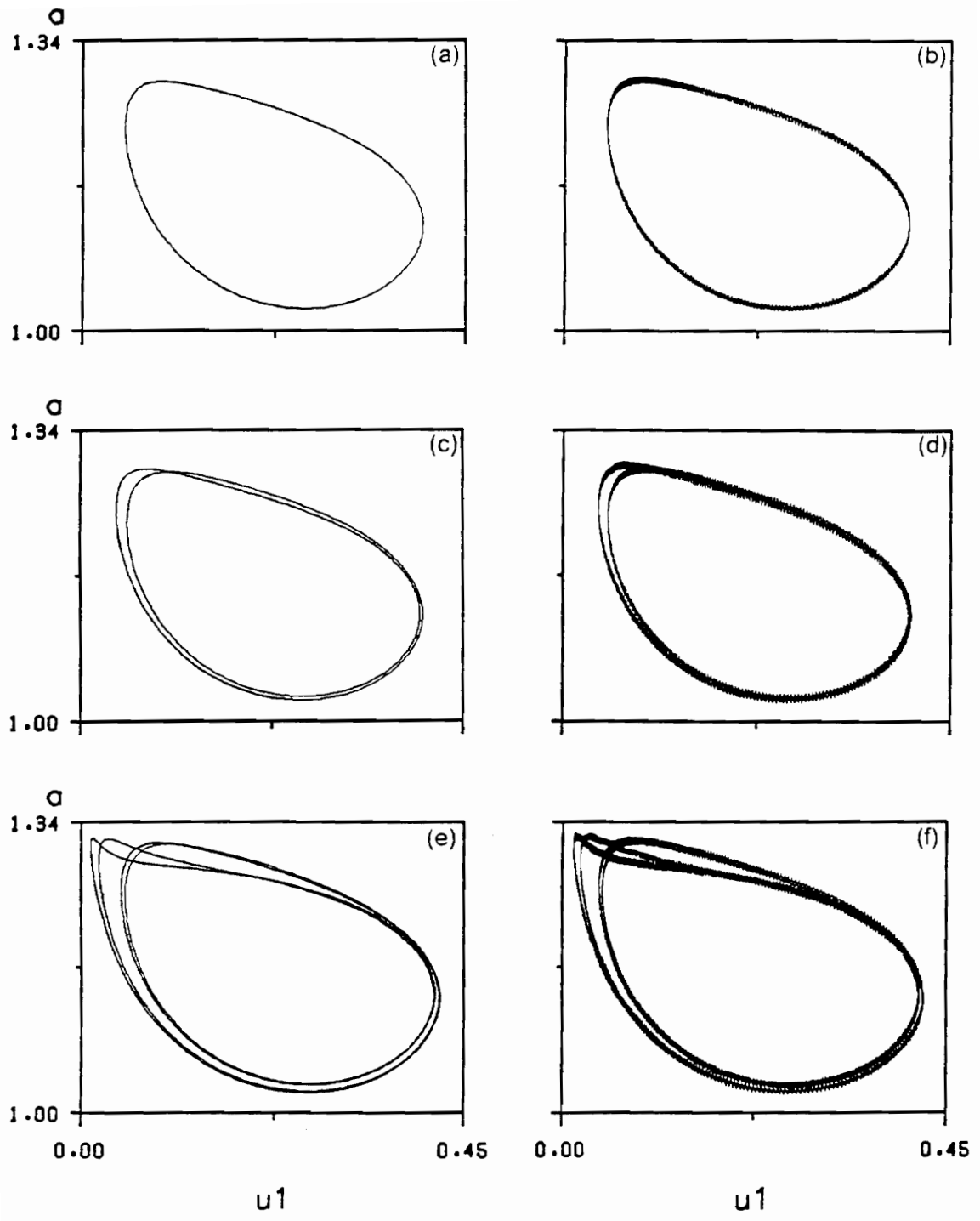

Figure 4.21. Comparison between the numerical time integration of the modulation equations (left) and the original equations for $\varepsilon = 0.01$ (right), where $\sigma = -0.47$ for (a) and (b); $\sigma = -0.472$ for (c) and (d); $\sigma = -0.51$ for (e) and (f).

CHAPTER 5

CONCLUSIONS AND RECOMMENDATIONS

5.1 Concluding Remarks

A closed-form solution of a given nonlinear system of equations may not be possible. In such a case, one often determines an approximate solution by perturbation methods, numerical methods, or geometrical methods. We use a numerical-perturbation approach to obtain approximate solutions for weakly nonlinear systems with repeated natural frequencies in Chapter 3 and systems with widely spaced modal frequencies in Chapter 4. In Chapter 2, we study a special class of solutions of a nonlinear system, namely, the so-called nonlinear normal modes. They are defined on the basis of geometrical concepts and analyzed by using a perturbation technique.

Bifurcation analyses are conducted throughout this dissertation using the modulation equations. For a parametrically excited system, the trivial solution is

possible for all values of the various parameters. Nontrivial solutions are possible for a restricted set of parameters. The local stability of a constant solution can be determined by the eigenvalues of the Jacobian matrix of the modulation equations. A static bifurcation occurs when a real eigenvalue crosses the imaginary axis into the right-half plane along the real axis. A Hopf bifurcation occurs when a pair of complex conjugate eigenvalues crosses the imaginary axis transversely into the right-half plane. Using a combination of center manifold reduction and the method of multiple scales, we obtain the normal form of the dynamics near these bifurcation values. The normal form is used to identify three types of static bifurcations of the trivial solution, namely, supercritical pitchfork, subcritical pitchfork, and transcritical bifurcations; one type of static bifurcation (saddle-node bifurcation) of the nontrivial constant solution; and one type of Hopf bifurcation (supercritical Hopf bifurcation) of the trivial or nontrivial constant solution. A codimension-two bifurcation (Bogdanov-Takens bifurcation) is located at the intersection of two codimension-one bifurcation varieties, the static bifurcation and the Hopf bifurcation of the trivial solution. The corresponding linear operator has a double-zero eigenvalue. The global bifurcation behavior arising from this local codimension-two bifurcation can be studied by the normal form of the dynamics near this nonhyperbolic fixed point.

A small limit cycle is born after a supercritical Hopf bifurcation occurs. This corresponds to an amplitude- and phase- modulated motion of the original system. A combination of a shooting technique and Floquet theory is used to calculate limit cycles and their stability. Since the modulation equations are autonomous, one of the Floquet multipliers is always one. The limit cycle is stable if the other Floquet multipliers lie within the unit circle; if at least one of them is outside the unit circle, the limit cycle is unstable. As a control parameter is varied, a period-doubling bifurcation occurs when any Floquet multiplier leaves the unit circle along the real

axis through -1; a cyclic-fold (saddle-node) or a symmetry-breaking bifurcation occurs when any Floquet multiplier leaves the unit circle along the real axis through +1; and a Neimark bifurcation (secondary Hopf bifurcation) occurs when a pair of complex conjugate Floquet multipliers leaves the unit circle. If a sequence of period-doubling bifurcations is complete, a chaotic attractor emerges. However, a homoclinic bifurcation occurs when an orbit homoclinic to a saddle occurs. This could result in either a jump to a far away attractor or to a chaotic attractor, depending upon the Shilnikov inequality $\delta = \lambda_2/\lambda_1$, where the Jacobian at the saddle point has the positive eigenvalue (real or complex pair) with smallest real part, λ_1, and the negative eigenvalue (real or complex pair) with real part of smallest modulus, λ_2. When $\delta > 1$, there is a periodic orbit on one side of the homoclinic orbit and there is no recurrent behavior on the other side. Consequently, the response jumps to a far away attractor. When $\delta < 1$, there is a periodic orbit on one side of the homoclinic orbit and chaos on the other side.

Several types of jump phenomena are found in this study. The trivial fixed point could jump via a subcritical pitchfork bifurcation; a nontrivial fixed point could jump via a saddle-node bifurcation; and a limit cycle could jump via a cyclic-fold bifurcation or a homoclinic bifurcation. Moreover, a chaotic attractor could jump via a boundary crisis (Grebogi et al., 1983) if it collides with its own basin boundary. As a result, the attractor and its basin are destroyed and the response jumps to a far away attractor.

When two of the Floquet multipliers are +1, a symmetric limit cycle may lose symmetry. An asymmetric limit cycle could also lead to a chaotic attractor via a homoclinic bifurcation, a jump, or an intermittent chaotic motion via a cyclic-fold bifurcation without the formation of a homoclinic orbit. The resulting attractors and isolated branches of attractors can sometimes be found by checking the unstable manifolds of nearby saddles. The complex motions are identified by using phase

planes, power spectra, Lyapunov exponents, and dimensions. The analytical results are verified by numerically integrating the original system for some cases.

5.1.1 Nonlinear Normal Modes

In Chapter 2, we construct the nonlinear normal modes of a weakly nonlinear discrete system with one-to-one and three-to-one internal resonances by using a complex-valued invariant-manifold approach. Cubic geometric nonlinearities are considered. The method of normal forms is used to simplify the dynamics on the invariant manifolds. The simplified system possesses similar nonlinear normal modes for the case of one-to-one internal resonance and nonsimilar nonlinear normal modes for the case of three-to-one internal resonance. In contrast with the case of no internal resonance, the number of nonlinear normal modes may be more than the number of linear normal modes. Bifurcations of the calculated nonlinear normal modes are investigated.

Next, for a continuous system without internal resonances, we consider a cantilever beam and compare two approaches for the determination of its nonlinear planar modes. In the first approach, the governing partial-differential system is discretized using the linear mode shapes and then the nonlinear normal modes are determined from the discretized system. In the second approach, the boundary-value problem is treated directly by using the method of multiple scales. The results show that both approaches yield the same nonlinear modes because the discretization is performed using a complete set of basis functions, namely, the linear mode shapes.

5.1.2 Systems with Repeated Natural Frequencies

In Chapter 3, we study the nonlinear response of multi-degree-of-freedom systems with repeated natural frequencies and cubic nonlinearities to various parametric resonances. The linear part of the system has a nonsemisimple one-to-one resonance. The character of the stability and various types of bifurcation are analyzed. The results are applied to the flutter of a simply supported panel in a supersonic airstream. In which case, a set of nonlinear autonomous first-order ordinary differential equations governing the slow-time modulation of the amplitudes and phases of the excited modes are derived and used to calculate the equilibrium solutions and their stability, and hence to identify the excitation parameters that suppress flutter and those that lead to complex motions. A combination of a shooting technique and Floquet theory is used to calculate limit cycles and their stability. It is shown that the trivial solutions can lose stability through three types of bifurcations: supercritical and subcritical pitchfork bifurcations, supercritical Hopf bifurcations, and Bogdanov-Takens bifurcations for the cases of principal and fundamental parametric resonances. Near the formation of an orbit homoclinic to a saddle focus, the Shilnikov theorem is used to explain the jump phenomenon as a control parameter is varied. For the case of combination parametric resonance, the trivial solution can lose stability via a supercritical or subcritical pitchfork bifurcation only. However, conditions for supercritical Hopf bifurcations are found for nontrivial constant solutions. The bifurcation diagrams show that the Hopf bifurcation island and the pitchfork bifurcation curve move closer to each other as a frequency detuning parameter σ^* decreases. Inside this island of unsteady solutions, the numerical

results indicate the existence of cyclic-fold bifurcations and sequences of period-doubling bifurcations that culminate in chaos.

Next, the effects of quadratic nonlinearities are investigated. For the case of fundamental parametric resonance, the quadratic nonlinearities qualitatively modify the response of the excited system. They change the static bifurcation of the trivial solution from a pitchfork to a transcritical bifurcation. Cyclic-fold and Hopf bifurcations of the nontrivial constant solutions are produced. Period-doubling sequences leading to chaos are also produced by the quadratic terms. However, the quadratic nonlinearities only quantitatively change the response of the system with cubic nonlinearities to the principal parametric resonance if the coefficient of the nonlinear term in the modulation equations does not change sign.

5.1.3 Systems with Widely Spaced Modal Frequencies

In Chapter 4, we investigate a recently discovered mechanism for transferring energy from a high-frequency excitation to a low-frequency mode. The method of averaging is used to analyze the response of a two-degree-of-freedom system with widely spaced modal frequencies and cubic nonlinearities to a principal parametric resonance of the high-frequency mode. The conditions under which energy can be transferred from high- to low-frequency modes are determined. Oscillations of the low-frequency mode are accompanied by slow amplitude and phase modulations of the high-frequency mode, as observed in the experiments. The analytical results are validated by numerically solving the original system.

Many interesting complexities due to nonlinear interactions are found in this simple model after an oscillation in the low-frequency mode occurs. These include

bubble structures (the occurrence of cascades of period-doubling and reverse period-doubling bifurcations), homoclinic bifurcations, the coexistence of multiple attractors, cyclic-fold and symmetry-breaking bifurcations, the merger of two chaotic attractors, boundary crises, intermittent chaos, and chaos quenching.

5.2 Recommendations

Some issues recommended for further study are:

(1) Construct nonlinear normal modes with internal resonances (e.g., combination internal resonance) by accounting for quadratic as well as cubic nonlinearities. A symbolic manipulator is recommended for this work.

(2) Experimentally check the validity of our theoretical results, which identify excitation parameters for the suppression of flutter.

(3) Here, we study the effects of structural nonlinearities for panel flutter. The aerodynamic nonlinear effects become significant only when the panel deflection is on the order of the panel length. Two other types of flutter (transonic buzz and stall flutter) are important and involve significant aerodynamic nonlinearities. The nonlinear aerodynamic/structure interaction can be modelled and finite-amplitude flutter oscillations can be predicted by using a combination of computational fluid dynamics (CFD) and discretization of the structure. Can one use the CFD results to produce an analytical model of the aerodynamic nonlinearities? If so, one may be

able to analyze their effects on the response of the structure, as described in this dissertation.

(4) Develop a strategy for controlling the identified undesirable dynamic behaviors, such as, amplitude-modulated motions and chaotically modulated motions.

(5) According to the nature of the discontinuous changes in a chaotic attractor, Grebogi, Ott, Romeiras, and Yorke (1987) distinguished three types of crises; namely, boundary crises, interior crises, and attractor merging crises. Some of them are observed in the numerical studies in Chapter 4. Nayfeh and Nayfeh (1993b) also obtained similar phenomena in the response of the same system to a primary resonance of the high-frequency mode. A detailed bifurcation analysis of the averaged equations in this case needs to be conducted.

REFERENCES

1. Anderson, T. J., Balachandran, B., and Nayfeh, A. H., 1992, "Observations of nonlinear interactions in a flexible cantilever beam," *AIAA Paper No. 92-2332*, 33rd AIAA Structures, Structural Dynamics and Material Conference, Dallas, Texas.

2. Anderson, T. J., Nayfeh, A. H., and Balachandran, B., 1993, "Coupling between high-frequency modes and a low-frequency mode: Theory and experiment," *Nonlinear Dynamics*, accepted for publication.

3. Asmis, K. G., and Tso, W. K., 1972, "Combination Resonance in a Nonlinear Two-Degree-of-Freedom System," *Journal of Applied Mechanics*, Vol. E39, pp. 832-834.

4. Asrar, W., 1991, "Two-Degree-of-Freedom Systems with Quadratic Non-Linearities Subjected to Parametric and Self Excitation," *Journal of Sound and Vibration*, Vol. 150, pp. 447-456.

5. Burton, T. D., and Kolowith, M., 1988, "Nonlinear Resonances and Chaotic Motion in a Flexible Parametrically Excited Beam," *Proceedings of the Second Conference on Non-linear Vibrations, Stability, and Dynamics of Structures and Mechanisms*, Blacksburg, VA.

6. Carr, J., 1981, *Applications of Center Manifold Theory* Applied Mathematical Sciences, Vol. 35, Springer-Verlag, New York.

7. Caughey, T. K., and Vakakis, A. F., 1991, "A Method for Examining Steady State Solutions of Forced Discrete Systems with Strong Non-Linearities," *International Journal of Non-Linear Mechanics*, Vol. 26, pp. 89-103.

8. Ciliberto, S., and Gollub, J. P., 1985, "Chaotic Mode Competition in Parametrically Forced Surface Waves," *Journal of Fluid Mechanics*, Vol. 158, pp. 381-398.

9. Crespo da Silva, M. R. M., and Glynn, C. C., 1978, "Nonlinear Flexural-Flexural-Torsional Dynamics of Inextensional Beams-I. Equations of Motion," *Journal of Structural Mechanics*, Vol. 6, pp. 437-448.

10. Cusumano, J. P., and Moon, F. C., 1989, "Low Dimensional Behavior in Chaotic Nonplanar Motions of a Forced Elastic Rod: Experiment and Theory," *Nonlinear Dynamics in Engineering Systems, IUTAM Symposium*, Germany.

11. Dowell, E. H., 1966, "Nonlinear Oscillations of a Fluttering Plate," *AIAA Journal*, Vol. 4, pp. 1267-1275.

12. Dowell, E. H., 1975, *Aeroelasticity of Plates and Shells*, Noordhoff, Leyden.

13. Dowell, E. H., 1982, "Flutter of a Buckled Plate as an Example of Chaotic Motion of a Deterministic Autonomous System," *Journal of Sound and Vibration*, Vol. 85, pp. 333-344.

14. Dowell, E. H., and Ilgamov, M., 1988, *Studies in Nonlinear Aeroelasticity*, Springer-Verlag, New York.

15. Dowell, E. H., and Voss, H. M., 1965, "Experimental and Theoretical Panel Flutter Studies in the Mach Number Range 1.0 to 5.0," *AIAA Journal*, Vol. 3, pp. 2292-2304.

16. Dugundji, J., and Mukhopadhyay, V., 1973, "Lateral Bending-Torsion Vibrations of a Thin Beam Under Parametric Excitation," *Journal of Applied Mechanics*, Vol. 40, pp. 693-698.

17. Evan-Iwanowski, R. M., 1976, *Resonance Oscillations in Mechanical Systems*, Elsevier, New York.

18. Farmer, J. D., Ott, E., and Yorke, J. A., 1983, "The Dimension of Chaotic Attractors," *Physica 7D*, pp. 153-180.

19. Feng, Z. C., and Sethna, P. R., 1989, "Symmetry-Breaking Bifurcations in Resonant Surface Waves," *Journal of Fluid Mechanics*, Vol. 199, pp. 495-518.

20. Fu, F. C. L., and Nemat-Nasser, S., 1972a, "On the Stability of Steady-State Response of Certain Nonlinear Dynamic Systems Subjected to Harmonic Excitations," *Ingenieur-Archiv*, Vol. 41, pp. 407-420.

21. Fu, F. C. L., and Nemat-Nasser, S., 1972b, "Stability of Solution of Systems of Linear Differential Equations with Harmonic Coefficients," *AIAA Journal*, Vol. 10, pp. 30-36.

22. Grebogi, C., Ott, E., Romeiras, F., and Yorke, J. A., 1987, "Critical exponents for crisis-induced intermittency," *Physical Review A*, Vol. 36, pp. 5365-5380.

23. Grebogi, C., Ott, E., and Yorke, J. A., 1983, "Crises, sudden changes in chaotic attractors, and transient chaos," *Physica D*, Vol. 7, pp. 181-200.

24. Gu, X. M., and Sethna, P. R., 1987, "Resonant Surface Waves and Chaotic Phenomena," *Journal of Fluid Mechanics*, Vol. 183, pp. 543-565.

25. Guckenheimer, J., and Holmes, P. J., 1983, *Dynamical Systems and Bifurcations of Vector Fields* Springer-Verlag, New York.

26. Haddow, A. G., and Hasan, S. M., 1988, "Nonlinear Oscillation of a Flexible Cantilever: Experimental Results," *Proceedings of the Second Conference on Non-linear Vibrations, Stability, and Dynamics of Structures and Mechanisms*, Blacksburg, VA.

27. Holmes, P. J., 1986, "Chaotic Motions in a Weakly Nonlinear Model for Surface Waves," *Journal of Fluid Mechanics*, Vol. 162, pp. 365-388.

28. Hsieh, S. R., Shaw, S. W., and Pierre, C., 1993, "Normal Modes for Large Amplitude Vibration of a Cantilever Beam," *International Journal of Solids and Structures*, to appear.

29. Ibrahim, R. A., 1985, *Parametric Random Vibration*, Wiley-Interscience, New York.

30. Ibrahim, R. A., and Barr, A. D. S., 1975, "Autoparametric Resonance in a Structure Containing a Liquid. Part I: Two Mode Interaction," *Journal of Sound and Vibration*, Vol. 42, pp. 159-179.

31. Kaplan, J., and Yorke, J., 1978, "Functional Differential Equations and the Approximation of Fixed Points," Proceedings, Bonn, July 1978, Lecture Notes in Math. 730, H.O. Peitgen and H.O. Walther, eds., (Springer, Berlin, 1978), p. 228.

32. Knobloch, E., and Weiss, N. O., 1983, "Bifurcations in a Model of Magnetoconvection," *Physics of Fluids*, Vol. 9, pp. 379-407.

33. Lock, M. H., and Fung, Y. C., 1961, "Comparative Experimental and Theoretical Studies of the Flutter of Flat Panels in a Low Supersonic Flow," *AFOSR Rpt.* TN 670.

34. Meron, E., and Procaccia, I., 1986, "Low-Dimensional Chaos in Surface Waves: Theoretical Analysis of an Experiment," *Physical Review A*, Vol. 34, pp. 3221-3237.

35. Miles, J. W., 1984, "Nonlinear Faraday Resonance," *Journal of Fluid Mechanics*, Vol. 146, pp. 285-302.

36. Miles, J. W., 1985, "Parametric Excitation of an Internally Resonant Double Pendulum," *Journal of Applied Mathematics and Physics (ZAMP)*, Vol. 36, pp. 337-345.

37. Month, L. A., and Rand, R. H., 1977, "The Stability of Bifurcating Periodic Solutions in a Two-Degree-of-Freedom Nonlinear System," *Journal of Applied Mechanics*, pp. 782-783.

38. Month, L. A., and Rand, R. H., 1980, "An Application of the Poincare Map to the Stability of Nonlinear Normal Modes," *Journal of Applied Mechanics*, Vol. 47, pp. 645-651.

39. Moon, F. C., 1987, *Chaotic Vibrations* . Wiley-Interscience, New York.

40. Namachchivaya, N. S., and Malhotra, N., 1992, "Parametrically Excited Hopf Bifurcation with Non-Semisimple 1:1 Resonance," *ASME Nonlinear Vibrations*, DE-50/AMD-144, pp. 29-46.

41. Nayfeh, A. H., 1973, *Perturbation Methods*, Wiley-Interscience, New York.

42. Nayfeh, A. H., 1981, *Introduction to Perturbation Techniques*, Wiley-Interscience, New York.

43. Nayfeh, A. H., 1983a, "Parametrically Excited Multidegree-of-Freedom Systems with Repeated Frequencies," *Journal of Sound and Vibration*, Vol. 88, pp. 145-150.

44. Nayfeh, A. H., 1983b, "The Response of Multidegree-of-Freedom Systems with Quadratic Nonlinearities to a Harmonic Parametric Resonance," *Journal of Sound and Vibration*, Vol. 90, pp. 237-244.

45. Nayfeh, A. H., 1983c, "The Response of a Two-Degree-of-Freedom Systems with Quadratic Nonlinearities to a Parametric Excitation," *Journal of Sound and Vibration*, Vol. 88, pp. 547-557.

46. Nayfeh, A. H., 1987a, "Parametric Excitation of Two Internally Resonant Oscillators," *Journal of Sound and Vibration*, Vol. 119, pp. 95-109.

47. Nayfeh, A. H., 1987b, "Surface Waves in Closed Basins under Parametric and Internal Resonances," *Physics of Fluids*, Vol. 30, pp. 2976-2982.

48. Nayfeh, A. H., 1993, *Method of Normal Forms*, Wiley-Interscience, New York.

49. Nayfeh, A. H., and Balachandran, B., 1989, "Modal Interactions in Dynamical and Structural Systems," *Applied Mechanics Reviews*, Vol. 42, pp. 175-201.

50. Nayfeh, A. H., and Balachandran, B., 1994, *Nonlinear Dynamics*, Wiley-Interscience, New York.

51. Nayfeh, A. H., and Mook, D. T., 1979, *Nonlinear Oscillations*, Wiley-Interscience, New York.

52. Nayfeh, A. H., and Nayfeh, J. F., 1990, "Surface Waves in Closed Basins Under Principal and Autoparametric Resonances," *Physics of Fluids*, Vol. A2, pp. 1635-1648.

53. Nayfeh, A. H., and Nayfeh, S. A., 1993a, "On Nonlinear Modes of Continuous Systems," *Journal of Acoustics and Vibration*, accepted.

54. Nayfeh, A. H., and Nayfeh, S. A., 1993b, "Nonlinear Normal Modes of a Continuous System with Quadratic Nonlinearities," *Journal of Acoustics and Vibration*, submitted.

55. Nayfeh, A. H., and Pai, P. F., 1989, "Non-Linear Non-Planar Parametric Responses of an Inextensional Beam," *International Journal of Non-Linear Mechanics*, Vol. 24, pp. 139-158.

56. Nayfeh, A. H., and Zavodney, L. D., 1986, "The Response of Two-Degree-of-Freedom Systems with Quadratic Non-Linearities to a Combination Parametric Resonance, *Journal of Sound and Vibration*, Vol. 107, pp. 329-350.

57. Nayfeh, S. A., and Nayfeh, A. H., 1993a, "Energy Transfer from High- to Low-Frequency Modes in a Flexible Structure via Modulation," *Journal of Vibration and Acoustics*, in press.

58. Nayfeh, S. A., and Nayfeh, A. H., 1993b, "Nonlinear Interactions Between Two Widely Spaced Modes - External Excitations," *International Journal of Bifurcation and Chaos*, Vol. 3, pp. 417-427.

59. Pak, C., Rand, R. H., and Moon, F. C., 1992, "Free Vibrations of a Thin Elastica by Normal Modes," *Nonlinear Dynamics*, Vol. 3, pp. 347-364.

60. Pomeau, Y. and Manneville, P., 1980, "Intermittent Transition to Turbulence in Dissipative Dynamical Systems," *Communications in Mathematical Physics*, Vol. 74, pp. 189-197.

61. Rand, R. H., Pak, C. H., and Vakakis, A. F., 1992, "Bifurcation of Nonlinear Normal Modes in a Class of Two Degree of Freedom Systems," *Acta Mechanica*, Vol. 3, pp. 129-145.

62. Rosenberg, R. M., 1962, "The Normal Modes of Nonlinear N-Degree-of-Freedom Systems," *Journal of Applied Mechanics*, Vol. 30, pp. 7-14.

63. Rosenberg, R. M., 1966, "On Nonlinear Vibrations of Systems with Many Degrees of Freedom," *Advances in Applied Mechanics*, Vol. 9, pp. 155-242.

64. Rosenberg, R. M., and Kuo, J. K., 1964, "Nonsimilar Normal Mode Vibrations of Nonlinear Systems Having Two Degrees of Freedom," *Journal of Applied Mechanics*, Vol. 31, pp. 283-290.

65. Schmidt., G., and Tondl, A., 1986, *Nonlinear Vibrations*, Akademie-Verlag, Berlin.

66. Shaw, S. W., and Pierre, C., 1991, "Non-Linear Normal Modes and Invariant Manifolds," *Journal of Sound and Vibration*, Vol. 150, pp. 170-173.

67. Shaw, S. W., and Pierre, C., 1993a, "Normal Modes for Non-Linear Vibratory Systems," *Journal of Sound and Vibration*, in press.

68. Shaw, S. W., and Pierre, C., 1993b, "Normal Modes of Vibration for Non-Linear Continuous Systems," *Journal of Sound and Vibration*, to appear.

69. Shilnikov, L. P., 1970, "A contribution to the problem of the structure of an extended neighborhood of a structurally stable equilibrium state of saddle-focus type," *Math. USSR Sbornik*, Vol. 10, pp. 91-102.

70. Simonelli, F., and Gollub, J. P., 1989, "Surface Wave Mode Interactions: Effects of Symmetry and Degeneracy," *Journal of Fluid Mechanics*, Vol. 199, pp. 471-494.

71. Streit, D. A., Bajaj, A. K., and Krousgrill, C. M., 1988, "Combination Parametric Resonance Leading to Periodic and Chaotic Response in Two-Degree-of-Freedom Systems with Quadratic Nonlinearities," *Journal of Sound and Vibration*, Vol. 124, pp. 297-314.

72. Szemplinska-Stupnicka, W., 1980, "The Resonant Vibration of Homogeneous Non-Linear Systems," *International Journal of Non-Linear Mechanics*, Vol. 15, pp. 407-415.

73. Tezak, E. G., Mook, D. T., and Nayfeh, A. H., 1978, "Nonlinear Analysis of the Lateral Response of Columns to Periodic Loads," *Journal of Mechanical Design*, Vol. 100, pp. 651-659.

74. Tezak, E. G., Nayfeh, A. H., and Mook, D. T., 1982, "Parametrically Excited Nonlinear Multidegree-of-Freedom Systems with Repeated Natural Frequencies," *Journal of Sound and Vibration*, Vol. 85, pp. 459-472.

75. Tso, W. K., and Asmis, K. G., 1974, "Multiple Parametric Resonance in a Non-Linear Two Degree of Freedom System," *International Journal of Non-Linear Mechanics*, Vol. 9, pp. 269-277.

76. Vakakis, A. F., and Caughey, T. K., 1992, "A Theorem on the Exact Nonsimilar Steady-State Motions of a Nonlinear Oscillator," *Journal of Applied Mechanics*, Vol. 59, pp. 418-424.

77. Vakakis, A., and Rand, R. H., 1992a, "Normal Modes and Global Dynamics of a Two-Degree-of-Freedom Non-Linear System-I. Low Energies," *International Journal of Non-Linear Mechanics*, Vol. 27, pp. 861-874.

78. Vakakis, A., and Rand, R. H., 1992b, "Normal Modes and Global Dynamics of a Two-Degree-of-Freedom Non-Linear System-II. High Energies," *International Journal of Non-Linear Mechanics*, Vol. 27, pp. 875-888.

Vita

The author was born on December 17th, 1961 in Taiwan. He attended National Taiwan University, Taiwan in 1979, studied Naval Architecture, and received his B.S. degree in 1983. From 1983 to 1985, he served as a Second Lieutenant Officer in the Army. In 1987, he received his M.S. degree in Aerospace and Ocean Engineering from Virginia Polytechnic Institute and State University. Then, he continued his studies for the degree of Ph.D. in the Department of Engineering Science and Mechanics.